The University Of Sheffield.

"Transglutaminase 2 in Chronic Kidney Disease of the Domestic Feline and its role in a rodent model of Renal Warm Ischaemia"

Armando Cristian Sánchez-Lara

Thesis submitted to the University of Sheffield for the degree of Doctor of Philosophy

Supervisor: Dr John L Haylor BPharm MEd PhD

Department of Infection and Immunity
Academic Nephrology Unit

September 2015

Acknowledgements

I would like to express my deepest appreciation, admiration and respect to my supervisor Dr John L Haylor. Without his guidance and persistent help, neither this thesis nor the papers published would not have been possible. Without his support and his high sense of empathy I would not have been able to become a Member of the Royal College of Veterinary Surgeons, which I am very proud of. Many thanks.

Many thanks to Professors Harriet Syme and Jonathan Elliott from the Royal Veterinary College for their unconditional support and for believing in this project. You are both inspirational people and role models in the veterinary world,

I am heartily thankful to:-

My mother. Senitillo ¡Lo logramos, mi mariposita blanca! Esta tesis te la dedico a ti, es tuya. En esta tesis estás tú y es el resultado de tu esfuerzo por hacer realidad mi sueño. Gracias por siempre creer en mis locuras, por estar allí siempre y por empujarme a romper paradigmas ¡te quiero mucho!

My aunt. Tía, en esta tesis están las develadas que nos dimos tu y yo; gracias por esas cartas en inglés que al final acababas escribiendo tú, la mejor maestra de inglés sin duda.

My father. Un paso más papá, y lo que le falta. Gracias por tu apoyo y por creer en esta aventura.

My brother. Bro, te quiero y admiro mucho. De alguna manera sé que estás cerca.

My sister. ¡Los sueños se pueden hacer realidad! Confío que lograrás los tuyos.

My soul-mate. Piojita hermosa, juntos terminamos la tesis y juntos empezamos un capítulo más de nuestro hermoso libro.

My friends and colleagues in Mexico and in the UK for their love, guidance and understanding at different stages of this academic adventure.

Dr Luis Antonio Calzada Nova and Dr Pedro Zamudio for their contagious love to science. Without their influence, knowledge and philosophy I would have never discovered the door to this fascinating World of Science.

Federation Canófila Mexicana and Dr José Luis Payró for their timely and effective support.

Imran Butt, for his friendship, patience and advice in the teaching of the kidney transplant technique. Also, many thanks for his guidance in the technical structure of the kidney transplant procedure described on Chapter 7.

Mabrouka Maamra for having the patient and finding time in her busy diary to teach me, advise me and correct me in the laboratory techniques. Also, for offering me her unconditional friendship.

All the academics, post-docs and technicians in the Medical School, particularly the Academic Nephrology Unit. Special thanks to Mr Ahmed Halawa for his support in the renal warm ischaemia study. A big thanks to Fiona Wright for her guidance and advice in the lab techniques, H & E staining, tissue cutting and slide mounting.

My examiners Dr David Buttle and Simon Oldroyd for their time spent to highlight key points for the improvement of this thesis.

The Clinical Chemistry Department from the University of Sheffield for running plasma and urine creatinine samples in the rat studies.

Finally, I wish to express my gratitude to the National Autonomous University of Mexico and the University of Sheffield, my beloved Alma Maters, where I had the opportunity to grow and develop myself personally and academically.

¡GOYA! ¡GOYA!
¡CACHUN, CACHUN, RA, RA!
¡CACHUN, CACHUN, RA, RA!
¡GOYA!
¡¡UNIVERSIDAD!!

Table of Contents

Table of Figures

Chapter 1

Chapter 2

Chapter 3

Chapter 4

Chapter 5

Chapter 6

Chapter 7

Chapter 8

Table of Figures

Chapter 1

Chapter 2

Chapter 3

Chapter 4

Chapter 5

Chapter 6

Chapter 7

List of Abbreviations

AMP	Adenosine monophosphate
ATN	Acute tubular necrosis
ATP	Adenosine triphosphate
CAN	Chronic allograph nephropathy
CKD	Chronic kidney disease
CPP	Continuous pulsatile perfusion
CRRT	Continual renal replacement therapy
CS	Cold storage
DAPI	4',6-diamidino-2-phenylindole
DGF	Delayed graft function
ECM	Extracellular matrix
ELISA	Enzyme-linked immunosorbent assay
ESRD	End stage renal disease
FGF	fibroblast growth factor
FITC	Fluorescein isothiocyanate
FN 1	fibronectin 1
FWIT	First Warm Ischaemia Time
GFR	Glomerular filtration rate
GTP	Guanosine-5'-triphosphate
H & E	Haematoxylin and eosin stain
HIF-α	Hypoxia inducible factor α
HRP	Horseradish peroxidase,
IFN-γ	Interferon γ
IL-2	Interleukin 2
IRI	Ischemia reperfusion injury
IRIS	International Renal Interest Society
kDa	Kilo dalton
KD value	Dissociation constant
L-TGF-β1	Latent TGF-β1
MHC	Major histocompatibility complex
MMP	Matrix metalloproteinase enzymes
MTS	Masson Trichrome Staining
NOP	Normothermic organ preservation
NF-κβ	Nuclear factor kappa enhancer of activated B cells
Nx	Nephrectomy
PASH	Periodic Acid-Schiff Haematoxylin
PDGF	Platelet derived growth factor
PECAM-1	Platelet endothelial cell adhesion molecule 1
PMNs	Polymorphonuclears
RAAS	Renin angiotensin aldosterone system
ROS	Reactive Oxygen Species
SNx	Subtotal nephrectomy

SWIT	Second Warm Ischemia Time
TG2	Transglutaminase 2
TGF-β	Transforming growth factor-β
Th1	Lymphocyte T helper
TMB	3,3',5,5'-Tetramethylbenzidine,
TNF-α	Tumour necrosis factor α
UNx	Unilateral Nephrectomy
UPC	Urinary protein/creatinine ratio
VEGF	Vascular endothelial growth factor
WHO	World Health Organization
WI	Warm ischaemia
α-MA	α-smooth muscular actin

List of pertinent publications

Published

1. **Sánchez-Lara AC**, Elliott J, Syme HM, Brown CA, Haylor JL (2014). Feline Chronic Kidney Disease Is Associated With Upregulation of Transglutaminase 2: A Collagen Cross-Linking Enzyme. *Veterinary Pathology.* DOI: 10.1177/0300985814542811.

2. Shrestha B, Butt I, Da Silva M, **Sánchez-Lara AC**, Wagner B, Raftery A*, et al.* (2014). Upregulation of transglutaminase and epsilon (gamma-glutamyl)-lysine in the Fisher- Lewis rat model of chronic allograft nephropathy. *BioMed research international* **2014:** 651608. DOI: 10.1155/2014/651608.

In Preparation

3. **Sánchez-Lara AC** and Haylor JL (2015). The Role of Renal Warm Ischaemia and Transglutaminase 2 in the rat, an experimental model to study CKD in the Domestic Cat. *Veterinary Pathology*.

4. **Sánchez-Lara AC** and Haylor JL (2015). Possible Mechanisms for the development of Feline Tubulointerstitial Fibrosis and Glomerular Fibrogenic Resistance.

Summary

Chronic kidney disease (CKD) in humans and cats is a major cause of death. In both species, tubulointerstitial fibrosis (TIF) is the major histopathological feature, which is the product of collagen accumulation and deposition in the extracellular matrix (ECM). Transglutaminase 2 (TG2) is a calcium-dependent enzyme, secreted by renal and inflammatory cells under stress. TG2 crosslinks collagen protein, promoting fibrosis deposition and progression of disease.

In this research project, azotaemic and non-azotaemic feline kidney tissue were employed to determine the TG2 association with renal fibrosis and to test (*in vitro*) the feasibility of the TG2 inhibition. A rodent model of renal warm ischaemia was used to generate tubulointerstitial fibrosis without glomerulosclerosis and to determine the effect of transglutaminase inhibitors on the development of TIF.

The transglutaminase pathway was associated with TIF in either the cat or the rat. In the feline kidney tissue, the inhibition of TG activity was achieved using both a TG2 inhibitory monoclonal antibody and a chemical TG inhibitor. In the rat model of RWI, reduction in TIF fibrosis deposition was achieved when using an intrarenal TG chemical inhibitor. Glomerular TG2 expression and fibrosis was not observed in either the cat or the rat.

The TG pathway inhibition may represent a novel approach to reduce or stop the development of TIF in cats and humans. RWI rodent model may be an interventional model to study TIF in the cat. The understanding of the glomerular resistance to develop fibrosis in the cat with CKD and the rat following RWI may be of relevance in the generation of treatments to prevent or delay glomerulosclerosis in the man. The naturally occurring model of feline CKD may be an important research approach to study CKD in the man and to generate evidence based veterinary medicine.

CHAPTER 1

Introduction

1.1. Chronic Kidney Disease in the Cat

Chronic kidney disease (CKD) is a major concern in small animal medicine (Bartlett *et al.*, 2010). CKD is defined as a progressive deterioration in the structure and function of the kidney, resulting in electrolyte imbalance and the retention of metabolic waste products, with a sustained decrease in GFR at least for 3 months (Elliott *et al.*, 2007).

1.1.1 Epidemiology

CKD is commonly seen in aged cats (Boyd *et al.*, 2008; Lund *et al.*, 1999) and it is the most common renal disease in elderly cats (Polzin, 2011). The incidence of CKD in cats is at least 3 times higher than in dogs (Polzin, 2011). A retrospective study from Veterinary Teaching Hospitals in the USA reported a CKD incidence in cats over 12 years of age to be as high as 28% (Bartlett *et al.*, 2010). Another study on age distribution of CKD reported that 63% of CKD feline patients were older than 10 year of age (Bartges, 2012). A more recent retrospective study in USA showed an incidence of CKD, in randomly selected cats, to be as high as 50% (Marino *et al.*, 2013b).

1.1.2 Staging

The International Renal Interest Society was created in 1998 by a group of 14 veterinarians focused on the study of companion animal nephrology in order to develop a staging system for dogs and cats with CKD (Elliott *et al.*, 2007). In cats, there is a CKD staging system to facilitate severity, progression of diagnosis as well as treatment decision support. The core marker for CKD staging is based on plasma creatinine, a blood marker measured on two or more occasions in the stable animal. The stages are divided in 4 levels, see Figure 1.1. Each level estimates the degree of renal functionality and, therefore, potential clinical signs.

Proteinuria and systemic systolic blood pressure serve as parameters to sub-stage CKD. Proteinuria, assessed from the urinary protein/creatinine ratio (UPC), is divided in three stages; non-proteinuric (0 - 0.2 UPC), borderline proteinuric (0.2-0.4 UPC) and proteinuric (0.4-0.6 UPC). Systemic systolic blood pressure (SSBP) is

divided in four levels; minimal risk (130-150 mm/Hg), low risk (150-160 mm/Hg), moderate risk (160-190 mm/Hg) and high risk (180-190 mm/Hg). Both sub-staging parameters vary independently of each other; therefore, the level of proteinuria or SSBP may occur at any stage of CKD (Elliott *et al.*, 2007), see Figure 1.2.

Stage 1 (plasma creatinine < 140 µmol/L), the cat may have normal renal function but early renal disease. Non-azotaemic CKD cannot be ruled out.

Stage 2 (plasma creatinine 140-250 µmol/L), the cat presents a low-mild azotaemia with metabolic imbalances that can lead to hyperparathyroidism and hypokalaemia (Elliott *et al.*, 2007). This stage has been subdivided in 2a (140-170 µmol/L) and 2b (170-250 µmol/L) with the purpose of isolating cases with substantial azotaemia and probably evident clinical signs as seen in patients with CKD 2, sub stage b (Syme *et al.*, 2006).

Stage 3 (plasma creatinine 250-440 µmol/L), the cat shows moderate azotaemia. Extrarenal clinical signs may be present- bone pain, uremic gastritis, normocitic normochromic non-regenerative anaemia and metabolic acidosis.

Stage 4 (plasma creatinine >440 µmol/L), the cat presents severe azotaemia with evident systemic clinical signs and uraemic crisis. A non-reversible high degree of renal azotaemia indicates end stage renal failure (Elliott *et al.*, 2007).

1.1.3 Risk factors

In a recent retrospective study, involving 1230 clinical cases in USA, it was determined that risk factors can include low body condition score, prior dental disease, cystitis, anaesthesia and neutering in male cats (Greene *et al.*, 2014).

1.1.3.1 Susceptibility factors

Breed: In the late 80's, the Maine Coon, Abyssinian, Siamese, Russian Blue and Burmese breeds were reported as breeds in high risk of developing CKD (DiBartola *et al.*, 1987). The most common familial renal diseases in cats are polycystic kidney disease (autosomal dominant) in the Persian and amyloidosis (autosomal dominant with incomplete penetrance) in the Abyssinian, Siamese and Oriental cat (Polzin, 2011).

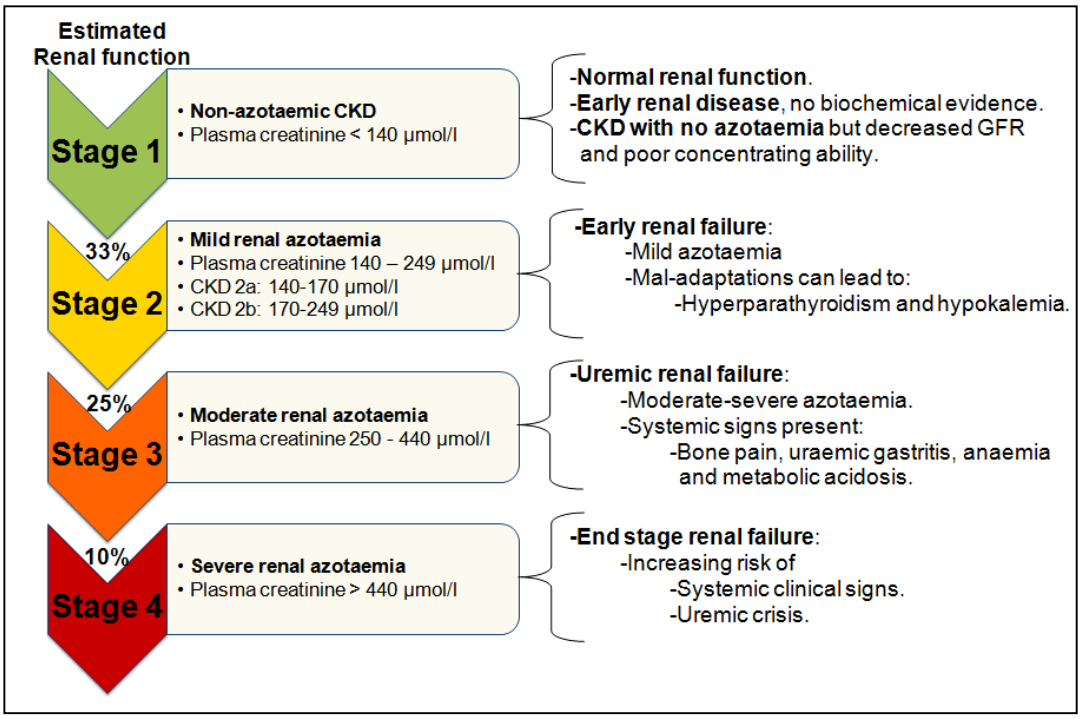

Figure 1.1: CKD staging system in the domestic cat

Scoring system showing the degree of renal function according to plasma creatinine as a core marker. Renal status and potential clinical signs are shown in brackets for each stage.

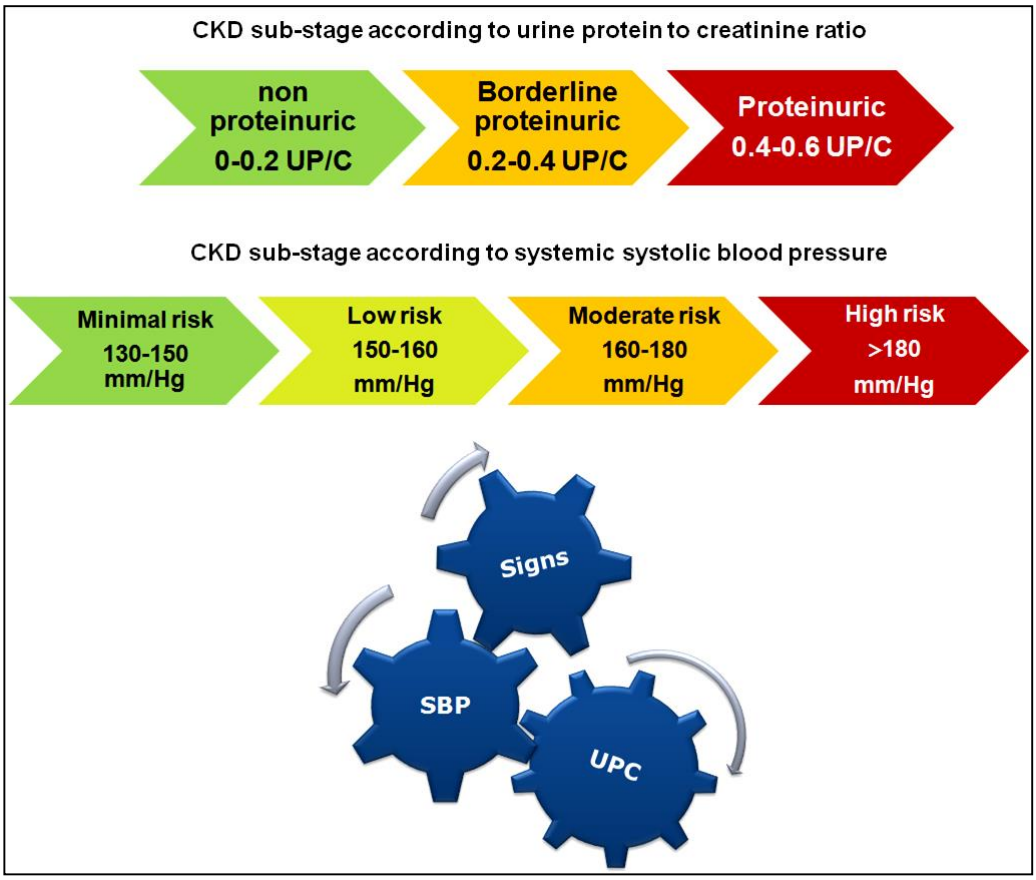

Figure 1.2: IRIS sub-stage based on proteinuria and systemic systolic blood pressure

Upper diagram shows the proteinuria sub-staging divided in three levels. Middle diagram shows the systemic systolic blood pressure sub-staging divided in four levels. The lower diagram shows that UPC, blood pressure and clinical signs may vary independently of each other but are closely interconnected when CKD is present.

Age: CKD is the most common renal disease in elderly cats (Bartges, 2012). An English study involving 80 feline cases showed the presence of CKD 2, 3 and 4 in cats of 8.3 ± 1.5, 14.4 ± 0.7 and 12.5± 0.9 years of age (Elliott *et al.*, 1998). However, the onset of familiar renal disease often presents earlier in young animals.

Gender: In cats there is not substantial evidence with regard to gender predisposition to develop CKD. There is data showing that males are more prone to develop clinical signs of CKD when compared to female cats (White *et al.*, 2006). However, this evidence does not rule out the possibility that females are just more capable to handling higher levels of uraemia, phosphataemia or electrolyte imbalances.

Environmental factors: Cats living in places with a high risk of infectious disease such as mycoplasmosis, feline immunodeficiency virus, feline leukaemia virus and feline infectious peritonitis may develop glomerulonephritis (Vaden, 2011). Recently, it has been reported that indoors and outdoors hunting cats can become infected with leptospirosis showing clinical signs and histopathological evidence of CKD (Arbour *et al.*, 2012). Another potential cause of CKD is urinary outflow obstruction (Nelson *et al.*, 2009) which can be driven by behavioural and environmental factors (Cameron *et al.*, 2004).

1.1.3.2 Initiation factors

Initiation factors are those related to kidney injury in acute, sub-acute, or sustained presentation. These factors affect the three basic components of kidney tissue; tubulointerstitial, glomerular and vascular space. Tubulointerstitial and glomerular disease have both been identified, although glomerular diseases are not so frequently seen in the domestic cat (Vaden, 2011; Yabuki *et al.*, 2010). Glomerular membranous nephropathy is the most common glomerular disease in the domestic cat (Vaden, 2011). Tubulointerstitial compartment damage is the most relevant alteration after acute kidney injury (AKI) in cats (Elliott *et al.*, 2007). AKI results in a wave of cellular damage with a potentially reversible loss of renal function. AKI has a mortality rate in cats and dogs of around 50% (Behrend *et al.*, 1996; Stokes *et al.*, 2004; Vaden *et al.*, 1997; Worwag *et al.*, 2008; Ympa *et al.*, 2005). According to two retrospective studies in companion animals, the prevalence of CKD from AKI survivors, was approximately 24% and 20% in dogs and cats, respectively (Vaden *et*

al., 1997; Worwag *et al.*, 2008). AKI may be divided into pre-renal, post-renal and intrinsic mechanisms, according to the anatomic area of injury (Stokes *et al.*, 2004).

Pre-renal AKI possible causes are associated with severe dehydration, haemorrhage, hypoalbuminaemia, anaphylaxis, sepsis, heart failure, anaesthetics, radiocontrast media, medications such as cyclosporine (Dager, 2008), overdose and/or mixture of non-steroidal anti-inflammatory drugs (NSAID's) and steroids (Lascelles *et al.*, 2005). **Post-renal AKI** causes are associated with urinary tract obstruction at any level from the renal tubule to the urethra (Dager, 2008). This is frequently found in companion animals. Other common causes of post-renal AKI are associated with blockage at different levels of the urinary tract; renal pelvis, ureteral, bladder and urethra (Berent, 2011; Lulich *et al.*, 1993). **Intrinsic AKI** results from hypotension, renal artery occlusion, vasoconstriction and/or intratubular obstruction (Schnellmann, 1999; Schrier *et al.*, 2004). The intrinsic AKI causes are associated to ischaemic, nephrotoxic and infectious aetiologies affecting vascular, glomerular, tubular or /and interstitial area. In humans, 85% of AKI cases are secondary to either ischaemic (50%) or nephrotoxic (35%) aetiologies (Dager, 2008). More than 90% of cases result in some degree of acute tubular necrosis (ATN), the main histopathological feature of AKI (Star, 1998). In cats, ATN secondary to renal ischaemia and nephrotoxic injury has been described (Bartges, 2011; Chew *et al.*, 2011). Possible common causes of tubulointerstitial damage associated in cats are shown in Table 1.1.

1.1.3.3 Progression factors

Hyperthyroidism and hypertension. Hyperthyroidism is an important metabolic disease that has been associated with CKD progression in the domestic cat (Peterson, 2012). The progression of CKD in the hyperthyroid cat has been linked to hypertension, which is present in 14-23% of cats. In the hyperthyroid cat, the renin-angiotensin-aldosterone system (RAAS) is activated as in the man. Interestingly, RAAS has not been associated with the development of hypertension in the hyperthyroid cat, however, it may contribute in the progression of CKD (Williams *et al.*, 2013). In the man, hypertension is closely associated with RAAS activation, which in turn, directly contributes to the development of CKD (Meguid El Nahas *et al.*, 2005). In hyperthyroid cats, hypertension is present in 14-23% of cats with CKD (Williams *et al.*, 2013). In cats with hypertension associated with CKD, there is not an increase in the plasma renin, thus angiotensin II is not increased either; however, plasma

aldosterone is elevated when compared to CKD normotensive cats (Jensen *et al.*, 1997). Furthermore, aldosterone is not influenced by levels of plasma renin (Williams *et al.*, 2013). Interestingly, there is evidence showing that exogenous aldosterone in the rat following AKI can promote hypertension (Syme, 2011). In cats hyperaldosteronism mediates and contributes in the progression of CKD (Javadi *et al.*, 2005). If aldosterone is not upregulated by renin-angiotensin in the cat, therefore a direct regulation of aldosterone via potassium ions may play an important role in cats with CKD, however, this mechanism might be more relevant in cats with CKD stage 4, as serum potassium tend to be lower in previous CKD stages. Feline primary hyperaldosteronism may also play a role in cats with CKD where hypertension and hypokalaemia are found together (Javadi *et al.*, 2005). Perhaps, there are other pathways for feline aldosterone regulation still to be discovered.

Diet: In man, diet plays an important role in the progression of CKD. Since cats are strictly carnivorous, a cat with CKD on a conventional diet would unavoidably generate higher levels of both urea and phosphorus (Roudebush *et al.*, 2009).

Proteinuria: In humans and dogs with CKD, proteinuria can be excreted in large amounts, as glomerulopathy is a common histopathological feature in these species. In cats with CKD, even though glomerular lesions are not very common, the low detectable levels of proteinuria have been associated with lower life survival compared to cats with CKD without proteinuria (Syme *et al.*, 2006).

Other factors: Smoker owners, metabolic acidosis, hypokalaemia, dehydration and anaemia have also been proposed as potential progression factors of CKD in the domestic cat (Polzin, 2011).

1.1.4. Treatment

Conservative management is based on the treatment of active renal diseases as well as the reduction of clinical signs. Some treatments for CKD are based on weak evidence or anecdotic experiences while others are based on exhaustive evidence-base veterinary medicine. An attempt to evaluate the evidence available to treat CKD in cats has been proposed recently using a grading system from I to IV. Grades I and II represents clinical evidence with a high level of reliability, whereas grade III and IV indicates either weak or low degree of evidence, respectively (Roudebush *et al.*, 2009).

Indirect tubulointerstitial damage
-Extended pre-renal kidney injury -Post-renal kidney injury
Direct tubulointerstitial damage
-Renal kidney injury
a) Ischaemic
Severe decompensation after anaesthesia Severe haemorrhage Renal artery thromboembolism IRI due to Kidney transplantation (De Cock et al., 2004) Acute allograft rejection (De Cock et al., 2004)
b) Nephrotoxic
Endogenous Myoglobin Haemoglobin Hypercalcaemia *Exogenous* Heavy metals Ethylene glycol Aminoglycosides Melamine/cyanotic acids Chemotherapeutics (cisplatin and doxorubicin) Amphotericin B Ciclosporin Lilies
c) Infectious
Bacterial Pyelonephritis, sepsis *Viral* FIP and FLV
d) Congenital
Amyloidosis
Juvenile renal dysplasia
Polycystic kidney disease
e) Immunogenic
Systemic lupus erythematosus
f) Neoplastic
Renal lymphoma

Table 1.1: Potential causes of Tubulointerstitial Damage in the Cat

Modified and combined table from (Ross, 2011) (Dager, 2008). IRI, ischaemia reperfusion injury; FIP, feline infectious peritonitis; FLV, feline leukaemia virus.

Grade I: Evidence obtained from one or more properly designed randomized controlled clinical trials performed in clinical patients of the target species.

Grade II: Evidence obtained from properly designed, randomized controlled studies performed using animals of the target species with spontaneous disease in a laboratory or research animal colony setting.

Grade III: Evidence obtained from appropriately controlled studies without randomization, appropriately designed cohort or case control studies, studies using acceptable models of disease or simulations in the target species, cases series or dramatic results from uncontrolled studies.

Grade IV: Evidence obtained from studies conducted in other species, reports of expert committees, descriptive studies, case reports, pathophysiological justification, and opinions of recognized experts developed on the basis of their clinical experience (Roudebush *et al.*, 2009).

1.1.4.1. Medical treatment

Diet: Dietary therapy has been shown to prolong survival for companion animals with CKD stage 2 to stage 4. Renal diets facilitate the absorption of nutrients with a reduced production of metabolic products (urea and phosphorus) slowing or preventing high levels of systemic toxic metabolites and potentially death if CKD progresses. Diets for CKD are lower in protein, phosphorus and sodium content. Also CKD diets are supplemented with vitamin B, soluble fibre, high caloric density, omega-3, polyunsaturated fatty acids and antioxidants. Potassium supplementation is used more in cats than other species (Polzin, 2011). There is strong evidence (grade I) for the use of low protein diets in cats with stage 2 and stage 3 CKD. With regard to the reduction of progression of CKD cats in stage 4, there is weak evidence (grade III) to show the benefit of renal diets (Polzin, 2011; Roudebush *et al.*, 2009). There is strong evidence (grade I) to support the benefit of dietary restriction of phosphorus, although evidence supporting the target ranges of phosphataemia to bring a benefit to the cat with CKD is weak (grade IV) (Roudebush *et al.*, 2009).

Gastrointestinal Uraemia: Gastrointestinal signs of uraemia include reduction of food intake, nausea, vomiting, uraemic stomatitis, halitosis, haematemesis and

haematochezia. Treatment is symptomatic using histamine H2 receptor antagonist, antiemetics, mucosal protection such as sucralfate (Polzin, 2011).

Hyperphosphataemia promotes renal secondary hyperparathyroidism, mineralization of tissues and progression of CKD. High levels of phosphorus increase mortality in humans and companion animals. Phosphate binders are important treatment in cats from CKD stage 2 to stage 4. This therapy can be combined together with dietary restriction of phosphorus. One third of cats with CKD require treatment with phosphate binders. The main phosphate binders available for companion animals are sevelamer, chitosan, lanthanum, calcium and aluminium salts. Calcium and aluminium salts have been used in the dogs and cats effectively (Polzin, 2011), however they have been associated with secondary effects such as hypercalcaemia and toxic systemic accumulation, respectively. Sevelamer has also been used successfully in human patients with CKD. In dogs and cats, although sevelamer has been shown to reduce hyperphosphataemia, its effectiveness has not been tested in randomized studies. Chitosan phosphate binders have been tested in short and long term studies showing a positive reduction in the progression of CKD, attributable to an effective reduction in plasma phosphate and urea, even if renal diets are not being used. On the other hand, this product has been associated with the development of hypercalcaemia, as it contains 10% of calcium carbonate. With regard to lanthanum salts, several studies have shown the effectiveness of the product reducing plasma phosphate and urea; however, randomization studies are slightly bias according to some experts. Overall, lanthanum salts and chitosan are effective products even when patients are fed with regular food (Kidder *et al.*, 2009).

Metabolic acidosis occurs in approximately 10% cats with CKD stages 2-3 and around 50% in feline patients with uraemic syndrome, most of them in CKD stage 4 (Elliott *et al.*, 1998). Parenteral alkalinisation therapy is required when severe cases are detected. In low metabolic acidosis, dietary therapy may be sufficient (Polzin, 2011).

Hypokalaemia is seen in 20-30% of cats with CKD stages 2 - 3 and may be associated with polyuria, low potassium intake, and activation of renin-angiotensin-aldosterone system (Lulich *et al.*, 1992). Also, hypokalaemia may be associated with hypokalemic myopathy, progressive renal injury, increase in water intake and urine production. Potassium gluconate or citrate are adequate options for oral supplementation. However, there is weak (grade III) evidence for the implementation

of potassium to prevent hypertension and reduce progression of CKD (Roudebush *et al.*, 2009). Hyperkalaemia is more evident in cats in CKD stage 4 (Polzin, 2011).

Dehydration is a common sign of CKD and significantly evident in CKD stage IV feline patients (Elliott *et al.*, 1998). Dehydration reduces renal function and induces acute uraemia. In cats, the lack of access to water and frequent vomiting/diarrhoea, signs of CKD, increase the level of dehydration promoting progression of renal disease. Water *ad libitum*, parenteral or empirical subcutaneous administration of lactated Ringer's have been used for patients with uremic crisis (Polzin, 2011). However, there is very weak evidence (grade IV) supporting the long term benefit of subcutaneous fluid therapy in cats with CKD (Roudebush *et al.*, 2009).

Anaemia occurs in patients with CKD stages 3 and 4. Erythropoietin is a glycoprotein hormone which main function in producing erythrocytes (main oxygen transporter units). Renal erythropoietin is produced by cortical interstitial fibroblasts in close relationship with peritubular capillaries and epithelial cells. The main effect of erythropoietin is on red blood cells progenitors and precursors localized in bone marrow. It is regulated by hypoxia inducible factor 2α (HIF-2α) under hypoxic condition (Paliege *et al.*, 2010). The low cortical oxygenation due to lack of erythrocytes maintain a hypoxic environment that may influence the progression of CKD. If the kidney cortex is particularly affected in a cat with CKD, a decreased level of erythropoietin and therefore anaemia should be expected to occur. Iron production is disrupted in patients with CKD. Also uraemia itself inhibits primary cells in the bone marrow (Nurko, 2006). Chronic gastrointestinal haemorrhage secondary to uraemia can also contribute to anaemia. Exogenous synthetic erythropoietin such as darbepoetin alfa or human recombinant erythropoietin have been used to control anaemia and reduce the need of blood transfusions. However, antibodies to exogenous erythropoietin may form producing refractory anaemia and hypoplasia of the erythroid bone marrow (Cowgill *et al.*, 1998). There is grade III evidence to use human recombinant erythropoietin in cats with anaemia secondary to CKD. No proper studies have been perform to establish the safety and efficacy of darbepoetin (Roudebush *et al.*, 2009).

Calcitriol therapy: Kidneys convert 25-hydroxycholecalciferol to 1,25-dihydroxycholecalciferol, also known as calcitriol. Calcitriol and parathyroid hormone are considered the main calcium metabolism modulators. Kidneys with chronic disease have low levels of calcitriol and this promotes renal secondary

hyperparathyroidism. Parathyroid hormone can be as toxic as urea and treatment with exogenous calcitriol may reverse the effects of hyperparathyroidism in feline patients with CKD (Roudebush *et al.*, 2009). Nevertheless, recent grade II and III evidence was not able to support the use of calcitriol therapy in cats with CKD (Roudebush *et al.*, 2009).

Proteinuria has been reported as a progression factor in the cat with CKD (Syme *et al.*, 2006). In humans, there is substantial evidence showing that the reduction of proteinuria correlates with survival and progression of CKD (Methven *et al.*, 2010). Treatments with angiotensin-converting enzyme inhibitor (ACEI) have been implemented in cats with UPC's above 0.5 for stages 2 and 3 and 0.4 for stage 4 (Polzin, 2011). There is grade I evidence for the reduction of proteinuria and survival in cats with CKD; however, there is very weak evidence to support the use of ACEI's to slow the progression or to prolong the survival of cats with CKD (King *et al.*, 2006; Roudebush *et al.*, 2009; Syme *et al.*, 2006). Although important trends towards an increased survival and reduction in the progression of disease were noted when reduction of proteinuria was achieved. Another approach to reduce proteinuria is by blocking angiotensin II receptors. Telmisartan has shown similar efficiency regarding the reduction of proteinuria in cats with CKD (Sent *et al.*, 2013), as seen in humans (Mann *et al.*, 2008).

Hypertension is a complication of CKD. Treatment is normally based on the use of angiotensin converting enzyme inhibitors (ACEI), benazepril or enalapril. Benazepril has hepatic excretion; therefore, is preferred in small animals, however in cats, angiotensin converting enzyme inhibitors are not as effective as in dogs, due to the role of renin angiotensin aldosterone system (RAAS) (Jensen *et al.*, 1997). In cats, calcium channel blockers are more effective alternative, where amlodipine is the drug of choice for cats as it increases vascular tone instead of RAAS stimulation (Polzin, 2011). However, so far there is just moderate evidence grade III for the use of amlodipine to treat hypertension in cats (Roudebush *et al.*, 2009).

1.1.4.2. Renal replacement therapy

Dialysis: Peritoneal dialysis and haemodialysis, a diffusion extracorporeal blood purification technique, have been used to treat a variety of conditions including AKI, CKD with severe azotaemia, acute kidney disease superimposed on CKD, pre-treatment for kidney transplantation in patients with CKD, feline patients with disorder

of fluids balance (oliguric, anuric and non-oliguric) and acute intoxications (Cowgill, 2011). The survival percentage for dogs and cats subjected to haemodialysis was from 21-38% for 1 year survival (Eatroff *et al.*, 2011). Haemodialysis has also shown superiority when compared to peritoneal dialysis, with regard to secondary effects (Eatroff *et al.*, 2011). However, peritoneal dialysis is still a good alternative due to its low cost and the technical simplicity (Ross *et al.*, 2013). In general, both peritoneal and haemodialysis have shown a remarkable benefit translated to patient survival in AKI cases (Roudebush *et al.*, 2009).

Continual renal replacement therapy (CRRT) is a blood purification modality that uses diffusion, convection and, to some extent, adhesion in contrast to intermittent haemodialysis where diffusion is the main mechanism of action. The slow and gradual blood purification and removal of large molecules allows a better control of electrolytes and acid base balance when compared to IHD. The maintenance cost for the CRRT is importantly lower when contrasted with IHD. However, CRRT tends to be a longer and more intensive procedure to perform than IHD (Acierno, 2011). Currently, enteric dialysis based on pro-biotics which metabolize uremic toxins has been used in USA. Another form of enteric dialysis uses polymers that adsorb uremic toxins. However, randomized controlled clinical trials are needed to support the initial anecdotal evidence (Roudebush *et al.*, 2009).

Kidney Transplantation: Kidney transplantation in veterinary practise is a technically challenging surgical procedure currently undertaken in the USA and also performed in one centre in Australia. The technique is becoming more popular in the USA, however its future as a renal replacement technique, at present, is still unclear. Management of CKD in cats can be divided into two main areas, the medical and surgical approach. The medical approach states that feline CKD is a long term progression course, where stabilization can be achieved using medical treatment without the employment of kidney transplantation, a technique considered by some experts to be an excessive approach for a cat with a short life expectancy since, the majority of cats with CKD present at over 13 years of age and the average life span of cats is 15 years (Zoran *et al.*, 2011). Moreover, a recent retrospective study has shown that 81% and 37% of cats with CKD stage 2 and 3 respectively, died without showing CKD progression to stage 4 (Chakrabarti *et al.*, 2012), which may question the usefulness of transplantation over medical treatment. Kidney transplantation procedure requires adequate recipient, donor selection, client education, intense pre-operative and post-operative care (Bernsteen *et al.*, 2000). The complex post-

operative care and kidney donor source factors can easily break the animal welfare homeostasis. Complications such as hypertension, delayed graft function, acute/chronic rejections, chronic allograft nephropathy, neurologic abnormalities, neoplasia, diabetes, hypertension, graft thrombosis, hind limb ischaemia and infections can be encountered either during or after surgical procedure. In 2008, the University of Wisconsin, reported that the survival percentage for cats with renal transplant was 59% and 42% at 6 months and at 3 years post-transplant, respectively (Schmiedt *et al.*, 2008). Currently, in the same University, the survival percentage with 6-month survival after renal transplantation is around 80% and 3-year survival is around 65%. In the long term, most cats die of diseases other than renal disease. The survival percentage is expected to improve with advances in surgical techniques and immunosuppressive drugs. However, as yet, there is not significant evidence for the benefit of kidney transplantation over conservative medical treatment (Roudebush *et al.*, 2009).

1.2. Comparative Medicine

A more novel and less common approach to study CKD in humans is based on the investigation of "naturally occurring CKD" in domestic or wild animals. This area of research comes under the general heading of comparative medicine, a discipline that compares similarities and differences between man and animals to enhance the understanding of disease processes (Bradley, 1927). The concept behind comparative medicine was initiated in the 18th century by Dr Giovanni Maria Lancisi, a physician who established a model to control Rinderpest in cattle, a lethal virus guilty of three pandemic hits and responsible of a major shortage in animal-based food, especially in Europe. The first veterinary school to be established in the world had its origins in Lyon (France) with the purpose of applying Lancisi's principles to the control of animal disease (Palmarini, 2007). Later, in the 19th century, the interdependence of animal and human health was emphasised by the German physician, Rudolf Virchow and the Canadian physician, William Osler (Virchow's pupil), both men labelled as 'the fathers of modern pathology and modern medicine' (Kahn *et al.*, 2007). Rudolf Virchow coined the term "zoonosis", to highlight the relevance of linking human with animal medicine; identifying in this way that progress in both areas are dependent on mutual scientific advances and technological discoveries. The quote from Virchow that:-

"Between *animal and human medicine there is no dividing line — nor should there be. The object is different, but the experience obtained constitutes the basis of all medicine"*,

still prevails today and is the fundamental principle of comparative medical research (Klauder, 1958). In the 1980s Calving Schwabe, strongly influenced by Virchow's philosophy, coined the term **"one medicine",** to establish the links between human and animal disease while the term **"one health"** is the evolution of one medicine, which takes into account the role played by the balance of ecosystems in the health of both man and animals (Zinsstag *et al.*, 2011).

1.2.1. Naturally Occurring Animal Diseases

Naturally occurring animal diseases (NOAD) in domestic animals are diseases generated with silent, acute or chronic clinical presentation as a result of a wide range of genetic and environmental factors / variables. These factors may be similar or identical to those responsible for human disease. Environmental factors can contribute to the development of illnesses by altering the onset, presentation, time course, diagnosis, control, prevention of diseases, as well as the outcome of treatments. Diet, habitat and habits (smoker owner with passive smoker pets) are some factors that cannot be fully replicated in the laboratory, as probably more than one variable is interconnected to generate a disease. Also, the wide genetic pool (heterogeneity) in both human and animal population is a major factor for disease generation that cannot be fully mimicked using laboratory animals. Diseases in animals and humans are the product of both environmental and genetic factors individually and interacting between the two (Hunter, 2005).

The domestic cat, dog, horse, cow, pig and sheep are species where naturally occurring diseases may offer a mutual value to both human and veterinary medicine (Wolfe, 2009), based on the histopathology, clinical presentation and/or genetic profile of disease similarities, see tables 1.2, 1.3 and 1.4. Furthermore, the recent mapping of the dog and cat genomes has allowed the identification of more than 250 genetic diseases, homologous to human disorders (Menotti-Raymond *et al.*, 2008; Pontius *et al.*, 2007). An important increase in the use of naturally occurring diseases in dogs and cats should be noticed in the following years due to the efforts of completing and refining the cat's and dog's genome.

The comparative study of gene-environment interactions for the development of diseases between animals and humans using *sequenced* animal *genomes*, may allow the following points:-

- A better understanding of the genetic and environmental risks factors and their interactions according to a suspected population predisposition (Hunter, 2005).
- Identification of the associations between environmental factors and diseases in animals with a genetic predisposition to develop a disease (Hunter, 2005).
- Analysis of disease mechanism by using information on susceptibility/resistance genes to determine the most suitable biological pathways in the disease and the environmental variables that are more important to the pathways in question (Hunter, 2005).
- Identification of factors that trigger or prevent diseases to occur in both animals and humans, as the study of the differences between species may help to identify new approaches of disease study and treatments.
- Drug safety with a more comparable lifespan to that in humans allowing a long term assessment of drugs to evaluate side effects.
- Generation of evidence-based veterinary medicine.

The study of human diseases based on comparative genetics has a wide range of approaches to enhance the understanding of disease. Some possible study designs are; the development of prospective studies, prospective interventional studies (potentially reducing the use of laboratory animals), prospective studies of genetic predisposition and prospective/retrospective basic epidemiological studies. However, at the moment, study designs of diseases in domestic animals are achievable only in species where the mapping of the genome has been completed or it has reached an advance degree of identification, such as in the domestic feline and canine.

Medical field	Animal aetiology or disease	Human disease	Reference
Horse			
Orthopedics	Osteoarthritis	Osteoarthritis	(Frisbie et al., 2000)
Oncology	Melanoma	Melanoma	(Seltenhammer et al., 2004)
Bovine			
Chemical Pathology - Metabolic Medicine	Citrillinemia	Citrillinemia	(Harper et al., 1989)
Parasitology	Onchocerciasis	River blind disease by onchocerciasis	(Gilbert et al., 2005)
Sheep			
Chemical Pathology - Metabolic Medicine	Krabbe disease	Krabbe disease	(Pritchard et al., 1980)
Ferret			
Nephrology	Ferret cystic renal disease	Cystic renal disease	(Jackson et al., 2008)

Table 1.2: Naturally occurring disease in domestic species

Medical field	Animal aetiology or condition	Human disease	Reference
Neurology	Myasthenia gravis	Myasthenia gravis	(Galin *et al.*, 2007)
	Canine muscular dystrophy	Duchenne muscular dystrophy	(Sharp *et al.*, 1992; Wang *et al.*, 2009)
	Narcolepsy	Narcolepsy	(Lin *et al.*, 1999)
	Canine neuronal ceroid lipofuscinosis	Human infantile and juvenile neuronal ceroid lipofuscinosis	(Lingaas *et al.*, 1998)
	Myotonia congenital	Myotonia congenita	(Rhodes *et al.*, 1999)
	B-amyloid accumulation in canine brain	Alzheimer	(Cummings *et al.*, 1993)
Ophthalmology	Canine retina degeneration	Human retinal degeneration	(Acland *et al.*, 1999)
	Progressive rod-cone degeneration	Retinitis pigmentosa	(Acland *et al.*, 1998)
	Cone degeneration	Achromatopsia	(Sidjanin *et al.*, 2002)
	Collie eye anomaly	Choroidal hypoplasia	(Lowe *et al.*, 2003)
	Human congenital stationary night blindness	Human congenital stationary night blindness	(Aguirre *et al.*, 1998)
	Canine hereditary retinal dystrophies	Human hereditary retinal dystrophies	(Veske *et al.*, 1999)
Rheumatology	Rheumatoid arthritis	Rheumatoid arthritis	(Ollier *et al.*, 2001)
Dermatology	Digital footpad hyperkeratosis	Inherited keratodermas	(Keller *et al.*, 1998)
Hepathology	Cooper toxicosis	Cooper deficiency (Menkes disease) and accumulation (Wilson disease)	(van De Sluis *et al.*, 2002)
Urology	Canine cystinuria	Human cystinuria	(Henthorn *et al.*, 2000)
Nephrology	Canine x-linked hereditary nephritis	Human x-linked hereditary nephritis	(Zheng *et al.*, 1994)
	Membranoproliferative glomerulonephritis / hereditary canine C3 deficiency	Membranoproliferative glomerulonephritis / hereditary human C3 deficiency	(Ameratunga *et al.*, 1998)
	Samoyed hereditary glomerulopathy and Bull terrier hereditary nephritis	Alport disease	(Hood *et al.*, 2000; Jansen *et al.*, 1986)
	Renal amyloidosis / recurrent fever of unknown origin	Mediterranean fever	(Rivas *et al.*, 1993)
	Polycystic kidney disease	Polycystic kidney disease	(Gharahkhani *et al.*, 2011)
	Renal dysplasia	Renal dysplasia	(Hoppe *et al.*, 1990)
	Renal cystadenocarcinoma and nodular dermatofibrosis (RCND)	Renal cancer syndrome Birt-Hogg-Dube	(Jonasdottir *et al.*, 2000; Lingaas *et al.*, 2003)
	Fanconi syndrome	Fanconi syndrome	(Bovee *et al.*, 1978)
	Membrano proliferative glomerulonephritis	Membrano proliferative glomerulonephritis	(Minkus *et al.*, 1994a)

Table 1.3: Naturally occurring diseases in the Domestic Canine

Medical field	Animal aetiology or disease		Human disease	Reference
Immunology	Feline immunodeficiency disease		AIDS by HIV	(Willett *et al.*, 1997)
	Feline leukaemia virus		AIDS by HIV	(Mullins *et al.*, 1989)
Oncology	Feline leukaemia virus		Oncogenesis	(Hardy *et al.*, 1976)
	Feline mammary carcinoma		Mammary carcinoma	(Vail *et al.*, 2000)
	Soft tissue sarcoma		Soft tissue sarcoma	(Spugnini *et al.*, 2007)
	Non-Hodgkin's lymphoma		Non-Hodgking's lymphoma	(Vail *et al.*, 2000)
Gastroenterology	*Helicobacter pilori*		*Helicobacter pilori* - Zoonotic risk	(Fox *et al.*, 1996)
Pneumology	Coronavirus (H5N1)		H5N1 - Zoonotic risk and epidemiology	(Kuiken *et al.*, 2004)
	Coronavirus		Severe acute respiratory syndrome	(O'Brien *et al.*, 2006)
Haematology	Feline leukaemia virus		Aplastic anaemia	(Cotter *et al.*, 1977)
Cardiology	Hypertrophic Cardiomyopathy		Hypertrophic Cardiomyopathy	(Fox *et al.*, 1995)
	Arrhythmogenic ventricular cardiomyopathy		Arrhythmogenic ventricular cardiomyopathy	(Fox *et al.*, 2000)
Chemical Pathology - Metabolic Medicine	Lysosomal storage disorders	β-glucuronidase deficiency	Mucopolysaccharidosis type VII	(Fyfe *et al.*, 1999)
		Mucopolysaccharidosis type VI	Mucopolysaccharidosis type VI	(Haskins *et al.*, 1981)
		alpha-mannosidosis	Alpha-mannosidosis	(Vite *et al.*, 2001)
		Globoid cell leukodystrophy	Krabbe disease	(Johnson, 1970; Sigurdson *et al.*, 2002)
		Mucopolysaccharidosis type I	Mucopolysaccharidosis type I	(He *et al.*, 1999)
		Feline Niemann Pick disease type C	Niemann-Pick disease type C	(Brown *et al.*, 1994)
		GM2-Gangliosidosis	Sandhoff disease	(Baek *et al.*, 2009)
	Endocrine	Diabetes mellitus type II	Diabetes mellitus type II	(Henson *et al.*, 2006)
Urology	Feline interstitial cistitis		Interstitial cistitis	(Lavelle *et al.*, 2000)
Nephrology	Polycystic kidney disease		Polycystic kidney disease	(Lyons *et al.*, 2004)
	Renal Amyloidosis		Renal Amyloidosis	(DiBartola *et al.*, 1986)

Table 1.4: Naturally occurring diseases in the Domestic Feline

Hypertrophic cardiomyopathy (HCM) in cats has been used to investigate human HCM (Fox *et al.*, 1995), while recently, the cat has been appointed as a model to study diabetes mellitus type II and obesity in humans (Henson *et al.*, 2006). In nephrology, the domestic cat has been proposed as a model to study of polycystic kidney disease (Lyons *et al.*, 2004) and renal amyloidosis (DiBartola *et al.*, 1986).

1.3. Animal Models of Chronic Kidney Disease

To study any disease, the most frequent experimental approaches are based on *in vitro* and animal experimentation. This allows the isolation of variables to investigate the pathology and pathogenesis of diseases in a specific experimental context. Animal models play a fundamental role to evaluate the efficacy and side effects of potential treatments under a complex physiological system. The use of laboratory animals is widely accepted by the scientific community and more recently includes the ability to knock out or over express genes, particularly in mice, allowing a narrower delimitation to study certain molecular pathways (Anders *et al.*, 2000). *In vitro* models using cells can be very useful approach to evaluate isolated molecular pathways, however, using cell models does not allow the evaluation of renal function or renal tissue protein dynamics under a complex biological system.

To generate a model of CKD in experimental animals, two main requirements have to be fulfilled; the generation of an effective acute insult (inflammatory process) and the chronic development of renal fibrosis (reparation process), following an acute renal injury. In this research project, ischaemia renal perfusion injury (IRI) was the renal insult chosen to study the role of the cross-linking enzyme transglutaminase in the progression of CKD. The criteria used to choose the rat model of RWI were:-

1. Acute and chronic hypoxic stress based model as an insult to develop CKD.

Tubulointerstitial hypoxia plays a pivotal role in renal fibrosis, it is a final step in ESRD in a variety of kidney diseases and mediates progression of renal injury in early and chronic kidney disease (Mimura *et al.*, 2010). Peritubular capillary damage, tubulointerstitial fibrosis and inflammatory cellular infiltration in the extracellular matrix are histopathological issues found in CKD independently of the cause. Peritubular capillary rarefaction mediates hypoxia, tubular damage and tubulointerstitial fibrosis (Kawakami *et al.*, 2014). RWI in the rat is able to develop peritubular capillary

rarefaction in chronic models of renal fibrosis (Basile, 2007; Basile, 2004; Basile *et al.*, 2001a). Therefore, this model may mimic the aetiology for the development of CKD in the cat and in the human.

2. Quantification of acute and chronic renal injury by assessment of renal function without development of proteinuria.

In the cat, proteinuria is not a prominent feature of renal damage, this is probably due to the low development of glomerulosclerosis in cats with CKD (Vaden, 2011). The model of RWI allows development of tubulointerstitial fibrosis without proteinuria. Proteinuria seems to be more evident after 16 weeks of RWI (Basile *et al.*, 2001a; Basile *et al.*, 2003; Torras *et al.*, 1999). This model provides a window from 28 days to 16 weeks where the development of tubulointerstitial fibrosis is evident without relevant amounts of proteinuria, as occurs in the cat with CKD.

3. Quantifiable development of tubulointerstitial fibrosis in the absence of glomerulosclerosis.

Tubulointerstitial fibrosis correlates with the reduction of renal function more than glomerular fibrosis in humans (Risdon *et al.*, 1968), experimentally in rodents and in the cat with CKD (Chakrabarti *et al.*, 2013). This feature, allows this model to be used for feline and human CKD studies. A measurable level of fibrosis, together with a reduction of renal function is vital to assess the association with the transglutaminase pathway.

4. Easy to replicate in a short period of time, with low mortality in long term, providing enough kidney tissue to perform kidney homogenates

The rodent model of RWI provides enough renal tissue for experimental techniques. Importantly, the low rat mortality after acute injury surviving long term, provides adequate numbers in experimental groups, important for chronic experiments when expensive drugs are employed for interventional studies.

The model of IRI in the rat generates tubulointerstitial fibrosis which is the core histopathological damage in humans and in the cat with CKD. The time dependent development of glomerulosclerosis in this model is highly relevant for the study of CKD in the cat and important to understand glomerulosclerosis in the human. The

histological similarities and differences in this models may bring a better understanding the disease for both the domestic feline and the man.

IRI induces a substantial reduction in intracellular adenosine triphosphate (ATP), promoting a number of metabolic consequences in tubular cells such as acute tubular necrosis (Devarajan, 2005). IRI has three consecutive phases; renal warm ischaemia, reperfusion and tissue damage. Tissue damage can be evident in the first two phases; however, major renal injury is reached during and after the reperfusion phase. The ischaemic event is caused by stopping or significantly reducing blood perfusion to the kidney by placing a microvascular clamp in the right renal hilus (renal artery and vein) for one hour. Reperfusion occurs when the clamp is removed causing a sudden restoration of oxygenated blood flow into the kidney (Collard *et al.*, 2001; Maxwell *et al.*, 1997), activating and increasing catalytic enzymatic activity promoting oxidative stress and cellular damage (Carden *et al.*, 2000). In general, the acute and chronic stage of IRI are triggered and continued by tissue hypoxia and inflammation secondary to the damage to the tubuloepithelial cells and the peritubular / glomerular capillary networking.

It is important to mention that apart from renal IRI, there are other common animal models employed to generate tubulointerstitial fibrosis, these include renal mass reduction (5/6th subtotal nephrectomy) (Johnson *et al.*, 2007) and diabetic nephropathy rat models. Unilateral ureteral obstruction (UUO) (Kim *et al.,* 2010; Shweke *et al.*, 2008) and models of nephrotoxicity (Debelle *et al.*, 2002) are also popular murine fibrogenic models. Even though hypoxia is an event encountered in all these models, glomerulosclerosis is a short term outcome in most of them, which may not be relevant to study CKD in the cat. UUO model does allow urine/plasma assessment for renal function, as urine is not coming from the damaged kidney and plasma renal analytes are the reflex of both the intact and the injured kidney; leaving histopathology as the only method to determine glomerular and tubular impairment.

1.3.1. Renal Ischaemia Reperfusion Injury

Renal warm ischaemia (RWI) is defined as the organ deprivation of blood flow, decreasing the tissue oxygen concentration. It is considered to be the prelude to major renal damage. When blood flow and oxygen concentration are re-established; the last event, is also called renal reperfusion injury. The kidney receives approximately 25% of the cardiac output, being the most well perfused organ in the

body in relation to its size (Brezis *et al.*, 1995). Once the renal arterial blood gets into the kidney, the cortex is the first renal zone to be oxygenated (30-50mmHg). On the other hand, the medulla has a low oxygen tension profile (15-20mmHg); this is due to the fact that the medulla has a high rate of oxygen exchange and therefore higher levels of carbon dioxide to preserve osmotic gradient, and urinary concentration (Brezis *et al.*, 1995; Nangaku *et al.*, 2007a). The most susceptible areas for ischaemia are the S3 segment of the proximal tubule (cortex close to the outer medulla) and the ascending limb of the loop of Henle in the outer medulla (Brezis *et al.*, 1995; Nangaku *et al.*, 2007a; Nielsen *et al.*, 1999); probably associated with either Na/K-ATPase or K^+ channel activity and sensitivity to ATP levels in the proximal tubules (Tsuchiya *et al.*, 1992). The effect of a 60 minute period of renal warm ischaemia on the surface colouration of the kidney following the release of a renal hilus clamp is shown for the anaesthetised rat in Figure 1.3.

1.3.1.1. Histopathology

The acute stage of IRI can be assessed by histopathology and is useful in establishing the level of damage and renal prognosis. Some histopathological features include the loss of apical brush border and basolateral interdigitations (Bonventre, 1993). After 5 minutes of renal ischaemia, the lipid composition of the membrane changes significantly (Jones, 1982; Jones, 1981). On the other hand, with more advanced damage, intracellular vacuoles and mitochondrial swell, as well as shrinking of nucleus and chromatin condensation (pyknosis), can be detected. Furthermore, an apparent tubular dilatation may be observed over the basement membrane due to the gaps produced by the cell separation from its base (Bonventre, 1993; Meadows, 1973). Also, histopathology detects cellular debris, intratubular proteins and even histopathological features suggesting oedema (Bonventre, 1993).

1.3.1.2. Hypoxia

There is evidence showing that an ischaemic process during AKI, in whichever modality (pre-renal, intrinsic and post-renal), triggers a cascade of inflammatory factors that overlaps the healing stage, promoting a substitution of functional parenchyma by fibrotic tissue (Dager, 2008; Rosenberger *et al.*, 2006). AKI is associated with aberrant intra-renal microcirculation and therefore oxygen misbalances. Low tensions of oxygen in the renal cortex promotes up-regulation of

hypoxia-inducible factor (HIF) in all types of AKI (Rosenberger *et al.*, 2006), which has been associated with the development of renal fibrosis (Higgins *et al.*, 2008).

There are three different forms of AKI. Pre-renal, renal and post renal AKI. Ischaemia in pre-renal and intrinsic AKI are the most common forms of AKI generated by renal hypoperfusion, however post-renal AKI has also a hypoxaemic component.

Pre-renal AKI: results from hypotension and/or hypovolemia leading to hypoxia with conserved renal microstructure when compensated on time (Dager, 2008). Hypovolemia leading to a severe fall in systemic blood pressure promotes vasoconstriction in different systems, including the renal system, preserving the basic immediate vital ones (cardiac output and cerebral perfusion) (Badr *et al.*, 1988).

Intrinsic AKI: Is associated to frank reduction in renal oxygen producing a direct effect in the vascular, glomerular and tubular or /and interstitial compartment (Dager, 2008).

Post-renal AKI. Post-renal AKI results from the increase of intrapelvic pressure leading to ischaemic atrophy, which can be reversible when intrapelvic blockage is corrected (Wen *et al.*, 1999). The most representative animal model to evaluate post-renal AKI is the unilateral ureteral obstruction (UUO)(Chevalier *et al.*, 2010). UUO produces tubuloepithelial apoptosis and necrosis due to hypoxia and oxidant injury as seen in intrinsic renal AKI (Thornhill *et al.*, 2007). Post-renal AKI secondary to UUO produces hypoxia with cellular proliferation, tubular basement membrane thickening and necrosis in proximal tubules, as seen in renal ischaemia reperfusion injury (Cachat *et al.*, 2003).

1.3.1.3. Molecular Pathophysiology of Ischaemia

Ischaemia promotes a decrease in cellular oxidative phosphorylation resulting in a deficit of ATP re-synthesis and phosphocreatine; this event is described as Krebs cycle paralysis. At this point, cellular metabolism follows the anaerobic pathway to obtain enough energy for cell survival. These pathways are mainly glycolysis and glycogenolysis and provide around 5% ATP production in contrast to the aerobic ATP synthesis (de Groot *et al.*, 2007).

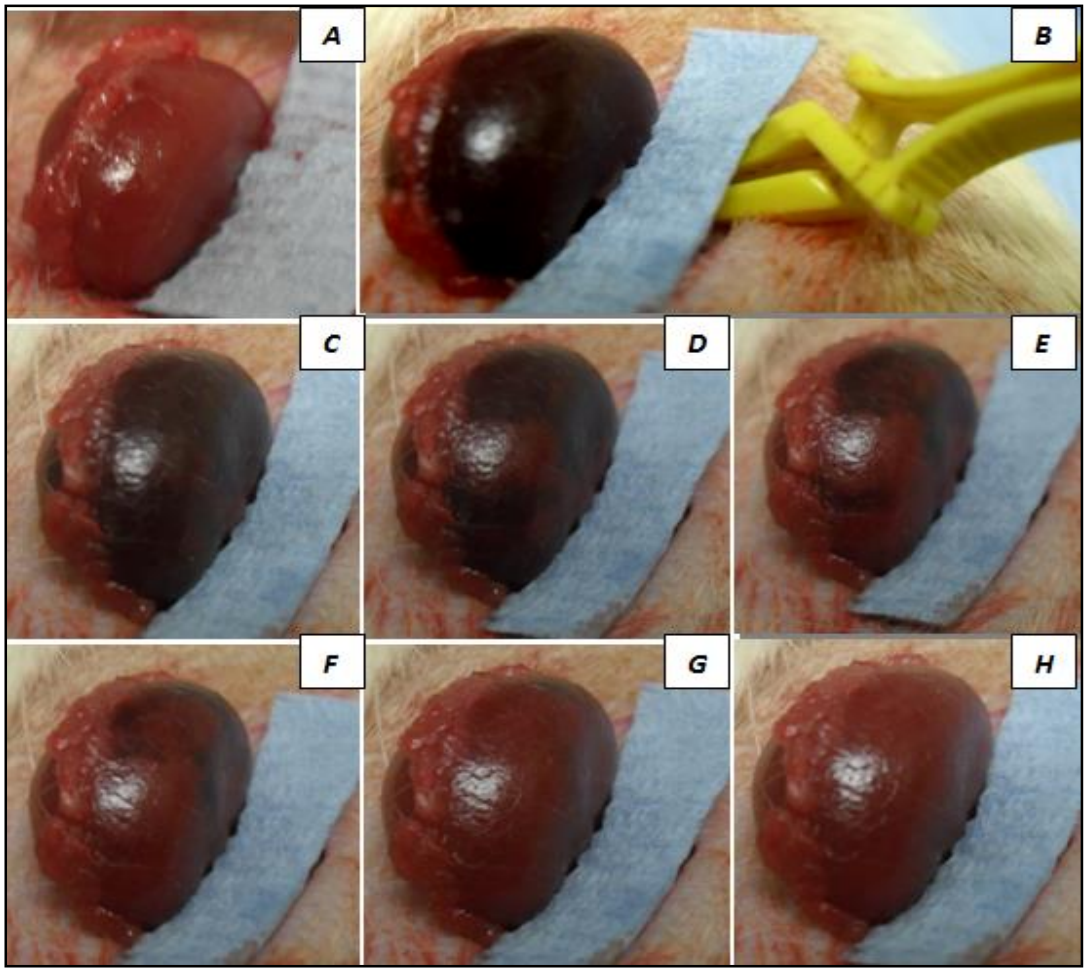

Figure 1.3: Effect of Renal Warm Ischaemia on the renal surface colouration

Sequence of renal surface colour from a Sprague Dawley rat before, during and after left renal hilar clamping. **A**: Normal colour; **B**: Colour of clamped kidney after 60 minutes. **C-H**: Colour after removing the clamp forceps for **C** = 5 seconds, **D** = 10 seconds, **E** = 15 seconds, **F** = 20 seconds of removing clamp; **G**: Colour after 30 seconds of removing clamp and **H**: Colour after 1 minute of removing.

Apart from generating high levels of lactic acid, increasing intracellular and extracellular pH with a later disturbance in liposome stability, ischaemic events also provoke an inadequate functioning of the transmembrane ionic pumps. The ionic disequilibrium is mainly due to the increase in the intracellular concentration of Ca^{+} and Na^{+}, dragging water into cells with the subsequent cellular swelling (Flores *et al.*, 1972). In an adequate cellular environment, ATP is normally hydrolysed by nucleoside triphosphate diphosphohydrolases (NTPDases) to ADP-AMP-adenine; and adenine is deaminated to inosine-hypoxanthine-xanthine-uric acid, see Figure 1.4. The enzyme responsible for the oxidation of hypoxanthine to xanthine is xanthine dehydrogenase. Interestingly, when there is a lack of oxygen, the enzyme is converted by Ca activated proteases to xanthine oxidase. Xanthine oxidase is an oxygen-dependent enzyme that is not able to degrade hypoxanthine to xanthine. A continuous increase of hypoxanthine is therefore unavoidable; see Figure 1.5 (Maxwell *et al.*, 1997). This catabolic product does not produce damage by itself. Hypoxanthine requires re-oxygenation to induce cellular disturbances.

1.3.1.4 Reperfusion

The pathophysiology of reperfusion can be explained through three main components; the role of reactive oxygen species (ROS), complement and leukocytes.

Reactive Oxygen Species (ROS): When reperfusion occurs, xanthine oxidase starts degrading the accumulated hypoxanthine to xanthine. In this process, high levels of reactive oxygen species such as superoxide and hydrogen peroxide are produced; however, hydroxyl radical and nitric oxide are also important products to take into account in this process, see Figure 1.6 (Maxwell *et al.*, 1997).

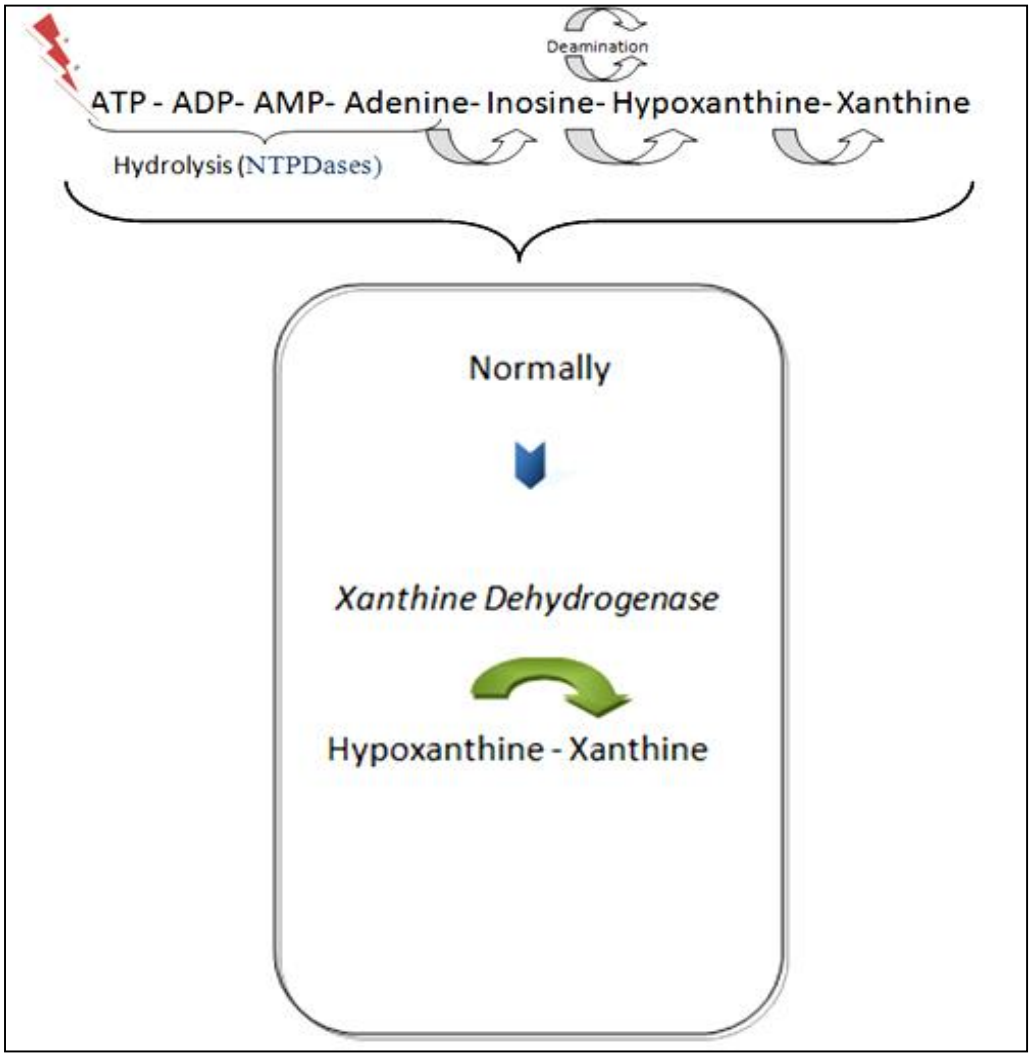

Figure 1.4: Xanthine dehydrogenase in the healthy kidney

The degradation of hypoxanthine to xanthine is performed by xanthine dehydrogenase in a normal cellular environment.

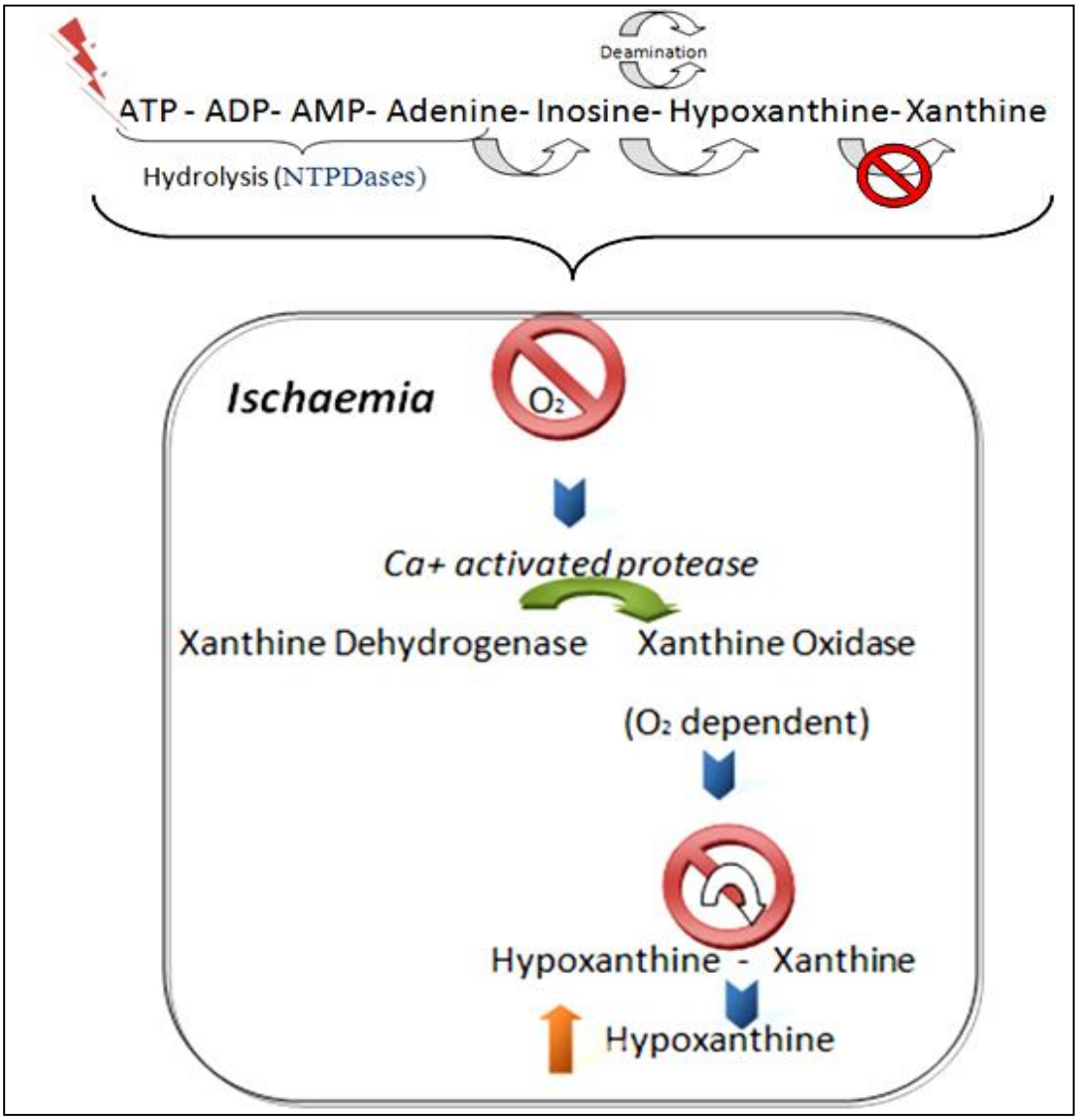

Figure 1.5: Renal ischaemia and the role of xanthine dehydrogenase

Due to a decrease in oxygen xanthine dehydrogenase is converted to xanthine oxidase, an oxygen-dependent enzyme to catalyse hypoxanthine to xanthine; therefore, an increase in hypoxanthine unavoidable

Eventually, ROS disrupts cells by damaging DNA, inducing apoptosis and oxidizing polydesaturated fatty acids and amino acids (Martin *et al.*, 2002). Interestingly, even though xanthine oxidase is a key enzyme in the development of ROS, its inhibition through allopurinol in acute renal ischaemia and kidney transplantation has not always been translated into improvements in renal integrity (Paller *et al.*, 1984).

Complement: IRI also interferes with the innate immune system. The complement system plays an important role in reperfusion by altering vascular permeability and integrity through the overexpression of adhesive endothelial molecules such as β2 integrin, E-selectin and P-selectin, promoting leukocyte adhesion. Moreover, complement is involved in the stimulation of the lipoxygenase pathway. The main anaphylatoxins responsible of such an event are C3a, iC3b, C5a and C5b-9. C5a has been the most widely studied in IRI (Collard *et al.*, 1999).

Leukocytes: The white cells are aggregated in vascular endothelium by the interaction of integrins, selectins and the endothelial intracellular adhesion molecules 1 (ICAM-1). The transmigration of leukocytes by diapedesis is augmented by platelet endothelial cell adhesion molecule 1 (Panes *et al.*, 1999). Mesangial/tubular cell death and development of thrombosis after IRI are promoted by leukocyte products released (ROS, elastases and proteases) in the oedematous interstitial space. In an IRI model of rat, the inhibition of P-selectin receptors by a soluble P-selectin ligand showed a significant decrease in the inflammatory response when compared to the diseased group without treatment (Takada *et al.*, 1997).

1.3.1.4 Companion Animals

The study of IRI in animal models has been widely used to understand the phenomena related to kidney transplantation, including delayed graft function, chronic allograft nephropathy and the effect of immunosuppressive drugs on the transplanted kidney (Ahmed *et al.*, 2004).

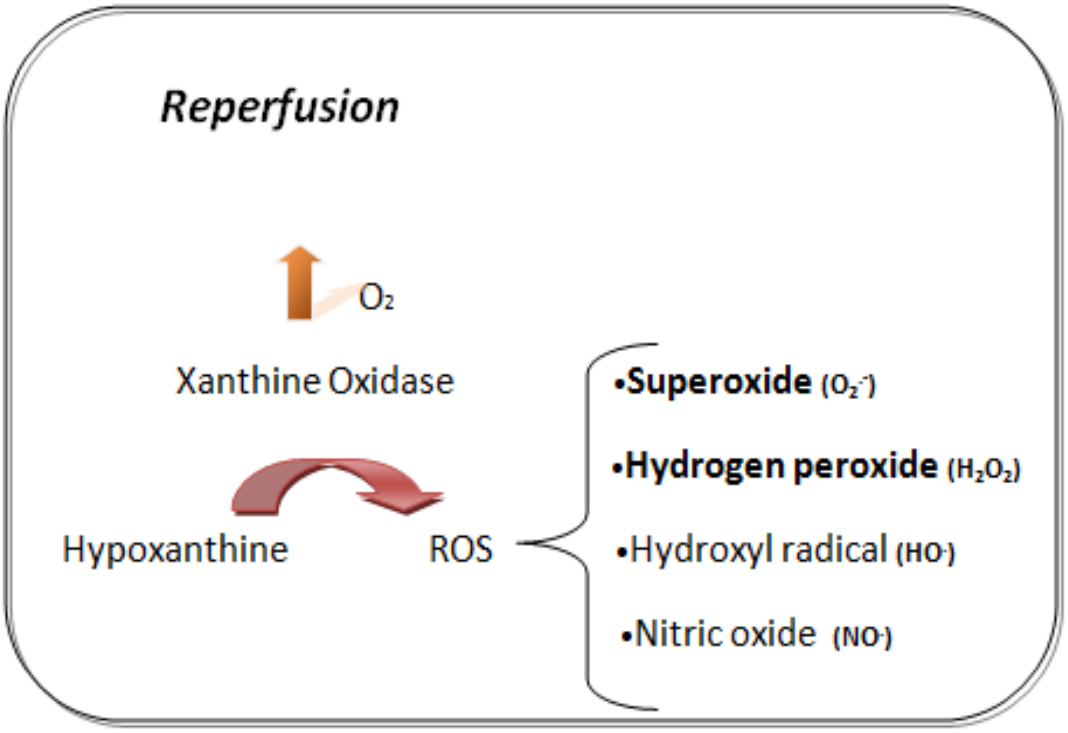

Figure 1.6: Summary of events during reperfusion and final cellular products

The sudden flow of oxygenated blood through the ischaemic kidney produces an increase in the xanthine oxidase activity with the subsequent formation of reactive oxygen species (ROS).

The model of ischaemia reperfusion injury using renal isografts in the rat allows the isolation of IRI from immunological alloantigenic factors and immunosuppressive drugs (Kusaka *et al.*, 2000). Similar phenomena can be isolated and studied in animal models of renal auto-transplantation. The animal model of IRI can also help to understand the development of chronic kidney disease since both the initial renal damage and the progression to CKD are closely related to hypoxic cellular events (Basile, 2007). In both CKD and CAN, the main final histopathological feature is tubulointerstitial fibrosis, responsible for disease progression.

In cats and dogs, a 60-minute period of RWI can produce sufficient damage to generate important functional and histological injury following 3 days of reperfusion (Jiang *et al.*, 2010; Kitada *et al.*, 2002; Schmiedt *et al.*, 2011). Similar acute phenomena have been shown in feline renal isografts (Bernsteen *et al.*, 1999) and in renal autograft models of cat (Mehl *et al.*, 2006) and dog (Dempster *et al.*, 1953). One kidney graft out of five developed generalized diffused interstitial fibrosis after 21 days (Mehl *et al.*, 2006). The studies above show the high degree of sensitivity in the acute response to IRI in both species. In the cat, IRI may be a potential complication for the development of renal fibrosis, suggesting that hypoxia may be an important factor for the development of CKD.

1.4 Chronic Kidney Disease (CKD)

1.4.1 CKD in Humans

In man, chronic kidney disease may be defined as the sustained and irreversible decrease in renal function with a disease progression of ≥ 3 months, irrespective of cause. CKD is the most common disease affecting kidneys. CKD is defined as a GFR <60ml/min per 1.73 m^2 or albumin-to-creatinine ratio > 30mg/g, the main parameters for CKD staging (Levey *et al.*, 2010).

Epidemiology: According to a recent national hospital survey in USA, 17% of people between 60-69 years of age presented moderate CKD (Coresh *et al.*, 2007). Cardiovascular disease is the most common cause of death in patients with CKD (Keith *et al.*, 2004; Tonelli *et al.*, 2006). In the UK, amongst the potential aetiologies of CKD, diabetes heads the list followed by glomerulonephritis (independent of aetiology) with hypertension in third place (Farrington *et al.*, 2009). Major medical risk

factors associated with CKD, in patients over 65 years of age, include hypertension, dyslipidemia, chronic lung disease, coronary heart disease, diabetes mellitus, stroke or transient ischemic attack and peripheral arterial disease (Go *et al.*, 2004). CKD aetiology can be divided according to susceptibility, initiation and predisposition factors.

Susceptibility and initiation factors: Familial predisposition, race, low birth weight, infant malnutrition, male and elderly people have been described as susceptibility factors whereas hypertension, diabetes, hyperlipidaemia, obesity, and smoking as initiation factors.

Progression factors: Familial diseases, race, age, and gender are defined as non-controllable factors; metabolic controllable factors are diabetes, obesity, hyperlipidemia, hyperuricemia and the subsequent systemic hypertension, cardiovascular and renal disease. Other progression factors include smoking, daily drinking of alcohol and frequent non-steroidal anti-inflammatories (Meguid El Nahas *et al.*, 2005).

Staging: CKD is divided into five stages, mainly in relation to the eGFR. Stage 1 (>90ml/min/1.73m^2); stage 2 (60-89 ml/min/1.73m^2); stage 3 (30-59 ml/min/1.73m^2); stage 4 (15-29 ml/min/1.73m^2) and stage 5 (<15ml/min/1.73m^2). Staging based on the albumin/creatinine ratio may be divided into stage A1 optimal (<10mg/g); stage A1, high normal (10-29mg/g); stage B, high (30-299 mg/g) and stage C, very high (>300mg/g) (Levey *et al.*, 2010).

General Management: The management of CKD has two approaches, life style modification (diet, exercise and weight reduction) and drug therapy. The aims for pharmacological intervention can be divided in early and late stages of CKD. In early stages of CKD, the main aims are: decreasing blood pressure, decreasing proteinuria and controlling hyperglycaemia (diabetic patients) and serum cholesterol. For the later stages of CKD, a broader range of treatments are available to cover other complications including hyperparathyroidism, anaemia, heart disease, malnutrition, hypovitaminosis A, hyperphosphataemia and iron deficiency (Meguid El Nahas *et al.*, 2005).

Replacement: Once the patient has been diagnosed with CKD stage 5, also known as end stage renal failure (ESRF), the only effective treatment is renal

replacement therapy. The aims of renal replacement are to remove cellular catabolic products and to maintain an adequate water/electrolytes balance, achieved by either dialysis or kidney transplantation. According to two global overview studies in patients with ESRF, around 23% of ESRF patients undertook kidney transplantation while the remaining 77% used dialysis (69% haemodialysis and 8% peritoneal dialysis) (Grassmann *et al.*, 2005; Moeller *et al.*, 2002). Peritoneal dialysis provides only approximately 10% of the normal renal excretory function (Sehgal, 2002) and has some important complications such as amyloidosis, diabetes mellitus, peritonitis, mineral and vitamin deficiencies. Haemodialysis, on the other hand, can trigger complications such as mineral imbalances, hypotension, fever, clot alteration, haemolysis and arrhythmias (Chadha *et al.*, 2010; Shroff *et al.*, 2009).

Chronic Allograft Nephropathy: Chronic Allograft Nephropathy (CAN) is defined as the decrease in renal function in the presence of tubulointerstitial fibrosis and tubular atrophy within the transplanted kidney. In a retrospective study, CAN showed a significant impact in more than one-fourth of patients subjected to kidney transplantation (Cecka, 2000). CAN risk factors are divided in two main areas; alloantigen independent and dependent factors. Regarding alloantigen independent factors, ischaemia reperfusion injury heads the list, followed by donor age, aetiology of renal failure and kidney size mismatch (Fellstrom, 2003; Paul, 1999). Concerning alloantigen dependent factors, these are related to human leukocyte mismatch and commonly associated with classic acute rejections (Fellstrom, 2003; Paul, 1999). During kidney transplantation, the ischaemic stage may be divided in two main conditions, warm ischaemia (WI) and cold ischaemia (CI). WI occurs when the kidney stops receiving blood supply with a temperature around 37°C. This stage is subdivided in two phases, first warm ischaemia (FWI) and second warm ischaemia (SWI) (Collard *et al.*, 2001).

FWI begins when the blood flow of the donor kidney, from either cadaveric donors (non-heart-beating donors) or heart-beating donors, is totally or partially blocked, and ends when the kidney is perfused with cold preservation solutions and stored in a cold environment. This phase has been associated with graft survival as FWI of more than 50 minutes has been shown to increase the possibility of graft rejection episodes significantly (Vanes *et al.*, 1983). On the other hand, less than 30 minutes of FWI prevents important cellular damage (Secin, 2008).

SWI goes from the time the kidney is not in a cold environment and free of cold preservation solution, to the time the donor kidney is anastomosed before reperfusion. In this phase, there is evidence showing that a higher development of acute tubular necrosis can occur when anastomosis of conduits lasts for more than 35 minutes (Halloran *et al.*, 1988). However, there is also evidence suggesting that a more relevant renal damage may take place during cold ischaemia time rather than SWI itself (Szostek *et al.*, 1999).

Cold ischaemia takes place outside the donor's body and involves a cold sequence which lasts from the time the kidney is stored in a cold environment (0 - 4 °C) with cold preservation solutions to the time it is placed in the recipient. An increase during the cold ischaemic time (CIT) has been associated with delayed graft function (DGF) (Kyllonen *et al.*, 2000). Moreover, the association of CIT with the overexpression of major histocompatibility complex II (MHC II) mRNA in rats has been shown in proximal tubular cells and vascular endothelium (Kouwenhoven *et al.*, 2001). A similar immunogenic phenomenon was also studied in mice where the expression of MHC I and II mRNA was noticed in proximal tubular cells after long CIT (Shoskes *et al.*, 1990). These findings suggest that ischaemia is not only an alloantigen independent factor, but also closely related to alloantigen dependent events.

1.4.2. Hypoxia

Experimental evidence has demonstrated that a reduction in renal oxygenation is a common and progressive final pathway in CKD (Nangaku, 2006). This hypothesis suggests that renal tissue under oxygen misbalances increases extracellular matrix deposition, mainly in the tubulointerstitial space, promoting fibrosis and therefore development and progression of CKD. This hypothesis has been validated by different researchers *in vitro, in vivo* and using human tissue (Heyman *et al.*, 2008; Norman *et al.*, 2006). The sustained loss of peritubular capillaries may continue the damage caused by ATN leading to tubulointerstitial fibrosis. This pathway has been represented in animal models of ischaemia reperfusion injury, 5/6th subtotal nephrectomy and models of AKI using nephrotoxic drugs (Badr *et al.*, 1988; Basile, 2004; Pillebout *et al.*, 2001; Yuan *et al.*, 2003) where hypoxia has been recognized as core trigger factor for CKD development and progression. Hypoxia promotes fibroblast activation, proliferation and epithelial mesenchymal transition, stimulating

extracellular matrix synthesis due to deposition of collagen proteins in the tubulointerstitial space (Desmouliere *et al.*, 2005; Norman *et al.*, 2000).

Kidney fibrosis is defined as the uncontrolled and progressive deposition of connective tissue in the tubulointerstitial and glomerular space. It has been suggested that renal fibrosis is a parallel event to the primary inflammatory response (Efstratiadis *et al.*, 2009). However, with more evidence, it has been proposed that renal ischaemia plays an important first step role in the development of renal fibrosis (Bonventre, 1993), as seen in chronic allograft nephropathy.

1.4.3 Renal Fibrosis

In humans, there is evidence of the association between AKI and the development of CKD (Finn, 1993; Venkatachalam *et al.*, 2010; Wald *et al.*, 2009). In vivo animal models have shown that renal recovery after IRI is often not complete; this lack of recovery predisposes the kidney to generate sequelae. Residual structural damage can progress inducing sustained tubular damage with the subsequent substitution of functional parenchyma by renal fibrosis (Devarajan, 2006; Venkatachalam *et al.*, 2010). Fibrogenesis is mainly carried out by fibroblasts and leukocytes. Nonetheless, particularly in kidney, endothelial, tubuloepithelial and mesangial cells are the crucial units which contribute to the development of fibrosis (Verderio *et al.*, 2004). A potential link between vascular endothelial damage and CKD has also been suggested to be a crucial factor for the development of renal fibrosis following acute kidney injury (Basile, 2007).

1.4.3.1 Pathophysiology

Acute: Renal IRI culminates in nephron death due to tubular epithelial cell death via necrosis and apoptosis (Ueda *et al.*, 2000). Later on, from the remaining nephrons, the severely injured ones experience a decrease in glomerular filtration rate (GFR) (Daughart.Tm *et al.*, 1974; Daugharty *et al.*, 1975). This is due to the fact that damaged tubules produce intratubular cellular debris increasing the tubular internal pressure. The blocked tubules increase the intratubular fluid pressure separating the tubular cells from the basement membrane. Afterwards, the uncovered basement membrane is not able to retain the fluid which leaks back into the peritubular capillaries with the subsequent reduction in glomerular plasma flow followed by decrease in GFR. Furthermore, the intratubular casts, composed of

cellular debris, lead to tubular blockage with the subsequent oedema due to the increase in pressure, proximal to the obstruction (Bonventre, 1993). The initial tubular epithelial cell inflammation apparently takes place more in the outer medulla, producing a mechanical secondary site of injury that keeps and enhances the ischaemic event (Yamamoto *et al.*, 1984). Therefore, probably the histopathological evaluation for acute damage should probably focus in both outer medulla and cortex. Regarding the less injured remaining nephrons, an increase in single nephron GFR might be noticed. However, due to the extensive damage, the nephrons still show an overall decrease in GFR. The increase of GFR for a single nephron seems to be associated with a compensatory glomerular hypertrophy, allowing an increase in the glomerular plasma flow and intracapillary pressure, followed by endothelial shear stress which in turn induces endothelial activation and the arrival of inflammatory cells (Seal *et al.*, 2005), see Figure 1.7.

Chronic: Once the main acute phase of the inflammatory cascade has developed, a transitional and overlapped tissue repairing phase takes place in the injured kidney. The main actors are the infiltrated and local fibroblasts in the interstitial space, which participate in the synthesis and deposition of collagen fibres, producing an expansion in the extracellular matrix translated as kidney scarring. This histopathological change together with tubular degeneration culminate in tubular malfunction leading to tubulointerstitial fibrosis, glomerulosclerosis and multilayering of peritubular capillaries (Remuzzi *et al.*, 1998). Histological changes are degenerative and irreversible (Boor *et al.*, 2007).

1.4.3.2 Molecular Pathophysiology

Acute: The first molecules involved after IRI are P and E-selectin, which reach their maximum level 6 hours after the initial injury. This phenomenon promotes leukocyte arrival (mainly neutrophils), adhesion and aggregation with the subsequent cellular transmigration to the interstitial space. On the other hand, after 2-5 days macrophages infiltrate interstitial space (Takada *et al.*, 1997) releasing different cytokines and growth factors, mainly transforming growth factor β (TGF-β), interleukin 6 (IL-6), IL-1, fibroblast growth factor (FGF), vascular endothelial growth factor (VEGF) and platelet derived growth factor (PDGF).

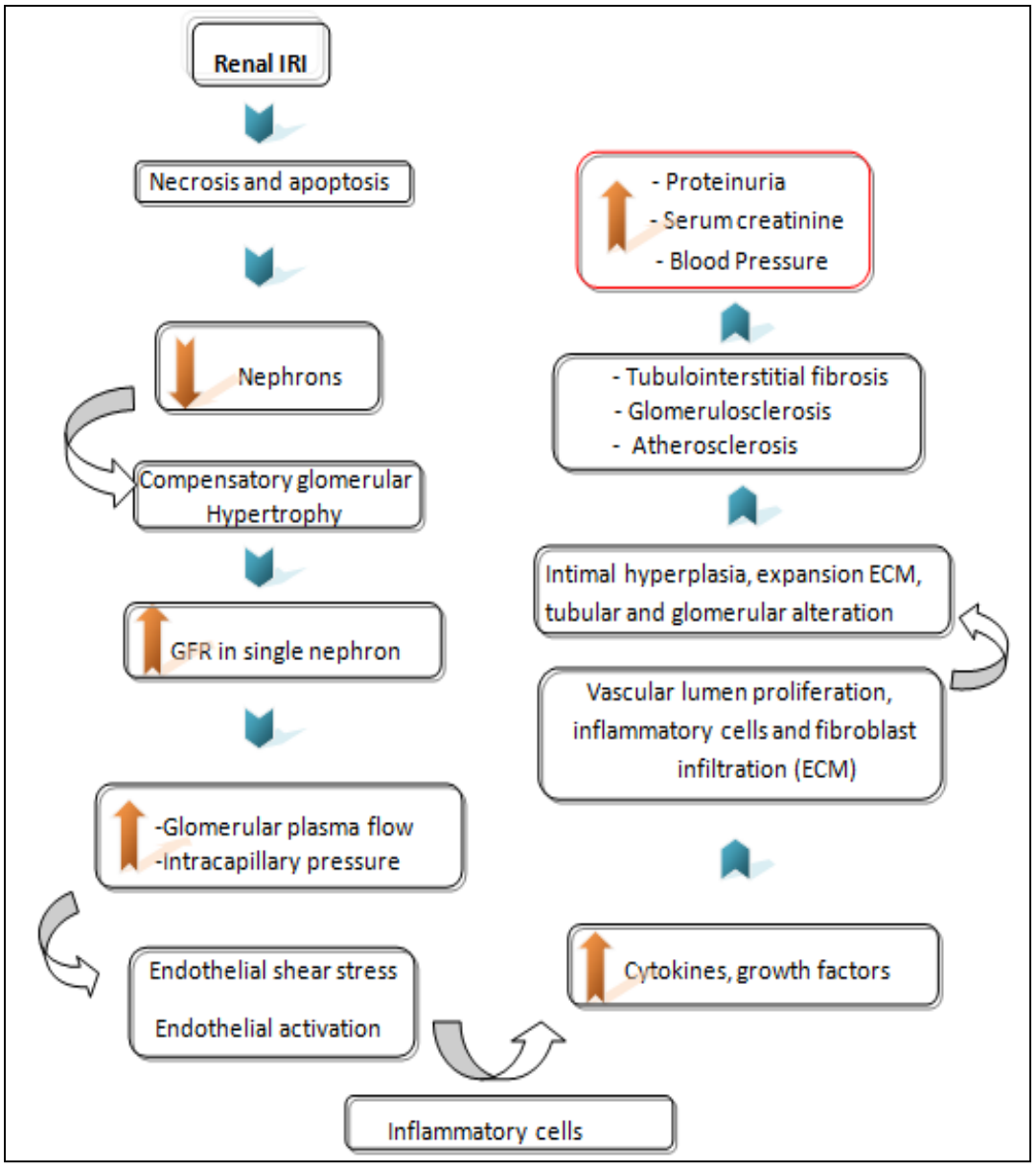

Figure 1.7: Development of renal fibrosis following ischaemia reperfusion injury

Renal IRI culminates in nephron death loss followed by hypertrophy of single nephron which in turn increases the GFR promoting endothelial and cytokines activation. An increase in vascular lumen proliferation together with infiltration of inflammatory cells and fibroblasts into the extracellular matrix will generate atherosclerosis, tubulointerstitial fibrosis and glomerulosclerosis.

The last two are described as wound healing factors (Verderio *et al.*, 2004). Concerning lymphocytes Th1; IL-2, tumour necrosis factor α (TNFα) and interferon gamma (IFN-γ) are the principal cellular products in the acute inflammatory stage (Verderio *et al.*, 2004). HIF also plays an important role. In a HIF-stimulated model of rat by inhibition of prolyl-hydroxylase, it was found that in approximately 90 % of the juxtamedullary cortex (inner cortex), the transcription of erythropoietin was localized in cortical fibroblasts and up-regulated through HIF-2α (Paliege *et al.*, 2010), suggesting that erythropoietin level might be proportional to HIF-2α expression in the juxtamedullary cortical tissue when hypoxia is present.

Chronic: This transitional phase is mainly orchestrated by two inflammatory cytokines TGF- β and FGF (Verderio et al., 2004), perhaps due to their close link with fibroblast activation and expansion of extracellular matrix. Furthermore, transformation of epithelial tubular cells into mesenchymal fibroblasts has been suggested as one of the main mechanisms to develop renal fibrosis (Strutz et al., 2006). *In vitro*, for instance, renal epithelial cells have shown significantly higher levels of collagen I, III and IV under TGF- β stimulation (Creely et al., 1992). Epithelial mesenchymal transition also occurs in pericytes in the mouse with normal kidney function and these cells are the major source of myofibroblast in the ureteral obstruction model of kidney fibrosis, generating mainly collagen I (Lin et al., 2008). HIF has been implicated in the cellular transition in tubuloepithelial cells *in vitro*. In the HIF-1α knock out mouse with unilateral ureteral obstruction, a substantial decrease of fibrosis was noticed in contrast to the wild type group (Higgins et al., 2007). The HIF signalling has been associated with the development of fibrosis through the activation of transforming growth factor-β1 (TGF-β1), its role in endothelial mesenchymal transition pathway and inflammatory processes (Haase, 2006).

After inflammation, fibroblasts provide stabilization and tissue development. These cells produce fibronectin collagen I, III and IV, which are the most important elements in the extracellular matrix (ECM) for fibrosis generation. Also metalloproteinase enzymes (MMP) are synthesized by fibroblasts. Other elements in the extracellular matrix include: glycoproteins, glycosaminoglycans, reticular and elastic fibres (Strutz *et al.*, 2006). Fibroblast activation is performed through PDGF, TGF- β1 or carried out by FGF 2, in an autocrine way (Strutz *et al.*, 2002). Interestingly, the renin-angiotensin system has been associated with the development of fibrosis through the indirect activation of fibroblast by increasing the

levels of TGF- β1 in tubular epithelial cells. Moreover, it has been shown that TGF-β1 stimulates *in vitro* the expression of renin in juxtaglomerular cells (Border *et al.*, 1998). However, other mechanisms such as hyperglycaemia, hypoxia and ECM – integrin interaction and fibroblasts activators have also been described (Qi *et al.*, 2006; Strutz *et al.*, 2006). Fibroblasts reach the injured area by migration of local fibroblasts from the medulla to the cortex or by differentiation of epithelial or endothelial cells (Zeisberg *et al.*, 2008). They can also adopt a myofibroblast phenotype expressing α-smooth muscular actin (α-SMA); this property compacts the injured area by contraction of actin fibres (Desmouliere *et al.*, 2005).

1.4.3.3 Extracellular Matrix

ECM can be easily defined as the acellular material around cells; it includes the interstitial space and the basement membrane. This meshwork-like substance is an intercellular scaffold substrate for cellular support, movement, development, differentiation, and intercellular networking (Hynes, 2009). It is mainly composed of collagen proteins I, III, IV and V. However, other important elements are found in the ECM: elastin, which keeps the anatomic form of tissue; fibronectin, important in cell adhesion migration and differentiation; proteoglycans, responsible for water retain; and glycosaminoglycans, vital for tissue resistance to high levels of compression (Strutz *et al.*, 2006). Normally, there is a balance between synthesis and degradation of ECM. However, in renal disease such as in CKD, the synthesis of ECM is altered. There are many pathways to understand the development of renal fibrosis during renal disease. In CKD, the normal rate of ECM degradation is thought to be overcome by the pathological deposition of collagen fibres resulting in expansion of ECM. Also, it has been shown that CKD itself reduces the degradation of the ECM with the following accumulation of matrix. Additionally, the pathological expansion of ECM can be further enhanced when cross-linking of collagen proteins occurs in the interstitial space and basement membrane. When collagen cross-linking occurs, **fibrosis accumulation** (reversible scarring stage) of extracellular matrix suffers a transition to **fibrosis deposition**, which is a stage where fibrosis cannot be easily degraded by natural proteolytic systems promoting fibrosis build up. The cross link of collagen fibres and elastin occurs mainly by three pathways; non enzymatic glycation / lipid peroxidation (Maillard reaction), lysyl oxidase and transglutaminase enzymes (Popov *et al.*, 2011).

Non-enzymatic glycation is a reaction between proteins and reducing sugars (ribose and glucose), it is implicated in aging of tissue proteins as well as in hyperglycaemia. This reaction produce chromophores and fluorophores called advanced glycation end products (AGEs) which react with amino groups of collagen producing collagen-AGEs cross link products (Copeland *et al.*, 1987).

Lysyl oxidases (LOXs) are a group of 5 characterized copper enzymes, responsible of the peptidyl lysine oxidation converting specific residues of hydroxylysine and lysine of α-aminoadipic-δ-semialdehyde; these converted residues produce an insoluble cross link in elastin and collagen fibres (Lucero *et al.*, 2006). Interestingly, these enzymes seem to be up regulated by TGF-β1 (Goto *et al.*, 2005). Animal models of lung, liver, dermal, renal (Di Donato *et al.*, 1997; Higgins *et al.*, 2007; Yang *et al.*) and arterial fibrosis have shown a reduction in the level of scarring when inhibiting LOX's; however, it has also been associated with the development of severe alterations in musculoskeletal, vascular and the respiratory system (Maki *et al.*, 2005).

Transglutaminases (TG's) were discovered in 1959 (Clarke *et al.*, 1959). In 1968 the first type was described as a fibrin stabilizing factor, better known as protein factor XIIIa (Pisano *et al.*, 1968). Currently, 9 types of transglutaminase have been identified in kidney, brain, skin, testis, liver, heart, lung and prostate (Selkoe *et al.*, 1982). Their more widely studied roles include wound healing and the erratic increase of extracellular matrix after cellular stress (Telci *et al.*, 2006).

1.5 Transglutaminase 2

TG2 is an enzyme expressed in organs such as bowel, skin, prostate, testicles, brain, lung, heart, liver and kidney. Macrophages, hepatocytes, skeletal, smooth muscle cells and astrocytes cells are able to secrete TG2 when these are exposed to stress factors (Haroon *et al.*, 1999b; Ientile *et al.*, 2007; Verderio *et al.*, 2004). In the kidney, TG2 has been identified in epithelial, mesangial, endothelial cells and can be secreted when cells are exposed to stress factors, such as hyperglycaemia and hypoxia (Ientile *et al.*, 2007; Verderio *et al.*, 2004).

TG2 in the human has a molecular weight of 80kDa and is composed of 687 aminoacids and it is transcribed in the chromosome 20 locus 12. In the cat, TG2 also consists of 687 amino acids as a secreted protein (protein ID ENSFCAP00000004444) (Flicek *et al.*, 2014). Interestingly, between human and the cat TG2 there is a 90% protein sequence homology, according to the Ensembl genome data base (Flicek *et al.*, 2014).

TG2 has calcium dependent and independent activities. Transamidation and deamidation are calcium dependent functions whereas G-protein, disulphide isomerase activity, protein kinase binding and hydrolysis of GTP are considered calcium independent activities. From all these functions the most studied is transamidation. Transamidation is the transfer of a NH_2 from glutamine to lysine. Transamidation can be explained in two main phases. First phase involves a nucleophilic attach, which is the binding of the thiol group from cysteine 277 to the carboxamide of a glutamine residue (acyl-donor). This phenomena releases ammonia and produces a thioester intermediate bond between the cysteine 277 and the substrate. In the second phase, the thioester intermediate can then be attacked by the surface amine (acyl-acceptor) of a second substrate (lysine residue). The residues in collagen protein are rich in lysine and glutamine (Gundemir *et al.,* 2012). Regulation of TG2 is achieved through the GTP/GDP hydrolysis regulation, Ca^{2+} concentration and regulation of disulphide bonds between cysteine residues via redox processes (Jin *et al.,* 2011).

TG2 transamidation accelerate the extracellular matrix build up through the creation of pro-fibrotic and irreversible cross linking products of epsilon (γ-glutamyl)-lysine dipeptide bonds, which are highly resistant to proteolytic degradation (Johnson *et al.*, 2004a; Johnson *et al.*, 1999; Verderio *et al.*, 2004). TG2 is an important phagocytic enhancer, plays important roles in fibroblast movement, adhesion and spreading (Gaudry *et al.*, 1999) and it has been implicated in other activities such as, cell death modulator by promoting intracellular cross link using fibronectin 1 (FN1) as substrate and preventing microtubular and substantial DNA damage (Verderio *et al.*, 1998).

Intracellularly, TG2 is inactive due to the low levels of Ca and the high levels of GDP/GTP (guanosine-5'-triphosphate/ guanosine-5'-diphosphate), maintaining a closed structural conformation avoiding the interaction of cysteine 277 with any substrate. TG2 expression can be found in nuclei, cytosol and plasma membrane. Interestingly, TG2 does not have a signal peptide, therefore, the common endoplasmic reticulum/Golgi secretion pathway is not utilised by this enzyme. FN1 is considered as important protein for TG2 secretion (Gaudry *et al.*, 1999; Telci *et al.*, 2006; Verderio *et al.*, 2004). However, other studies have suggested other proteins for TG2 externalization (Telci *et al.*, 2006). Zemskov et al (2013) showed that TG2 may be exteriorised through perinuclear recycling endosomes. This mechanism allows TG2 protein to be delivered inside these vesicles to the plasma membrane and then externalized to the extracellular space. However, further research has to be done to clarify the exact mechanism to transport TG2 extracellularly.

TG2 enzyme has four domains, amino terminal sandwich, first, second barrel domain and a core domain, where the catalytic triad is located. The triad is composed of cystein-277, histidine-335 and aspartame-358 aminoacids allowing the transamidation activity of the enzyme (Liu *et al.*, 2002). TG2 monomer in ribbon drawing is shown in Figure 1.9. Second barrel and amino terminal sandwich have been identified as vital TG2 elements for externalization and therefore potential targets for drug inhibitors (Hang *et al.*, 2005). The mechanisms can be divided in two pathways, direct and indirect increase of extracellular matrix.

Direct Increase in ECM: When the specific cells are damaged by hypoxia, oxidative stress, hyperglycaemia, glutamate exposure, UV or inflammatory cytokines (Ientile et al., 2007), TG2 is mobilized to the extracellular space. In the new environment, the enzyme encounters a high concentration of Ca^{+} that interacts with the catalytic core triggering a transamination reaction. Through this reaction, a new amino bond is formed linking mainly two peptides localized in collagen proteins, γ-carboxamide glutamic acid and epsilon-amino group of lysine, see Figure 1.8.

Also, low levels of guanosine-5'-triphosphate interact and improve the catalytic transamination. TG2 also cross links, at a lower rate with other substrates such as apolipoproteins, fibronectin, vimentin and dermatan sulphate proteoglycans (Gupta *et al.*, 2007). The cross link products are highly resistant to proteolytic, mechanical or chemical interactions (Fisher *et al.*, 2009; Griffin *et al.*, 2002; Johnson *et al.*, 2003; Johnson *et al.*, 2007; Verderio *et al.*, 2004).

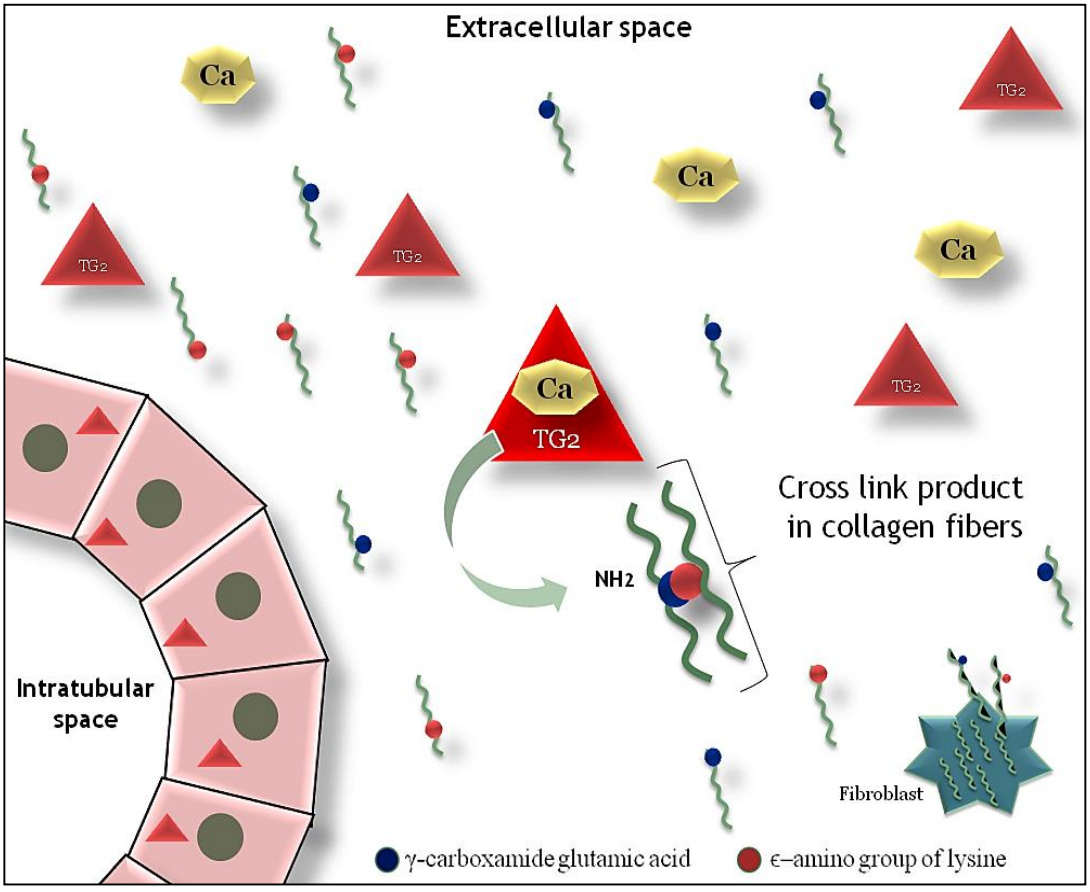

Figure 1.8: Cross linking product of collagen fibres through the TG2 pathway

Once Transglutaminase 2 is externalized to the extracellular space, interacts with calcium promoting the formation of an amino bond which binds γ-carboxamide glutamic acid and ϵ-amino group of lysine peptides in collagen fibres.

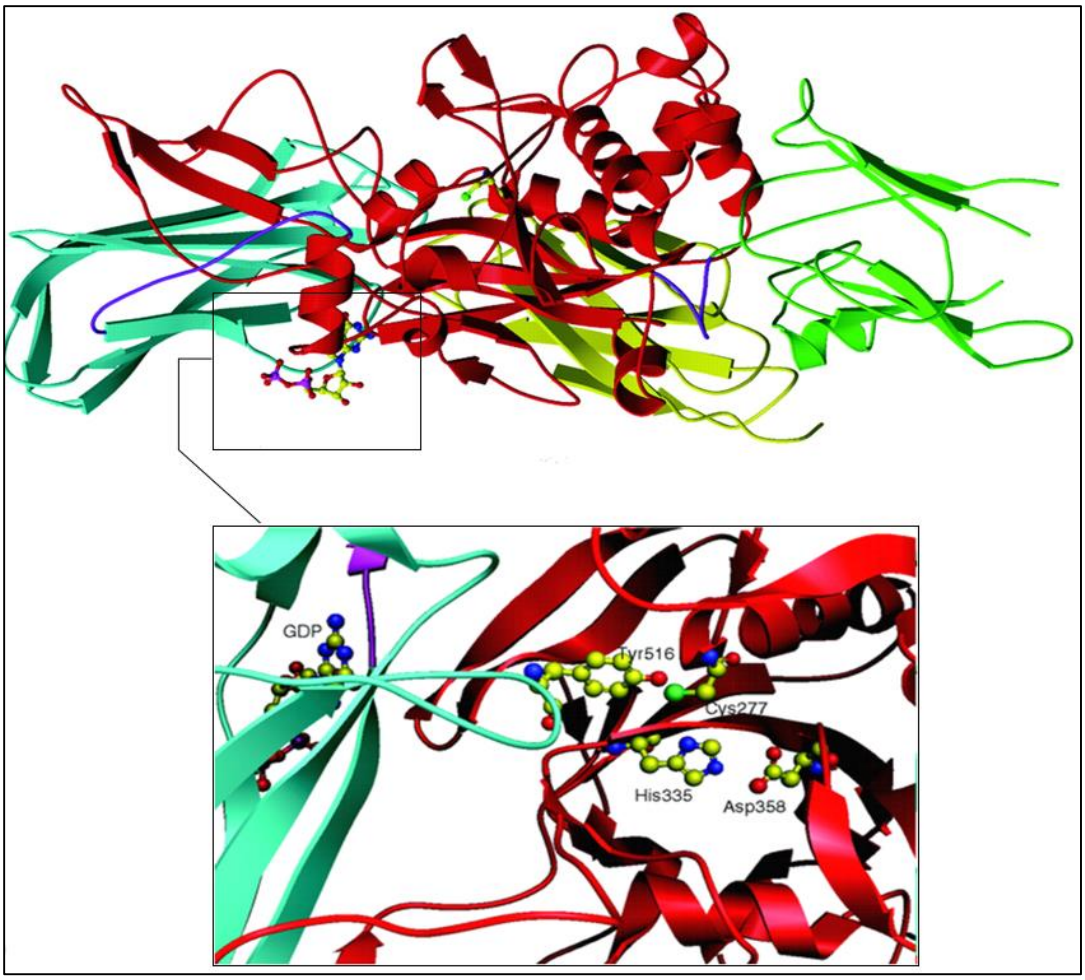

Figure 1.9: Ribbon drawing of a human TG2 monomer with bound GDP

Upper drawing. Green, red, cyan and yellow represents the sandwich domain, catalytic core, first and second barrel domain, respectively. GDP is shown as a ball and stick model between the catalytic core and the first barrel. Lower framed drawing represents the magnification of the catalytic core consisting of Cys-277, His-335, Asp-358, Tyr-516 and GDP using a ball and stick model. Upper and lower drawing were taken from (Liu *et al.*, 2002).

Indirect Increase in ECM*:* TG2 can regulate one of the most well-known fibrogenic cytokines, TGF-β1 (Huang et al., 2010; Khalil, 1999). Studies have shown that TGF-β1 is secreted inactively as latent form of TGF- β (L-TGF-β1) and later this is catalysed by TG2. Also, TG2 may recruit the latent form of TGF-β1 to the extracellular matrix followed by cytokine activation (Huang *et al.*, 2010; Kojima *et al.*, 1993; Nunes *et al.*, 1997). Researchers from the Academic Nephrology Unit / The University of Sheffield showed that a partial reduction (approximately 20%) in the expression of TGF -β1 can be achieved when cell lines overexpressing TG2 are subjected to TG2 inhibitors (Huang et al., 2010).

Inhibition of transglutaminase activity: Currently, four interventional studies have been achieved to evaluate the role of TG2 in the development of renal fibrosis, these studies can be divided in two different approaches:- TG2 gene ablation in a models of UUO (Kim *et al.*, 2010; Shweke *et al.*, 2008); and based on pharmacological transglutaminase inhibitors in the rodent model of diabetic nephropathy (Huang et al., 2009) and subtotal nephrectomy (Johnson et a 2007). However, neither gene ablation, nor pharmacological approach has ever been attempted using a RWI stimuli in the rat.

The compound used in the present research project is a chemical drug produced by Zedira biotech company under the name of D003, called in this thesis as TGI. TGI is a 2-[(2-oxopropyl)thio] imidazolium derivate, 220.70 molecular weight and a IC_{50} of about 1.0 µM (Zedira, Germany). TGI was originally developed to inhibit factor XIIIa as a therapeutic approach in the treatment of thrombosis (Freund *et al.*, 1994). However, further evaluation showed that its effectiveness to inhibit factor XIIIa was similar to drugs developed to inhibit transglutaminase 2 in the extracellular matrix (Skill *et al.*, 2004). Using proximal tubular cells, Skill et al (2004) evaluated the *in vitro* effectiveness of TGI to inhibit TG2 activity. The drug was tested to determine its effect without a direct effect on either TGF-β regulation (Skill *et al.*, 2004) or caspase 3, an enzyme involved in apoptosis (Johnson *et al.*, 2007). Skill et al (2004) also ruled out the possibility that the inhibitory effect of TGI on collagen I/IV deposition was due to a down regulation in cellular collagen secretion or collagen transcription. Johnson et al (2007) showed TGI to reduce collagens *in vivo* (Johnson *et al.*, 2007).

TGI has access to both the intracellular and extracellular space (Lortat-Jacob *et al.*, 2012), whilst a second inhibitor derived from the same chemical family N-benzyloxycarbonyl-L-phenylalanyl-6-dimethyl-sulfonium-5-oxo-L-norleucine is not

able to access intracellularly due to its higher molecular weight (Baumgartner *et al.*, 2004); both TG inhibitors have just an extracellular effect. The transglutaminase enzyme, when active, transfers an acyl group from the substrate to the transglutaminase cysteine residue (active site). This action results in a thiol ester group which subsequently is catalysed via enzymatic aminolysis or hydrolysis. The thiol group can be easily inactivated by alkalinic compounds; however highly reactive alkalinic compounds can also affect other enzymes with a thiol group, decreasing specificity (Folk *et al.*, 1977; Freund *et al.*, 1994). TGI exerts its inhibitory effect via acetonylation of the active site cysteine residue, with release of the complementary thione; moreover, it has also a low reactivity as an alkylating agent (Freund *et al.*, 1994), improving specificity. Similar transglutaminase inhibitors to TGI have been tested *in vitro* at a concentration of 1mM without any effect on several serine protease and thiol sensitive enzymes showing a high selectivity for the transglutaminase family enzymes (Freund *et al.*, 1994).

A novel approach to inhibit the activity of transglutaminase 2 isoform is by targeting the active site of the enzyme using antibodies to a specific epitope. The mouse inhibitory antibody to human TG2 (BB7) used in Chapter 4 is an antibody derived from a single murine clone B cell. For its development, different antigens containing specific epitopes from the active site of the human TG2 were injected in mice. B cells were isolated from spleen and mixed with myeloma cells generating immortal hybridomas. Each hybridoma cell produced a single type of antibody against a single epitope. The single hybridoma cells were separated into individual wells of a microtiter plate and tested for their ability to produce monoclonal antibodies. These antibodies were isolated, purified and then tested for their ability to inhibit the activity of TG2. After an extensive screening, BB7 antibody targeted an epitope in the TG2 core domain resulting in the inhibition of human TG2 activity. The epitope is identical to the residues in the feline TG2 active site and just 82% identical to the one it the rat and mouse. Even though BB7 showed a useful level of *in vitro* inhibition in the rat TG2, it was not employed for *in vivo* studies due high risk of immunogenicity to the rat and production issues. Therefore, in the end, the employment of BB7 was just restricted to inhibition of feline TG2 in kidney tissue with CKD.

The development, screening and previous *in vitro* testing of BB7 antibody were exclusively performed by Dr Phil Watson, Dr Mabrouka Maamra and Professor Tim Johnson from the Department of Infection and Immunity - Medical School, University of Sheffield.

1.6 Hypothesis and Aims

Hypothesis

Is TG2 elevated in the domestic feline with CKD? Does the inhibition of TG2 reduce the development of tubulointerstitial fibrosis in a rodent model of RWI which mimics CKD in the domestic feline and renal fibrosis secondary to CAN?

Aims

Firstly, a companion animal approach was employed. Kidney tissue, obtained post mortem, from domestic cats with/without azotaemia was analysed. Kidney tissue samples were obtained from the biorepository at the Royal Veterinary College (London, UK) in collaboration with Professors Jonathan Elliott and Harriet Syme.

Chapter 3: To determine if the development of azotaemia in the domestic cat was associated with the progression of tubulointerstitial fibrosis in the kidney.

Chapter 4: To determine if the development of tubulointerstitial fibrosis and azotaemia in the domestic cat was associated with an upregulation of the transglutaminase pathway, an enzyme system involved in protein cross-linking and matrix deposition. Additional studies were also performed, *in vitro*, to establish whether renal transglutaminase enzyme activity in the cat could be decreased by either (a) a mouse monoclonal, neutralising antibody to human TG2 (selective inhibitor) or (b) by a non-selective, small molecule, chemical inhibitor of the transglutaminase enzyme group.

Secondly, an *in vivo* laboratory model of renal fibrosis was employed. Tubulointerstitial fibrosis was induced in the Sprague-Dawley rat following a period of renal warm ischaemia (RWI) applied to the left kidney.

Chapter 5: To establish if changes in renal function and the development of renal fibrosis were associated with an increase in the expression of TG2 protein and TG enzyme activity in the Sprague-Dawley rat using a unilateral model of RWI.

Chapter 6: To undertake an interventional study using a nonselective, small molecule, transglutaminase inhibitor (D003, Zedira, Germany) to establish whether the inhibition of renal TG following a period of RWI in the Sprague-Dawley rat is associated with a reduction in renal fibrosis, specifically in the tubulointerstitial space.

Thirdly, a technique of kidney transplantation was developed in the rat with the aim of undertaking TG2 interventional studies in a model of chronic allograft nephropathy, a renal fibrosis model largely influenced by renal warm ischaemia.

Chapter 7A: Describes the precise details of the surgical technique employed.

Chapter 7B: The donor and recipient techniques were carefully evaluated.

Disappointingly however, while the intricate technique of kidney transplantation in the rat was successfully established, TG2 neutralising antibodies were ultimately unavailable for use.

CHAPTER 2

Material and Methods

2.1. Domestic Cat

Blood samples were obtained via jugular vein. Plasma biochemical profiles were obtained almost at the time of sample collection. UPC measurements were obtained from samples that had been stored at -80°C. Plasma analysis was performed by Idexx Laboratories (Wetherby, UK). Urine protein and creatinine were measured using pyrogallol red and picric acid methods, respectively.

Systemic blood pressure was performed using a doppler flow detector with a 9.5 MHz probe as described previously (Syme *et al.*, 2002).Time-averaged systolic blood pressure (SBPOT) was calculated using an average of 5 measurements of systolic blood pressure against time dividing the area under the curve by the interval between the first and last blood pressure measurements (Chakrabarti *et al.*, 2013).

Post-mortem kidney tissue was obtained for 15 cats from a bio-repository bank stored at -80°C. An informed consent had been obtained from cat owners following euthanasia (Royal Veterinary College, London, UK). 14/15 cats were of domestic shorthair varieties (DSH), 1/15 was a Burmese. The average age at euthanasia was 16.2 years (range 9 - 23.7). An essential inclusion criteria was the presence of a plasma biochemical profile obtained within a maximum of 2 months prior to euthanasia.

The following normal ranges were employed: plasma creatinine 40-140 µmol/L; plasma urea; 2.7-9.2 µmol/L; plasma phosphate 1.29-2.84 mmol/L; urinary protein creatinine ratio (UPC), non-proteinuric < 0.2, borderline proteinuric 0.2 - 0.4 and proteinuric > 0.4.

The degree of CKD was assessed according to the International Renal Interest Society (IRIS) staging system for feline CKD (Elliott *et al.*, 2007). Plasma creatinine 140-250 µmol/L (CKD stage 2); 251-440 µmol/L (CKD stage 3) and > 440 µmol/L (CKD stage 4) (Elliott *et al.*, 2007; Syme *et al.*, 2006) . Cats were divided in two groups; **non-azotaemic** control group, where plasma creatinine and urea were within the normal range (n=5), and **azotaemic** group (n=10). The azotaemic group included cats with CKD stage 2 (n=3), stage 3 (n=3) and stage 4 (n=4).

2.2. Sprague Dawley Rat

All the procedures were carried out according to the regulations of the Home Office (Animals Scientific Procedures Act 1986, United Kingdom). An intensive course, composed of four modules, was undertaken at the University of Sheffield (Biological Services) to obtain a personal license to perform animal handling and surgical procedures in rats. Topics included UK legislation on animal experimentation, ethical and welfare issues together with a review of animal handling, husbandry, human methods of killing rats, anaesthesia and the basis of surgery.

Male Sprague-Dawley rats (Harlan, UK), 8-10 weeks, with an initial weight of 250-300 grams were maintained at 20°C, 45% humidity and with a light cycle of 12 hours. Rats were housed in pairs with water and food *ad libitum* (Harlan 2018 Tecklad Global, 18% protein rodent diet).

2.2.1. Anaesthesia

Induction of anaesthesia was performed by placing the rat in an anaesthetic chamber with 5% isoflurane and 8 L/min oxygen (Figure 2.1). Analgesia was provided by intramuscular (left rear limb) injection of buprenorphine 50µg/kg. Maintenance of anaesthesia was achieved with 1.5% of isoflurane and 1 L/min oxygen.

2.2.2. Temperature

The rat was placed on an operating board covered with a homeothermic blanket. The body temperature was measured using a homeothermic blanket control unit (Harvard apparatus, USA) (Figure 2.2) by introducing a probe in the rectum. The blanket was servo-controlled, increasing its temperature automatically when the reading was below 36.5°C until reaching 37°C. The tight control of animal body temperature is of particular importance in studies using warm ischaemia as the renal insult.

2.2.3. Aseptic Technique

The rat was shaved on the cranio-dorsal side of the lateral abdominal wall (6 cm^2). The shaved area was cleaned three times using chlorhexidine solution. The excess of solution was removed using a sterile swab. Sterile double layer paper roll

(30 cm^2) with a middle 5cm^2 central opening was used as surgical drapes to narrow the surgical field. The surgical procedure was performed with surgical mask, cap, sterile gloves and gown (Figure 2.3). The surgical procedure started when a diagonal (4 cm) skin incision was made in the left abdominal wall from the dorsal corner (close to the last rib) of the shaved area to the ventral-caudal shaved corner.

2.2.4. Renal Warm Ischaemia

After the skin incision, an incision through the abdominal oblique external, internal and a portion of the transverse muscles was performed. The abdominal fat was identified and displaced on one side in order to visualize the kidney. Subsequently, Adson forceps were used to grab the perirenal fat from the caudal pole pulling the kidney out from the abdominal cavity without injury. With the aid of a surgical microscope (10x magnification), the adrenal gland and main conduits of the renal hilus (renal artery with the respective branches, renal vein and ureter) were identified. Later on, the excess of perinephric fat tissue near the renal hilus was carefully separated from the renal vascular conduits creating a small window of 0.5cm length in the each side of the renal vascular bundle. Afterwards, the renal artery and renal vein were clamped for 60 minutes with a 45◦ angled vascular bulldog clamp, exerting 75-80 grams of pressure according to the manufacturer information (Vascu-statt II, SCALAN international). Special care was taken to avoid clamping adrenal gland blood supply and ureter. To ascertain whether the kidney was being clamped properly; visual evaluation on the kidney surface was carried out in order to see the change of colour from reddish bright brown to dark brown (Figure 2.4). The kidney with the clamp was placed back in the abdominal cavity to avoid heat loss. The muscular layers together with the skin were closed with a Bakus towel clamp. The wound and clamp were covered with a sterile gauze bandage soaked in NaCl 0.9%. After 60 minutes, the clamp was removed and the total recovery of colour was evaluated for 3 minutes (Figure 1.3, panel A, B and H).

The abdominal muscular layers (abdominal transverse, oblique internal /external muscular layers) were sutured as one layer with polyglycolic acid 4-0 (braided coated fast absorbable suture, 3/8c, 19mm needle, B. Braun) using a simple continuous pattern. The skin was sutured using 4 single separated knots. The rat was placed in an incubator to recover consciousness. During all procedures the body temperature was kept between 36 - 37 ◦C.

Figure 2.1: Anaesthetic equipment

Black arrow: anaesthetic chamber. **Red arrow:** Isoflurane adsorber. **Yellow arrow:** Oxygen meter. **White arrow**: Isoflurane vaporizer**.**

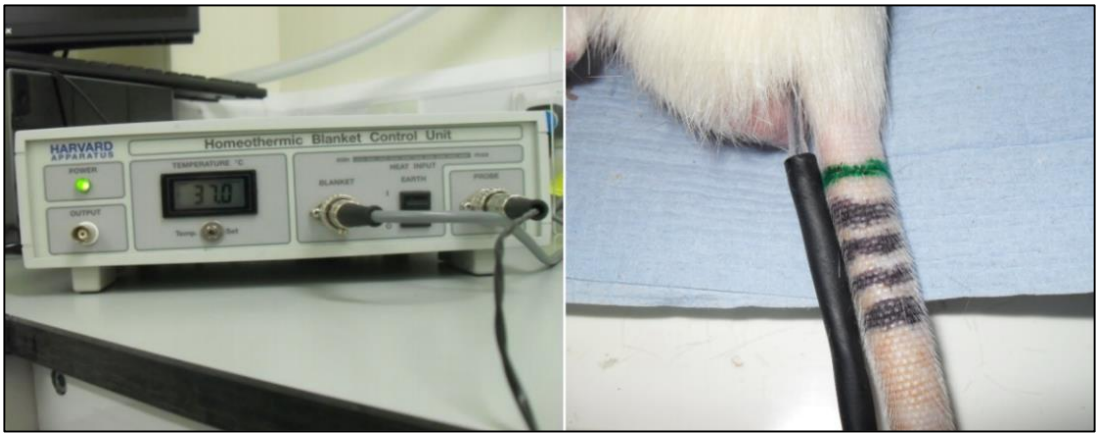

Figure 2.2: Homeothermic blanket control unit

Left panel: Homeothermic Unit board displaying an optimal temperature. **Right panel:** Rectal probe in the rat.

Figure 2.3: Surgeon using a microscope during a surgical procedure in a rat

2.2.5. Nephrectomy

Rats were nephrectomised by removal of the right kidney. Ligation of the ureter, renal artery and vein was undertaken by placing a Rochester forceps in the renal hilus. A 3-0 polyglycolic acid suture was placed below the forceps to ligate the area (Figure 2.5). Another pair of Rochester forceps were placed 0.5cm above the first forceps. The pedicle was cut using microvascular scissors in the free space between forceps. The other forceps were removed slowly to evaluate the effectiveness of the knot by visually assessing any degree of haemorrhage coming from the ligated pedicle.

2.2.6 Renal Tissue Infusion

For interventional drug studies in rat models of RWI, drugs were delivered by renal tissue infusion allowing both a marked reduction in total drug dose and reduced potential for the development of side effects. The principle of intrarenal drug delivery using a subcutaneous osmotic pump was based on previous published methodologies (Huang *et al.*, 2009; Johnson *et al.*, 2007; Oldroyd *et al.*, 1999).

2.2.6.1. Fenestrated Cannula.

Fenestrated cannula was produced with the aid of a light microscope (10x magnification), using sterile gloves over a sterile working surface. The heat sealing end was tested inserting a 23 gauge needle in the open end, attached to a 3 ml air filled syringe. Air was injected into the sealed cannula followed by immersion of the heat sealing end in a universal container with sterile NaCl 0.9% for the detection of bubbles. Disposal of cannulas was done when air leakage (bubbles) was detected. Using a preheated 27 gauge needle with the aid of a thermocautery pencil, six bilateral fenestrations were performed on the polyethylene tubing between 2 and 12mm from the sealed side. To visually ensure the fenestrations were inside the kidney when inserted, the cannula was ring marked with a permanent marker between 1.5 and 15 mm from the seal (Figure 2.6); therefore, when the cannula was correctly positioned in the kidney, the markings were not visualized. The plastic debris were flushed away by injecting sterile NaCl 0.9% into the cannula and then cannulas were dried out by centrifugation.

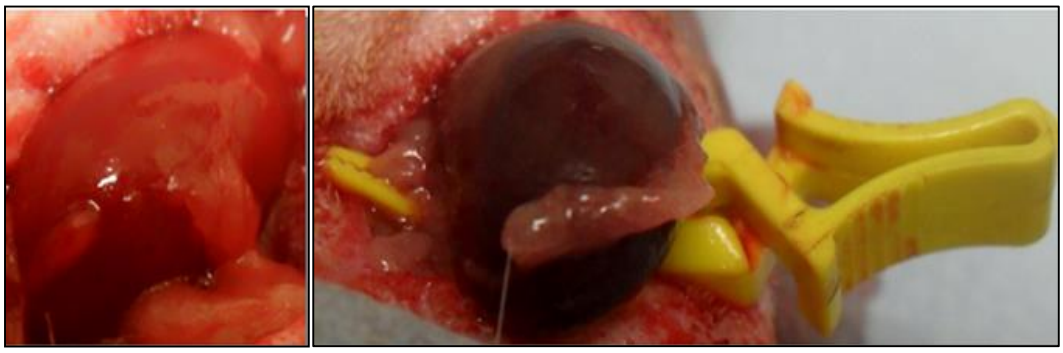

Figure 2.4: Effect of renal warm ischaemia on the renal surface colouration

The **left panel** shows the normal kidney colour. The **right panel** represents the dark brown colour after 5 minutes of renal vascular clamping.

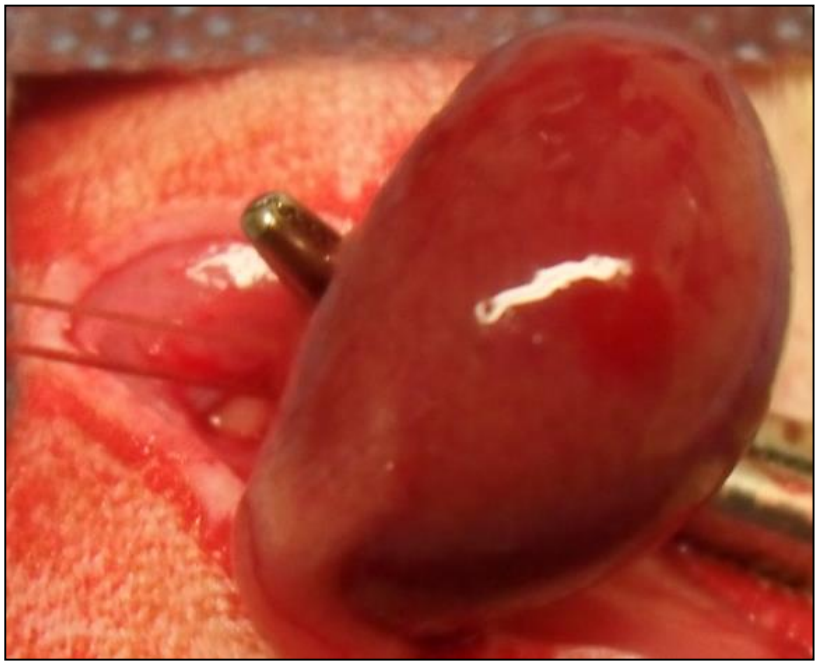

Figure 2.5: Right nephrectomy

Rochester forceps clamping renal hilar conducts and suture placed to ligate renal hilar conducts.

2.2.6.2. Osmotic Minipump

The complete osmotic pump has a length, diameter and weight of 5.1 cm, 1.4 cm and 5.1 grams, respectively. The body is composed of cellulose ester blend osmotic (outer layer) and thermoplastic hydrocarbon elastomer (drug reservoir). The flow moderation is a stainless steel (56 gauge), 4.6 cm length metallic tube with a plastic removable plastic cap on top. The outer and inner diameters of the flow moderation are 0.08 and 0.05 cm, correspondingly. The pump consists of a cylindrical drug compartment, inert to aqueous drug formulations including bases, diluted acids and alcohols. The drug reservoir is encapsulated by an osmotic layer material, which in turn is surrounded by a semi-permeable non-expandable membrane, (Figure 2.7).

The semi-permeable membrane allows the subcutaneous fluids to get in contact with the osmotic layer. The expanded osmotic layer compresses the cylindrical drug compartment promoting the expulsion of the drug solution at specified rates and volumes (Theeuwes *et al.*, 1976). 2ML4 pump model was used to deliver 2.5 µl/hr of 50 mmol/L of TG inhibitor (D003) or vehicle solution.

2.2.6.3. Pump Loading

Osmotic minipumps were filled under aseptic conditions using a laminar flow hood. The pumps were manipulated using sterile gloves over a sterile surface (sterile blue roll paper or gloves inner wrapping) Figure 2.8, panel A. The steps to load an osmotic minipump are described below:-

1. The pump was weighed without solution together with its flow moderator.
2. The filling cannula was attached to a 3ml syringe and the solution was drawn up, taking care not to introduce air (bubbles).
3. The pump was held with the exit port pointed upright (vertically).
4. The filling cannula was inserted and maneuvered to the bottom of the pump.
5. The plunger of the syringe was slowly pushed, holding the pump in an upright position and slightly inclined to allow the exit of the displaced air by the injected solution (Figure 2.8, panel B).
6. Excess solution was removed and the flow moderator fully inserted into the body of the pump without the plastic cab, Figure 2.8, panels from C to E.
7. The filled pump was weight with the flow moderator in place.
8. The volume loaded was calculated from the difference in weight obtained in step

1 and step 6. All the loaded pumps were completely filled, with no less than 2ml.

9. The cannula was inserted in the exit of the flow moderator (Figure 2.8, panel F).
10. The cannula was glued to the pump using a small drop of cyanoacrylate base solution followed by a drop of sterile NaCl 0.9% (Figure 2.8, panel G).
11. To prime the cannula. The pump with the attached cannula was placed in a universal container with 7ml of sterile NaCl 0.9%, just enough to cover 90% of the pump's body, (Figure 2.8, panel H). The universal containers were closed and placed in a 37°C incubator overnight.

2.2.6.4. Renal Tissue Cannulation

The insertion of the cannula into the kidney was performed using an intravenous catheter 18 gauge. Intra-renal cannulation was achieved using the following steps. The needle of the catheter is removed. The needle is bent several times using forceps to separate 3.5 cm length of the needle from the cutting edge tip (Figure 2.9, panel A). The 3.5 cm needle is reintroduced into the catheter until the sharp tip gets 0.5cm out of the plastic catheter (it can be pushed with the large portion of the cut needle) (Figure 2.9, panel B and C), The cannula is then cut with scissors allowing 4 cm length (Figure 2.9, panel D) . A free space of 1 cm between the blunt side of the needle and the plastic catheter is allowed to insert the plastic cannula (Figure 2.9, panel E and F). To ensure the cannula will remain attached to the pump during the study, a loop of silk 3-0 is displayed and knotted around the cannula embracing the external flow moderator (Figure 2.9, panel E).

The catheter/needle works as guide to insert the cannula straight and smoothly within the kidney. The insertion starts from the caudal pole to the cranial pole slightly towards the convex side of the kidney. Afterwards, the guide is pulled out from the catheter, (Figure 2.10, top right and left panel).

The fixation of the intra-renal cannula was achieved by placing a double knot (silk 3-0) in the cannula, cranial and caudal to the renal parenchyma. The knots were covered with cyanoacrylate to ensure fixation (Figure 2.10, bottom panel).

Figure 2.6: Fenestrated cannula for drug delivery

Left panel shows a 12 cm 0.58-mm-polyethylene bore cannula with a fenestrated seal heated side. **Right panel** shows the intra-renal fenestrated cannula with 6 double side fenestrations. The cannula is ring market to delimitate the intra and extra renal parts.

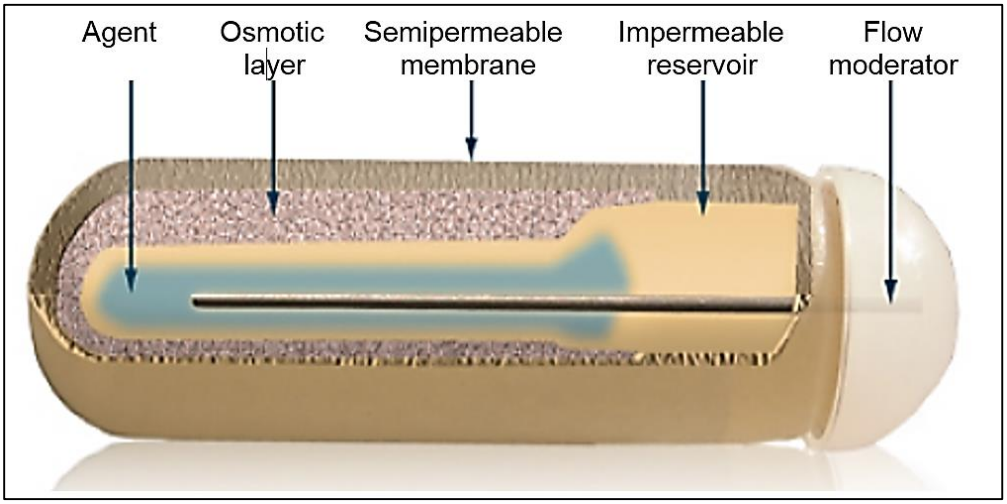

Figure 2.7: Minipump compartments

From left to right the blue arrows are showing the agent loaded in the pump, osmotic layer, semipermeable membrane, impermeable reservoir and the external portion of the moderator covered by a plastic cab. Diagram from Alzet, USA.

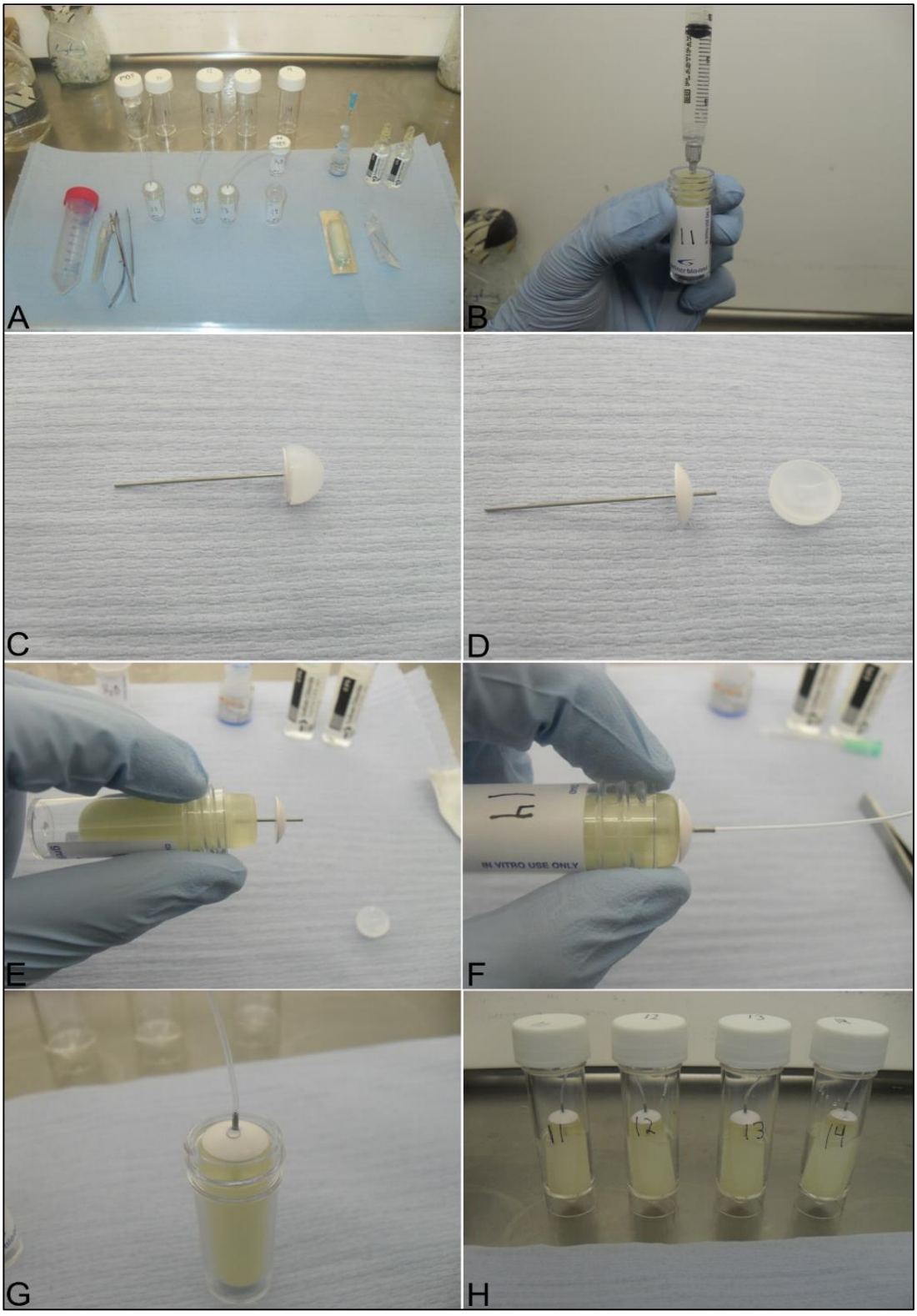

Figure 2.8: Sequence for mini-pump loading

Panel **A**. Preparation for pump loading in the hood laminar chamber. Panel **B.** The filling cannula attached to the syringe was inserted vertically into the pump. Panel **C** and **D:** Flow moderator with and without the plastic cab, respectively. Panel **E:** Partially inserted flow moderator into the pump. Panel **F:** Fully inserted flow moderator with a cannula attached. Panel **G:** Cannula glued with cyanoacrylate base solution. Panel **H:** Pumps in universal containers with 7ml of sterile NaCl 0.9%, ready for priming in incubator at 37°C.

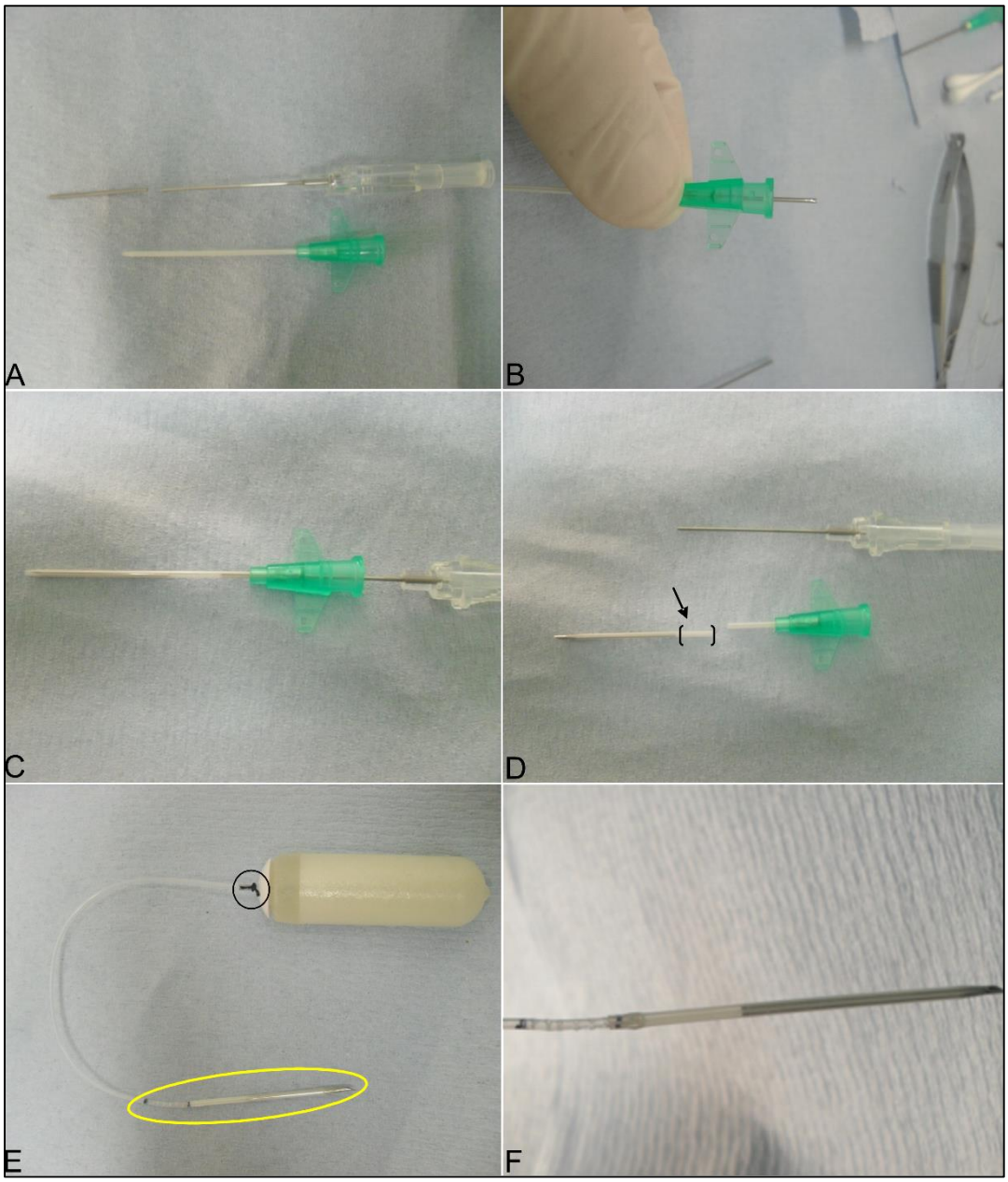

Figure 2.9: Sequence to prepare the cannula for renal insertion

Panel **A.** The needle is removed from the intravenous catheter and cut 3.5 cm from the cutting edge tip. Panel **B**. The needle is reintroduced in the cannula. Panel **C.** The needle is then pushed with the cut cannula until the sharp tip is 0.5cm out of the catheter. Panel **D.** Black arrow and brackets are showing 1 cm space between the blunt side of the needle and the end of the catheter. Panel **E.** The cannula is inserted into the 1cm space of the catheter (yellow oval). Knot embracing the cannula to the flow moderator (black circle). Panel **F.** Image magnification from yellow oval in panel E.

Osmotic Minipump Position

Using a left lateral abdominal incisional approach, a small window was created between skin and muscle (dorsal corner of the incision) using blunt dissection towards the back of the rat, aligned slightly left along the spinal thoracic processes. This manoeuvre allowed the creation of a subcutaneous tunnel to insert the osmotic mini-pump in the back of the rat (Figure 2.12, panel A and B). Subcutaneous blunt dissection was performed 7cm caudal of the lateral abdominal incision. The cannula was displayed forming a loop subcutaneously in the abdominal wall allowing the cannula to get into the abdominal cavity through the ventral corner of the muscular layer (Figure 2.12, panel from C to F. To avoid intra-abdominal displacement of the cannula, 3 single stitches were placed between the subdermal tissue and muscular fascia along cranial side of the loop. The purpose of displaying the cannula in this way was to avoid changing the natural position of the kidney when the cannula gets stretched during the daily activity of the rat. Furthermore, to avoid the subcutaneous displacement of the pump from the back of the rat towards the abdominal incision, a partial space narrowing using a continuous purse-string suture (allowing 1 cm diameter opening, smaller than the pump's diameter) was performed in between the cannula and the pump (Figure 2.12, panel G and H). The intention of avoiding displacement of the pump was mainly to avoid pushing the fixed intra-renal cannula, inducing possible renal torsions and potential positional reduction of renal blood flow. Wound closure was performed as described previously. After 3 days infusion of TG inhibitor or vehicle, left renal hilar clamping was performed as previously described (section 2.2.4) to induce renal warm ischaemia, Figure 2.11.

2.2.7. Urine collection, water/food intake and body weigh

The rats were placed in metabolic cages for 24 hrs to determine urine production and water intake (Figure 2.13). Terminal food intake was evaluated by subtracting the remaining food after 24hrs from the initial 75 grams of food previously placed in the food container.

To avoid protein degradation, the urine was collected and preserved in chilled plastic containers (ice block). The urine was collected, filtered using Whatman filter paper 3MM, aliquoted and stored at – 20 °C.

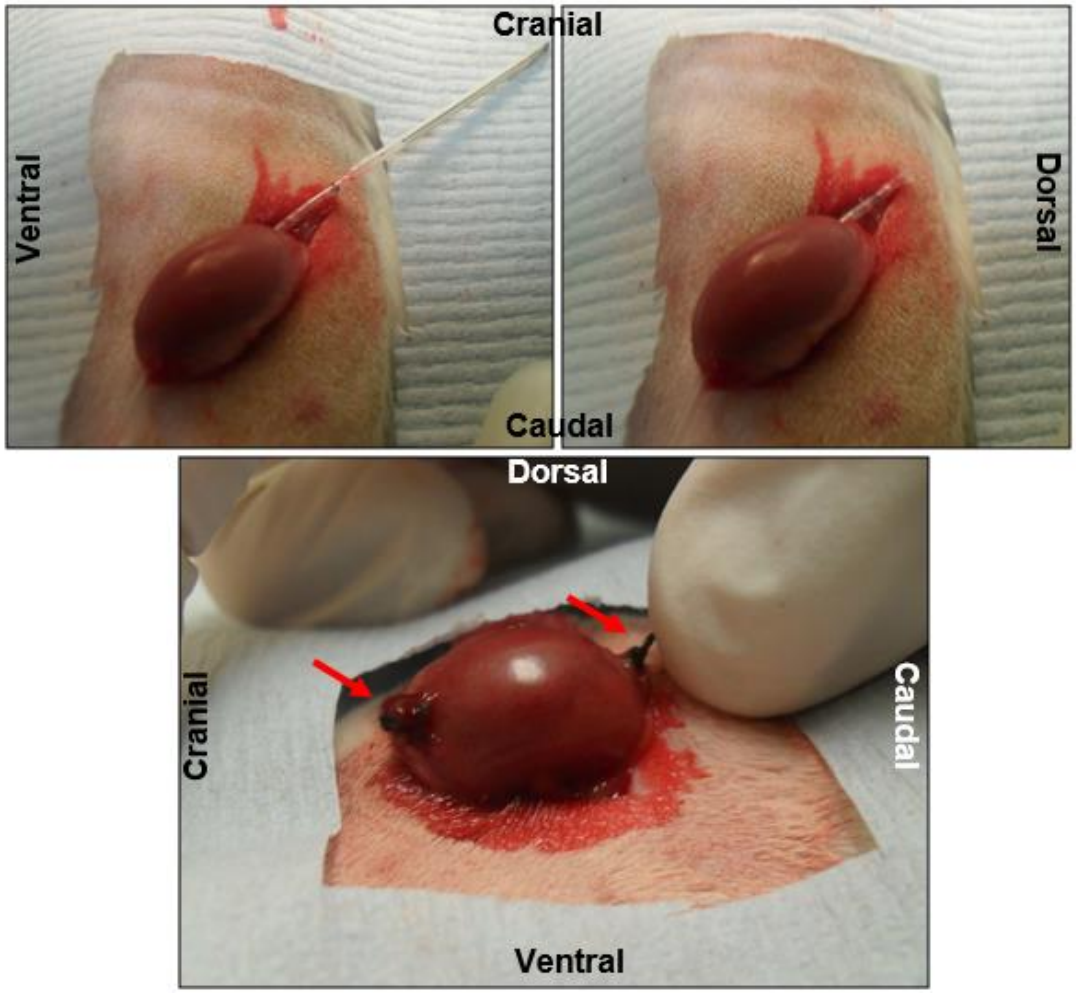

Figure 2.10: Intra-cannulation and fixation

Top left panel shows the cannula insertion from the caudal pole to the cranial pole of the left kidney using a modified catheter/needle as guide to insert the cannula along the kidney. **Top right panel** shows the cannula without the guide ready to be fixed. **Bottom panel** shows the fixation of the cannula by placing double knots of suture in the cannula (red arrows), cranial and caudal of the renal parenchyma. The text around the images (dorsal, ventral, caudal and cranial) indicates the lateral display of the rat on the surgical board.

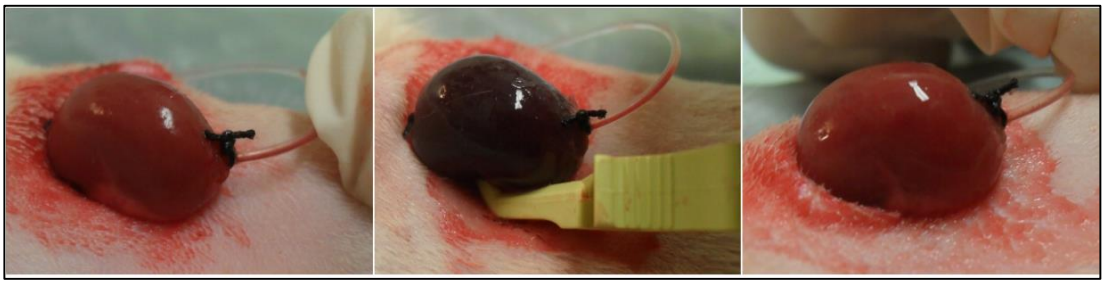

Figure 2.11: Colour of renal surface before, during and after renal warm ischaemia

Left panel shows the normal red colour in a cannulated kidney. **Middle panel** shows the dark brown colour after 60 minutes of renal warm ischaemia; black arrow indicates a microvascular clamp. **Right panel** shows the renal colour after reperfusion in a cannulated kidney.

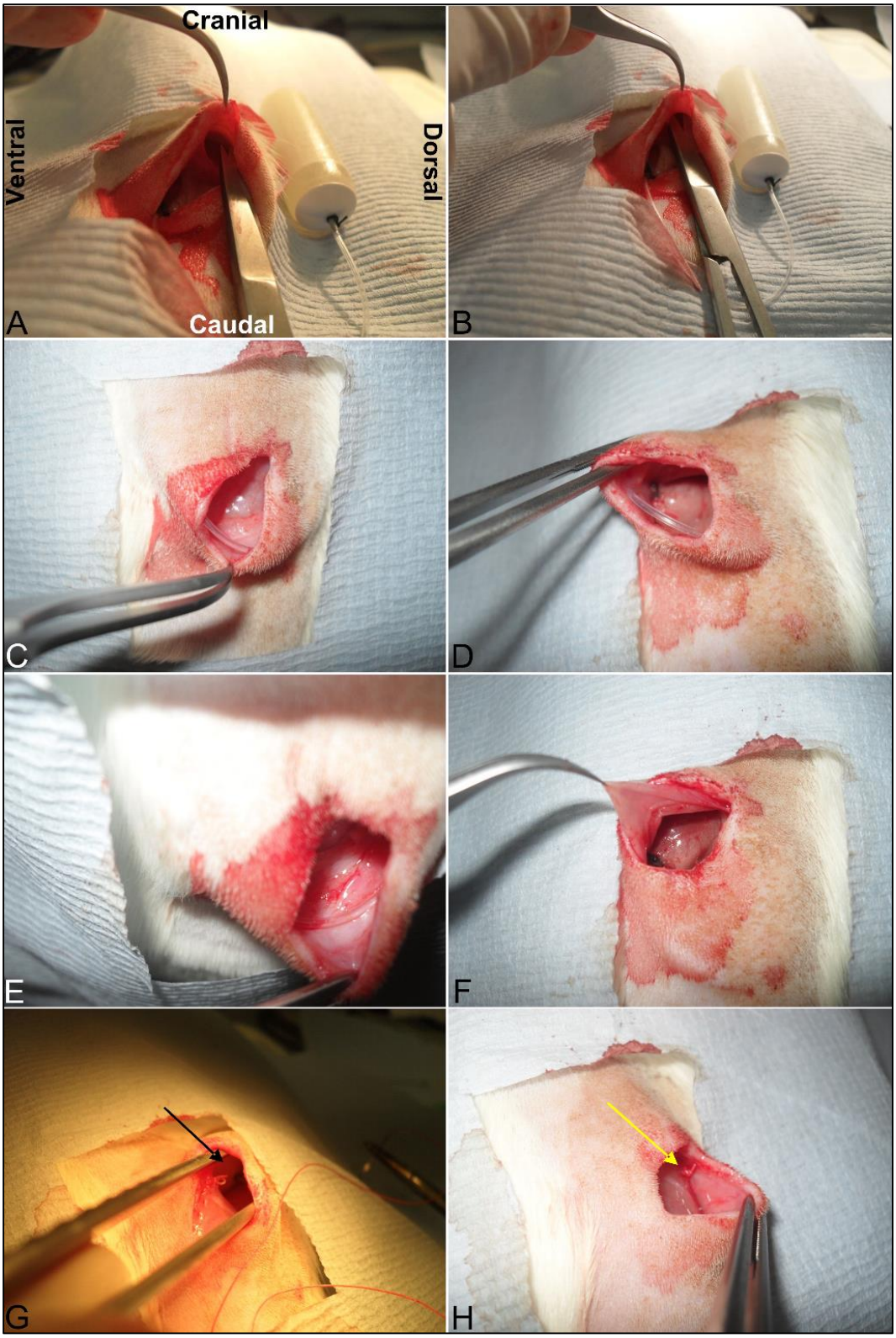

Figure 2.12: Subcutaneous positioning of osmotic pump

Panel **A** and **B.** Subcutaneous blunt dissection on the dorsal thorax to positioning an osmotic pump. Panel **from C to D.** Panel **E**. Display of the plastic cannula under the skin. Panel **F**. Position of kidney after cannulation, the cannula is displayed subcutaneously forming a loop. Panel **G.** Visualization of the plastic portion of the flow moderator (black arrow). Panel **H.** Partial narrowing of the pump exit using a continuous purse-string suture (yellow arrow).

Body weight monitoring was performed every 48 or 72 hours. The % of gained body weight was calculated by measuring the initial rat weight in grams before any surgical procedure (regarded as 100% body weight) and compared with the last recorded weight measurement.

2.2.8. Blood

For longitudinal blood sampling, rats were anesthetized as previously described (section 2.2.1). A butterfly needle (23G) was introduced into one of the collateral caudal veins obtaining approximately 500µl of blood. The sample was allowed to clot and then centrifuged. The serum obtained was aliquoted in eppendorfs (50µl) and stored at - 20°C. Terminal blood samples were collected by heart puncture through the diaphragm and centrifuged. Serum was aliquoted (100 µl) and stored at -20°C.

2.2.9. Systolic blood pressure

2.2.9.1. Principle

Systemic blood pressure (SBP) was measured using a tail cuff plethysmography. The tail cuff exerts pneumatic pressure on the base of the rat tail occluding the blood flow through an air inflation system cuff. The first pulse of the caudal collateral tail arteries was recorded while deflating the occlusion cuff. The data is captured photoelectrically from the tail cuff sensor and the signals are sent to the central amplifier (IITC life science BP amplifier) and codified to obtain the systemic systolic / diastolic blood pressure, mean and heart rate. The equipment to measure systemic blood pressure is shown in Figure 2.15.

2.2.9.2. Procedure

Each rat was placed in a pre-warmed rat restraint cage. A tail cuff sensor was placed in the base of the tail and screwed to the cage. Approximately after three minutes in the restraint cage, when the rat was quiet and calmed, the tail cuff was placed in the base of the tail (Figure 2.14), left panel and eventually covered with blue paper role. A warm environment was achieved by using heat lamp (Figure 2.14, right panel). Five readings per rat were carried out. This procedure was performed after 28 days of ischaemia reperfusion injury or every 28 days for the 5 months study. The time spent per rat was approximately 10 minutes.

Figure 2.13: Metabolic cages

White arrow shows the cage where the rat is placed. **Yellow arrow** shows the water container. Green arrow shows the food container. **Black arrow** shows the funnel to separate urine from faeces. **Blue arrow** shows ice block to store urine and faeces.

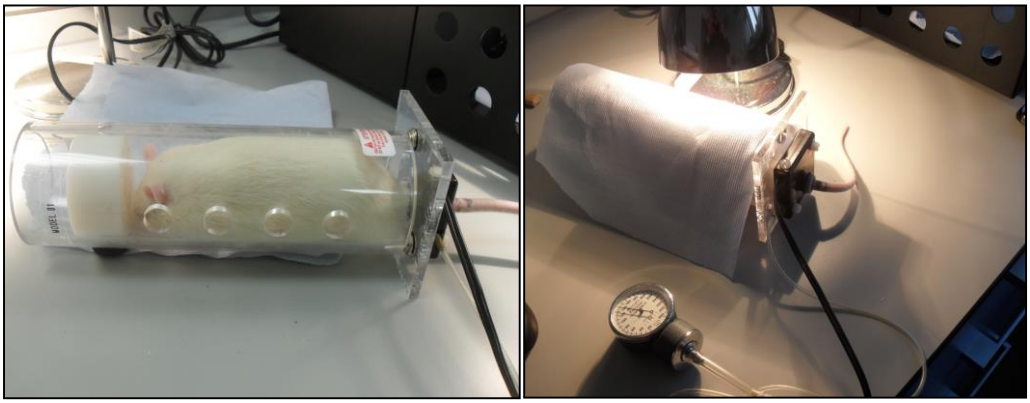

Figure 2.14: Systemic systolic and diastolic blood pressure procedure

Left panel shows a rat in a restraining cage with a tail cuff attached to the tail's base. **Right panel** shows the rat covered and warmed with the aid of a lamp.

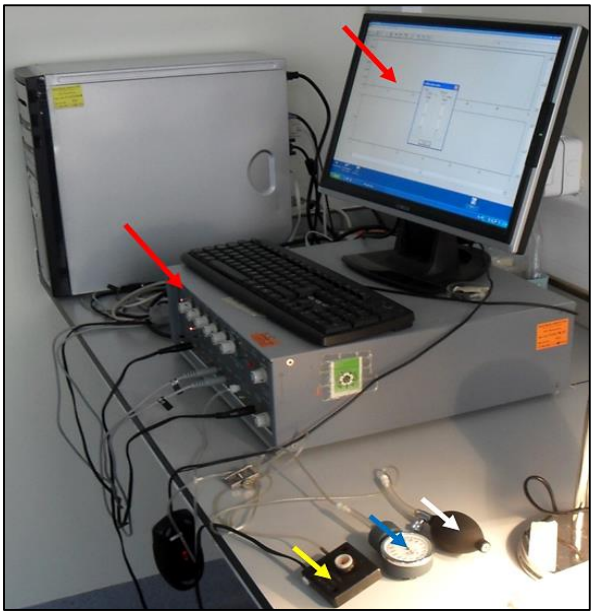

Figure 2.15: Equipment for systemic blood pressure in the rat

Red arrows show the monitor (top arrow) and central amplifier unit (bottom arrow). **Yellow, blue** and **white arrows** show a tail cuff sensor, a sphingometer to measure the pressure on the tail cuff and a pump to inflate the tail cuff, respectively.

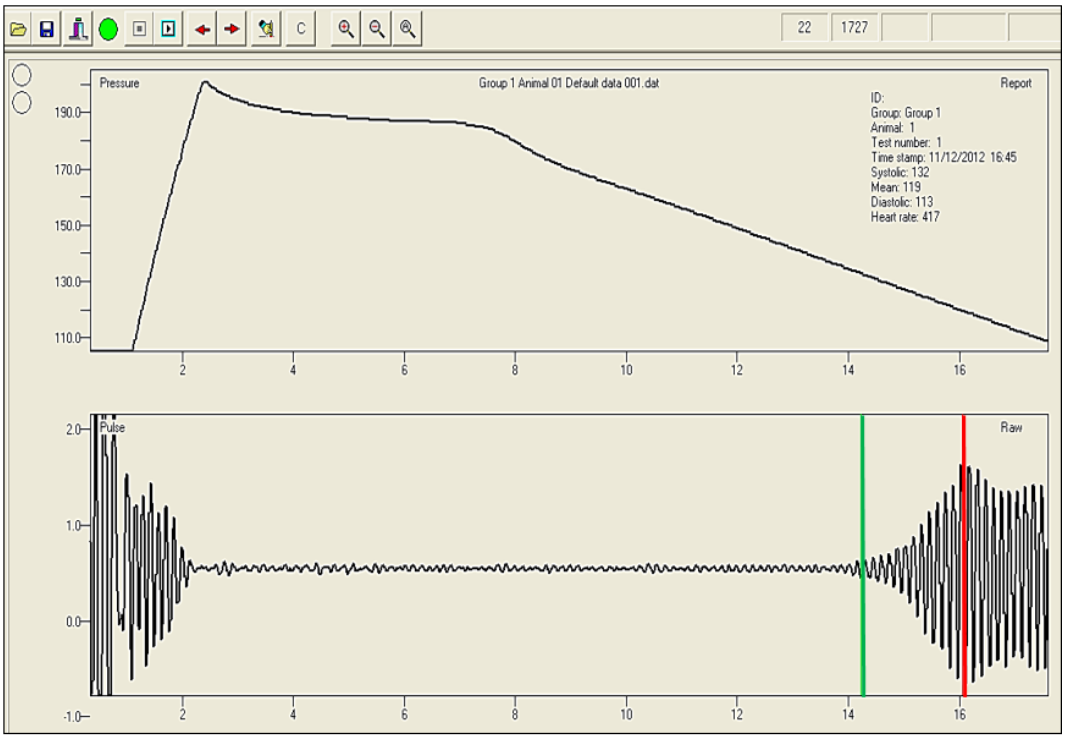

Figure 2.16: Telemetry for systemic systolic and diastolic blood pressure

Top linear graph represents the pressure (mmHg) exerted on the base of the rat's tail with a pneumatic tail cuff. **Bottom linear graph** represents the blood pulsation of the caudal collateral tail arteries. The **green line** represents systole and the **red line** represents diastole.

The results for each measurement were displayed on the blood pressure monitor (IITC software). The determination of systole and diastole was determined manually according to the chart recording. The green line (systole) was placed where the pulsation began. The red line (diastole) was placed where the pulsation wave expanded the most (Figure 2.16). The results were obtained by calculating the mean of the values excluding the highest and lowest measurements.

2.2.10 Kidney Tissue

At the end of the study the rats were anesthetized as previously described. A longitudinal incision was performed from xyfoids to pubis. The left kidney was sized, pictured and weight without renal capsule. The kidney was incised longitudinally from the convex to the concave side; afterwards each half was cut in the middle to obtain four pieces of tissue. One piece was placed in formalin 10% for 24 hrs and changed to PBS afterwards. The other three pieces were placed in cryovials and stored in liquid nitrogen.

2.3 Chemical Assays

2.3.1. Creatinine

2.3.1.1. Principle

Creatinine phosphate is a break-down product of muscle metabolism. Its production is constant depending on the muscle body mass. This catabolic product is used to estimate the glomerular filtration rate by calculating its renal clearance from measurements of creatinine in the serum and urine.

2.3.1.2. Procedure

Creatinine was analysed in urine and serum by the Jaffe rate method (Levey *et al.*, 1988), which utilises the colorimetric reaction between alkaline picrate and creatinine. The change in colour is quantifiable photometrically through absorbance readings at 520 nanometres (Bartels *et al.*, 1969; Fabiny *et al.*, 1971). The samples were run in a SYNCHRON ® System (Beckman Coulter Inc.) machine using CREm reagents (Beckman Coulter Inc.). The data was expressed in µmol/L and mmol/L for

serum and urine respectively. The measurements of creatinine in urine and blood were performed by the Department of Clinical Chemistry, Royal Hallamshire Hospital in Sheffield and supervised by Dr Martin Loxley. Cat samples were analysed by the Royal Veterinary College, Hatfield, UK. Assessment of serum creatinine was performed at day 0, 8 and 28 after, 56, 84, 112 and 140 of RWI according to each study.

2.3.2 Rat Albumin

2.3.2.1. Principle

Rat albumin was measured in urine by enzyme-linked immunosorbent assay (ELISA). A 96 well plate was coated with sheep anti-rat albumin antibody and the sample added to the plate. The secondary sheep anti-rat albumin antibody containing horseradish peroxidase (HRP) was then added followed by the enzyme substrate 3,3',5,5'-tetramethylbenzidine (TMB). The enzymatic colour reaction was proportional to the amount of secondary antibody bound to the primary antibody, which in turn, is bound to albumin. The optical signal was measured by spectrophotometry at 450 nm.

2.3.2.2. Materials

Coating buffer; 0.05 M Carbonate-Bicarbonate with a pH of 9.6; washing solution, 50mM Tris, 0.14 M NaCl, 0.05% Tween 20, pH 8.0; blocking solution, 50mM Tris, 0.14M NaCl, 1% BSA, pH8.0; sample/conjugate diluent: 50mM Tris, 0.14M NaCl, 1% BSA, 0.05% Tween 20, pH 8.0. For enzyme substrate and stopping solution 3,3',5,5'-tetramethylbenzidine (TMB) and 2 M H_2SO_4 were used, respectively.

2.3.2.3. Procedure

For coating with capture antibody and blocking, 100µl of sheep anti-rat albumin (Lot A110-134A-2, BETHYL, 30mg/ml) were diluted in 10ml of coating buffer to pipette from the final solution 100µl in each well. The plate was incubated for 60 minutes at room temperature and washed. The washing procedure was repeated three times. 200µl blocking solution was added, incubated for 30 minutes and washed 3 times. The standards were diluted in sample diluent according to the chart provided by the manufacturer (Rat reference Serum, Lot: RS10-100-4, BETHYL). Control group samples (Nx) were diluted from 1:500 to 1:128,000; disease group samples (RWI)

where dilute from 1:2,000 to 1: 1,024,000. 100µl of the diluted samples and standards were added to their specific wells and incubated for 60 minutes. Afterwards, the plate was washed 5 times.

For HRP detection a sheep anti-rat albumin HRP conjugated (Lot A110-134P-10, BETHYL) was diluted 1:10,000 in sample conjugate and 100µl pipetted in the wells followed by 60 minutes incubation. Later, the plate was washed to remove the unbound antibody-enzyme conjugate. For the enzyme substrate reaction, a tablet of 3,3',5,5'-tetramethylbenzidine (TMB) was diluted in 1ml dimethyl sulfoxide (DMSO). Once the tablet was dissolved, 9ml of phosphate buffer was added together with 2µl hydrogen peroxide (H_2O_2). 100µl substrate buffer was added to each well, and the plate incubated for 10 minutes at room temperature. The colour reaction was stopped by adding 100µl 2M H_2SO_4. The plate was read at 450nm. A standard curve is shown in Figure 2.17. The concentration of albumin in the urine was expressed in milligram/millilitre. Assessment of urine albumin was performed at day 0, 8 and 28 after, 56, 84, 112 and 140 of RWI according to each study.

2.4 Kidney Histology

2.4.1. Haematoxylin and Eosin

2.4.1.1. Principle

Haematoxylin and eosin (H & E) is considered the gold standard staining for medical diagnosis. The staining consists in the oxidation of haematoxylin, which produces aluminium ions and haematein, staining in blue nuclei of cells, keratohyalin granules and calcium-based material. The blue nuclear staining is due to binding of the dye-metal complex to DNA. Other colour shades such as pink, red and orange are achieved by using an aqueous or alcoholic solution of eosin Y. H & E staining was performed by Fiona Wright, from the Academic Nephrology Unit, Medical School-the University of Sheffield.

2.4.1.2. Procedure

5µm paraffin embedded sections were deparaffinized and rehydrated using a standard protocol; 100% xylene (10 minutes); 100% ethanol (5 minutes); 90% ethanol

(5 minutes); 70% ethanol (5 minutes). After that, haematoxylin nuclear staining was applied in the sections and rinsed in tap water getting a blue colour. To remove the excessive background stain (differentiation step), a weak acid alcohol was used and sections were rinsed again. Later on, the eosin counterstain was applied. Slides were passed through several changes of alcohol to remove traces of water and then rinsed in several baths of xylene to clear the tissue. The slides were mounted in DPX mountant for histology.

10 sections containing glomeruli (1 glomerulus per section) and tubules (4-5 transverse tubules per section) per rat kidney were assessed by measuring the diameter of the Bowman's capsule and tubules in μm (vertical and horizontal red lines) and the internal area of the Bowman's capsule and tubules in μm^2 (red line enclosing intra capsular and tubular white space), see Figure 2.18. The quantification of measurements was determined by the mean diameter in μm and area in μm^2 of 10 sections per tissue sample.

2.4.2 Periodic acid Schiff & Haematoxylin

2.4.2.1. Principle

The periodic acid Schiff and Haematoxylin (PASH) protocol is based on the demonstration of extracellular polysaccharides such as glycogen and collagens through an oxidative process (Thompson, 1966). It also allows the detection of mucosubstances such as glycoproteins, glycolipids and mucins. The oxidation results in the formation of aldehyde grouping through carbon to carbon bond cleavage. The dialdehyde compound is then detected by the Schiff reagent. The purple-magenta colour is the result of the restoration of the quinoid chromophoric group.

Haematoxylin on the other hand, which is obtained from the log-wood tree, is a dye called haematein that is used in combination with aluminium ions. It stains acidic / basophilic structures giving to the nucleus a purplish colour. DNA and RNA are both basophilic. Eosin is a negatively charged acid dye, which stains basic or acidophilic structures in red or pink. Eosinophilic or acidophilic structures includes filaments in muscle cells, intracellular membranes and extracellular fibres.

2.4.2.2. Procedure

Kidneys were fixed in 10% neutral-buffered formalin and evaluated by a specialist veterinary pathologist (Dr Cathy Brown – University of Georgia) masked of all clinical history. Paraffin-embedded sections (3µM) were stained with haematoxylin and eosin (HE). A second section was stained with haematoxylin and periodic acid-Schiff, for morphometric evaluation.

Glomerulosclerosis scoring system ranged from 0 to 3 (Hughson *et al.*, 2002). Twenty five glomeruli per sample (600x) were evaluated for the degree of mesangial matrix expansion. Score 0 = matrix encircling no more than 1 nucleus (no fibrotic tuft); 1 = matrix could surround several nuclei but no extended to the peripheral capillary loops (between 1% to 25% fibrotic); 2 = moderate matrix expansion involving peripheral capillary loops affecting less than 50% of the glomerulus (between 26% to 50% fibrotic tuft); 3 = moderate matrix expansion affecting more than 51% to 75% of the glomerulus. The score for each glomerulus was averaged and divided by the number of glomeruli measured. % obsolescence index was determined by counting all glomeruli in two 70-mm^2 fields and recording the number that were obsolescent. Obsolescent glomeruli (score 4, matrix expansion affecting > 75% of the glomerulus) and the obsolescence index was combined with the mean glomerular score using the following formula: combined glomerular score = 0.04 **x** obsolescence index **+** mean glomerular score **x** (1 – obsolescence index/100) (Hughson et al., 2002).

Tubulointerstitial fibrosis and inflammation scoring system ranged from 0 to 3 with 0.5 intervals (Chakrabarti *et al.*, 2013). Score 0 = no fibrosis/inflammation or rare small foci; 1 = mild or scattered multifocal areas of fibrosis/inflammation affecting less than 5% of the tissue section; 2 = moderate fibrosis/inflammation affecting 25% to 50% of the section; 3 = diffuse or coalescing fibrosis / inflammation affecting more than 50% of the section (Chakrabarti et al., 2013).

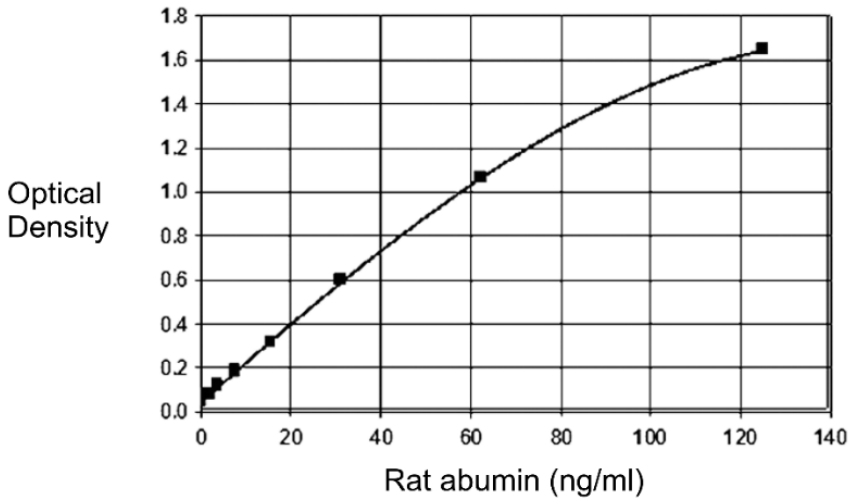

Figure 2.17: Standard curve used to calculate ng/ml of albumin

The Y axis represents the optical density (absorbance reading at 450 nm). The X axis represents the albumin concentration, Standard curve and albumin concentrations detected using a spectrophotometer.

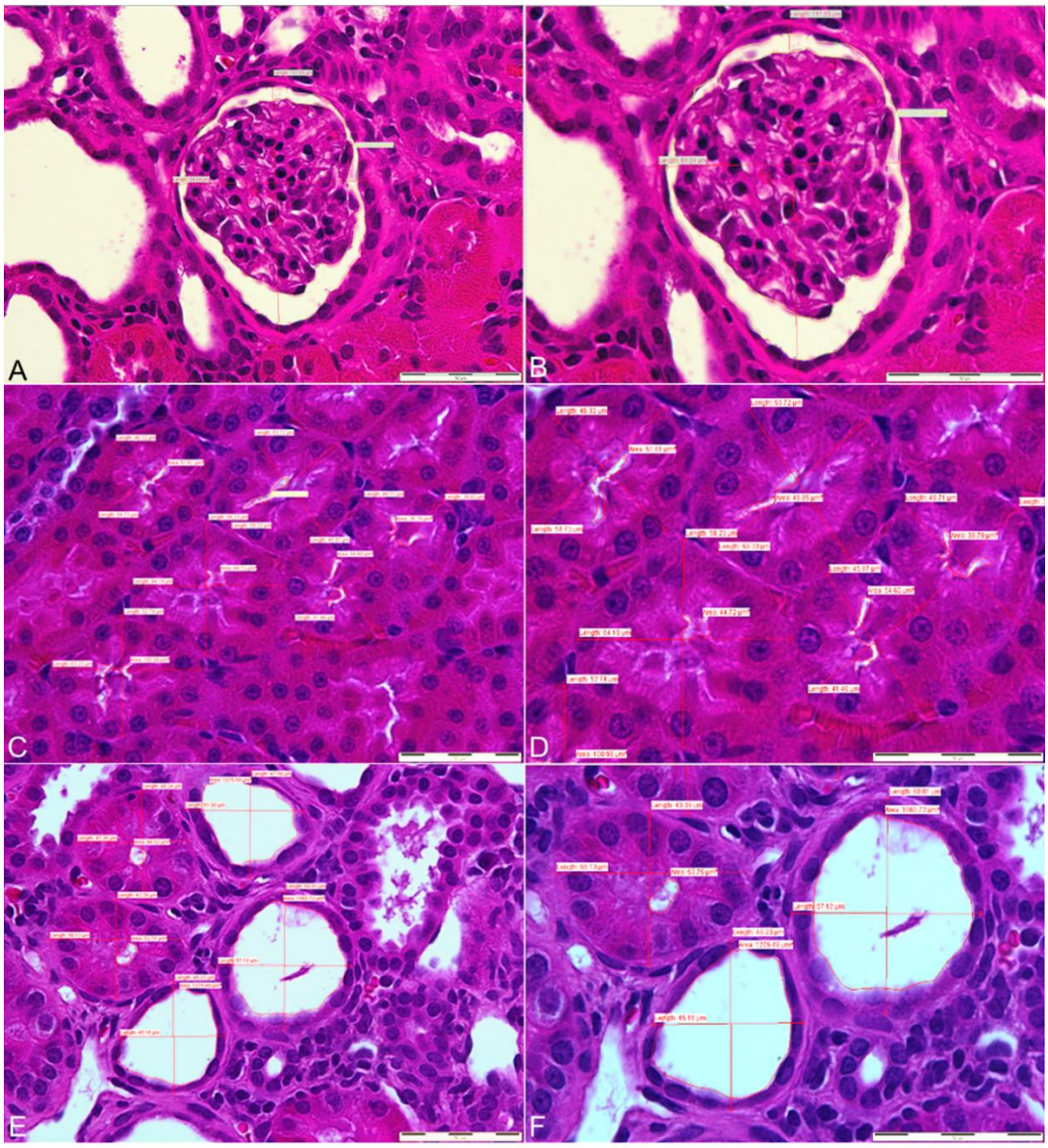

Figure 2.18: Glomerular and tubular histomorphometry

Panels **A**-**B**, **C**-**F**. Representative images of glomeruli and tubules, respectively, under 400x (**A**, **C** and **E**) and 600x (**B**, **D** and **F**) magnification. Panels **A**-**B**, show measurements for glomerular diameter (vertical and horizontal red lines) and Bowman´s capsule (yellow line enclosing the white Bowman's area). Panels **C**-**F**, show intratubular area (red line enclosing the intratubular white space) and tubular diameter (vertical and horizontal red lines transecting transverse tubules) measurements and structural differences between Nx (**C** and **D**) and RWI tissue samples (**E** and **F**).

2.4.3 Masson's Trichrome

2.4.3.1. Principle

This technique stains the extracellular matrix (mainly collagen proteins) in blue; therefore, blue colour correlates with the degree of kidney fibrosis. MTS can also stain in pink/red cytoplasm, nuclei in dark blue / black; therefore, erythrocytes, epithelial, endothelial, mesangial and infiltrated inflammatory cells can be stained. The quantification of the colours can be achieved using multiphase image analysis allowing the identification of specific shade of colours.

2.4.3.2. Materials

Bouin's solution; working Weigert's iron haematoxylin solution; Biebrich scarlet-acid fucshin, aniline blue solution (Sigma-Aldrich, UK), distyrene / plasticizer / xylene media (DPX) from BHD England and cold ice acetone were employed for this technique.

2.4.3.3. Procedure

5µm paraffin embedded sections were deparaffinized and rehydrated by using a standard protocol; 100% xylene (10 minutes); 100% ethanol (5 minutes); 90% ethanol (5 minutes); 70% ethanol (5 minutes). The slides were placed in Bouin's solution overnight at room temperature and washed in tap water until no yellow colour was detected. The slides were placed in working Weigert's iron haematoxylin solution for 5 minutes (rinsed in deionized water), Biebrich scarlet-acid fuchsin, working phosphotungstic/phosphomolybdic acid and aniline blue solutions followed by 1% acetic acid for 2 minutes. The slides were dehydrated by rinsing them for one second in 70% ethanol, 90% ethanol and 100% xylene and mounted in DPX (Johnson *et al.*, 2007).

2.4.3.4. Quantification

Intra-glomerular mesangial area (IGMA): Using a CC-12 digital camera (Imaging Systems, Germany), a minimum of 10 IGMA fields (400x) were assessed. The assessed area was delimited by centring a squared frame on the glomerular tuft, excluding glomerular parietal epithelial cells and Bowman's capsule. Measurements

were achieved by multiphase image analysis (Cell F, Olympus, Software Digital Image System, USA). The analysis of blue, red and white colour was performed using 3 different colour phases. Indigo blue was used to highlight blue staining (extracellular matrix), green for red/pink staining (cellularity) and black to isolate white colour (free space), see Figure 2.19, panels A and D. 96% of colour coverage per image was required as minimum to assure the images were being properly evaluated.

Tubulointerstitial space: For cortical tubulointerstitial space, at least 12 cortical fields were acquired (200x). The image analysis was performed as described before, Figure 2.19, panels C and D. For either the glomerular or tubulointerstitial space, the ratio of ECM to cell volume was calculated by dividing the percentage of indigo blue (ECM) between % of green (cellularity) as described by Johnson et al (2007). In the cat study, the area of positive stain was expressed as a percentage of the total field.

2.5 Kidney Homogenates

2.5.1. Homogenization

2.5.1.1. Principle

Tissue homogenization is a process where a tissue sample is brought to a state such that all fractions of the same sample are equal in composition. The mechanical action of tissue homogenization together with hyperosmotic solution used to preserve proteins promotes cell membrane disruption. This allows an accurate measurement of protein and enzymatic activity for both intra and extracellular compartments.

2.5.1.2. Materials

Protease inhibitors, solutions and equipment used are displayed in Table 2.1.

2.5.1.3. Procedure

A portion of kidney tissue is cut, weighted and chopped. If 1 gram of tissue is obtained, this is suspended in 9 ml of STE + 1 tablet protease inhibitor in a 15 ml centrifuge tube (10% tissue homogenate).

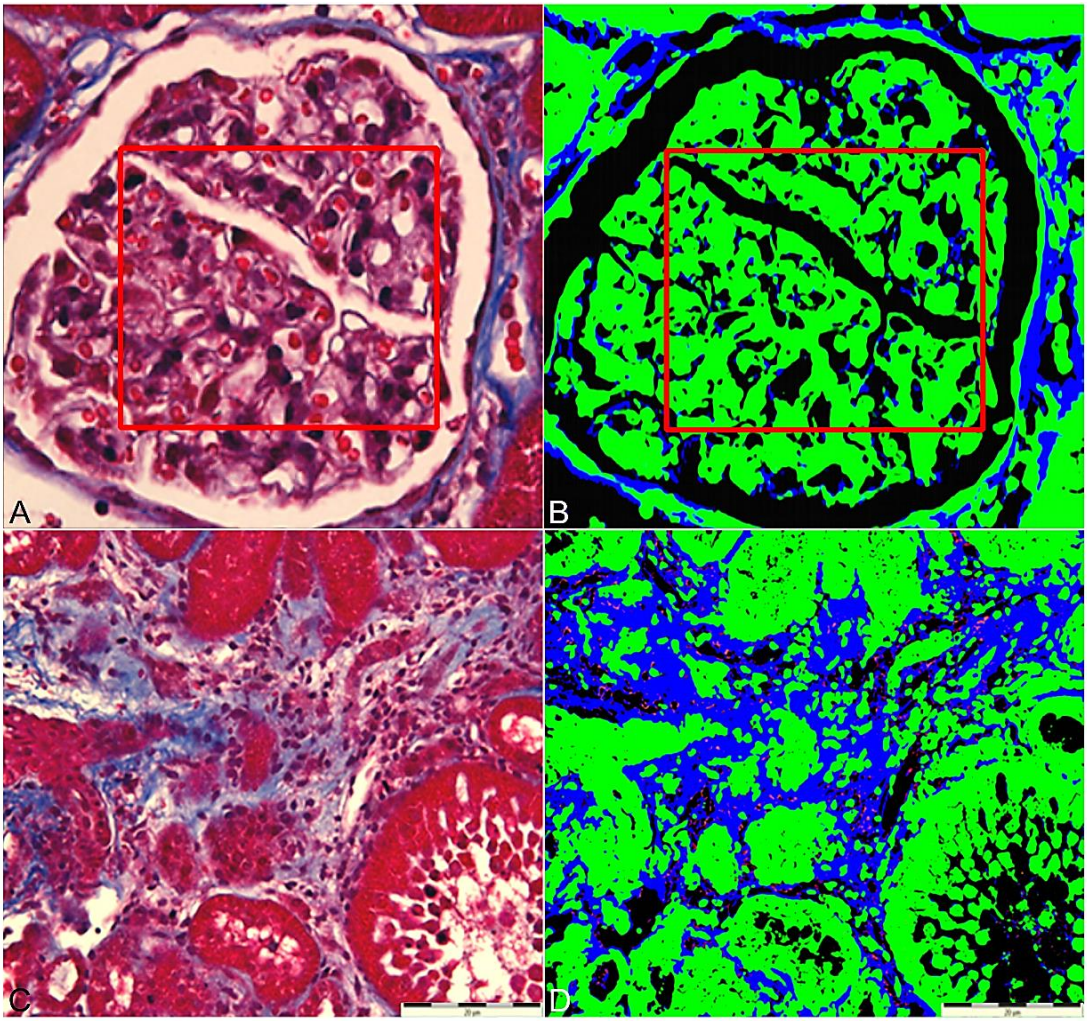

Figure 2.19: Masson's trichrome staining image analysis

Panels **A** and **C** show representative images of diseased glomeruli and tubulointerstitial space, respectively. The intra-glomerular mesangial area (IGMA) is delimited by a red square. **Panels B** and **D** are examples of multiple colour substitution from panels A and C, respectively; blue (extracellular matrix) is highlighted in indigo-blue; red (cellularity) in green and white (free space) in black.

The centrifuge tube is placed on a box with flaked ice. The tube is half embedded in liquid nitrogen for 2 seconds followed by the homogenizer probe introduction and homogenization of tissue for no more than 10 seconds, 3 times and 24000 rpm. For each time, the homogenate is cooled down in liquid nitrogen for two seconds. Between homogenization of different tissue samples the homogenizer probe is thoroughly rinsed. 1 ml of homogenate is pipetted in an eppendorf previously load with stainless steel beads. Eppendorfs are placed in the bullet blender in the cold room setting the controls for speed 8 during 5 minutes and centrifuged for 10 seconds to remove burrs of metal beads and non-homogenized tissue. See Figure 2.20.

2.5.2 Kidney Protein

2.5.2.1. Principle

The assay is based on the reaction of proteins with an alkaline copper tartrate solution (reagent A) and folin reagent (reagent B)(Lowry *et al.*, 1951). The mixture of reagent A with B into the protein samples allows the reaction between protein and copper at alkaline pH, with the subsequent reduction of Folin regent by the copper-treated protein. The development of the yellowish colour in the samples is due to the reaction with the amino acids tyrosine and tryptophan; however, other aminoacids, cysteine, cysteine and histidine, contribute to a less extend.

2.5.2.2. Materials

Protease inhibitors, solutions, hardware and software used are displayed in Table 2.2.

2.5.2.3. Procedure

Serial dilutions of BSA were prepared (0.2-1.5mg/ml) starting with 1.5mg/ml in a microplate (96 wells) in STE + protease inhibitors. 5µl of standards or samples were pipetted into the wells. 25µl of working reagent A was pipetted to each well and mixed thoroughly using a microplate mixer. After that, 200µl of reagent B was added into each well with the subsequent microplate agitation. The microplate was incubated at room temperature for 5 minutes and then measured absorbance at 750nm.

Figure 2.20: Equipment and process of tissue homogenization

Panel **A**. Homogenizer and probe, yellow arrow. Panel **B**. Homogenizer settings, revolutions per minute. Panel **C**. Styrofoam box with a 15 ml centrifuge tube (right black arrow) on flaked ice. Dewar for liquid nitrogen, right arrow. Panel **D**. Two tubes with homogenized tissue from different samples using a probe homogenizer. Arrow showing matrix tissue sediment. Panel **E**. Stainless steel beads for bullet blender homogenizer. Panel **F**. Beads in eppendorf ready to be loaded with 10% tissue homogenates. Panel **G** and **H**. Bullet blender. Panel **I**. Samples from Panel **D** after homogenization with bullet blender.

2.5.3 Transglutaminase Enzyme Activity

2.5.3.1. Principle

This technique is based on the incorporation of a radioactive (3H) amine substrate (putrescine) into an acceptor protein (dimethylcasein), as described previously (Lorand *et al.*, 1972). Both elements are transglutaminase substrates, which bond between each other by transglutaminase protein activity in the tissue homogenate. The tissue homogenization itself and the STE buffer used for homogenization break up the membrane cell by both physical and osmotic mechanisms, respectively. Hence, the measurement of activity in this assay covers the intra and extracellular compartments. The activation is triggered by adding calcium chloride and dithiothreitol (DTT) to the mixture. Once activated, the mixture is incubated at body temperature during different time points and placed in small squares of filter paper. The filter paper is embedded in trichloroacetic acid to stop the reaction and to promote protein precipitation. The filter paper is placed in ethanol and then air dried. The paper is placed in tubes with scintillation fluid to enhance radioactivity detection from the scintillation machine. The incorporation of labelled groups into proteins by the transglutaminase activity are attached and/or embedded into the filter paper, therefore, the radioactivity detected by the scintillation machine counter is the protein precipitated on the paper.

2.5.3.2. Materials

Materials for TG activity by 3H-putrescine assay are displayed in Table 2.3

2.5.3.3. Procedure

Kidney homogenates (10% w/v) in STE buffer and protease inhibitors were incubated (37˚C) with 60mM 3H-putrescine (65Ci/mmol), 40mM dithiothreitol, 25mg/ml NN'-Dimethylcasein, 25mM $CaCl_2$ in a final volume of 50 µl. Recombinant rat TG2 1:1000 was used as the positive control. Negative controls were obtained using either the 50 µM of TGI (D003, Zedira, Germany) or 100mM EDTA. 10µl of the mixture was spotted into 3 mm filter paper at 0, 5, 10, 20, and 60 minutes and precipitated with cold 10% and 5% trichloroacetic acid, 5 minutes (2x) and 10 minutes (4x) respectively. The filter papers were placed washed twice in 100% ethanol for 5 minutes. The filter papers were dried off over night at room temperature. The

precipitated protein was determined by scintillation counting, Figure 2.21. The EDTA controls were subtracted from the samples values. One unit of TG activity was equivalent to 1nmol of 3H-putrescine incorporated per hour at 37˚C. The results were expressed units per mg of protein. Unit of activity is equivalent to 1nmol of putrescine incorporated per hour at 37°C. The technique was performed as described previously.

2.5.4 Transglutaminase Protein

2.5.4.1. Principle

Western blot is a technique to detect and quantify specific proteins in tissue homogenates. It uses gel electrophoresis to separate proteins by structure and molecular weight (Laemmli, 1970). Once the proteins are separated, these are transferred to a polyvinylidene difluoride membrane. The proteins in the membrane are targeted using a primary and secondary antibody. The secondary antibody is linked to a reporter enzyme. The enzymatic chemiluminescent signal is triggered when exposed to appropriate substrates. The chemical signal is detected by a high resolution / sensitivity camera. The signal is quantified by image analysis.

2.5.4.2. Materials

Powders, solutions, antibodies, control antibodies, control proteins, software and hardware used are displayed in Tables 2.4a and 2.4b.

2.5.4.3. Procedure

Cat and rat kidney homogenates (10% w/v) in STE buffer were separated on a 10% polyacrilamide gel (27µg/lane), transferred (14v, cold room) overnight to PVDF membrane, washed and blocked with 10% skimmed milk. Human recombinant TG2 was used as a positive control. For negative controls an unspecific antibody to TG2, IgG and serum were employed. The blot was probed with a primary antibody and revealed using a secondary polyclonal HRP antibody. Chemiluminescent blots were captured by a ChemiDoc MP Image System. Determination of molecular weight was performed by comparing the colour bands in the blot (molecular weight marker) with the bands obtained in the enzymatic reaction using the ChemiDoc Image System Software, Figure 2.23. Results were shown as optical density mm^2 per µg of protein.

Figure 2.21: Scintillation machine counter

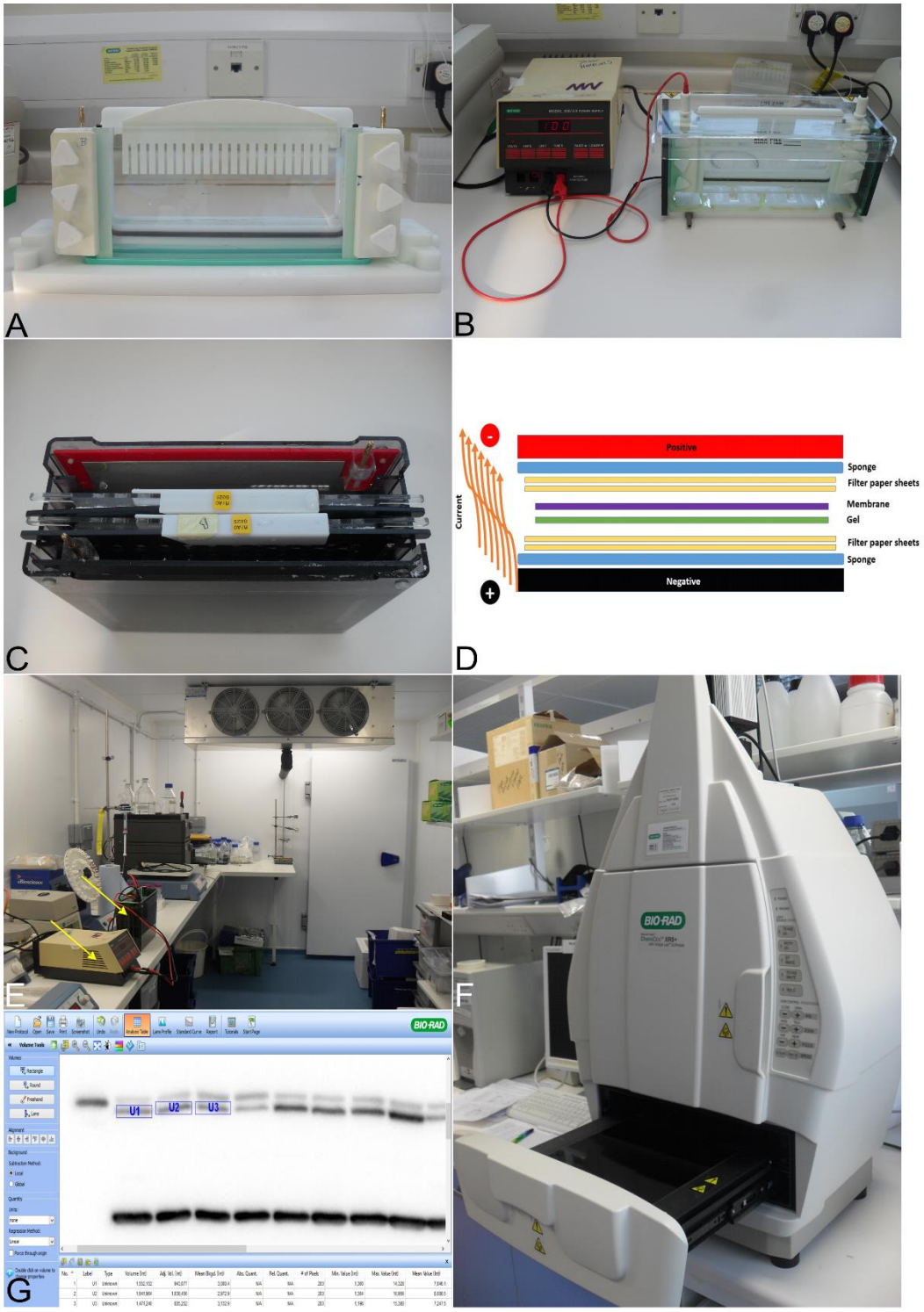

Figure 2.22: Western blot basic equipment

Panel **A**. Dual gel caster. Panel **B**. Power source (left) and buffer tank (right). Panel **C**. Transfer tank loaded with cassettes. Panel **D**. Order of material in a transfer cassette. Panel **E**. Power source and transfer tank in a cold room, lower and upper yellow arrow respectively. Panel **F**. Chemidoc machine. Panel **D**. Chemidoc software for protein quantification.

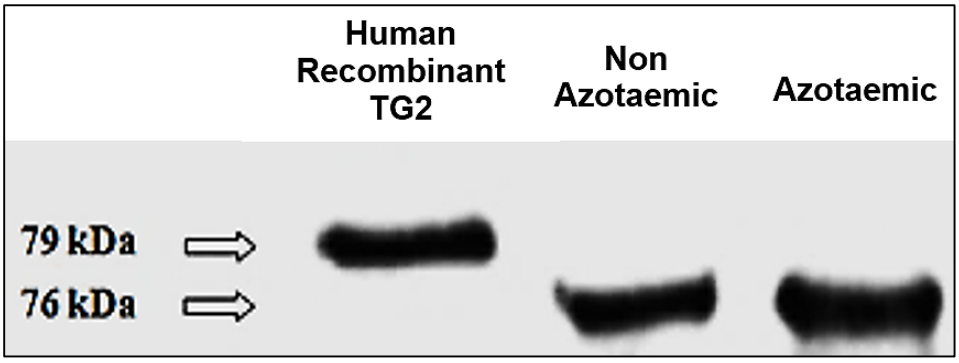

Figure 2.23: Representative Western blot for transglutaminase 2

Representative kidney tissue homogenates from cats with and without azotaemia. The samples were immunoprobed with a mouse monoclonal TG2 antibody BB7, using human recombinant TG2 as positive control. From left to right, human recombinant TG2 shows a band of 78-79 kDa, whereas both the normal function and CKD cat tissue show a band of 75 and 66 kDa. 66kDa bands possible inactive fragments of TG2.

2.6. *In situ* assays

2.6.1. Immunofluorescence

2.6.1.1. Principle

A primary antibody binds on a specific tissue protein; afterwards, a secondary antibody labelled with a fluorochrome binds to the primary antibody. Subsequently, an optical microscope is used to quantify the amount fluorescence from the secondary antibody. The microscope emits fluorescent light with a specific wave length which in turn excites the fluorochrome attached to the secondary antibody, emitting light captured by the microscope receptors. The quantification is performed applying the same bases as described for MTS technique.

2.6.1.2. Material

To make up the washing buffer, a tablet of protease inhibitor cocktail (Complete Mini, Roche Diagnostics, GmBH, Germany) was dissolved in 10 ml of PBS + 0.1% Triton X-100. For blocking buffer, 5% goat serum was added to 5ml of washing buffer. Primary and secondary antibodies used in the cat and in vivo studies are displayed in Table 2.5.

2.6.1.3. Procedure

8µm thick cryostat sections on adherent slides, previously stored at -80°C were placed in an incubator chamber at 37°C for 10 minutes. The slides were ringed with a paraffin pen marker to avoid spillage of reagents.

Primary antibody. 50µl blocking buffer was added to the slides incubating them for 10 minutes. The solution was removed by tilting the slide over a tissue paper. The tissue samples were washed with 50µl washing buffer followed by 5 minutes incubation at room temperature with the subsequent removal of solution. This procedure was performed two more times. The primary antibody was diluted in blocking buffer. 50µl were added and incubated in a humidity chamber overnight at 4°C. For controls, blocking buffer without primary antibody and unspecific primary antibody to the protein in analysis (e.g. Collagen IV when looking for TG2) were used in some sections.

Fixation. The slides were washed twice in blocking buffer as described before and placed in cold acetone for 10 minutes in a -20°C and air-dried was allowed. The sections were washed using PBS for two more times.

Secondary antibody. The secondary antibody was diluted in PBS + 3% bovine serum albumin (w/v). 50µl was added to the slides with subsequent incubation in a humidity metal tray placed on a dark room for 2 hours. The slides were washed 3 times with PBS and air dried. Finally, a drop of mounting medium with DAPI was added (MOWIOL + DAPI) to stain nuclei in blue and covered with a cover slip. The slides were left in a dark place at room temperature overnight. Sections were analysed using an optical microscope (BX61 Olympus) with the appropriate UV filter. The sections were covered with foil and stored at -20°C for subsequent analysis.

2.6.1.4. Quantification

No less than 10 or 15 fields were randomly pictured for IGMA (400x) and cortical tubulointerstitial space (200x), respectively (Olympus Systems, F-view II digital camera). The quantification of Alexa red (red), FITC (green) and DAPI (blue) was performed using 2 different colour phases. Yellow or white were used to highlight the brightest red or green signal, respectively, depending on the secondary antibody fluorochrome; whereas green or red were used for quantification of DAPI staining,

see Figure 2.25. The analysis a 96% of colour coverage per image was required as minimum to assure the images were being evaluated properly using white to cover the black space. For either IGMA or tubulointerstitial space, the ratio of collagens or TG2 to cell number was calculated by dividing percentage of yellow (collagens or TG2 expression: green or red fluorescent signal, respectively) between the percentage are of green (DAPI: fluorescent blue staining) (Huang *et al.*, 2009). In the cat study, the area of positive stain was expressed as a percentage of the total field instead of ration of protein target to cell number. Equipment for image analysis is displayed in Figure 2.24. Examples for protein quantification by image analysis are shown in Figure 2.25.

2.6.2. TG Activity assay

2.6.2.1. Principle

The technique is based on the incorporation of a fluorescent TG substrate (cadaverin) into the endogenous TG substrates in the cryostat section such as collagens. The binding of substrates is performed by the endogenous transglutaminases localized in the extracellular space. The section is incubated with biotinylated cadaverin. The activation is triggered when calcium chloride and DL-Dithiothreitol (DTT) are added to the section. The catalysed reaction attaches the biotinylated cadaverin to the tissue section. Later on, the slide is incubated with a fluorescent fluorochrome attached to streptavidin. Streptavidin and biotin have a high affinity between each other; therefore, the fluorochrome labelled streptavidin attaches to biotin working as a fluorescent tag for TG activity. The more fluorochrome is detected the more activity is present. This technique was performed as previously described (Johnson *et al.*, 1999).

2.6.2.2. Material

The main material is displayed in Table 2.6a. Rehydration buffer and washing buffer reagents are displayed in Table 2.6b. Reaction buffer and controls reagents are shown in Table 2.6c.

2.6.2.3. Procedure and quantification

Cryostat kidney sections (8µm) were rehydrated and incubated 30 minutes at room temperature. The slides were washed up twice. The sections were incubated 1h at 37°C with the reaction buffer. Three controls were set up by incubating some sections with either 10mmol/L EDTA, 200 µmol/L of TGI (DOO3, Zedira, Germany) or anti-TG2 mouse monoclonal antibody, 1:50. Sections were washed twice, fixed with cold acetone for 10 minutes in a -20°C freezer, air dried and blocked with 3% BSA in PBS at 4°C overnight. The sections were washed twice, probed with Alexa labelled streptavidin 1:300 in 3% BSA / PBS and incubated 2h at 37°C. Sections were washed in PBS and mounted using MOWIOL-DAPI mounting media. IGMA and tubulointerstitial fields were pictured and quantified as described for the immunofluorescent techniques. Examples for TG activity and protein quantification by image analysis are shown in Figure 2.26.

2.7. Statistical analysis

2.7.1. Cat study

Data analysis and presentation were performed using Prism 5 software (GraphPad). The cross-sectional data was analysed by unpaired two-tailed Student's t-test with Welch's correction. To evaluate group correlations, r^2 was calculated by linear regression analysis. The statistical significant level was defined as $P<0.05$.

2.7.2. *In vivo* studies

Longitudinal measurements were assessed using two way analysis of variance (two-way ANOVA); whereas the cross sectional measurements were analysed by both unpaired t test (for two groups) and one way ANOVA (more than two groups) followed by Bonferonni's multiple comparisons test to compare more than two groups. To assess correlations between different experiments, analysis r^2 and p values were calculated. For all the statistical analysis, a probability higher than 95% ($p<0.05$) was taken as significant. The calculations, histograms and linear plots were performed using Graph Prism version 5 software.

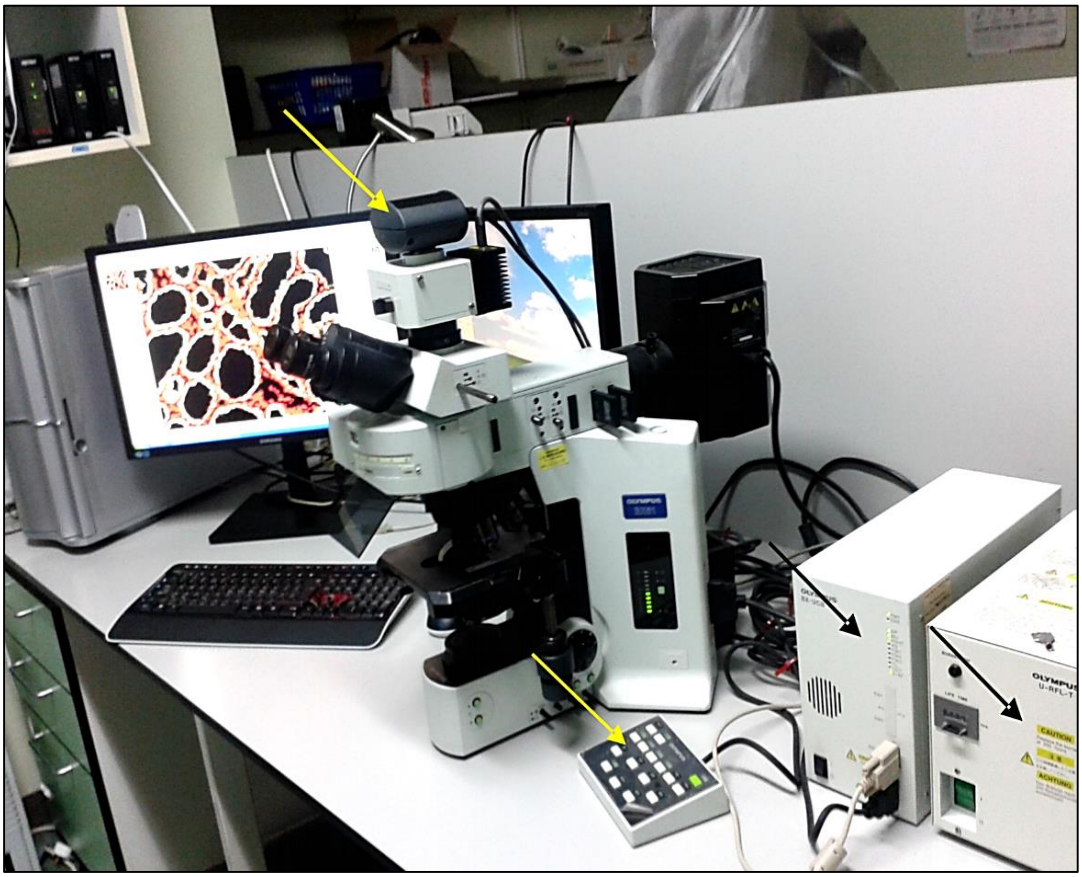

Figure 2.24: Microscopy equipment

Camera and manual control for microscope, upper and lower yellow arrow, respectively. Microscope voltage regulator and fluorescent light source, upper and lower black arrow, respectively.

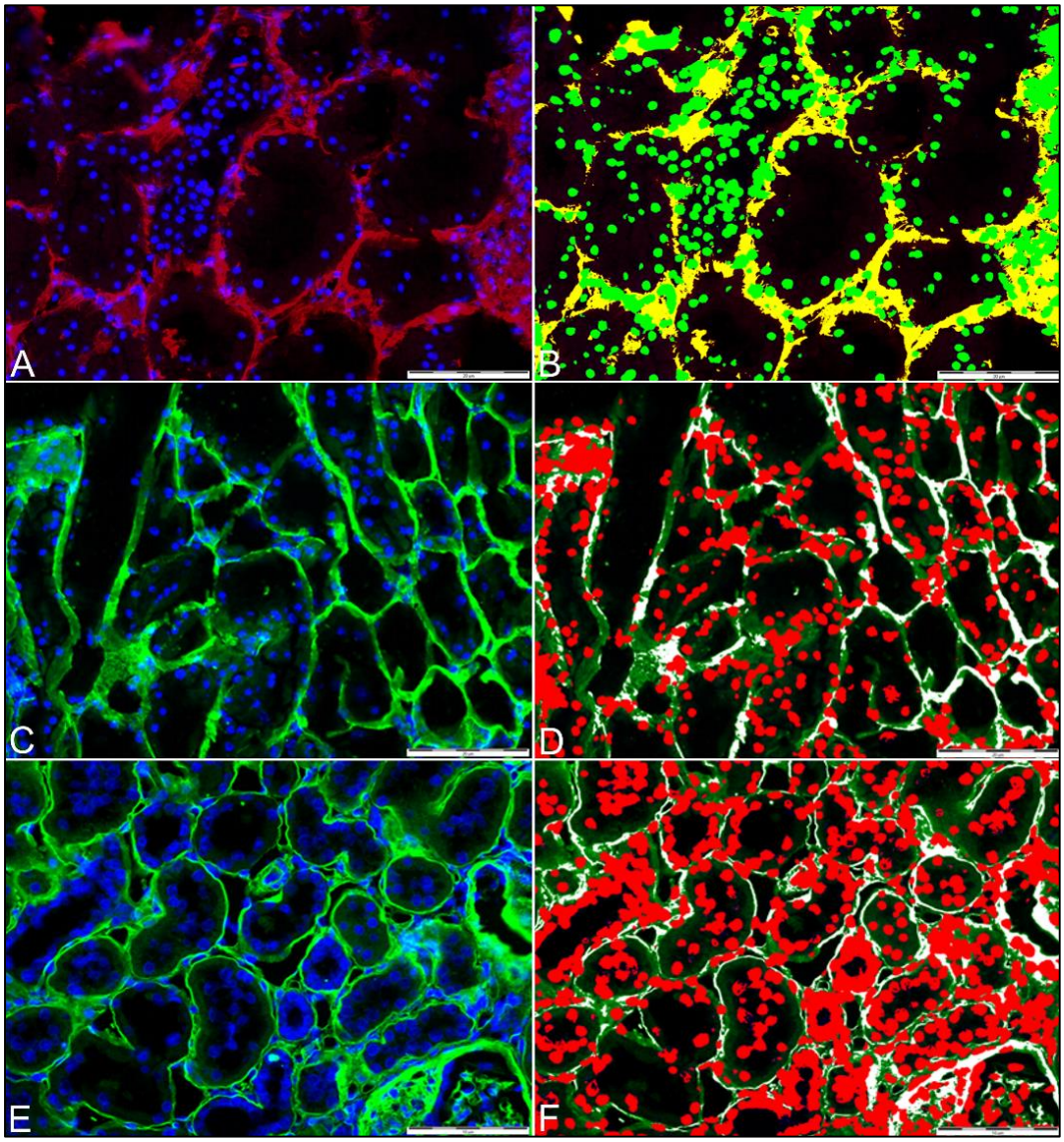

Figure 2.25: Identification and quantification of target proteins by image analysis

Panel **A**, **C** and **E** are representative images of the tubulointerstitial area by immunstained for collagen I, III and IV immunofluorescence. Panel **A**-**B** and **E**-**F** correspond to cat tissue. Panel **C**-**D** corresponds to rat tissue. Panel **A**. Intense red fluorescence (Alexa red) indicates the presence of collagen I protein, whereas the green fluorescent (FITC) indicates the presence of collagen III and IV, Panel **C** and **E**, respectively. The blue dots (DAPI) represent cell nuclei for all images. Panel **B**, **D** and **F** show the colour substitution by image analysis from panel **A**, **C** and **E**, respectively. Intense red fluorescence is highlighted in yellow and green fluorescence in white. Blue (DAPI) in green or red.

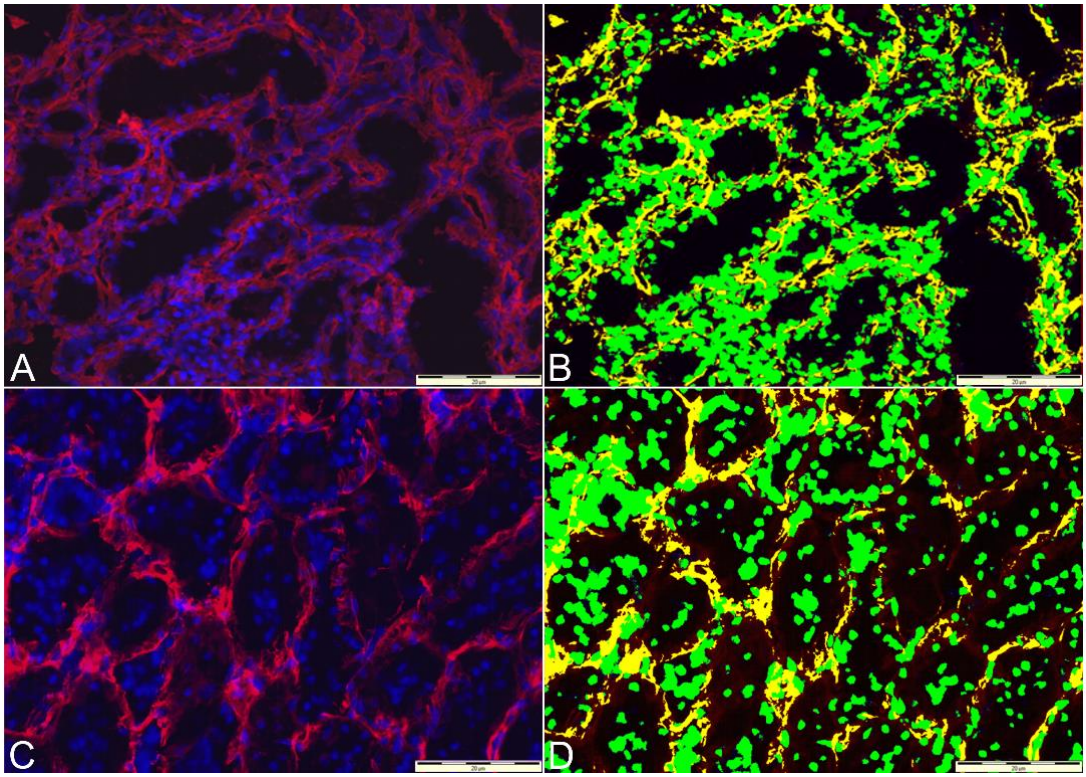

Figure 2.26: TG act and TG2 identification and quantification by image analysis

Panel **A and C** are representative images of the tubulointerstitial area for TG activity and TG2 protein identification. Panel **A**-**B** and **C**-**D** are tissue samples from rat and cat, respectively. Intense red fluorescence (Alexa red) indicates the presence of TG activity and TG2 protein, Panels **A** and **C**, respectively. The blue dots (DAPI) represent cell nuclei. Panel **B** and **D** shows the colour substitution by image analysis from panel **A** and **B, respectively**. Intense red fluorescent is highlighted in yellow. Blue (DAPI) in green.

Protease inhibitors
-Complete Free EDTA protease Inhibitor, 1 tablet in 10 ml (Roche, USA)
Solutions and equipment
-STE buffer (0.25 M *sucrose*, 0.03 M Tris, 0.05 M EDTA) + protease inhibitors -Homogenizer, Janke Kunkel (IKA Labothechnik T25, Germany) -Bullet blender + Stainless steel beads 0.9-2mm, (Next Advance, Inc, USA) -15 ml centrifuge tubes and 1.5 ml eppendorfs -Liquid nitrogen -Styrofoam box with flaked ice.

Table 2.1: Material for tissue Homogenization

Protease inhibitors
-Complete Free EDTA protease Inhibitor Cocktail (Roche, USA)
Solutions
-Colorimetric assay kit (DC Protein Assay, 500-0120, Bio-rad, UK). *Reagent A*: Alkaline copper tartrate solution and *Reagent B*: Folin reagent -STE buffer (0.25 M *sucrose*, 0.03 M Tris, 0.05 M EDTA) -Bovine serum albumin standard 1.43mg/ml (protein standard II, Bio-rad, UK).
Hard and Software
-Microplate for ELISA (96 wells) -Thermo Lab Systems Ascent, microplate reader/software V2.7, USA.

Table 2.2: Material for protein concentration measurement

Powders and tablets
-NN'-Dimethylcasein -Trichloroacetic acid (TCA) -Sucrose -Tris base -EDTA -Complete Free EDTA protease Inhibitor Cocktail (Roche, USA) -$CaCl_2$
Solutions
-Putrescine dihydrochloride ([1,4-^{3}H(N)] 1mCi (37MBq), 65Ci/mmol, PE, USA. -STE buffer (0.25 M sucrose, 0.03 M Tris, 0.05 M EDTA) -50mM and 1.05M Tris-HCl (pH 7.4) -25mM $CaCl_2$ -Ethanol 100% -Scintillation solution (L8286,Ultima Gold LSC Cocktail, Sigma)
Recombinant proteins and inhibitors
-Recombinant rat TG2 1:1000 (T038, Zedira. Germany) -TG inhibitor, 1,3-dimethyl-2[(oxopropyl)thio]-imidazolium chloride (50µM; D003, Zedira, Germany)
Others
-1cm^2 filter paper squares Whatman 3MM
Hard and Software
-Scintillation Machine (Beckman Coulter, LS 6500 scintillation counter, USA)

Table 2.3: Material for TG activity by 3H-putrescine assay

Powders and Tablets	
-Tris base -NaCl -Acrylamide -Sodium lauryl sulphate (SDS) -Ammonium per sulphate (APS)	-Tetramethylethylenediamine (TEMED) -Glycine -Bromophenol blue -Complete protease Inhibitor Cocktail (Roche, USA)
Solutions	
-**SDS page 10%:** H_2O (6.3ml), 1.5M Tris HCL pH 8.8 (4ml), 30% Acrylamide (5.4ml), 10% SDS (160 µl), 10% APS (160 µl), TEMED (16µl). -**Stocking gel:** H_2O (3.05ml), 0.5M Tris HCL pH 6.8 (1.25ml), 30% Acrylamide (0.67ml), 10% SDS (50 µl), 10% APS (50 µl), TEMED (12µl). -**Running Buffer** for 1L: Tris (3g) + glycine (14.4g) + SDS (1g) in d.d H_2O. -**Transfer buffer** for 1L: Tris (3g) + glycine (14.4g) + 800ml d.d H_2O + 200 methanol -**2x Protein buffer** for 80ml**:** 0.5M Tris pH 6.8, 4% SDS, 80% glycerol, 0.5% Bromophenol blue **-Loading buffer** for 1ml: 2x Protein loading (900 µl) + mercaptoethanol (100 µl) -**10X Tris buffered saline (TBS)**: 0.5M Tris HCl, 1500mM NaCl, pH 7.4: -**Washing buffer:** Tris buffered saline TBS + Tween 20 1% -**BM chemiluminiscence blotting substrate (POD)** (Roche, Germany)	

Table 2.4a: General materials for Western Blotting

Primary antibodies	**Secondary antibodies**
-Rabbit polyclonal TG2 antibody (1:5000, Abcam, Ab421, USA)	-Polyclonal goat anti-rabbit HRP antibody (1:10,000, P0448, DAKO, UK)
-Goat polyclonal TG2 antibody (1:1000, Ab62819, Abcam)	-Polyclonal rabbit anti-goat HRP antibody (1:5000, P0449, DAKO, UK)
-Mouse monoclonal TG2 antibody (1:1000, CUB 7402, Abcam, UK)	-Goat anti-mouse HRP antibody (1:5000, A3673, Sigma, UK)
-Mouse monoclonal TG2 BB7 Ab (1:5000, U of Sheffield, UK)	**Control Antibodies** -Goat IgG -Rabbit IgG -Rabbit polyclonal cyclophilin A Ab (1:1000, Ab 42408, US) -mAb B-actin (1:2000, Ab 6276, UK)
Positive control and protein weight marker	
-Human recombinant TG2, 78 kD (1:250, T002, Zedira, Germany) -Guinea pig liver TG2, 76.5 kD (1:250, T006, Zedira, Germany) -Molecular weight marker: Precision Plus Protein dual colour molecular weight markers (Bio-rad, 16-03-64, UK)	
Hard and Software	
-PVDF membrane (Immobilon-P, Millipore, USA) -Whatman paper 3MM and sponges -Wet electroblotting equipment (Dual gel caster, buffer tank, gel transfer cassettes, transfer tank, electrode assembly, power source) -ChemiDoc MP Image System (170-8280, Bio-rad, USA) -ChemiDoc Image System Lab Software (4.1v, Bio-rad, USA). See Figure 2.22, panel F.	

Table 2.4b: General materials for Western Blotting

Protein target	Cat study				*In vivo* rat studies			
	Primary Ab		Secondary Ab		Primary Ab		Secondary Ab	
Collagen I	Mouse monoclonal Abcam, Ab 6308	1:20	Goat Polyclonal FITC Santa Cruz, sc362277	1:50	Rabbit polyclonal Abcam 34710	1:100	Swine polyclonal FITC Dako F0054	1:15
Collagen III	Goat polyclonal Southern Biotech, 1330-01	1:15	Rabbit polyclonal FITC Vector, FI5000	1:150	Goat polyclonal Southern Biotech, 1330-01	1:10	Rabbit polyclonal FITC Vector, FI5000	1:150
Collagen IV	Rabbit MP Biomedicals 681241	1:35	Swine polyclonal FITC Dako F0054	1:15	Rabbit MP Biomedicals 681241	1:35	Swine polyclonal FITC Dako F0054	1:15
TG2	Rabbit polyclonal Abcam, Ab421	1:100	Goat polyclonal Alexa Invitrogen, A.Fluor 594 A11012	1:300	Rabbit polyclonal Abcam, Ab421	1:100	Goat polyclonal Alexa Invitrogen , A.Fluor 594 A11012	1:300

Table 2.5: Primary and secondary antibodies used for tissue analysis

Solutions
-Goat serum -Triton X-100 -Biotin cadaverin (A1594, Molecular Probes, Invitrogen, USA) -Streptavidin Alexa red fluor conjugate 594 1:300 (Invitrogen, USA)
Powders and tablets
-DTT -Streptavidin (Sigma, USA) -Tris (hydroxymethyl)aminomethane -Complete Free EDTA protease Inhibitor Cocktail (Roche, USA)
Inhibitor
-1,3-dimethyl-2[(oxopropyl)thio]-imidazolium chloride (D003, Zedira, Germany)
Hardware and Software
-Light Microscope (Olympus) -F-View digital camera (Soft Imaging Systems, Germany) -Multiphase image analysis software (Cell F, Olympus, Germany)

Table 2.6a: General materials used for TG *in situ* activity experiment

Rehydration buffer	Washing buffer
5% goat serum	
10mmol/L EDTA	10 mmol/L EDTA
0.01% (v/v) Triton X-100	
5 µg/ml streptavidin	
Protease inhibitors	Protease inhibitors
In 50 mmol/Tris 7.4	In PBS 7.4 pH

Table 2.6b: Reagents for rehydration and washing buffers

Reaction buffer	Negative Control 1	Negative Control 2	Negative Control 3	Control 4
5mmol/L $CaCl_2$		5mmol/L $CaCl_2$	5mmol/L $CaCl_2$	5mmol/L $CaCl_2$
5mmol/L DTT	5mmol/L DTT	5mmol/L DTT	5mmol/L DTT	5mmol/L DTT
0.5 mmol/L Biotin cadaverin	0.5 mmol/L Biotin cadaverin	0.5 mmol/L Biotin cadaverin	0.5 mmol/L Biotin cadaverin	0.5 mmol/L Biotin cadaverin
Protease inhibitors	Protease inhibitors	Protease inhibitors	Protease inhibitors	Protease inhibitors
In 50 mmol/Tris 7.4 pH	In 50 mmol/Tris 7.4 pH	In 50 mmol/Tris 7.4 pH	In 50 mmol/Tris 7.4 pH	In 50 mmol/Tris 7.4 pH
	10mmol/L EDTA	20mmol/L EDTA	100 µmol/L DOO3	Anti-mouse TG2

Table 2.6c: Reagents for reaction buffer and controls

CHAPTER 3

Renal Fibrosis and Chronic Kidney Disease in the Cat

3.1. Introduction

Feline CKD affects over 50% of senior cats (Marino *et al.*, 2013a), therefore, a large case load requires renal targeted treatment where the cornerstone treatment is mainly modification of diet. Other approaches such as drugs to reduce hypertension and proteinuria (RAAS and ARB) may contribute to feline wellbeing. However, extended and large scale studies are needed to determine if angiotensin inhibition is effective with regard to life survival, as seen in humans with CKD. Feline CKD presents two main challenges in veterinary medicine, the silent onset of CKD and the lack of reversibility once the disease has been established. Therefore, approaches to tackle CKD can be focused in:- a) detection of early CKD (plasma, urinary markers), where affected kidneys may have better chances to stop the progression or even reverse the disease and b) treatments to treat mature CKD, where symptomatic therapy plays an important role and where inhibition of profibrotic proteins may allow a substantial reduction in the substitution of functional parenchyma by fibrotic tissue, main characteristic of CKD.

Renal fibrosis is characterized by deposition of collagen proteins in the extracellular matrix. Extracellular matrix is a meshwork-like substance found within the extracellular space and in association with the basement membrane of the cell surface. It promotes cellular proliferation, provides supporting structure, influences cell development and differentiation, coordinates cellular functions through signalling with cellular adhesion receptors, integrates cells into tissues and influences cell shape and it is vital for cell movement. When functional renal parenchyma (endothelial, epithelial tubular and mesangial cells) is substituted by fibrotic tissue, function in the kidney is progressively reduced with important disturbances of function at glomerular and tubulointerstitial level.

Once collagen protein is accumulated in the extracellular area, this is stabilized and matured when the disease is not controlled and hence fibrosis becomes deposited and resistant to natural degradation. In humans there is a large amount of evidence showing that tubulointerstitial fibrosis highly correlates more with renal function than with glomerulosclerosis (Rodriguez-Iturbe *et al.*, 2005). A recent study has shown similar results in the domestic cat (Chakrabarti *et al.*, 2013). This finding suggests that tubulointerstitial space is a cardinal subject to study over glomeruli, independently of the low regenerative ability of the later. Therefore, to study fibrogenic

pathways in renal tissue from cats with CKD has to fulfil two main features, deterioration of renal function and a considerable level of tubulointerstitial fibrosis.

The aim of this study was to analyse the level of renal fibrosis in feline kidney tissues with different levels of renal function provided by the RVC biorepository bank. Renal function correlates with the level of renal fibrosis in man and in numerous *in vivo* studies, therefore, it was expected to generate two groups, a non-azotaemic (n=5) and azotaemic (n=10) groups, with low and high level of fibrosis, respectively.

Renal fibrosis analysis was performed employing Masson's trichrome staining and quantified by image analysis. Similar results to those in MT staining were obtained when analysing collagen I by immunofluorescence. This data was further confirmed by a Diploma holder from the American College Veterinary Pathologists, based in the USA; who evaluated renal fibrosis and inflammation by stereology on periodic acid-Schiff / haematoxylin (PASH) stained tissue. The importance of determining the level of fibrosis was vital in this study to further investigate the association of tubulointerstitial fibrosis with transglutaminase 2 enzyme, a pro-fibrotic enzyme.

3.2. Material and methods

3.2.1. Renal tissue source and function

Kidney tissue was obtained from the Royal Veterinary College biorepository bank. Breed, age, gender, last treatment and cause of euthanasia for each kidney samples are described in Table 3.1. The selection of renal samples was based on the presence of plasma biochemical profile obtained in a maximum of 2 months prior to euthanasia. From over 100 samples, the group was reduced to 27 samples. 10/27 tissues were obtained from cats with hyperthyroidism and therefore discarded. 2/23 showed borderline values of hyperazotaemia and were discarded too. The remaining samples were further separated according to the level of renal function using mainly plasma creatinine as a marker. Groups were divided in non-azotaemic (n=5) and azotaemic group (n=10) according to plasma creatinine, however other parameters such as urea, phosphate, urinary protein creatinine ratio (UPC), urinary specific gravity and blood pressure were also recorded, Table 3.2.

Case No.	Breed	Age	Gender	Last treatment	Cause of Euthanasia
1	DSH	18.0	F	None	Died/unknown
2	DSH	21.4	F	CCB	Neurological
3	DSH	11.0	F	None	Stomach tumour
4	DSH	17.3	M	CCB	Seizures
5	DSH	23.7	F	CCB	Liver tumour
6	DSH	19.9	M	None	Lung tumours
7	DSH	17.9	M	ACE	NA
8	DSH	10.5	F	ACE,CCB	Bladder tumour
9	DSH	16.1	M	CCB	Behaviour change
10	Burmese	20.5	M	None	Collapsing
11	DSH	15.7	F	None	Intestinal tumour
12	DSH	9.0	M	None	CKD
13	DSH	13.8	M	None	CKD
14	DSH	10.0	M	None	CKD
15	DSH	17.7	F	CCB	CKD

Table 3.1: Clinical history from kidney tissue

DHS, domestic short hair; CKD, chronic kidney disease; ACE, angiotensin converting enzyme inhibitor; CCB, calcium channel blocker. Age is displayed in years at death.

Groups	Sample	Plasma creatinine µmol/L	Plasma urea mmol/L	Plasma phosphate mmol/L	UPC	Blood pressure mmHg	USG
Non Azotaemic	1	53.7	15.8	1.07	NA	89	NA
	2	91	12.5	1.58	1.91	142	1.015
	3	92.2	8.3	1.25	0.18	105	1.029
	4	124	9.4	1.85	0.26	155	1.046
	5	133	14.8	1.18	NA	138	1.014
Azotaemic	6	180	11.8	1.26	0.19	135	1.018
	7	221	17	0.96	0.47	151	1.016
	8	244	30.9	2.29	5.8	183	1.014
	9	251	24.5	1.84	0.51	181	1.024
	10	260.3	27.3	2.19	NA	141	1.016
	11	352	19.4	1.4	1.28	137	1.016
	12	450	67.3	5.67	4.78	149	1.021
	13	489	48	5.38	1.58	140	1.016
	14	513.5	34.4	3.84	0.24	139	1.012
	15	847.6	72.3	5.17	0.76	144	1.011

Table 3.2: Individual renal function parameters

UPC, urinary protein creatinine ration; USG, urinary specific gravity

3.2.2. Renal histomorphology

Kidneys were fixed in formalin 10%. Paraffin-embedded sections for each kidney were cut (3μM thickness). The slides were deparaffinised and rehydrated to stain with periodic acid-Shiff haematoxylin (PASH) or Haematoxylin and eosin, in different sections. Fibrosis and inflammation were evaluated in both tubulointerstitium and glomeruli, whereas obsolescence was only assessed in the glomeruli. Staining and analysis of tissue was carried out by a certified veterinary pathologist masked of all clinical history. See Chapter 2, section 2.4.2.

3.2.3. Renal fibrosis

3.2.3.1. Masson's trichrome staining

5μm, formalin-fixed, paraffin embedded sections were deparaffinized and rehydrated. The slides were placed in Bouin's solution overnight, washed and placed in working Weigert's iron haematoxylin solution for 5 minutes. The slides were stained with Biebrich scarlet-acid fuchsin, aniline blue solutions, dehydrated and mounted in DPX. For IGMA and tubulointerstitial expansion of extracellular matrix, no less than 10 glomeruli (x 400) and (x 200) of cortex tubules were acquired. The fibrosis index was determined calculating the blue area percentage of total field. Quantification was performed by image analysis. See Chapter 2, section 2.4.3.

3.2.3.2. Immunofluorescence

8μm thick cryostat sections on adherent slides, previously stored at -80°C. The slides were blocked and washed. The tissue was probed with a primary antibody (collagen I and III) overnight at 4°C followed by fixation and serial washings. The slides were immunoprobed with a secondary antibody and left at room temperature for 2 hours. Finally, a drop of mounting medium with DAPI was added. No less than 10 glomeruli (x 400) and (x 200) of cortex tubules were acquired. The immunofluorescent fibrosis index was determined calculating the intense Alexa red (collagen I) and FITC (collagen III) fluorescent area percentage of the total field. Quantification was performed by image analysis. See Chapter 2, section 2.6.1.

3.2.4. Statistics

The cross-sectional data was analysed by unpaired two-tailed Student's t-test with Welch's correction. To evaluate group correlations, r^2 was calculated by linear regression analysis. The statistical significant level was defined as $P<0.05$.

3.3. Results

3.3.1. Renal function

The measurements of plasma creatinine, urea and phosphorus in the azotaemic group showed a significant 4-fold, 3 fold and 3 fold increase, respectively, when compared to the non-azotaemic group. UPC, blood pressure and USG did not show any significant difference between groups; however, the azotaemic group showed a higher mean UPC and blood pressure mean together with a lower urinary density trend when compared to the non-azotaemic group, Table 3.3.

Parameters	Non-azotemic (n=5)	Azotemic (n=10)
Plasma urea (mmol/L)	12 ± 1.5	35 ± 6.6 **
Plasma creatinine (µmol/L)	98 ± 14	381 ± 64 ***
Plasma phosphate (mmol/L)	1.4 ± 0.4	3 ± 0.6 *
Urinary specific gravity	1.026 ± 0.0075 (4)	1.016 ± 0.0012
Urine protein/creatinine	0.8 ± 0.6 (3)	1.7 ± 0.7 (9)
Blood pressure (mmHg)	126 ± 12	150 ± 5.6

Table 3.3: Grouped renal function parameters

Results are expressed as mean ± sem. *$P<0.05$, ** $P<0.01$, ***$P<0.005$. Nos. of samples assayed are shown in brackets.

3.3.2. Renal fibrosis, inflammation and specific renal diseases

3.3.2.1. Periodic Acid-Schiff / Haematoxylin (PASH)

Glomerular fibrosis score and glomerular obsolescence. Measurements of glomerular fibrosis score and glomerular obsolescence for the azotaemic and non-azotaemic groups, expressed as score unit and index %, respectively, did not show

any significant difference between groups. Glomerulosclerosis, non-azotaemic, 1.15 ± 0.20 score; azotaemic, 1.22 ± 0.17 score, NS. Glomerular obsolescence, non-azotaemic, 8.4 ± 3.7 index %; azotaemic, 21.4 ± 6 index %, NS.

Tubulointerstitial fibrosis score and inflammation. The azotaemic group for tubulointerstitial fibrosis score was associated with a significant 2.8 fold increase in the unit score when compared to the non-azotaemic group. Non-azotaemic, 0.8 ± 0.34; azotaemic, 2.25 ± 0.21 score, P<0.01. No significant difference was seen for the inflammation score between groups. Non-azotaemic, 0.9 ± 0.33; azotaemic, 1.6 ± 0.16 score, NS.

Specific renal diseases, papillary necrosis, hypertensive arteriosclerosis and lymphoma were diagnosed in tissue samples 8, 10 and 11, respectively. All renal histomorphology parameters per sample generated by stereology are displayed in Table 3.4.

3.3.2.1. Masson's trichrome

Intraglomerular mesangial area. Representative examples of glomeruli from MTS sections are shown for the non-azotaemic and the azotaemic group in Figure 3.1, panels A and C, respectively**.** The intraglomerular mesangial area (IGMA) in the representative images do not show any visual difference in blue staining between images. Cross-sectional measurements of IGMA for the azotaemic and non-azotaemic groups, expressed as mean blue area % did not show a significant difference. See Figure 3.1 panel E for IGMA changes. Non-azotaemic, 5.65 ± 2.4; azotaemic, 4.73 ± 1.8 area %, NS.

Tubulointerstitial area. Representative examples of glomeruli from MTS sections are shown for the non-azotaemic and the azotaemic experimental group in Figure 3.1, panels B and D. The tubulointerstitial area from the azotaemic image shows a high level of blue staining localized in the interstitial area when compared to the non-azotaemic representative section. The azotaemic image also shows a higher degree of intratubular and intertubular space in contrast to the non-azotaemic representative image. Measurements of the tubulointerstitial in the azotaemic and non-azotaemic groups, expressed as mean of blue/red ratio, showed a significant change between groups. Non-azotaemic, 1.95 ± 0.5; azotaemic, 5.5 ± 1 blue area %, P<0.005. See Figure 3.1, panel F.

Case No.	CKD stage	Interstitial fibrosis score	Degree	Glomerular fibrosis score	Degree
1	Non-azotemic	1	Mild	0.96	Normal
2	Non-azotemic	2	Moderate	1.88	Mild
3	Non-azotemic	0	Normal	0.72	Normal
4	Non-azotemic	0.5	Normal	1.08	Mild
5	Non-azotemic	0.5	Normal	1.12	Mild
6	2	1	Mild	0.44	Normal
7	2	1.5	Mild	1.32	Mild
8	2	2.5	Moderate	2.2	Moderate
9	3	2.5	Moderate	2.08	Moderate
10	3	2	Moderate	1.12	Mild
11	3	2	Moderate	1.32	Mild
12	4	2	Moderate	1.2	Mild
13	4	3	Severe	0.88	Normal
14	4	3	Severe	0.96	Normal
15	4	3	Severe	0.72	Normal

Table 3.4: Renal histopathology

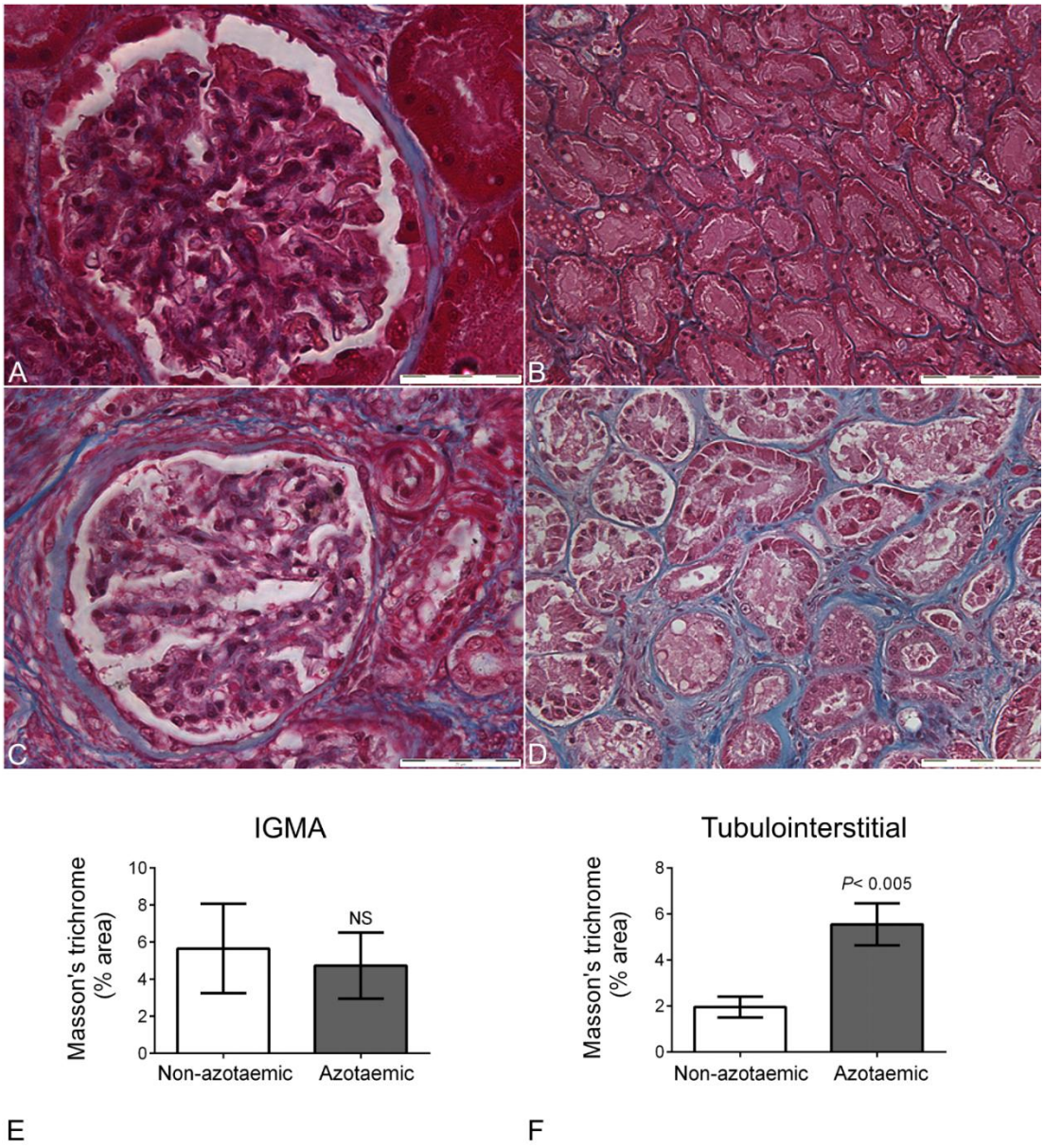

Figure 3.1: Expansion of extracellular matrix in the cat kidney tissue

Panel **A**, **C** and B, **D**. Representative images of glomeruli (400x) and tubulointerstitial (200x) area, respectively, showing coloration (blue – extracellular matrix and red-cellularity) and structural differences between the Non-azotaemic (**A** and **B**) and azotaemic (**C** and **D**) samples, respectively. Panel **E** and **F**. The histograms represents the mean blue area % in the IGMA and tubulointerstitial area, respectively. Non-azotaemic group (n=5) and Azotaemic group (n=10). Vertical bars indicate +/-SEM.

3.3.2.2. Collagens

Intraglomerular mesangial area for collagens I and III. Representative examples of IGMA for collagen I (Figure 3.2) and III (Figure 3.3) fluorescent stained sections are shown for the non-azotaemic and azotaemic group, panels A and C, respectively. The intraglomerular mesangial area (IGMA) in the representative images do not show any visual difference in red or green staining between groups for collagen I or collagen III. Terminal measurements of collagens in the IGMA for the non-azotaemic and azotaemic groups, expressed as mean Alexa red and FITC area %, did not show any significant change between groups, Figure 3.2 and Figure 3.3 panels E, respectively.

Tubulointerstitial area for collagens I and III. Representative examples of tubulointerstitial space for collagen I (Figure 3.2) and III (Figure 3.3) fluorescent stained sections are shown for the non-azotaemic and azotaemic group, panels B and D, respectively.

The tubulointerstitial example for collagen I in the azotaemic group shows a higher level of red fluorescence when compared to the non-azotaemic image. Measurements of the tubulointerstitial area for collagen I in the non-azotaemic and azotaemic groups, expressed as Alexa red area %, showed a significant change between groups. Non-azotaemic, 5.4 ± 1.3; azotaemic, 11.89 ± 1.6 area %, $P<0.01$. See Figure 3.2, panel F.

The tubulointerstitial examples for collagen III show a similar level of green fluorescence in both groups. No significant difference between groups was observed for collagen III. See Figure 3.3, panel F.

3.3.3. Correlations

Interstitial fibrosis showed positive linear correlations with both renal function and interstitial inflammation parameters. All the renal function markers showed a moderate but significant level of correlation with fibrosis, see Table 3.5 and 3.6.

Positive linear correlations were obtained between techniques to quantify fibrosis by image analysis (MT and Collagen I) and stereology (PASH), see Table 3.7 and Figure 3.4.

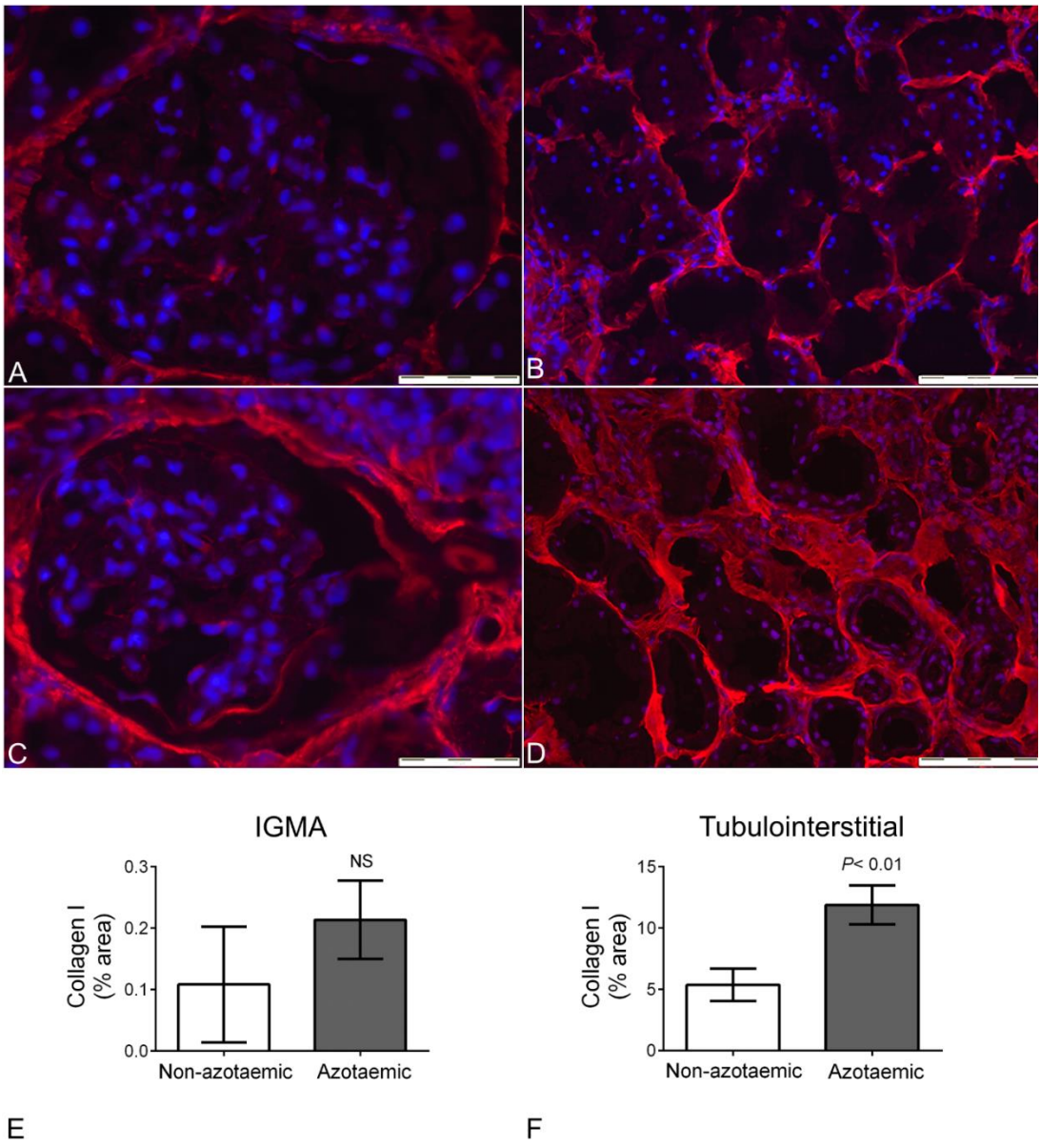

Figure 3.2: Collagen I in the cat kidney with CKD

Panel **A**, **C** and **B**, **D**. Representative images of glomeruli (400x) and tubulointerstitial (200x) area, respectively, showing coloration (Alexa red – collagen I and DAPI – nuclei) and structural differences between the Non-azotaemic (**A** and B) and azotaemic **(C** and **D**) samples, respectively. Panel **E** and **F**. The histograms represents the mean Alexa red area % in the IGMA and tubulointerstitial area, respectively. Azotaemic group (n=10) and non-azotaemic group (n=5). Vertical bars indicate +/-SEM.

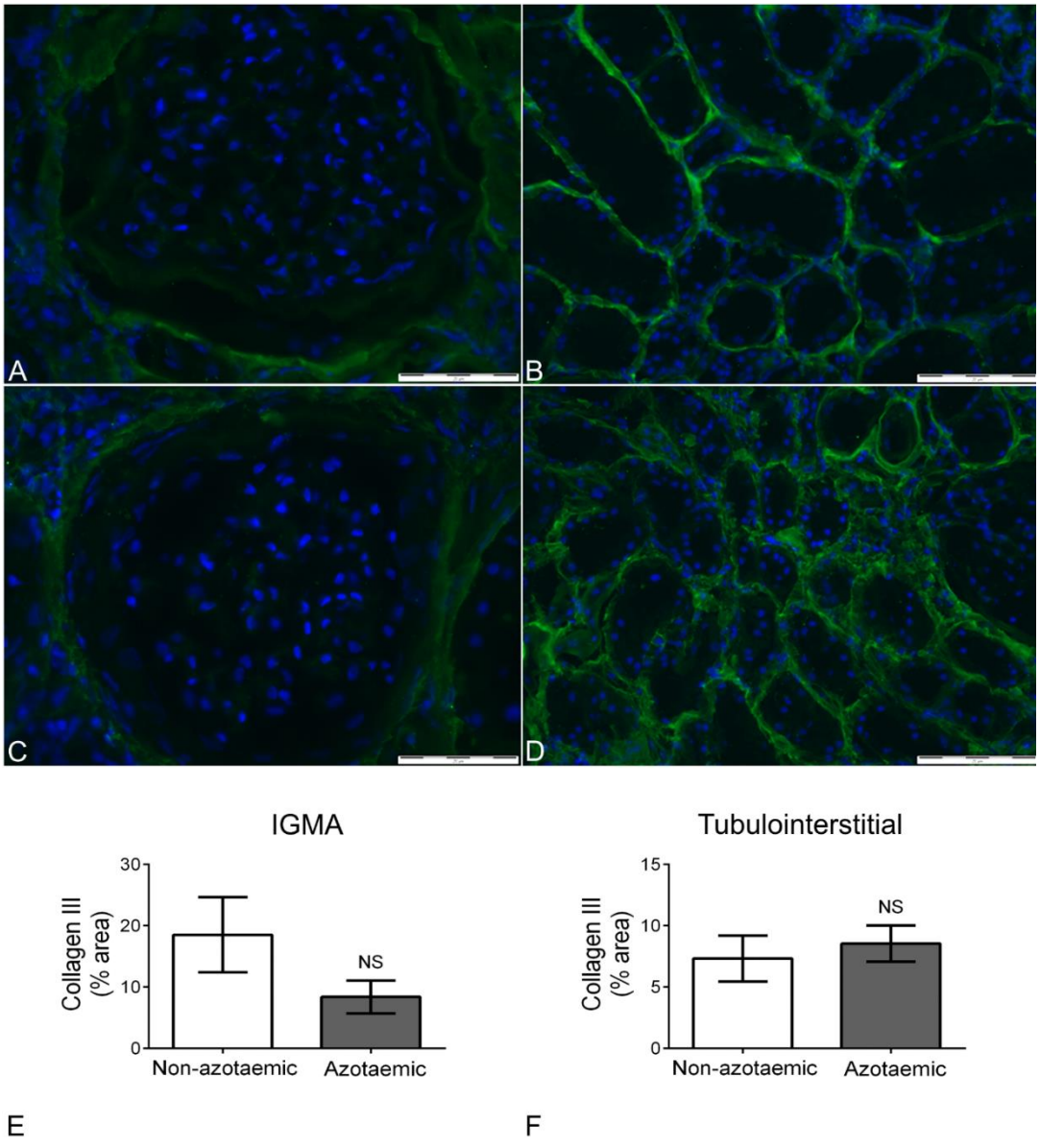

Figure 3.3: Collagen III in the cat kidney with CKD

Panel **A**, **C** and **B**, **D**. Representative images of glomeruli (400x) and tubulointerstitial (200x) area, respectively, showing coloration (FITC green – collagen III and DAPI – nuclei) and structural differences between the Non-azotaemic (**A** and **B**) and azotaemic (**C** and **D**) samples, respectively. Panel **E** and **F**. The histograms represents the mean % green area in the IGMA and tubulointerstitial area, respectively. Azotaemic group (n=10) and non-azotaemic group (n=5). Vertical bars indicate +/-SEM.

Fibrosis	Renal function	r^2	P value <
Fibrosis by MTS	Creatinine	0.44	0.008
Fibrosis by MTS	Urea	0.57	0.002
Fibrosis by MTS	Phosphate	0.44	0.008
Fibrosis by PASH	Creatinine	0.56	0.005
Fibrosis by PASH	Urea	0.48	0.005
Fibrosis by PASH	Phosphate	0.45	0.007
Collagen I	Creatinine	0.56	0.002

Table 3.5: Positive linear regressions between fibrosis and renal function

Technique A	Technique B	r^2	P value <
Inflammation by H&E*	Fibrosis by MTS	0.35	0.03
Inflammation by H&E*	Fibrosis by PASH	0.65	0.001

Table 3.6: Positive linear regressions between fibrosis techniques

Technique A	Technique B	r^2	P value <
Fibrosis by PASH	Fibrosis by MTS	0.28	0.05
Fibrosis by PASH	Collagen I	0.38	0.02

Table 3.7: Positive linear regressions between inflammation and fibrosis techniques

H&E, haematoxylin and eosin; PASH, periodic acid-Schiff + haematoxylin; MTS, Masson's trichrome staining; *, n=14.

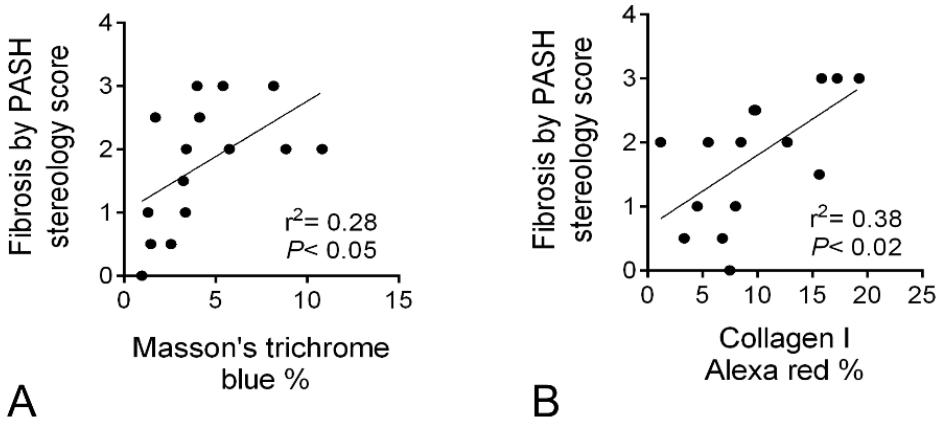

Figure 3.4: Tubulointerstitial fibrosis correlations.

3.4. Discussion

3.4.1. Renal function

Post-mortem kidney tissue was obtained from primary renal azotemic and non-azotaemic cats. Plasma blood analysis showed a significant low level in renal function in the azotaemic group. On the non-azotaemic group, even though plasma analysis did not show evidence of renal impairment we cannot rule out the possibility of incipient forms of CKD. Their old age (11 to 23.7 years) itself is considered a risk factor for the development of renal dysfunction (Greene *et al.*, 2014). Low urinary specific gravity is frequently associated with early and severe stages of CKD in geriatric cats. However, this technique normally has to be consistent with other parameters of renal dysfunction to gain diagnostic relevance. A cat with extra-renal impaired antidiuretic hormone activity could have normal renal function with USG <1.035, however this is not common in cats (Watson, 1998).

3.4.2. Renal fibrosis assessment

With regard to the techniques employed to assess fibrosis, stereology by PASH was the only technique showing a positive correlation with both collagen I and MTS. It also showed a slightly higher correlation when compared to renal function parameters. Professor Cathy A Brown from the University of Georgia, responsible for the tissue analysis by stereology in this study, has used this technique to assess renal tissue in the cat providing very relevant information of interest in the feline CKD field (Chakrabarti *et al.*, 2013; Schmiedt *et al.*, 2009).

Concerning methods to quantify fibrosis, image analysis is faster than interactive stereological methods but requires a high contrast of tissue between the object (blue staining in case of MT) and the background for the software to detect specific shades of colour (Kubinova *et al.*, 2004). MTS blue coloration can vary according to the level of fibrosis, thickness of tissue and age of staining products, however this technique is more specific for collagens than PASH. In my experience, setting the blue threshold using MTS can be challenging in kidney tissue with early fibrosis and hence it cannot be captured in its totality. PASH staining is not specific for collagens as it also stains polysaccharides. Therefore, complete assessment of fibrosis cannot just rely in one technique and should be thoroughly assessed by

combination of semi-quantitative methods. Collagen immunostaining has to be performed parallel to either MT or PASH independently of its quantification method.

3.4.3. Glomerular fibrosis

Glomerulosclerosis is thought to be a less consistent feature of CKD in the cat when compared to dogs or humans (DiBartola *et al.*, 1987; Lucke, 1968; Minkus *et al.*, 1994b; Yabuki *et al.*, 2010). However, in a recent English study, mild forms have been reported in a cat population of 80 individuals (Chakrabarti *et al.*, 2013). In humans, a strong correlation between tubulointerstitial fibrosis and renal function has been documented, independent of glomerulosclerosis (Bohle *et al.*, 1981). As reported previously by Chakrabarti et al (2013), renal dysfunction seen in azotaemic cats with CKD is related most clearly to tubulointerstitial damage rather than glomerular injury, perhaps suggesting that progressive fibrosis drives progressive deterioration in renal function. This may indicate that the survival of nephrons depends on the quick tubular restoration to allow the glomeruli to undertake their reparative process or any structural salvage mechanism; hence, the glomerular capillary system may be dependent on the peritubular capillary network. The high regenerative tubular process may be supported by regenerative cells and cytokines coming from the peritubular capillary network and not just tubular or resident interstitial cells. The glomerular reparative process may be dependent on oxygenation and some regenerative material coming the peritubular capillary system. Another approach to explain the lack of correlation between glomerulosclerosis and renal function may be found in Gandhi et al (1998) study, where a subtotal nephrectomy animal model showed that atubular glomeruli exceeded the number of glomeruli with total sclerosis, suggesting that periglomerular interstitial fibrosis, without major mesangial fibrosis, may lead to peritubular scarring due to the obstruction of the blood flow into the proximal tubule and therefore the glomeruli may seem structurally normal but in essence is atubular (Gandhi *et al.*, 1998).

3.4.4. Tubulointerstitial fibrosis

The presence of tubulointerstitial fibrosis in the post-mortem kidney tissue obtained from primary renal azotaemic cats was demonstrated by both quantification by multiphase image analysis and by a veterinary pathologist without knowledge of the samples' clinical history. Kidney collagen I was elevated whereas collagen III remained at the same level of the non-azotaemic group. The absence of elevated

collagen III deposition in kidneys from azotemic cats supported the presence of a mature form of renal fibrosis since collagen III, a scaffold for collagen I, is the predominant isoform of collagen when deposited in the early stages of renal fibrosis (Lavaud *et al.*, 2001; Zager *et al.*, 2009). A study performed by Chakrabarti et al (2012) in cats with different levels of CKD showed the relevance of tubulointerstitial fibrosis and its correlation with the reduction of renal function parameters such as azotaemia, hyperphosphatemia, proteinuria and anaemia. The data presented in this chapter showed similar results.

The formation of tubulointerstitial fibrosis has been extensively studied *in vitro* and *in vivo* models with many mediators for its development, most of them within inflammatory and hypoxic processes. In human medicine, research approaches to understand renal fibrosis have been focused on inflammation and pro-fibrotic processes and the generation of urine and plasma markers for each process are topics of high priority.

Detecting early stages of renal inflammation allows early treatment with the subsequent reduction of pro-fibrotic events. In human medicine detecting early stages of renal disease is accomplished by health checks, which, in developed countries, are subsidised by governments. As an example, regular blood test analysis to assess renal status can be carried out in a regular basis after 65 years of age, in the UK. This action reduces long term cost to the government, as prevention is better than treating for many years any chronic condition. In the veterinary setting, even though preventive medicine is becoming more popular and insurance plans allow a better health check coverage, the culture of worldwide preventive medicine in pets is still immature.

Regarding pro-fibrotic pathways, research approaches to detect and to block fibrogenic proteins have been attempted for many years, using *in vitro* and *in vivo* models. Some of them have shown promising results to reduce and even to reverse nephropathy (Perico *et al.*, 2008; Perico *et al.*, 2005). In veterinary medicine, specifically in feline CKD, proteins such as TGF-β (Arata *et al.*, 2005), endothelin 1 (Uchide *et al.*, 2006) and renin, angiotensin, aldosterone system (King *et al.*, 2006; Mizutani *et al.*, 2006; Watanabe *et al.*, 2007) have been studied, with controversial findings. These proteins represent potential markers of fibrosis, as well as potential target treatments due to their association and causal link in the development of fibrosis in different experimental models. Large scale randomized, control and

prospective studies in cats are needed to generate evidence based veterinary medicine. Veterinary based medicine has to be boosted using also approved animal models and, if there is an adequate rationale, testing approved drugs for human use in feline patients in large scale trials may speed up the finding of suitable treatments for feline CKD. Even though, there are phenotypic differences amongst animal models, cats and humans, careful extrapolation of findings from veterinary research to human medicine and *vice versa* may be possible, taking into account the many functional and histopathological similarities of CKD. The trigger point to develop kidney failure has not being studied in depth in the cat, however, a common hypoxic cellular pathway may be importantly involved in its development (Nangaku, 2006; Norman *et al.*, 2000), as this is an intimate path in both inflammatory and fibrogenic processes (Manresa *et al.*, 2014). These processes have been found in any form of acute and chronic renal injury in many animal models and in human tissue with CKD. In the present research project, the varied level of fibrosis in the feline kidney samples allowed us to study the association of the transglutaminase 2 protein in the tubulointerstitial area, adding another protein to the short list of pro-fibrotic proteins investigated in the cat with CKD.

3.4.5. Conclusion

According to the renal function information provided by the Royal Veterinary College, two groups (non-azotaemic and azotaemic) have been established in this chapter. The azotemic group showed significantly higher level of tubulointerstitial fibrosis, by different techniques, when compared to the non-azotaemic group. This results allows the investigation of the association between tubulointerstitial fibrosis and the transglutaminase pathway in Chapter 4.

CHAPTER 4

Feline Chronic Kidney Disease and the Transglutaminase pathway

4.1. Introduction

The beginning and evolution of CKD is determined by the progressive deposition of collagen proteins in the tubulointerstitial space. The progressive behaviour of the disease has been associated with constant cellular insults that perpetuate chronic wound healing. Hypoxia has been proposed to play a pivotal role in tubulointerstitial fibrosis (Nangaku, 2006). An effective pathological deposition in the kidney is importantly aided by cross-linking enzymes such as transglutaminase 2, an isoform of a transglutaminase group of enzymes.

Transglutaminases are calcium-dependent enzymes able to cross link collagen proteins through the generation of an Ɛ-(γ-glutamyl)-lysine dipeptide bond, making them highly resistant to proteolytic degradation (Lorand *et al.*, 2003; Verderio *et al.*, 2004). The cross-link reaction is triggered following calcium activation when TG is exported into the extracellular space (Verderio *et al.*, 2004; Verderio *et al.*, 2009). From the 8 isoforms of transglutaminases in vertebrates, transglutaminase 2 (TG2) have been frequently studied due to its biochemical functions and ubiquitous expression in many cell types and core organs such as liver, heart and kidney. In the kidney TG2 is expressed by infiltrating macrophages (Haroon *et al.*, 1999a) together with a number of resident renal cell types including endothelial, mesangial (Fesus *et al.*, 1988) and tubular cells (Johnson *et al.*, 1999). TG2 transcription may be stimulated by stress factors such as hypoxia, acidosis, oxidative stress, hyperglycaemia or inflammatory cytokines (Ientile *et al.*, 2007; Skill *et al.*, 2004; Verderio *et al.*, 2004).

In the man, TG2 has been associated with the development of CKD by assessing TG2 protein and renal fibrosis in kidney biopsies (Johnson *et al.*, 2003). In experimental animal models, a causal link has been established between TG2 and tubulointerstitial fibrosis in interventional pharmacology studies using a rat model of diabetic nephropathy and subtotal nephrectomy (Huang *et al.*, 2009; Johnson *et al.*, 2007). Moreover, genetic modification has also shown the TG2-renal fibrosis link in the TG2-knock mouse models of unilateral ureteral obstruction (Kim *et al.*, 2010; Shweke *et al.*, 2008).

In the cat, naturally occurring CKD has been recently investigated to determine causes, risk and predisposition factors, to allow prevention, early identification and treatment of the disease. The impact of the CKD study in cats does not only rely in

the high incidence of the disease in this species, it is also of high importance due to the similarities of CKD between humans and domestic felines. By understanding the development of the disease in the cat and by finding a common disease pathway, this study intended to allow the establishment of a bridge between both species through the understanding CKD. A common factor for CKD between species may be hypoxia. Current research in cats have shown that renal tissue hypoxia may pay a role in generation of feline CKD (Habenicht *et al.*, 2013; Schmiedt *et al.*, 2012; Williams *et al.*, 2014) as seen in animal models and in the man (Eardley *et al.*, 2008). The importance of this evidence is the possibility of stabilising a common fibrogenic route of disease to enhance the understanding of the disease for and quicker generation of treatment in both human and veterinary medicine. The common fibrogenic route between hypoxia and renal fibrosis may be transglutaminase 2, which could be a potential maker of renal damage and a potential therapeutic target in this species.

The aim of this study was to determine whether TG is expressed in the feline kidney obtained from tissue non-azotaemic and azotaemic samples with different degrees of renal fibrosis. Total TG enzyme activity and total TG2 protein expression were measured in kidney homogenates whereas extracellular TG enzyme activity and TG2 protein expression were determined *in situ* by immunofluorescence.

In vitro inhibition of TG2 enzyme activity was assessed in this study to establish the relevance of TG2 over the other TG isoforms and to explore a potential therapeutic option in CKD inhibiting the TG pathway by using monoclonal antibodies to TG2 or chemical inhibitors of transglutaminases.

4.2. Material and methods

4.2.1. Transglutaminase activity

4.2.1.1. Total TG activity by 3H-putrescine assay.

Transglutaminase activity was measured by the incorporation of 3H-putrescine into N,N´dimethylcasein in tissue homogenates. The incorporation reaction was triggered by the addition of $CaCl_2$ and dithiothreitol (DDT). A sample of homogenate was spotted onto 3-mm filter paper and precipitated with ice cold

trichloroacetic acid (TCA) 10%. The filter paper was washed several times and the precipitated protein quantified to measure the incorporated 3H-putrescine. Each sample was re-assessed with 100 μM of a non-selective transglutaminase inhibitor compound developed at Aston University, N-benzyloxycarbonyl-L-phenylalanyl-6-dimethyl-sulfonium-5-oxo-L-norleucine developed, and the selective TG2 neutralizing monoclonal antibody BB7 (3.3nM). The results were expressed units per mg of protein. Unit of activity is equivalent to 1nmol of 3H-putrescine incorporated per hour at 37°C. See Chapter 2, section 2.5.2, for kidney homogenates and section 2.5.3 for TG 3H-putrescine assay methodology.

4.2.1.2. Extracellular *in situ* activity

8μm thick cryostat sections on adherent slides, previously stored at -80°C. Sections were incubated with biotin cadaverin and $CaCl_2$. The main negative control required the substitution of $CaCl_2$ by EDTA. The extracellular matrix incorporated biotin cadaverine was revealed by probing the tissue sections with streptavidin Alexa red. Sections were visualized using a fluorescent light microscope. Finally, a drop of mounting medium with DAPI was added. No less than 10 glomeruli (x 400) and 10 fields of tubulointerstitial space (x 200) were acquired. The fluorescent TG activity index was determined calculating the intense Alexa red area percentage of the total field. Quantification was performed by image analysis. See Chapter 2, section 2.6.2.

4.2.2. Transglutaminase 2

4.2.2.1. Total TG2 by Western blot

Tissue homogenates, obtained as described in Chapter 2, section 2.5.2, were separated on a 10% polyacrylamide gel and then electro-blotted. Human recombinant TG2 was used as a positive control. For negative controls a non-specific antibody to TG2, IgG and whole rabbit serum were employed. The blot was probed with either a monoclonal (BB7), rabbit polyclonal (Ab421), goat polyclonal (Ab62819) or mouse monoclonal (CUB7402) TG2 antibody. Primary antibodies were revealed using a secondary alkaline phosphatase antibody with the subsequent employment of a chemiluminiscence blotting substrate. The blots were placed in a ChemiDoc machine (Image system, Bio-rad, USA) and quantification was performed using a ChemiDoc

software (Image system lab software, Bio-rad, USA). The results obtained were shown as optical density mm^2 per µg of protein. See Chapter 2, section 2.5.4.

4.2.2.2. Extracellular TG2

8µm thick cryostat sections on adherent slides, previously stored at -80°C. The slides were blocked and washed. The tissue was probed with a primary antibody (TG2) overnight at 4°C followed by fixation and serial washings. The slides were immunoprobed with a secondary antibody and left at room temperature for 2 hours. Finally, a drop of mounting medium with DAPI was added. No less than 10 glomeruli (x 400) and (x 200) of cortex tubules were acquired. The immunofluorescent fibrosis index was determined calculating the intense Alexa red) area percentage of the total field. Quantification was performed by image analysis. See Chapter 2, section 2.6.1.

4.2.3. Statistics

The cross-sectional data was analysed by unpaired two-tailed Student's t-test with Welch's correction. To evaluate group correlations, r^2 was calculated by linear regression analysis. The statistical significant level was defined as $P<0.05$. Chapter 2, section 2.7.

4.3. Results

4.3.1. Total kidney transglutaminases

4.3.1.1. TG2 antibody

Representative western blots of recombinant human TG2 (rhTG2) and renal TG2 protein are shown for kidney sample No.15 immunoprobed with four different TG2 antibodies. rhTG2 (positive control) gave a single band at approximately 78kDa.

Cat kidney homogenate (35µg protein/lane approx.) showed two bands with both BB7 and Ab421 antibody at 75kDa / 83kDa and 75kDa / 66kDa, respectively. CUB7402 and Ab62819 showed a band at 75kDa, see Figure 4.1. As negative control western blots were probed with just secondary antibody, no signal was observed. To

further assess Ab421, a rabbit IgG, whole rabbit serum and guinea pig TG2 were employed, no evidence of bands overlapping either 83kDa or 75kD area was seen. Figure 4.2.

4.3.1.2. Total TG2 protein

A representative western blot of total TG2 protein in the kidney is shown for non-azotaemic cats (n=5) or azotaemic cats (n=10), Figure 4.3, panel A. Recombinant human TG2 (positive control) gave a single band at 78kDa. Cat kidney homogenates (27µg protein/lane) gave two bands at 75 kDa (TG2) and 83 kDa. For both primary antibodies rpTG2 antibody (Ab421) and TG2 monoclonal antibody (BB7), the mean volume density /µg protein of the 75kDa band obtained from cats with azotaemia was approximately 3-fold higher than that from non-azotaemic cats. When immunoprobing with BB7: Non-azotaemic, 151500 ± 9769; azotaemic, 222800 ± 26690 OD mm^2/µg protein, $P<0.05$, Figure 4.3 panel C. When immunoprobing with Ab421: Non-azotaemic, 21 270 ± 4 046; azotaemic, 60 300 ± 14 870 OD mm^2/µg protein, $P<0.05$, Figure 4.3 panel D.

A strong positive linear correlation was obtained between total TG2 protein and total enzyme activity, measured in tissue homogenates from cat kidneys by western blotting and 3H-putrescine incorporation assays, respectively, Figure 4.3, panel D.

4.3.1.3. Total TG enzyme activity

The azotaemic group was associated with a significant 3 fold higher level in the total TG enzyme activity when compared to the non-azotaemic group. Non-azotaemic, 10.9 ± 2.3 nmol; azotaemic, 37.2 ± 8.1 nmol 3H-putrescine per hour at 37°C, $P<0.02$, Figure 4.4, panel A. A positive linear correlation was obtained between total TG enzyme activity and total TG2 protein, see Figure 4.4. A strong positive linear correlation was obtained between total TG2 protein and total enzyme activity, measured in tissue homogenates from cat kidneys by western blotting and 3H-putrescine incorporation assays, respectively, Figure 4.5.

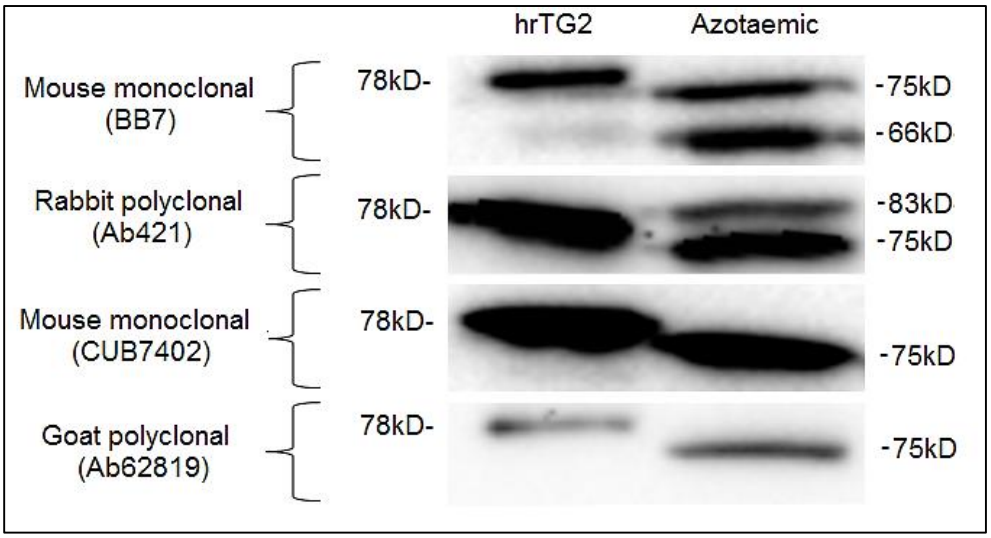

Figure 4.1: Western blot for Transglutaminase 2 using different antibodies

Western blot for cat kidney TG2 from a representative kidney tissue homogenate from an azotaemic cat sample (cat No. 15). Sample was immunoprobed with four different antibodies, using human recombinant TG2 as positive control were immunoprobed with BB7 antibody.

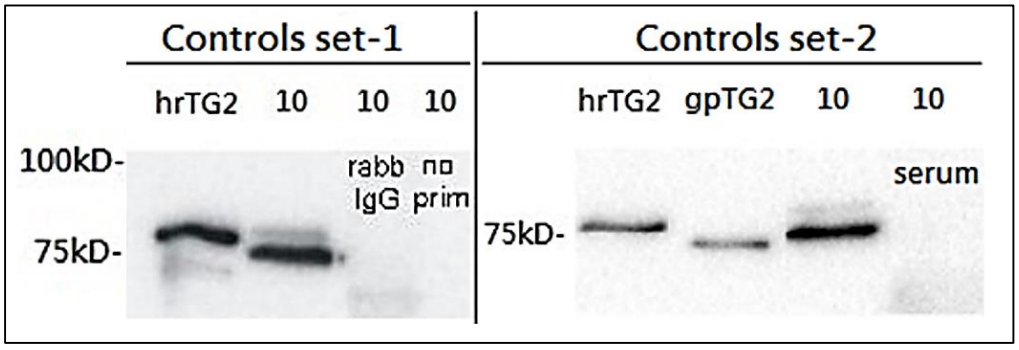

Figure 4.2: Western blot for TG2 using different positive and negative controls

Western blot for cat kidney TG2 from an azotaemic kidney homogenate (cat kidney tissue No. 10). Antibody was assessed using two positive controls, human recombinant TG2 (control set-1 and 2, first lanes) and guinea pig TG2 (control set-2, second lane). For negative controls, blots were probed with or without rabbit IgG (, control set-1, lane 3 and 4, respectively) and rabbit serum (control set-2, lane 4).

4.3.2. Extracellular kidney transglutaminase

4.3.2.1. TG *in situ* activity

Intraglomerular mesangial area. Representative examples of glomeruli from fluorescent sections are shown for each experimental group in Figure 4.6, panels A and C**.** The intraglomerular mesangial area (IGMA) in the representative images do not show any visual difference in red fluorescence between representative images. Measurements of IGMA for the azotaemic and non-azotaemic groups, expressed as mean of area % did not show a significant difference. Non-azotaemic, 4.5 ± 1.8; azotaemic, 9.5 ± 2.6 area %, NS. See Figure 4.6 panel E.

Tubulointerstitial area. Representative examples of tubulointerstitial area from fluorescent sections are shown for the azotaemic and non-azotaemic group in Figure 4.6, panels B and D, respectively. The tubulointerstitial area from the azotaemic image shows an intense red fluorescence extracellularly in both peritubular and interstitial space when compared to the non-azotaemic representative section. Measurements of the tubulointerstitial in the azotaemic kidney tissue, expressed as mean of area %, showed a 3.8 fold higher significant values. Non-azotaemic, 7.9 ± 2.1; azotaemic, 30.1 ± 3.1 area %, $P<0.005$. See Figure 4.6, panel F.

4.3.2.2. TG2 protein

Intraglomerular mesangial area. Representative examples of glomeruli from fluorescent sections are shown for each experimental group in Figure 4.7, panels A and C. The intraglomerular mesangial area (IGMA) in the representative images do not show any visual difference in red fluorescence between representative images. Terminal measurements of IGMA for the azotaemic and non-azotaemic groups, expressed as mean of area % did not show a significant difference. Non-azotaemic, 3.3 ± 1.5; azotaemic, 5 ± 1.7 area %, NS. See Figure 4.7 panel E.

Tubulointerstitial area. Representative examples of tubulointerstitial area from fluorescent sections are shown for the azotaemic and non-azotaemic group in Figure 4.7, panels B and D, respectively. The tubulointerstitial area from the azotaemic image shows an intense red fluorescence extracellularly in both peritubular and interstitial space when compared to the non-azotaemic representative section. Significantly higher values (2.7 fold) were obtained for kidney tissue from cats with

azotaemia compared with non-azotaemic samples. Non-azotaemic, 9.7 ± 2.7; azotaemic, 26.4 ± 3.3 area %, *P*<0.002). See Figure 4.7 panel F.

4.3.3. *In vitro* inhibition of TG enzyme activity

The effect of N-benzyloxycarbonyl-L-phenylalanyl-6-dimethyl-sulfonium-5-oxo-L-norleucin a small MW TG inhibitor on TG enzyme activity in cat kidney homogenates is compared with a TG2 selective mouse monoclonal antibody (BB7) in Figure 4.8. Both N-benzyloxycarbonyl-L-phenylalanyl-6-dimethyl-sulfonium-5-oxo-L-norleucine and mAb BB7 inhibitors almost completely inhibited all the activity in the cat kidney.

4.3.4. Correlations

Extracellular TG enzyme activity gave positive linear correlations with both a marker of renal function (plasma creatinine r^2 =0.30, *P*<0.05) and a marker of matrix deposition (collagen I, r^2 = 0.35, *P*<0.05). Extracellular TG2 protein in the tubulointerstitium showed a highly significant positive linear correlation with plasma creatinine (r^2=0.75, *P*<0.0001), plasma urea (r^2=0.81, *P*<0.0001) and plasma phosphate (r^2=0.76, *P*<0.0001), Table 4.1.

A significant positive linear correlation was also obtained between extracellular TG2 protein and extracellular TG enzyme activity (r^2=0.41, *P*<0.02) and also between total TG activity with both total TG2 protein and extracellular TG activity, Table 4.2. Regarding correlation between the TG pathway and tubulointerstitial fibrosis, significant positive linear correlations could also be demonstrated with markers of matrix deposition including, Masson's trichrome and collagen I, (r^2 =0.39 and 0.39, respectively, *P*<0.05). Also, when fibrosis was assessed by PASH, positive correlations were found with extracellular TG activity ad TG2 protein, see Figure 4.9.

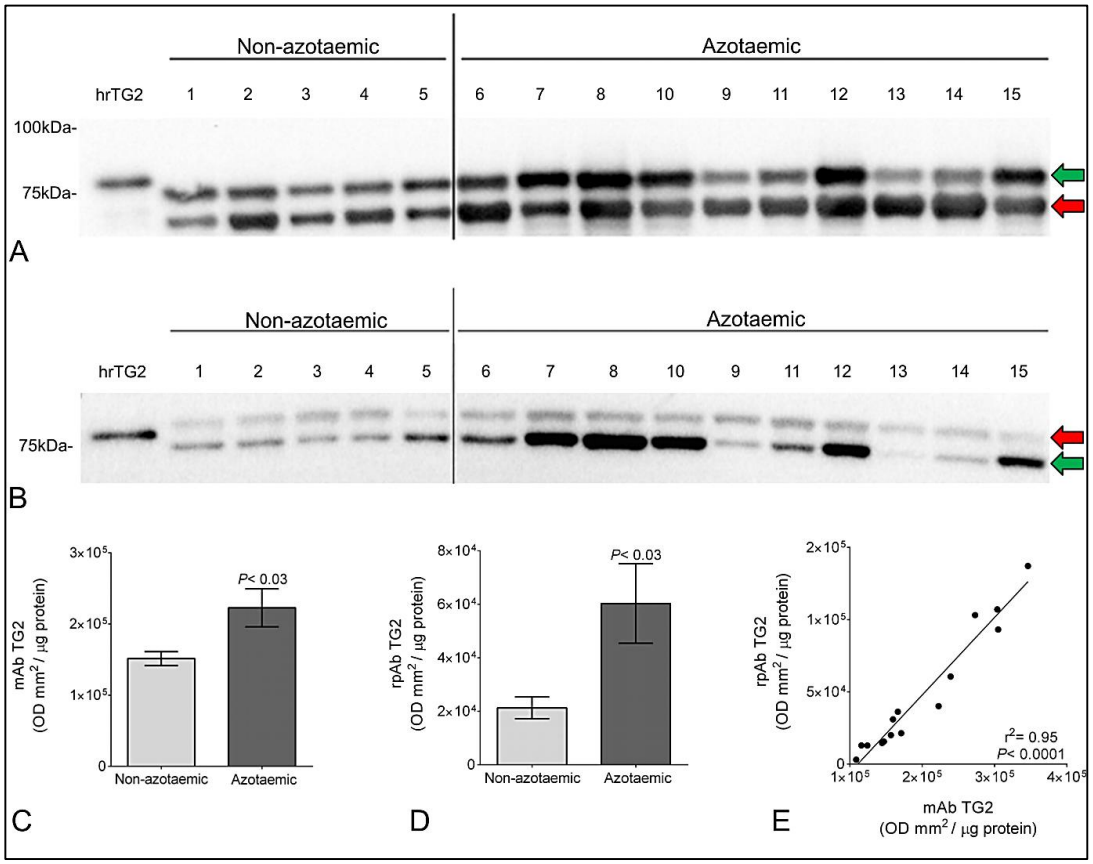

Figure 4.3: Representative Western blots for the quantification of feline TG2

Panel A. Western blot for cat kidney TG2 from non-azotaemic (cat Nos. 1–5) and azotaemic animals (cat Nos. 6–15). Kidney homogenates were immunoprobed with BB7 antibody. Human recombinant TG2 (hrTG2) was employed as a positive control (78 kDa). Kidney homogenates gave 2 bands at 75 kDa (TG2-green arrow) and 66 kDa (possible inactive TG2 fragments-red arrow). Panel B. Each feline tissue sample were reassessed using rabbit polyclonal TG2 antibody (rpTG2). Kidney homogenates gave 2 bands at 83 kDa (factor XIIIa-red arrow) and 75 kDa (TG2-green arrow). Panel C and D. Significantly higher total TG2 protein in cat kidneys obtained from azotaemic compared with non-azotaemic animals when immunoprobed with BB7 and rpTG2, respectively. Vertical lines on columns are ±SEM. Panel E. Positive linear correlation between total TG2 protein using BB7 and total TG2 protein using rpTG2 in kidneys from azotaemic and non-azotaemic cats (n = 15).

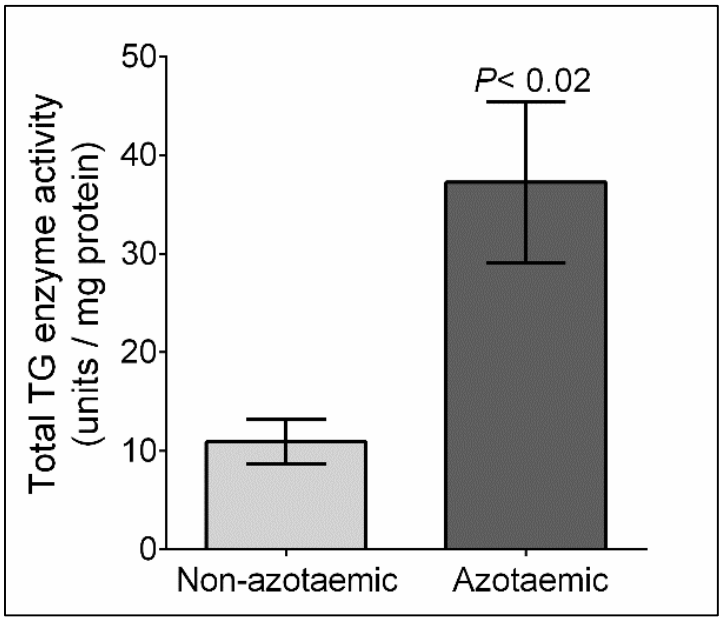

Figure 4.4: Total Transglutaminase activity

Significantly higher total TG enzyme activity in cat kidneys obtained from azotaemic (n = 10) compared with non-azotaemic animals (n = 5), determined by 3H-putrescine incorporation. Vertical lines on columns are ± SEM.

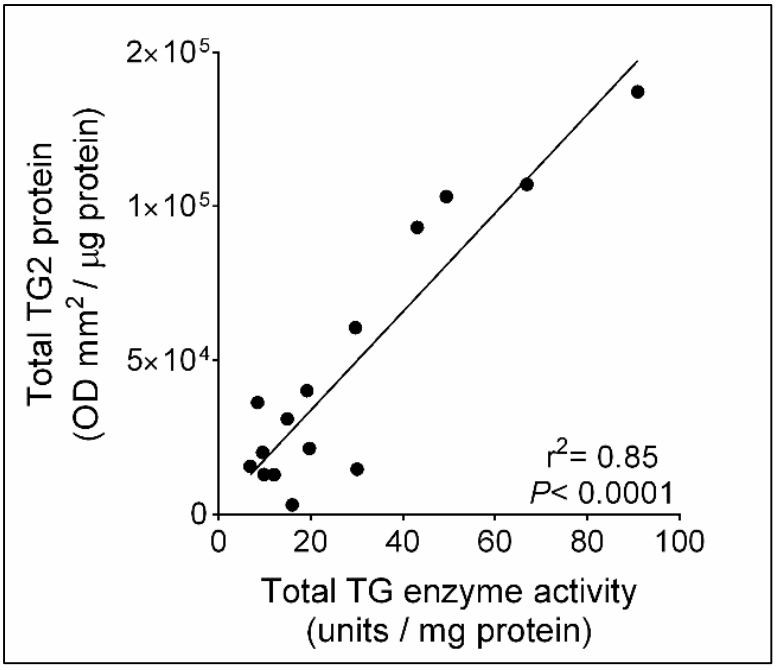

Figure 4.5: Linear regression between total TG activity and total TG2 protein

Positive linear correlation between total TG2 protein and total TG enzyme activity in kidneys from azotaemic and non-azotaemic cats (n = 15).

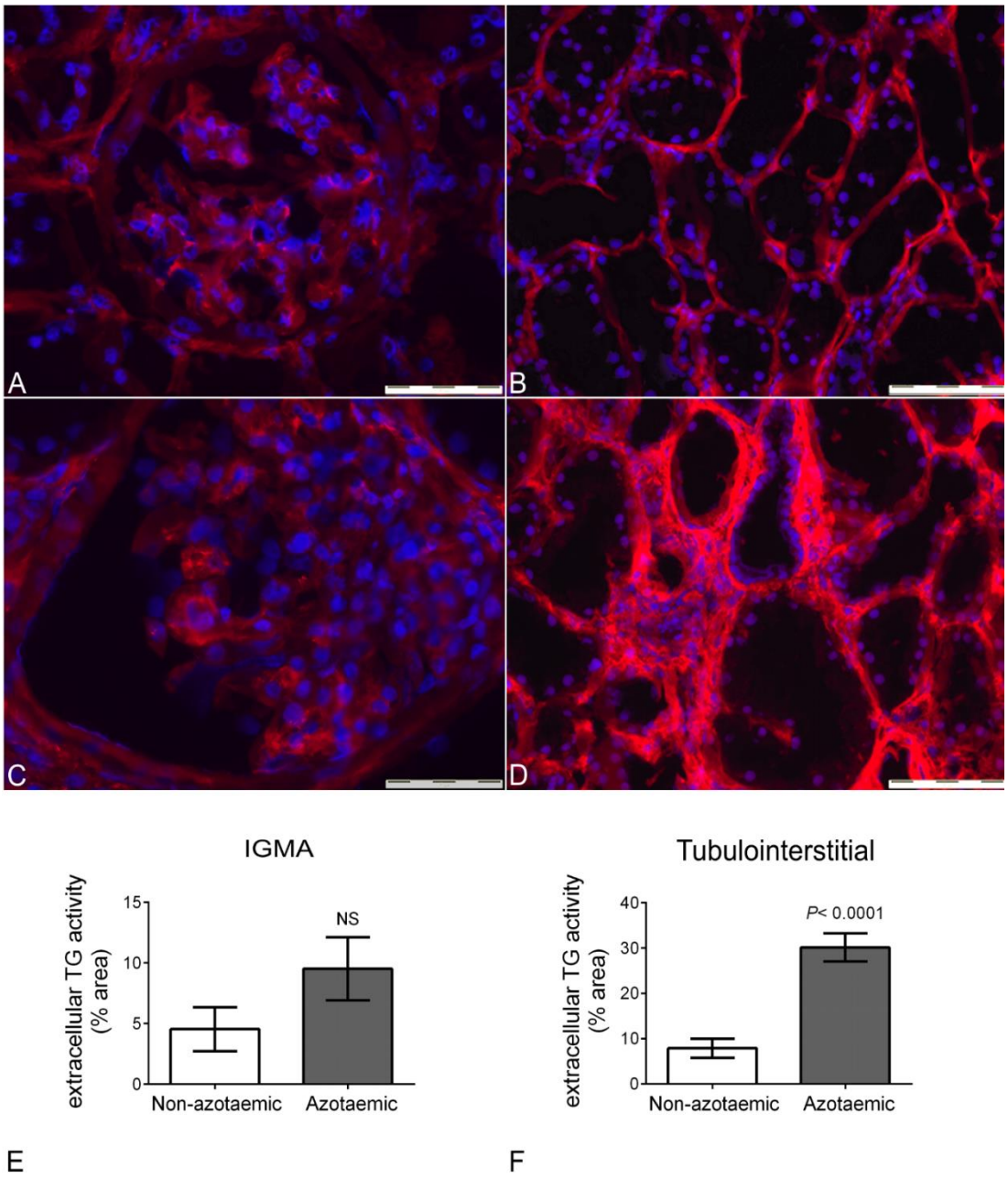

Figure 4.6: Transglutaminase activity in the cat kidney with CKD

Panel **A**, **C** and **B**, **D**. Representative images of glomeruli (400x) and tubulointerstitial (200x) area, respectively, showing coloration (Alexa red - TG activity and DAPI - nuclei) and structural differences between the Non-azotaemic (**A** and **B**) and azotaemic (**C** and **D**) samples, respectively. Panel **E** and **F**. The histograms represents the mean % red area in the IGMA and tubulointerstitial area, respectively. Azotaemic group (n=10) and non-azotaemic group (n=5). Vertical bars indicate +/-SEM.

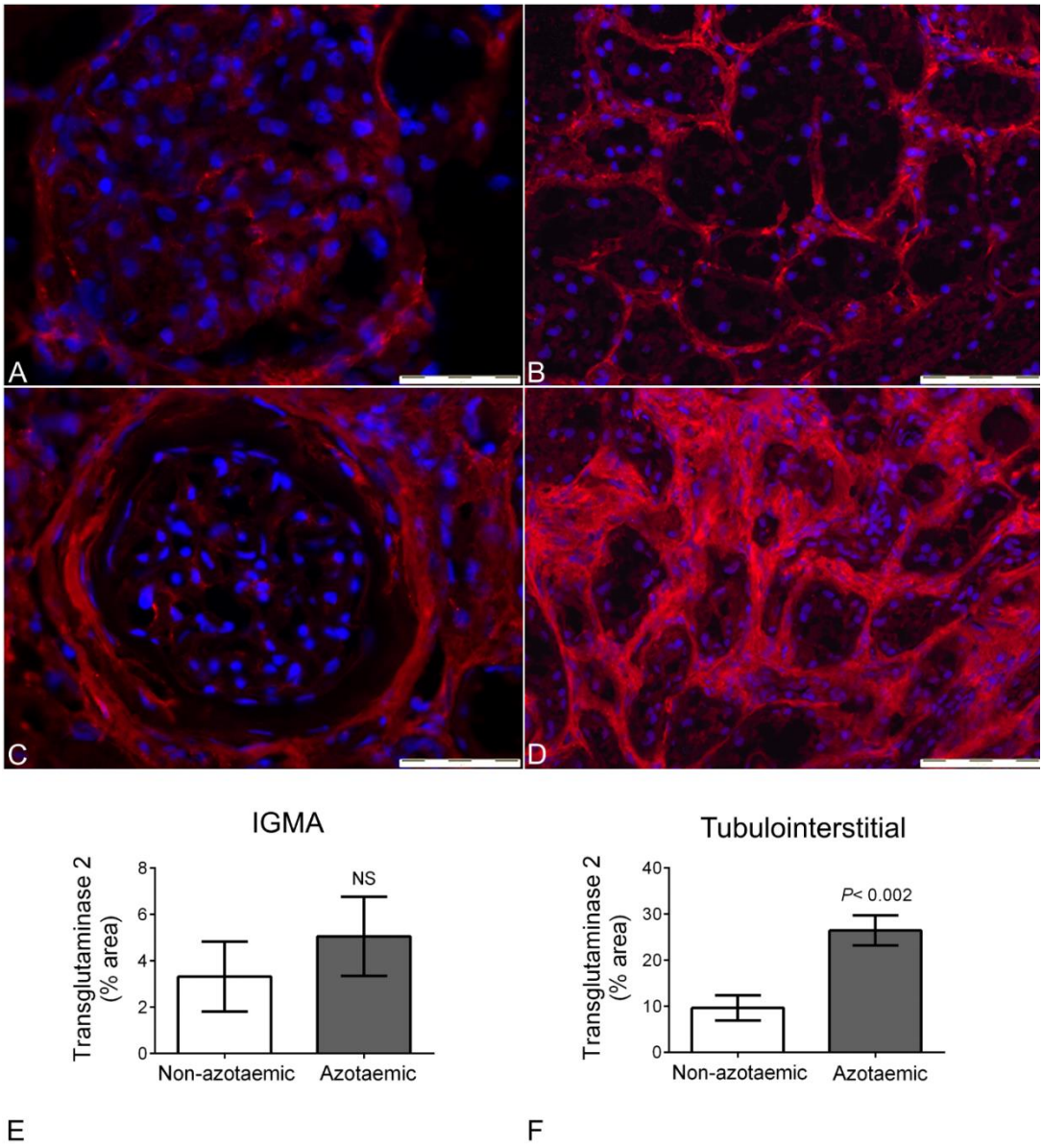

Figure 4.7: Transglutaminase 2 in the cat kidney with CKD

Panel **A**, **C** and **B**, **D**. Representative images of glomeruli (400x) and tubulointerstitial (200x) area, respectively, showing coloration (Alexa red-TG2 and DAPI-nuclei) and structural differences between the Non-azotaemic (**A** and **B**) and azotaemic (**C** and **D**) samples, respectively. Panel **E** and **F**. The histograms represents the mean % red area in the IGMA and tubulointerstitial area, respectively. Azotaemic group (n=10) and non-azotaemic group (n=5). Vertical bars indicate +/-SEM.

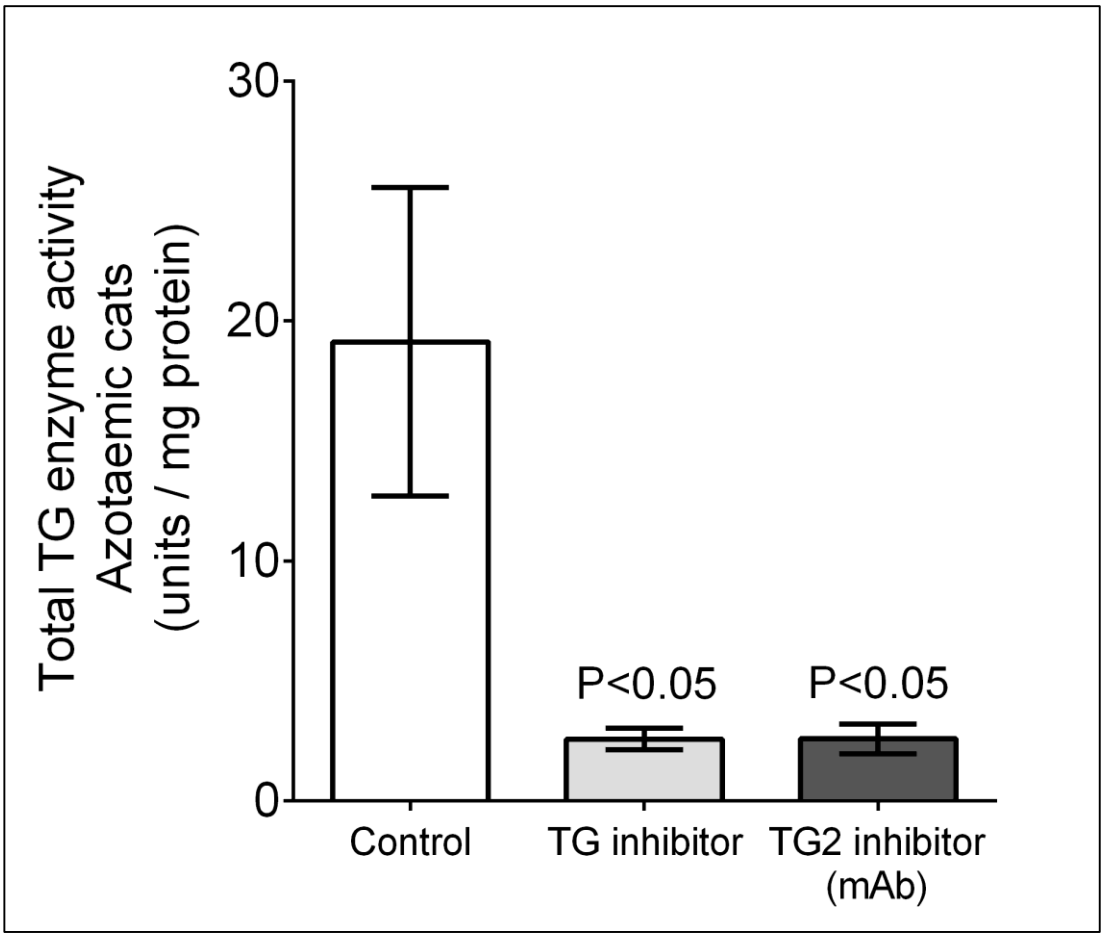

Figure 4.8: Inhibition of total transglutaminase

TG enzyme activity in cat kidney tissue by a low MW, nonselective TG inhibitor and a TG2-selective mouse monoclonal antibody (BB7 mAb) *in vitro*. Kidney homogenates were prepared from azotaemic cats Nos. 6, 7, 8, 10, 12 and 15. Vertical lines on columns are ± SEM (n=6).

Technique A	Technique B	r^2	P value <
Extracellular TG activity	Creatinine	0.30	0.05
Extracellular TG activity	Urea	0.27	0.05
Extracellular TG2 protein	Creatinine	0.75	0.0001
Extracellular TG2 protein	Urea	0.81	0.0001
Extracellular TG2 protein	Phosphorus	0.76	0.0001

Table 4.1: Correlation between tubulointerstitial TG pathway and renal function

Technique A	Technique B	r^2	P value <
Extracellular TG activity	Extracellular TG2 protein	0.41	0.02
Total TG activity	Extracellular TG activity	0.34	0.03
Total TG activity	Total TG2 protein	0.85	0.0001

Table 4.2: TG pathway correlations

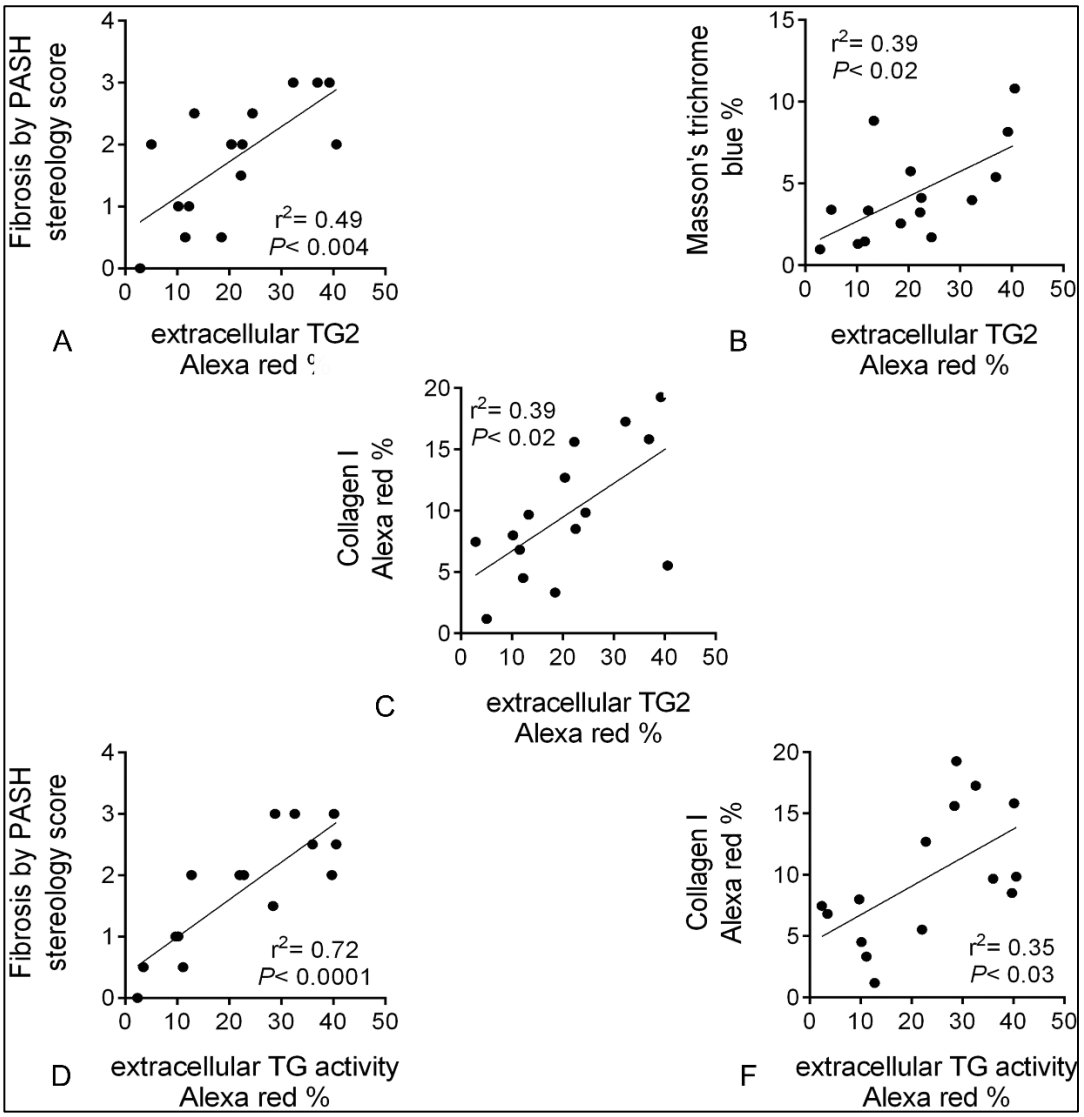

Figure 4.9: Correlations between tubulointerstitial TG pathway and fibrosis

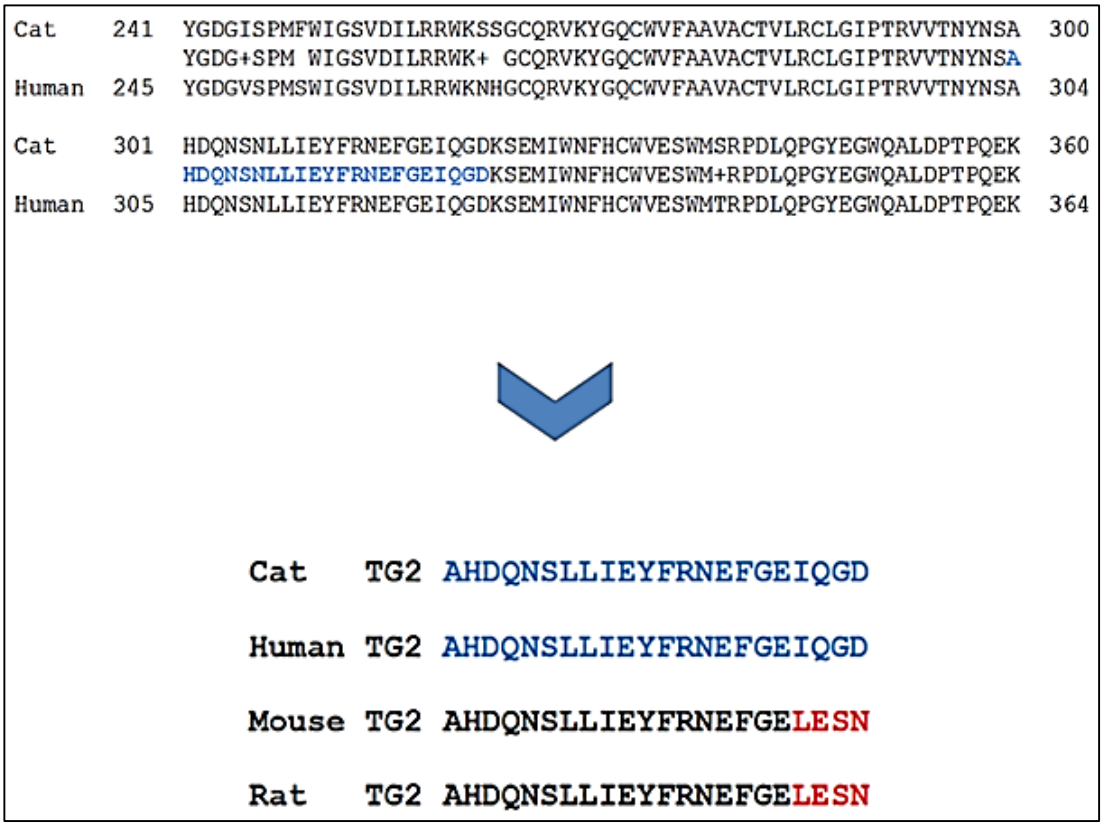

Figure 4.10: Epitope binding site of BB7 Ab on human and feline TG2

Upper image. Segment of TG2 aminoacid sequence and differences between the cat and the human; blue residues denote the BB7 epitope binding site. **Lower image**. BB7 epitope binding site is shown in blue for both cat and human (blue) showing 100% identities. Red residues in the mouse and rat aminoacid segment show the differences in the BB7 epitope binding site when compared to the cat and human.

4.4. Discussion

4.4.1. TG2 protein antibodies

When using the rabbit polyclonal TG2 (Ab421) western blot analysis showed two bands at 75kDa (TG2) and 83kDa. According to the molecular weight, the upper band is compatible with factor XIIIa (ENSFCAP00000014378) (Flicek *et al.*, 2014), a member of the transglutaminase group that is found in blood plasma. Factor XIIIa does not interfere with extracellular TG2 analysis in cryostat section, as the technique washes out all blood plasma from tissue sections. The positive controls (human recombinant TG2) gave a single band at 78kDa. Both human and feline TG2 are composed of 687 aminoacids, however, recombinant human TG2 (hrTG2) is N-terminally fused with a hexahistidine-tag generating a bigger protein of 693 aminoacids, which may explain the slight higher molecular weight for the recombinant TG2.

TG2 detection was further assessed testing four different TG2 antibodies by western blot. Three of those antibodies were commercially available by Abcam (goat polyclonal TG2 antibody, mouse monoclonal TG2 antibody and a rabbit polyclonal TG2 antibody) and the other, a monoclonal antibody named BB7, which was developed by our Academic Nephrology Unit (P Watson, T Johnson and M Mabrouka), see Chapter 2, section 2.5.4, Table 2.4. BB7 antibody, which was originally designed to inhibit human TG2, matched 100% the epitope binding site in the cat TG2, Figure 4.10. All the 4 antibodies showed a consistent band at 75kDa. However, a double, well-defined band was detected at 66kD which may be compatible with a degradation fragment of TG2 (Belkin *et al.*, 2004), Further discussion for the 83 and 66kD bands will be addressed in Chapter 8.

When using the goat TG2 antibody, a polyclonal antibody obtained from immunised goats with a synthetic peptide identical to the cat TG2, the positive control (recombinant human TG2) and feline renal TG2 showed a faint signal in both bands. Different blocking methods and antibody concentrations were attempted, however similar results were obtained, probably due to the susceptibility of cat TG2 protein to denature at that protein portion. For these reasons, the goat polyclonal antibody was not employed. The monoclonal TG2 antibody CUB7402 did not match 100% the epitope binding site to the cat TG2 (69% identities in the aminoacid sequence), hence, it was discarded too. BB7 antibody, on the other hand, matched 100% the feline

epitope binding site. However, due to patent in progress, the employment of BB7 antibody was restricted to the *in vitro* TG2 inhibitory study.

The rabbit polyclonal antibody (Ab421, immunogen: full length TG2 protein purified from guinea pig) was chosen in this project for the following reasons:-

a) Assets of a polyclonal antibody

   -It recognizes multiple epitopes on any one antigen, therefore, it can help to amplify signal with low expression (multiple epitopes provide more robust detection).

   -It is more tolerant to minor changes in antigen, such as polymorphism, heterogeneity of potential glycosylation sites and preferred choice for detection of denature proteins.

   -Identify proteins of high homology to the immunogen protein in question, hence suitable when the nature of the antigen in an untested species is not known, as in cat TG2.

b) The band at 75 kDa showed a high positive linear regression in the OD mm^2/µg protein when compared to the 75 kDa band generated by our TG2 monoclonal antibody BB7 (r^2= 0.95, P<0.0001), see Figure 4.3, panel A-E.

c) The lower band 75 kDa generated by this antibody is a neat and high definition band with no major background, easy to replicate experimentally, Figure 4.3, panel B.

d) It is a commercially available antibody, easy to obtain, thus information obtained in this research project can be published and further investigations can be done or replicated by any research group interested in the field.

4.4.2. Transglutaminase pathway and CKD in the cat

The azotaemic cats showed a higher TG activity and TG2 protein expression when compared to non-azotaemic cats in both extracellular and in tissue homogenates. Kidney homogenate studies showed a 3-fold higher total TG enzyme

activity in cats with azotaemia when contrasted with non-azotaemic cats. Extracellular TG enzyme activity and TG2 protein showed a significant linear correlation with markers of renal function, including plasma creatinine, urea, and phosphate, and with tubulointerstitial fibrosis, including the deposition of matrix protein and collagen I.

In the present study, triggering factors for TG2 expression and activity may be primary hypoxia or secondary, linked to phosphate, urea and creatinine levels. Combination of factors may be important to trigger or perpetuate TG2 transcription and cellular exportation o TG2 to the ECM.

4.4.2.1. Phosphate

An imbalance in calcium and phosphate homeostasis is a common feature of CKD (Barber *et al.*, 1998). Hyperphosphataemia has been found to be an independent predictor for CKD progression and associated with low survival and high morbidity when present in cats (Geddes *et al.*, 2013). The relevance of hyperphosphataemia in CKD and its suppressive effect on renal vitamin D3 metabolism has been studied in both humans and domestic felines (Barber *et al.*, 1998; Nolan, 2005). On the other hand, vitamin D analogues are known to have renoprotective effects (Li, 2010). A significant upregulation for both renin and TGF-β was reported in a model of CKD in vitamin D receptor knockout mice (Zhang *et al.*, 2008). Moreover, it has been shown that vitamin D receptor knockout fibroblasts show upregulation of NF-Kβ (Sun *et al.*, 2006). Interestingly, transglutaminase 2 is strongly associated with the upregulation of TGF- β (Khalil, 1999; Nunes *et al.*, 1997; Shin *et al.*, 2008) and NF-Kβ (Kim *et al.*, 2010), both main fibrogenic and inflammatory proteins, respectively (Morrissey *et al.*, 1998). Moreover, activation of NF-Kβ has been shown to activate TG2.

4.4.2.2. Urea

Regarding the link between azotaemia and TG2 in CKD, urea and creatinine may be importantly involved in the activation of TG2. Azotaemia is a blood condition by abnormally high levels of nitrogen containing compounds. Urea is considered to be the main compound to generate hyperosmolarity (Levine *et al.*, 2001) and metabolic acidosis, hence urea itself, through generation of reactive oxygen species (Vaziri, 2004), may be considered a TG2 triggering factor (Lee *et al.*, 2003).

4.4.2.3. Creatinine

The impact of high levels of creatinine in the cat has not been studied experimentally. In a model of acute kidney injury in the rat (bilateral nephrectomised rats) creatinine or urea injections where able to shorten life survival (Levine *et al.*, 2001). In dogs when chronic creatinine intoxication was induced, mild anaemia and gastroduodenitis were present (Giovannetti *et al.*, 1969). With this evidence, we could speculate that plasma creatinine might not have a direct role in TG activation, however, its potential effect to produce anaemia and inflammation may contribute to some extent.

4.4.2.4. Hypoxia

Triggering and perpetuating factors for TG2 may be associated with hypoxic tissue status. Upregulation of NF-Kβ following unilateral ureteral obstruction in the mouse could not be demonstrated in the TG2 knockout mouse (Kim *et al.*, 2010). Renal hypoxia generates reactive oxygen species (Nangaku, 2006) and systemic acidosis, all potential triggers for TG2 activation (Lee *et al.*, 2003).

In the cat, there are two pieces of evidence showing that hypoxia may be involved in feline CKD (Schmiedt *et al.*, 2012; Williams *et al.*, 2014). Schmiedt et al (2012) showed the effect of renal ischaemia reperfusion in a model of bilateral renal reperfusion injury in the cat, where the acute changes in plasma urea and creatinine were compatible with acute kidney disease that eventually may predispose to the development of CKD, as seen in many other experimental animal models. In Habenicht et al (2013) and Williams et al (2014) studies, vascular endothelial growth factor (VEGF) was assessed in urine from cats with CKD. VEGF is an angiogenic protein produced by cells when low oxygen levels are detected (Levy *et al.*, 1995). Hyperthyroid azotaemic cats showed a significant increase in urinary VEGF when compared to the normal renal function cats (Williams et al., 2014). Conversely, Habenicht et al (2013) showed that in non-hyperthyroid cats with CKD there is a significant reduction of urinary VEGF when comparing to normal renal function cats. Interestingly, in an acute model of RWI in the Sprague Dawley rat, increase in renal VEGFR-2 transcription occurs without the increase in expression of VEGF and VEGFR-1 showing that perhaps VEGF may not be a urinary sensitive marker of hypoxia (Kanellis *et al.*, 2002).

4.4.3. *In vitro* inhibitory studies

Both the mAb BB7 and N-benzyloxycarbonyl-L-phenylalanyl-6-dimethyl-sulfonium-5-oxo-L-norleucine almost completely inhibited all the activity in the cat kidney. The transglutaminase inhibitor compound is able to inhibit the activity of all 9 isoforms of transglutaminase whereas BB7 antibody is specific for TG2. These results suggest that factor XIIIa (blood plasma transglutaminase) does not play a major role in the kidney from cats with CKD, taking into account the homogenized kidney samples assessed in this study were obtained from euthanized cats without previous blood flushing out before -80°C storage. According to our findings TG2 is the major isoform in the cat kidney tissue with CKD.

4.4.4. Conclusion

This study has shown for first time the following points:

a) The association of TG2 with feline CKD
b) TG2 is the major transglutaminase isoform in the cat kidney.
c) We have identified an epitope in the cat TG2 that inhibits (*in vitro*) its activity when targeted by a monoclonal antibody.
d) Identification of a commercial TG2 antibody for future studies in the cat with CKD.
e) The *in vitro* inhibition of TG2 activity in the cat kidney tissue is possible using both approaches monoclonal and chemical inhibitors of transglutaminases.

The renal TG pathway represents an important and plausible new therapeutic target to reduce the development and slow the progression of CKD in the domestic cat. However, due to ethical concerns, experimentation to determine effectiveness of antibodies cannot be performed in cats in this study, hence a rat model of renal warm ischaemia was employed due the accumulative evidence showing that hypoxia may be a cornerstone factor for the development of renal fibrosis. The association and causal link between the TG2 pathway and tubulointerstitial fibrosis induced by RWI will be analysed in chapters 5 and 6, respectively.

CHAPTER 5

The Transglutaminase pathway following Renal Warm Ischaemia in the Rat

5.1. Introduction

Many of the animal models used to study the development of chronic kidney disease involve the induction of acute renal injury at a pre-renal, a renal or a post-renal level. Ischaemia has been identified as a major contributor to acute kidney injury in humans (Abuelo, 2007) significantly increasing the risk of developing CKD (Bellomo *et al.*, 2012). The development of oxidative stress is a common denominator following the induction of acute renal disease triggered by hypoxia (Nangaku, 2006; Shah *et al.*, 2007). The induction of acute renal injury following RWI has also been described in the cat where the histopathological features are compatible with the development of chronic kidney disease (Schmiedt *et al.*, 2012). Mechanisms associated with such events may be examined in animal models following the induction of renal warm ischaemia (RWI) (Weight *et al.*, 1996). Animal models of RWI have also been used to understand the pathogenesis of chronic allograft nephropathy, a fibrogenic condition which may develop following human kidney transplantation. Interestingly, chronic allograft nephropathy has been also recognised following kidney transplantation in cats (De Cock *et al.*, 2004).

RWI in the rat induces ischaemia reperfusion injury involving cellular infiltration and extracellular matrix accumulation leading to the development of chronic renal failure (Forbes *et al.*, 2000). The degree of RWI correlates with the level of renal damage in the functional and structural setting (Azuma *et al.*, 1997). Different rat models of RWI have been established to study the degree of acute renal injury after renal warm ischaemia and its implication in the development of renal fibrosis. Differences in these models rely on the clamping of renal pedicles (unilateral or bilateral), time of clamping (30, 45 and 65 minutes) and the time for contralateral nephrectomy after RWI (0, 5, 7 and 14 days). The less the clamping time the lower the acute renal injury and the degree of fibrosis in chronic studies (Becker *et al.*, 2013). Bilateral renal clamping tends to develop less renal fibrosis when compared to unilateral clamping + early contralateral nephrectomy (Basile *et al.*, 2001a; Lloberas *et al.*, 2001; Torras *et al.*, 1999); this is probably associated with the elevation of renal pressure, hyperfiltration and metabolism, increasing renal oxygen requirements (major tissue hypoxic state) in the unilaterally injured kidney (Brenner *et al.*, 1996; Brezis *et al.*, 1995).

Regarding the time for contralateral nephrectomy, the recovery and survival of the clamped kidney after 60 minutes of RWI kidney was importantly associated

with the time of contralateral nephrectomy in previous pilot studies; this is probably associated, apart from the tissue oxygen requirements above described, with the levels of hyperazotaemia (elevation of plasma urea and creatinine) that produces an acidotic systemic state affecting renal function and other rat organs, generating complete renal failure and death. On the other hand, long recovery of clamped kidney by contralateral renal support may produce a lower level of fibrosis in contrast to early contralateral nephrectomised rats. Temperature, plays an important role for the development of acute kidney in rat RWI. In Sprague Dawley rats, an acute association between RWI and the development of renal injury has been established according to the rat´s body temperature ranging from 32 to 39 °C, the higher the temperature the lower the renal function (Delbridge *et al.*, 2007). Therefore, an adequate balance amongst, temperature, timing for RHC and contralateral nephrectomy are pivotal for the development of tubulointerstitial fibrosis and level acute and long term mortality.

In the present study, a rat model of RWI was employed to assess changes in the transglutaminase pathway associated with the accumulation of extracellular matrix and impairment of renal function. Ischaemia reperfusion injury was induced in male Sprague Dawley rats subjected to left renal hilar clamping for 60 minutes (37°C body temperature) followed by a right nephrectomy 7 days later. Due to histology requirements, this study consisted of a series of 3 cross-sectional experiments where kidney tissue was harvested after 8, 28 and 140 days. Renal function was measured sequentially throughout. A time course was undertaken to establish whether the development of fibrosis in the rat kidney is associated with the transglutaminase pathway at different time points following renal warm ischaemia.

5.2. Material and methods

5.2.1. Animals and anaesthesia

Male Sprague-Dawley rats (Harlan, UK), 8-10 weeks, with an initial weight of 250-300 grams were maintained at 20°C, 45% humidity and with a light cycle of 12 hours. For surgical procedure, rats were induced in an anaesthetic chamber with 5% isoflurane and 8 L/min oxygen. Analgesia was provided by intramuscular injection of buprenorphine 50µg/kg. Maintenance of anaesthesia was achieved with 1.5% of isoflurane and 1 L/min oxygen. The rat was placed on an operating board covered

with a homeothermic blanket to keep the rat temperature between 36-37°C. Surgical area was clipped and cleaned aseptically.

5.2.2. Experimental protocol

The groups consisted of nephrectomised rats (Nx) composed of sham operated rats subjected to right nephrectomy at day 7. The disease group (RWI), composed of rats subjected to 60 minutes of left renal hilar clamping and right nephrectomy at day 7; both groups with a disease progression of 8, 28 or 140 days. In the 8-day experiment, a rat did not reach an adequate change in coloration suggesting inadequate clapping of renal hilus, therefore, it was removed from the study. A rat in the 28-day died after contralateral nephrectomy. Number of rats for each terminal experiments are displayed in Table 5.1.

Days after RWI	Number of rats per group	
	Nx	RWI
8	5	4
28	8	7
140	6	10

Table 5.1: Number of rats for each study

5.2.3. Renal function

5.2.3.1. Blood serum and urine

Blood serum and urine were pipetted into plastic test tubes. Creatinine was assayed in serum and urine by the Jaffe rate method (Levey *et al.*, 1988) using a SYNCHRON ® System (Beckman Coulter Inc.) machine (section 2.3.1). Assessment of serum and urine creatinine was performed at day 0, 8, 28, 56, 84, 112 and 140 of RWI, according to each study.

5.2.3.2. Rat albumin

Rat albumin was measured in urine by enzyme-linked immunosorbent assay (ELISA). A 96 well plate was coated with sheep anti-rat albumin antibody and the sample added to the plate. The secondary anti-sheep antibody containing horseradish peroxidase (HRP) was then added followed by the enzyme substrate. The change in colour was proportional to the amount of secondary antibody bound to the primary antibody which in turn is bound to albumin. The optical signal was measured by spectrophotometry at 450 nm (section 2.3.2). Assessment of albumin excretion was performed at day 8, 28, 56, 84, 112 and 140 of RWI, according to each study.

5.2.3.3. Systemic blood pressure

Systemic blood pressure was measured using a tail cuff plethysmography. The blood pressure was captured by a central amplifier (IITC life science BP amplifier) and the information was displayed through a software IITC life science (section 2.2.9).

5.2.4. Renal morphology

5.2.4.1. Haematoxylin and Eosin

5µm paraffin embedded sections were deparaffinized and rehydrated. The slides were stained with haematoxylin, rinsed and stained with eosin. Slides were passed through several changes of alcohol and xylene to clear and dehydrate tissue sections. The slides were mounted in DPX mountant. Bowman's space, glomerular diameter, tubular dilatation space and tubular luminal area were assessed using a software for image analysis (Cell F, Olympus, Software Digital Image System, USA). H and E staining was only performed for the 28-day RWI study (section 2.4.1).

5.2.5. Renal fibrosis

5.2.5.1. Masson's trichrome staining

5µm, formalin-fixed, paraffin embedded sections were deparaffinized and rehydrated. Tissue sections were placed in Bouin's solution overnight, washed and

placed in working Weigert's iron haematoxylin solution for 5 minutes. Slides were stained with Biebrich scarlet-acid fuchsin, aniline blue solutions, rinsed in tap water, dehydrated and mounted in DPX. For IGMA and tubulointerstitial expansion of extracellular matrix, no less than 10 glomeruli (x 400) and (x 200) of cortex tubules were acquired. The fibrosis index was determined calculating the blue (Masson´s trichrome) / red (cellularity) ratio of total field. Quantification was performed by image analysis (section 2.4.3). Tissue assessment of extracellular matrix expansion by MTS was performed at day 8, 28 and 140 days, according to each RWI study.

5.2.5.2. Immunofluorescence

8µm thick cryostat sections on adherent slides, previously stored at -80°C. The slides were blocked and washed. The tissue was then probed with a primary antibody (collagen I, III and IV) overnight at 4°C followed by fixation and serial washings. The slides were immunoprobed with a secondary antibody and left at room temperature for 2 hours. A drop of mounting medium with DAPI was added and a cover slide was placed on top. No less than 10 glomeruli (x 400) and (x 200) of cortex tubules were acquired. The immunofluorescent fibrosis index was determined calculating the intense FITC (collagens) / DAPI (nuclei) ratio of the total field. Quantification was performed by image analysis (section 2.6.1). Tissue assessment of collagens by immunofluorescence was performed at day 8, 28 and 140 days, according to each RWI study.

5.2.6. Renal transglutaminase

5.2.6.1. Immunofluorescence

8µm thick cryostat sections on adherent slides were blocked and washed. The tissue was probed with a primary antibody (TG2) overnight at 4°C followed by fixation and serial washings. The slides were immunoprobed with a secondary antibody and left at room temperature for 2 hours. A drop of mounting medium with DAPI was added and a cover slide was place on top. No less than 10 glomeruli (x 400) and (x 200) of cortex tubules were acquired. The immunofluorescent fibrosis index was determined calculating the intense Alexa red (TG2) / DAPI (nuclei) of the total field. Quantification was performed by image analysis (section 2.6.1). Tissue assessment of TG2 by immunofluorescence was performed at day 8, 28 and 140 days, according to each RWI study.

5.2.6.2. TG *in situ* activity

8µm thick cryostat sections were rehydrated. Sections were incubated 1h at 37°C with the reaction buffer. Three controls were set up by incubating some sections with either 10mmol/L EDTA, 200 µmol/L DOO3 or anti-TG2 mouse monoclonal antibody, 1:50. Sections were washed twice, fixed with cold acetone for 10 minutes in a -20°C freezer, air dried and blocked with 3% BSA in PBS at 4°C overnight. The sections were washed twice, probed with Alexa labelled streptavidin 1:300 in 3% BSA / PBS and incubated 2h at 37°C. Sections were washed in PBS and mounted using MOWIOL-DAPI mounting media. IGMA and tubulointerstitial fields were pictured and quantified as described for the immunofluorescent techniques. Examples for TG activity and protein quantification by image analysis are shown in Figure 2.26.

5.2.7. Statistics

Studies were assessed by unpaired t-test and two-way ANOVA for longitudinal studies. To assess correlations between different experiments, analysis r^2 and p values were calculated. For all the statistical analysis, a probability higher than 95% ($p<0.05$) was taken as significant. The calculations, histograms and linear plots were performed using Graph Prism version 5 software (section 2.7.2).

5.3. Results

5.3.1. Renal Warm Ischaemia - day 8 study

5.3.1.1. Renal function

Serum creatinine. The RWI group showed a significantly higher serum creatinine level, expressed as mean of µmol/L, when compared to the Nx group. Nx, 51.6 ± 4; RWI, 334.3 ± 34 µmol/L, $P<0.0001$.

Creatinine Clearance. The RWI group showed a significantly lower creatinine clearance, expressed as mean of milliliters per minute, when compared to the Nx group. Nx, 1.53 ± 0.21; RWI, 0.125 ± 0.04 ml / min, $P<0.001$.

Albumin excretion, water intake and urine production. Measurements did not show any significant difference between groups. Albumin, Nx, 0.8 ± 0.6; RWI, 2.36 ± 0.16 mg / 24hrs, P=0.06. Water intake, Nx, 29 ± 1; RWI, 36 ± 3 ml / 24 hrs, P=0.055. Urine production, Nx, 20.2 ± 6.5; RWI, 34.2 ± 4.15 ml / 24 hrs, P=0.13.

Renal weight. Terminal measurement of renal weight for the RWI group, expressed as mean of grams per kidney, showed a significantly higher change when compared to the Nx group. Nx, 1.24 ± 0.12; RWI, 2 ± 0.06 grams, P<0.01.

5.3.1.2. Renal fibrosis

Masson's Trichrome Staining

Intraglomerular mesangial area. The RWI group was associated with a significantly higher blue/red ratio at day 8 when compared to the Nx group. Nx, 2 $x10^{-4}$ ± 2.5 $x10^{-5}$; RWI, 10 $x10^{-4}$ ± 20 $x10^{-5}$ blue/red ratio, P<0.005.

Tubulointerstitial area. The RWI group was associated with a significantly higher in the blue/red ratio at day 8 when compared to the Nx group. Nx, 0.007 ± 0.001; RWI, 0.04 ± 0.01, P<0.001.

Collagen III

Intraglomerular mesangial area. Measurements of collagen III in the IGMA did not show any significant difference in the FITC/DAPI ratio between groups. Nx, 2.3 $x10^{-3}$ ± 0.7 $x10^{-3}$; RWI, 2.1 $x10^{-3}$ ± 10.5 $x10^{-3}$ FITC/DAPI ratio, P=0.9.

Tubulointerstitial area. The RWI group was associated with a significantly higher FITC/DAPI ratio when compared to the Nx group. Nx, 0.085 ± 0.02; RWI 0.3 ± 0.03 FITC/DAPI, P<0.0003.

5.3.1.3. Renal transglutaminase

TG *in situ* activity

Intraglomerular mesangial area. Measurements of TG activity in the IGMA did not show any significant difference in the Alexa red / DAPI ratio between groups. Nx, 0.54 ± 0.13; RWI 0.33 ± 0.22 Alexa/DAPI, P=0.43.

Tubulointerstitial area. The RWI group was associated with a significantly higher Alexa red / DAPI ratio when compared to the Nx group. Nx, 0.24 ± 0.07; RWI 0.55 ± 0.07 FITC/DAPI, P<0.02.

TG2 immunofluorescence

Tubulointerstitial area. The RWI group was associated with a significantly higher Alexa red / DAPI ratio when compared to the Nx group. Nx, 0.7 ± 0.05; RWI 0.9 ± 0.04 FITC/DAPI, P<0.05. Table 2.52 shows a summary for RWI-day 8 results.

5.3.2. Renal Warm Ischaemia - day 28 study

5.3.2.1. Renal function

Serum creatinine. The RWI group was associated with a significantly higher serum creatinine, expressed as mean µmol/L, when compared to the Nx group. Nx, 48.75 ± 2.3; RWI, 68.1 ± 3.4 µmol/L, P<0.001.

Albuminuria. Measurements did not show any significant difference between groups. Nx group. Nx, 0.7 ± 0.08; RWI, 0.6 ± 0.1, mg / 24 hrs, P<0.001.

Water intake and urine production. Measurements did not show any significant difference between groups. Water intake, Nx, 10.2 ± 2.3; RWI, 12.6 ± 2.3, ml / 24 hrs, P=0.5. Urine production. Nx, 12.06 ± 1.9; RWI, 15.14 ± 1.6, ml / 24 hrs, P=0.25.

Renal weight. Measurement of renal weight for the RWI group, expressed as mean of milligrams per kidney, showed a significant change when compared to the Nx group. Nx, 1.24 ± 0.12; RWI, 2 ± 0.06 grams, P<0.01.

Assessment	Groups		Units	RWI change	P value <
	Nx	RWI			
Renal function					
Serum creatinine	51.6 ± 4	334.3 ± 34	µmol/L	6.4 fold▲	P<0.0001
Creatinine clearance	1.53 ± 0.21	0.125 ± 0.04	ml / min	94%▼	P<0.001
Kidney weight	1.24 ± 0.12	2 ± 0.06	mg	1.6 fold▲	P<0.01
Albumin excretion	0.8 ± 0.6	2.36 ± 0.16	mg / 24hrs	66%▼	NS
Water intake	29 ± 1	38 ± 3	ml / 24 hrs	1.3 fold▲	NS
Urine production	20.2 ± 6.5	34.2 ± 4.15	ml / 24 hrs	1.7 fold▲	NS
Intraglomerular mesangial area					
MT	$2x10^{-4}$±$2.5x10^{-5}$	$10x10^{-4}$±$20x10^{-5}$	blue/red	5 fold▲	P<0.01
Collagen III	$2.3\ x10^{-3}$±$0.7\ x10^{-3}$	$2.1\ x10^{-3}$±$10\ x10^{-3}$	FITC/DAPI	8.7%▼	NS
TG *in situ* activity	0.54 ± 0.13	0.33 ± 0.22	Alexa/DAPI	39%▼	NS
Tubulointerstitial					
MT	0.007 ± 0.001	0.04 ± 0.01	blue/red	5.7 fold▲	P<0.001
Collagen III	0.085 ± 0.02	0.3 ± 0.03	FITC/DAPI	3.5 fold▲	P<0.0005
TG *in situ* activity	0.24 ± 0.07	0.55 ± 0.07	Alexa/DAPI	2.3 fold▲	P<0.02
TG2	0.7 ± 0.05	0.9 ± 0.04	Alexa/DAPI	1.3 fold▲	P<0.05

Table 5.2: Measurements after 8 days of RWI

5.3.2.2. Renal histomorphology

Bowman's space and glomerular diameter. The RWI group did not show a significant higher diameter when compared to the Nx group. Bowman's space, Nx, 847 ± 99.2; RWI, 1404 ± 278 μm^2, P=0.068. Glomerular diameter, Nx, 121 ± 2.8; RWI, 116 ± 5.7 µm, P=0.46.

Tubular luminal area. Representative examples of tubular luminal measurements from H & E sections are shown for each experimental group in Figure 5.1, panels A and B. The tubular section from the RWI group shows a considerable increase in tubular luminal area when compared to the Nx group. The RWI group was associated with a significantly higher tubular luminal area (μm^2) compared with Nx group (P<0.0001), see Figure 5.1 panel C. Nx, 105 ± 7.5; RWI, 670 ± 79 μm^2, P<0.0001.

External tubular diameter. Representative examples of external tubular diameter measurements from H & E sections are shown for each experimental group in Figure 5.1, panels A and B The tubular section from the RWI group shows no difference in the external tubular diameter area when compared to the Nx group. The RWI group did not show any difference or trend in the external tubular diameter area (µm) when compared to the Nx group, see Figure 5.1, panel D. Nx, 58 ± 1.2; RWI, 56.4 ± 1.4 µm, P=0.44

5.3.2.3. Renal fibrosis

Masson's Trichrome Staining

Intraglomerular mesangial area. Representative examples of glomeruli are from MTS sections at day 28 are shown for each experimental group in Figure 5.2, panels A and C. The intraglomerular mesangial area (IGMA) in the representative images do not show any visual difference in blue staining between Nx (panel A) and RWI (panel C) representative image. Measurements of IGMA for the Nx and RWI groups, expressed as mean of blue/red ratio did not show a significant difference at day 28. See Figure 5.2 panels E. Nx, $0.43x10^{-2} \pm 0.17 x10^{-2}$; RWI, $0.8 x10^{-2} \pm 0.3 x10^{-2}$ blue/red ratio, P=0.32.

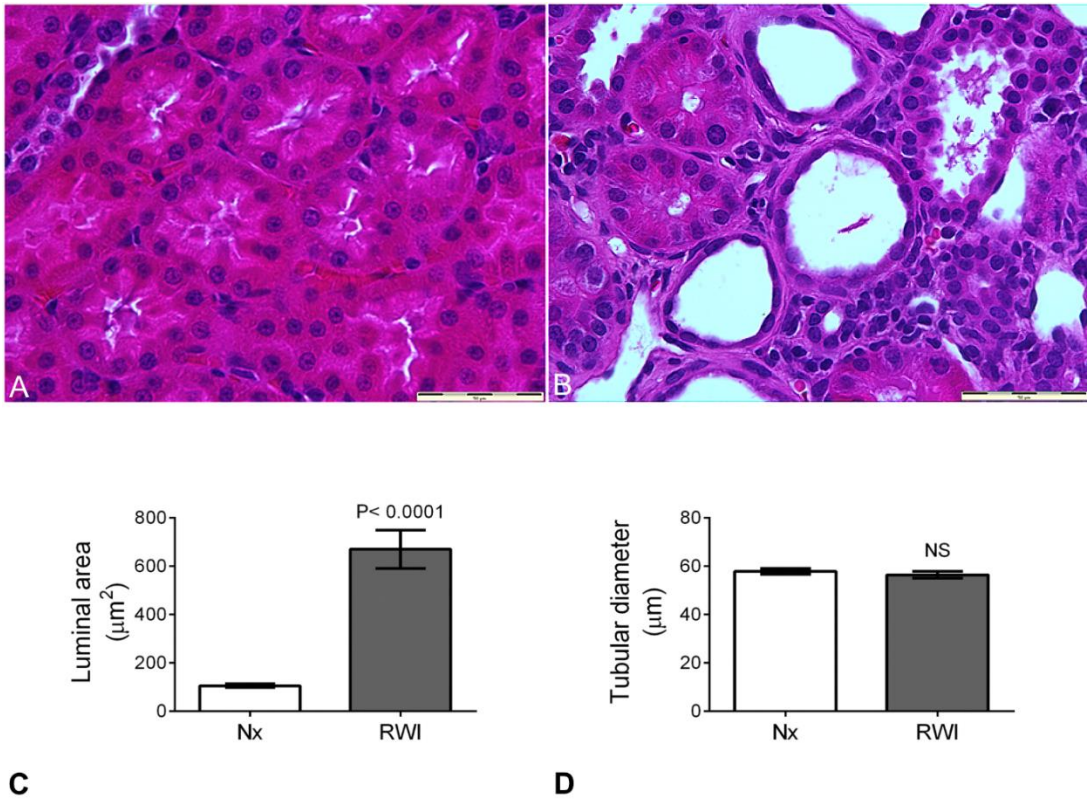

Figure 5.1: Effect of RWI on tissue morphology after 28 days

Panel **A** and **B**. Representative images of tubules under 400x magnification showing structural differences between the Nx (Panel A) and the RWI (Panel B) samples. The histogram in panel **C** and **D** represents the mean of tubular luminal area and external tubular diameter. RWI = renal warm ischaemia (60 min) plus right nephrectomy (n=7), Nx = right nephrectomy alone (n=8). Vertical bars indicate +/- SEM.

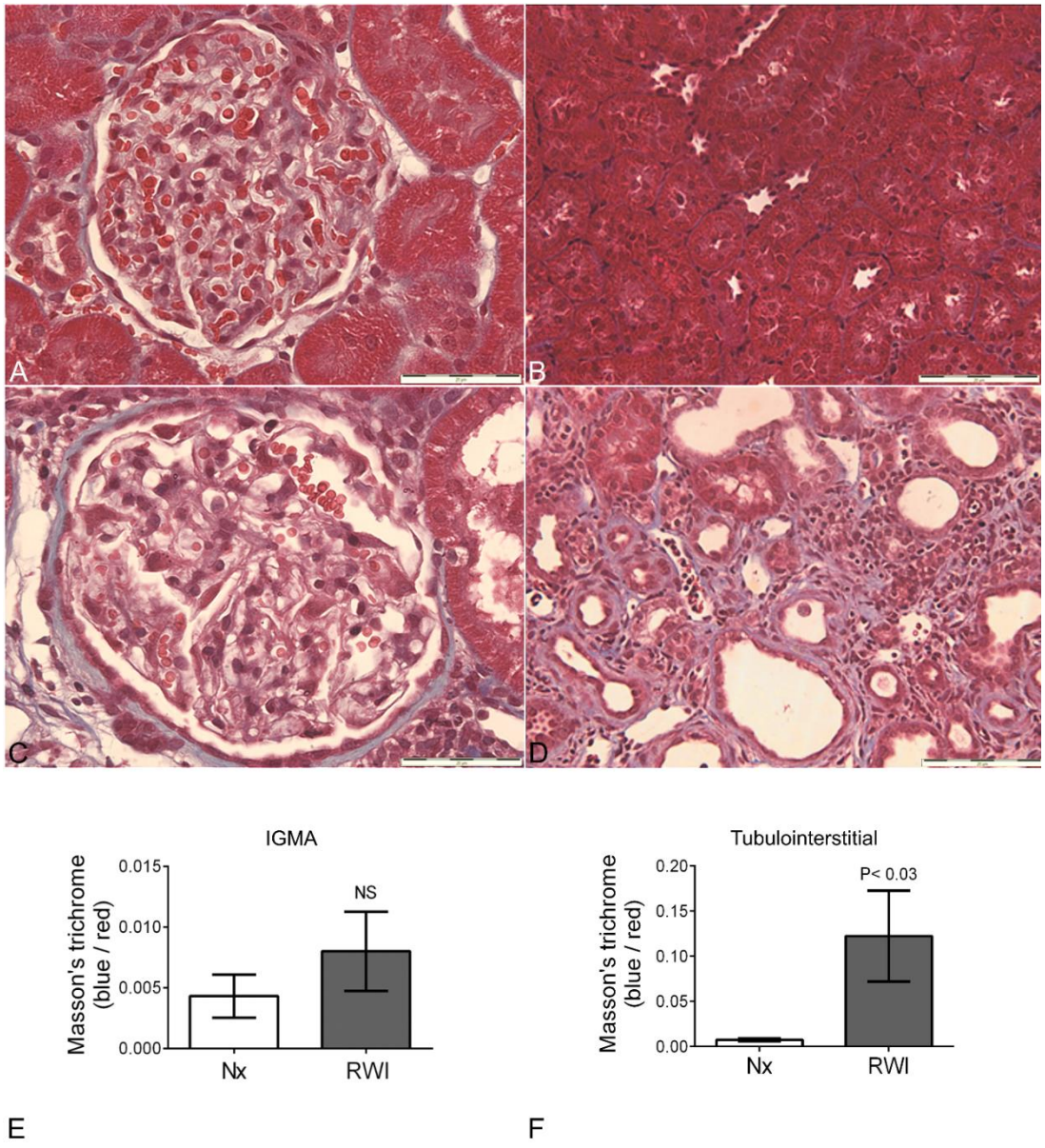

Figure 5.2: Effect of RWI on the IGMA and tubulointerstitial matrix after 28 days

Panel **A**,**C** and **B**,**D**. Representative images of IGMA and tubulointerstitial area under 400x and 200x magnification, respectively, are showing coloration (blue-extracellular matrix; red-cellularity) and structural differences between the Nx (**A** and **B**) and RWI (**C** and **D**) samples, respectively. The histogram **E** and **F** represents the mean blue/red ratio in the intraglomerular mesangial area and tubulointerstitial area after 28 days of RWI, respectively. Nx = right nephrectomy, n=8; RWI = renal warm ischaemia (60 min) plus right nephrectomy, n=7. Vertical bars indicate +/-SEM

Tubulointerstitial area. Representative examples of tubules from MTS sections at day 28 the RWI and Nx group are displayed in Figure 5.2, panels B and D, respectively. The tubulointerstitial area from the RWI image (panel D) shows a high level of blue staining localized in the tubular basement membrane and interstitial area when compared to the Nx image (panel B). Moreover, the RWI group shows a higher degree of intratubular and intertubular space in contrast to the Nx group. Measurements of the tubulointerstitial area for the Nx and RWI groups, expressed as mean of blue/red ratio, showed a significantly higher level in the RWI group when compared to the Nx group. Nx, 0.007 ± 0.001; RWI 0.12 ± 0.05 blue/red ratio, P<0.03. See Figure 5.2 panel F.

5.3.2.4. Renal transglutaminase

TG2 immunofluorescence

Intraglomerular mesangial area. Measurement of TG2 in the IGMA for the Nx and RWI groups, expressed as mean of Alexa/DAPI ratio, did not show any significant change between groups. Nx, $1.8x10^{-2} \pm 5.5x10^{-3}$; RWI, $5.3x10^{-2} \pm 28x10^{-3}$ Alexa red / DAPI, P=0.3.

Tubulointerstitial area. Cross-sectional measurements of TG2 in the tubulointerstitial space were associated with a significantly higher Alexa/DAPI ratio between groups. Nx, 0.9 ± 0.09; RWI 1.35 ± 0.13 Alexa/DAPI, P<0.02.
A summary of results is displayed in Table 5.3.

5.3.3. Renal Warm Ischaemia - day 140 study

5.3.3.1. Renal function

Serum creatinine. Longitudinal measurements of serum creatinine, expressed as a mean of µmol/L are shown in Figure 5.3, panel A. The RWI group was associated with significant 7 fold increase at day 8 (24hrs after right nephrectomy) when compared to the Nx group. Nx, 52 ± 1.7; RWI, 348 ± 18 µmol/L, P<0.0001. However, by the measurement at day 28, the levels of serum creatinine from the RWI group decreased considerably staying slightly higher than the Nx group for the rest of the study. At day 140, the RWI group was associated with a significant higher serum creatinine level when compared to the Nx group. Nx, 54.2 ± 2.8; RWI, 65.7 ± 3.4 µmol/L, P<0.04.

Assessment	Groups		Units	RWI change	P value <
	Nx	RWI			
Renal function					
Serum creatinine	48.75 ± 2.3	68.1 ± 3.4	µmol/L	0.7 fold ▲	P<0.001
Albumin excretion	0.7 ± 0.1	0.56 ± 0.1	mg / 24hrs	2.2 fold ▲	P<0.0001
Water intake	10.2 ± 2.3	12.6 ± 2.3	ml / 24hrs	1.2 fold ▲	NS
Urine production	12.06 ± 1.9	15.14 ± 1.6	ml / 24hrs	1.2 fold ▲	NS
Histomorphometry					
Glomerular diameter	121 ± 2.8	116 ± 5.7	µm	4%▼	NS
Bowman's space	847 ± 99.2	1404 ± 278	μm^2	1.6 fold ▲	NS
Tubular diameter	58 ± 1.2	56.4 ± 1.4	µm	2.7%▼	NS
Tubular luminal area	105 ± 7.4	670 ± 79	μm^2	6.4 fold ▲	P<0.0001
Intraglomerular mesangial area					
MT	$0.43x10^{-2}$±$0.17x10^{-2}$	$0.8x10^{-2}$ ± $0.3x10^{-2}$	blue/red	5 fold ▲	NS
TG2	$1.8x10^{-2}$ ± $5.5x10^{-3}$	$5.3x10^{-2}$ ± $28x10^{-3}$	Alexa/DAPI	2.9 fold ▲	NS
Tubulointerstitial					
MT	0.007 ± 0.001	0.12 ± 0.05	blue/red	17 fold ▲	P<0.03
TG2	0.9 ± 0.09	1.35 ± 0.13	Alexa/DAPI	1.5 fold ▲	P<0.02

Table 5.3: Measurements after 28 days of RWI

Creatinine Clearance. Longitudinal measurements of creatinine clearance, expressed as a mean of millilitres per minute, are shown in Figure 5.3, panel B. The RWI group showed a moderate decrease after 24hrs of renal hilar clamping ($P<0.05$), followed by an important decrease (94% its original value) at day 8 when compare to the Nx group. Nx, 1.3 ± 0.1; RWI, 0.1 ± 0.1 millilitres / minute, $P<0.0001$). At day 28, the creatinine clearance in the RWI group increased considerably staying slightly lower during the rest of the time course study in contrast to the Nx group. The creatinine clearance trend showed, an inverse pattern to the one seen for serum creatinine in Figure 5.3, panel A. The terminal measurements of creatinine clearance for the Nx and RWI groups did not show a significant difference between groups at day 140. Nx, 1.9 ± 0.3; RWI, 1.7 ± 1.1 mls / min, $P=0.5$.

Albumin excretion. Longitudinal measurements of albumin excretion, expressed as mg per 24 hours, are shown in Figure 5.3, panel C. The albumin levels in the RWI group increased steadily from day 28 to day 112 followed by a significant 5.5 fold rise compared to the Nx group at day 140 ($P<0.0001$). A gradual increase in the levels of albuminuria for the Nx group was evident from day 56 to day 120. Albumin excretion at day 8 did not show any significant difference between groups. However, the terminal measurements of albumin excretion showed a significant increase in the RWI group at day 140. Nx, 90.6 ± 2.8; RWI, 378 ± 95.9 mg / 24hrs, $P<0.05$.

Systolic blood pressure. Longitudinal measurements of systolic blood pressure for each experimental group, expressed as mmHg are shown in Figure 5.3, panel D. The RWI group was associated with a steady significant increase from day 28 to day 140 in contrast to the Nx group, which remained relatively constant within normal range (mean 124.6 ± 1.45 mmHg). At day 140, the RWI group showed a significantly higher blood pressure when compared to the Nx group. Nx, 128 ± 2.4; RWI, 150 ± 3.73 mmHg, $P<0.001$.

Water intake and urine production. The RWI group showed a moderate significant increase in water intake and urine production when compared to the Nx group. Water intake, Nx, 26.2 ± 0.4; RWI, 36.3 ± 2.4 ml / 24 hrs, $P<0.01$. Urine production, Nx, 14.7 ± 1.5; RWI, 25.5 ± 2.2 ml / 24 hrs, $P<0.01$.

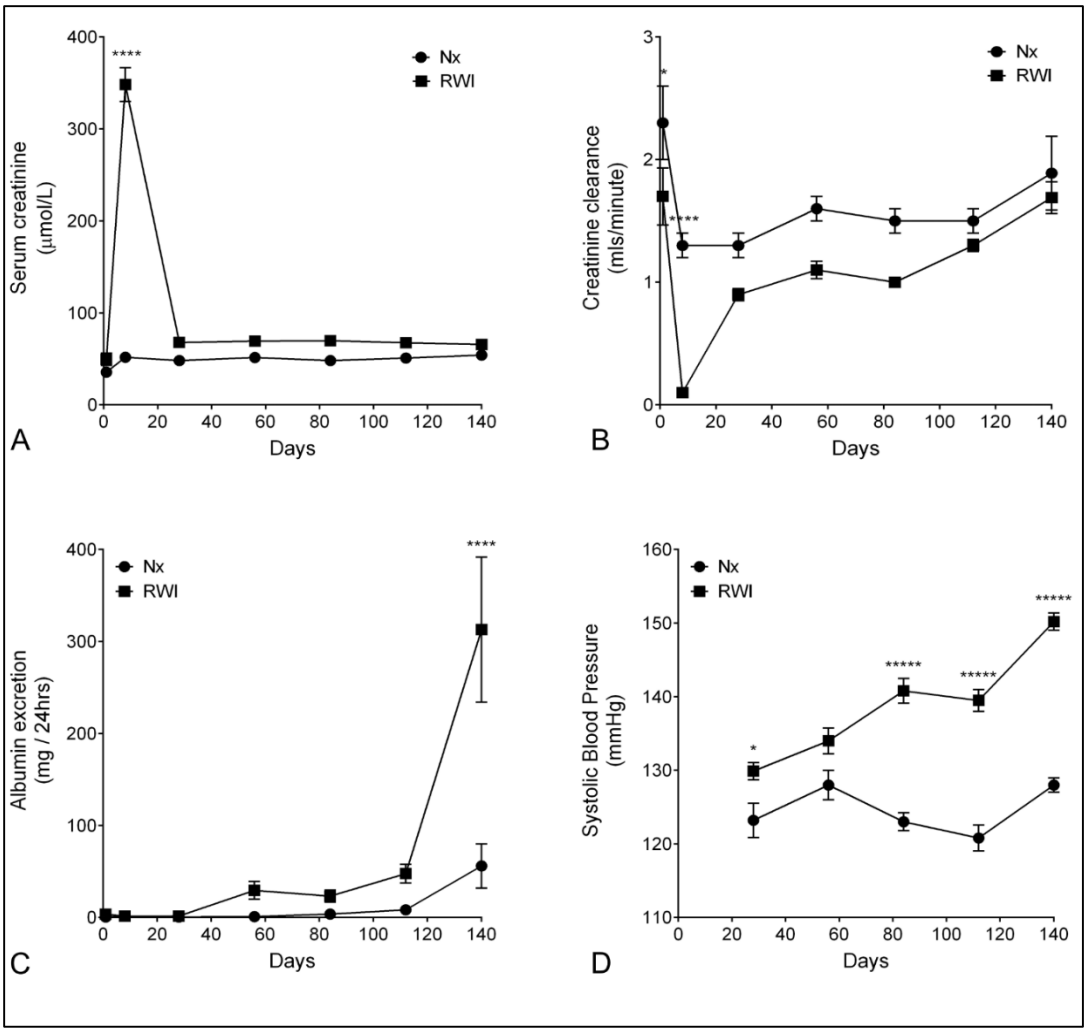

Figure 5.3: Effect of RWI on renal function during 140 days

The plot line graph represents the mean of serum creatinine (**A**), creatinine clearance (**B**), albumin excretion (**C**) and systolic systemic blood pressure (**D**) measurements at different time points after surgery. RWI = renal warm ischaemia (60 min) plus right nephrectomy (n=10), Nx = right nephrectomy alone (n=6). Vertical bars indicate +/-SEM. ***** = P< 0.05; ******** =P<0.0001.

5.3.3.2. Renal fibrosis

Masson's Trichrome Staining

Intraglomerular mesangial area. Representative examples of glomeruli from MTS sections are shown for each experimental group in Figure 5.4, panels A and C. The IGMA from the RWI image (panel C) shows almost the same level of blue staining than the mesangial matrix as the Nx image (panel A). Measurements of IGMA for the Nx and RWI groups, expressed as mean of blue/red ratio did not show a significant difference at day 140 of RWI. Nx, $0.7x10^{-2} \pm 0.5x10^{-2}$; RWI, $1.4x10^{-2} \pm 0.3x10^{-2}$ blue/red ratio, P=0.2. See Figure 5.4, panel E.

Tubulointerstitial area. Representative examples of tubules from MTS sections are shown for the RWI and Nx group in Figure 5.4, panels B and D. The RWI representative image (panel D) shows a higher level in blue staining when compared to the Nx group (panel B). The RWI group was associated with a significant increase in the blue/red ratio in comparison to the Nx group. Nx, 0.04 ± 0.01; RWI, 0.16 ± 0.03 blue/red ratio, P<0.01, Figure 5.4, panel F.

Collagens

Intraglomerular mesangial area for collagens I, III and IV. Measurements of collagens in the IGMA for the Nx and RWI groups, expressed as mean of FITC/DAPI ratio, did not show any significant change between groups at day 140. Collagen I, Nx, $13x10^{-2} \pm 4.5x10^{-2}$; RWI, $9.7x10^{-2} \pm 1x10^{-2}$ FITC/DAPI, P=0.31. Collagen III, Nx, $0.4x10^{-2} \pm 0.5x10^{-3}$; RWI, $0.4x10^{-2} \pm 0.3x10^{-3}$ FITC/DAPI, P=0.84. Collagen IV, Nx, 0.13 ± 0.03; RWI0.10 ± 0.04 FITC/DAPI, P=0.65.

Tubulointerstitial area for collagens I, III and IV. Representative examples of tubulointerstitial area from immunofluorescence stained sections are shown for each experimental group for collagen III and IV in Figure 5.5, panels A-C and B-D, respectively. The tubulointerstitial area for collagen I showed a similar level of green signal (FITC) in both groups. Collagen III and IV from the RWI representative sections show a higher level in green fluorescence in the interstitial and peritubular, respectively, when compared to the Nx group. The RWI group for collagen III and IV was associated with a significantly higher FITC/DAPI ratio when compared to the Nx group. Nx, 0.09 ± 0.14; RWI, 0.38 ± 0.02 FITC/DAPI, P<0.0001 for collagen III and Nx, 0.08 ± 0.02; RWI, 0.19 ± 0.03 FITC/DAPI, P<0.03 for collagen IV. No significant difference was seen for collagen I between groups. Nx, 0.14 ± 0.03; RWI, 0.16 ± 0.02 FITC/DAPI, P=0.44.

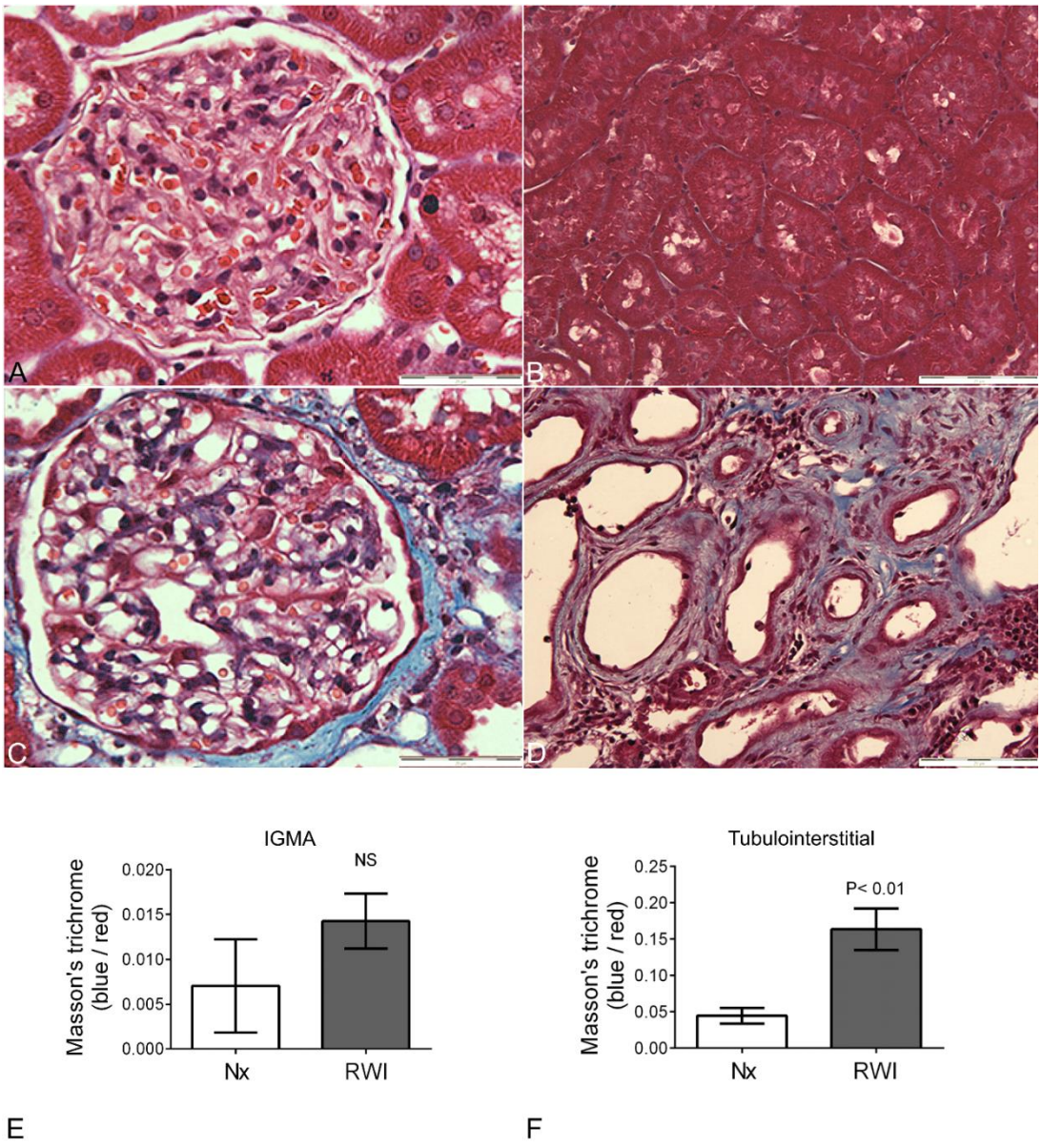

Figure 5.4: Effect of RWI on the IGMA and tubulointerstitial matrix after 140 days

Panel **A**,**C** and **B**,**D**. Representative images of IGMA and tubulointerstitial area under 400x and 200x magnification, respectively, are showing coloration (blue-extracellular matrix; red-cellularity) and structural differences between the Nx (**A** and **B**) and RWI (**C** and **D**) samples, respectively. The histogram **E** and **F** represents the mean blue/red ratio in the intraglomerular mesangial area and tubulointerstitial area after 140 days of RWI, respectively. Nx = right nephrectomy, n=6; RWI = renal warm ischaemia (60 min) plus right nephrectomy, n=10. Vertical bars indicate +/-SEM

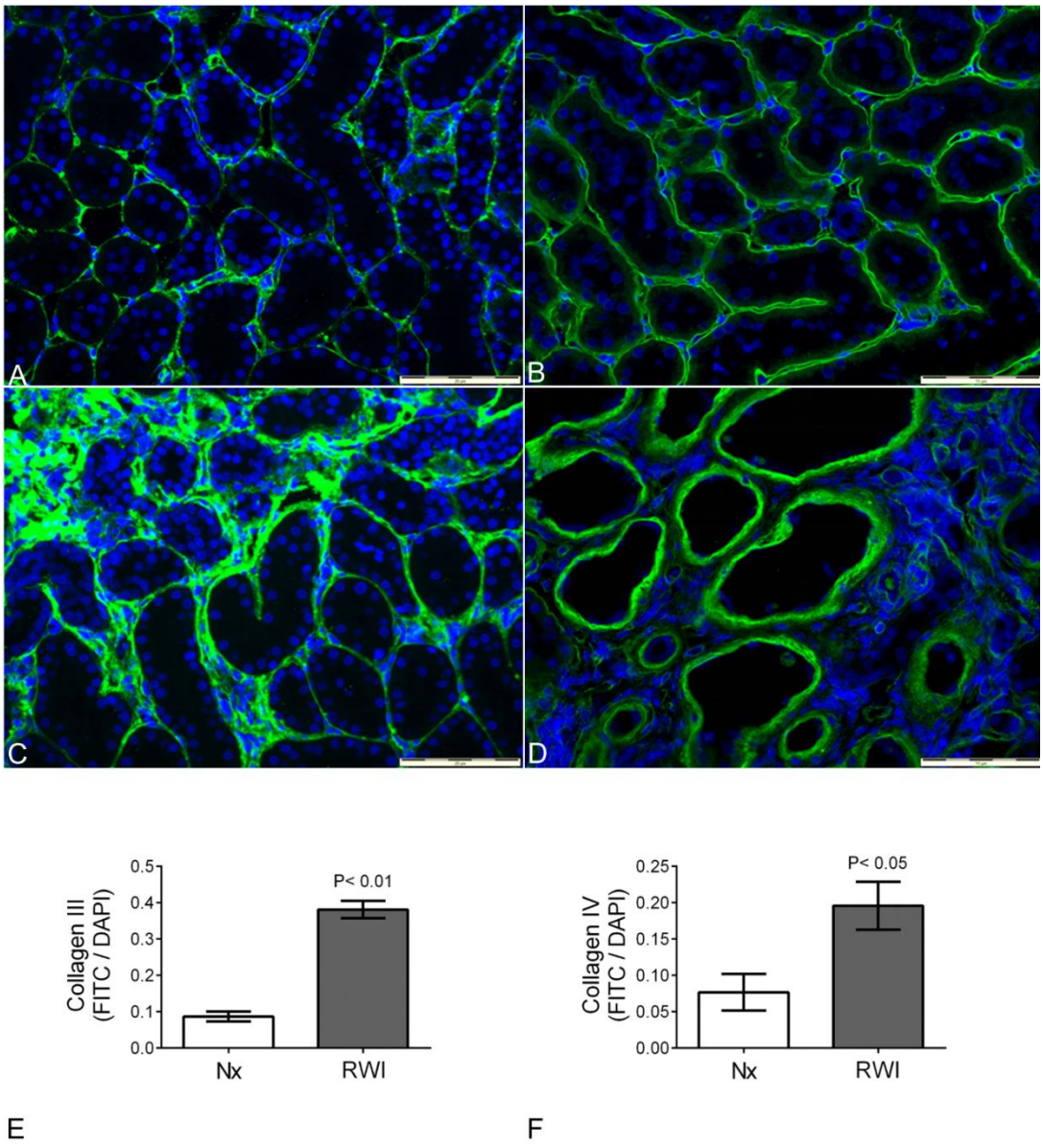

Figure 5.5: Effect of RWI on tubulointerstitial collagen III and IV after 140 days

Panel **A**-**D**. Representative images of tubulointerstitial (200x) area for collagen III (**A** and **C**) and IV **(B** and **D**) are showing coloration (collagens-FITC and blue nuclei-DAPI) and structural differences between the Nx (**A** and **B**) and RWI (**C** and **D**) samples. Panel **E** and **F**. The histograms represents the mean FITC/DAPI in the tubulointerstitial area for collagen III and IV, respectively. Nx = right nephrectomy alone (n=6). Vertical bars indicate +/-SEM. RWI = renal warm ischaemia (60 min) plus right nephrectomy (n=10).

5.3.3.3. Renal transglutaminase

TG *in situ* activity

Intraglomerular mesangial area. Representative examples of the IGMA from TG activity fluorescent stained sections are shown for the Nx and RWI experimental groups at 140 days of RWI in Figure 5.6, panels A and C. Measurements of TG activity in the IGMA for the Nx and RWI groups, expressed as mean of Alexa red / DAPI ratio did not show any significant change between groups at 140 days of renal warm ischaemia. Nx, $1.8x10^{-2} \pm 0.6x10^{-2}$, RWI, $1.8x10^{-2} \pm 12x10^{-2}$ Alexa red / DAPI ratio, P=0.5. Figure 5.6, panel E.

Tubulointerstitial area. Representative examples of the tubulointerstitial area from TG activity fluorescent stained sections are shown for the Nx and RWI experimental groups at 140 days of RWI in Figure 5.6, panel B and D, respectively. The example from the RWI group shows a higher intense red signal (Alexa) in the tubulointerstitial area when compared to the Nx representative image. The RWI group was associated with a significantly higher TG activity Alexa/DAPI ratio in contrast to the Nx group. Nx, 0.17 ± 0.01; RWI, 0.25 ± 0.02 Alexa/DAPI, P<0.02. Figure 5.6, panel F.

Transglutaminase 2

Intraglomerular mesangial area. Representative examples of the IGMA from immunofluorescent stained sections are shown for the Nx and RWI experimental groups at 140 days of renal warm ischaemia in Figure 5.7, panels B and D. Measurements of TG2 in the IGMA for the Nx and RWI groups, expressed as mean of Alexa/DAPI ratio, did not show any significant change between groups at 140 days of RWI. Nx, $0.2x10^{-2} \pm 0.9x10^{-3}$, RWI, $1.6x10^{-2} \pm 8.5x10^{-3}$ Alexa red / DAPI ratio, P=0.2. Figure 5.7, panel E.

Tubulointerstitial area. Representative examples of the tubulointerstitial area from immunofluorescent stained sections are shown for the Nx and RWI experimental groups at 140 days of RWI in Figure 5.7, panel C-D, respectively. The example from the RWI group shows a higher intense red signal-Alexa red in the tubulointerstitial area when compared to the Nx representative image. The RWI group was associated with a significantly higher TG2 Alexa/DAPI ratio in contrast to the Nx group. Nx, 0.07 ± 0.02; RWI, 0.3 ± 0.08 Alexa/DAPI, P<0.02. Figure 5.7, panel F. A summary of results is displayed in Table 5.4.

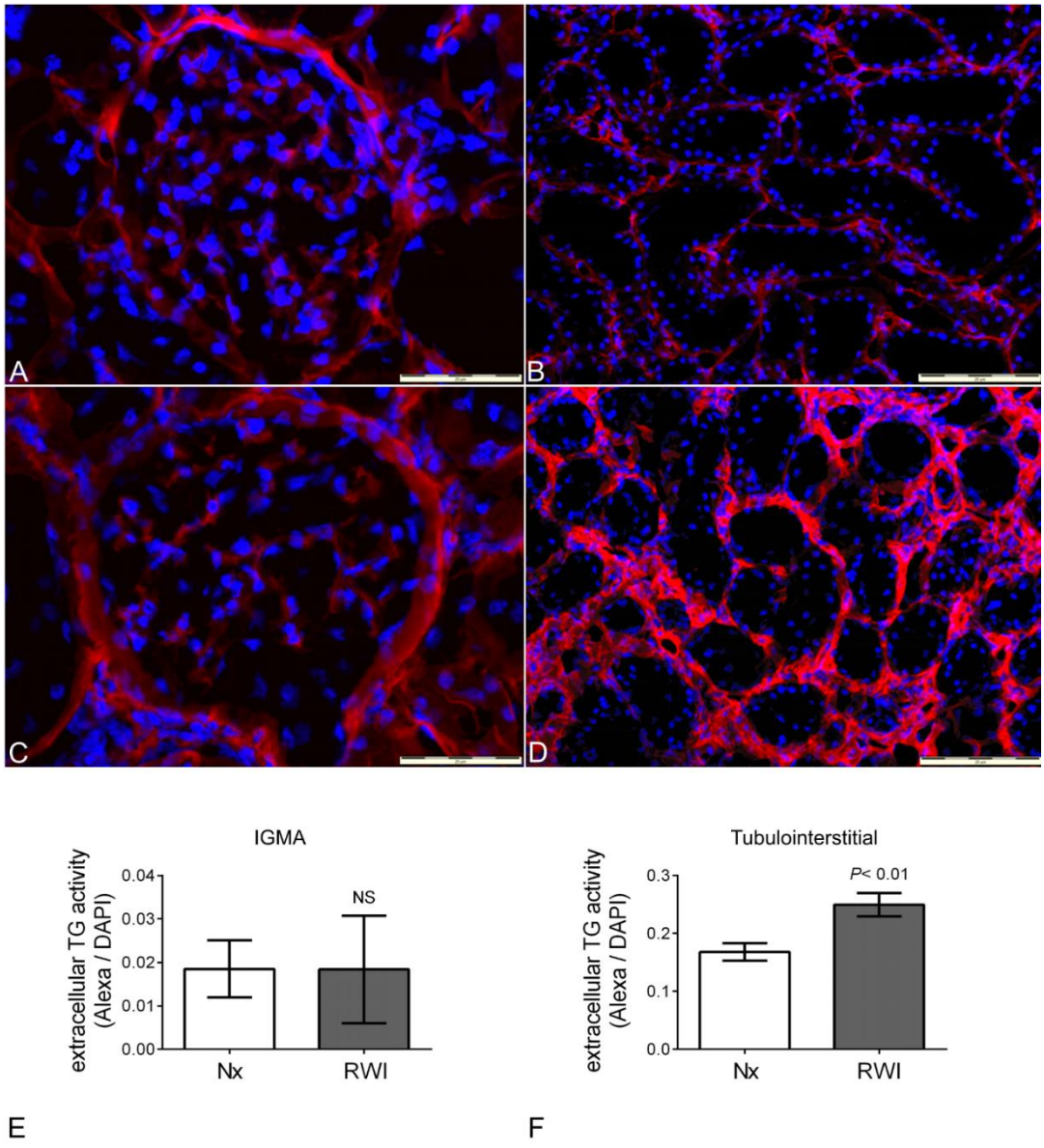

Figure 5.6: Effect of RWI on the IGMA and tubulointerstitial TG act after 140 days

Panel **A**, **B** and **C**, **D**. Representative images of glomeruli (400x) and tubulointerstitial (200x) area, respectively, showing coloration (TG activity-Alexa red and blue nuclei-DAPI) and structural differences between the Nx (**A** and **C**) and RWI (**B** and **D**) samples, respectively. Panel **E** and **F**. The histograms represents the mean Alexa/DAPI in the intraglomerular mesangial (IGM) and tubulointerstitial area, respectively. RWI = renal warm ischaemia (60 min) plus right nephrectomy (n=10), Nx = right nephrectomy alone (n=6). Vertical bars indicate +/-SEM.

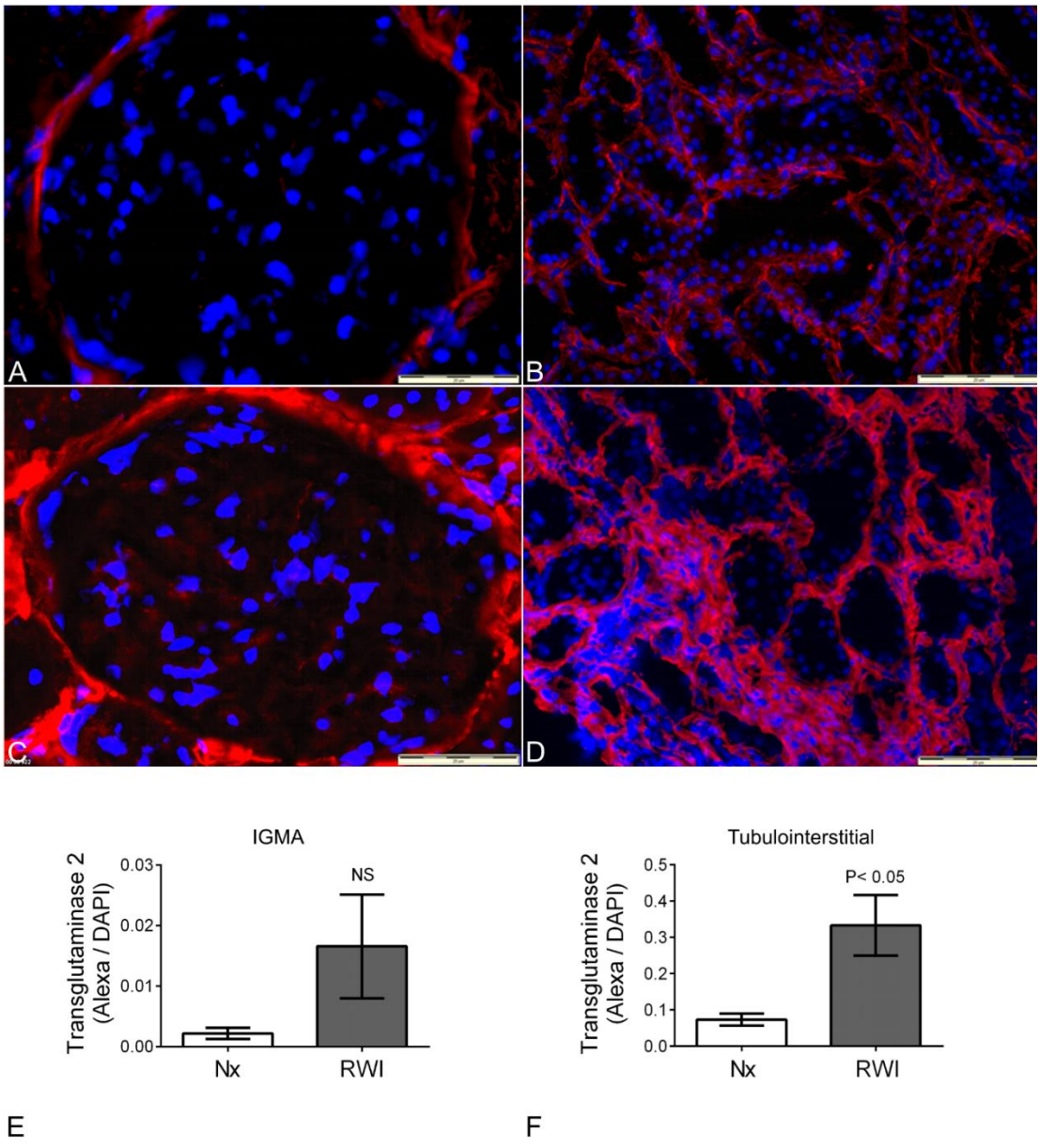

Figure 5.7: Effect of RWI on the IGM and tubulointerstitial TG2 after 140 days

Panel **A**, **B** and **C**, **D**. Representative images of glomeruli (400x) and tubulointerstitial (200x) area, respectively, showing coloration (TG2-Alexa red and blue nuclei-DAPI) and structural differences between the Nx (**A** and **C**) and RWI (**B** and **D**) samples, respectively. Panel **E** and **F**. The histograms represents the mean Alexa/DAPI in the intraglomerular mesangial (IGM) and tubulointerstitial area, respectively. RWI = renal warm ischaemia (60 min) plus right nephrectomy (n=10), Nx = right nephrectomy alone (n=6). Vertical bars indicate +/-SEM.

Assessment	Groups		Units	RWI change	P value <
	Nx	RWI			
Renal function					
Serum creatinine	54.2 ± 2.8	65.7 ± 3.4	µmol/L	6.4 fold ▲	P<0.04
Creatinine clearance	1.9 ± 0.3	1.7 ± 1.1	mls / minute	10%▼	NS
Albumin excretion	90.6 ± 50	378.2 ± 96	mg / 24hrs	4.1 fold ▲	P<0.05
SBP	128 ± 2.4	150.2 ± 4	mmHg	1.2 fold ▲	P<0.001
Water intake	26.17 ± 0.4	36.3 ± 2.4	ml / 24hrs	1.4 fold ▲	P<0.01
Urine production	14.67 ± 1.5	25.5 ± 2.24	ml / 24hrs	0.6 fold ▲	P<0.01
IGMA					
MT	$0.7x10^{-2}$±$0.5x10^{-2}$	$1.4x10^{-2}$ ±$0.3x10^{-2}$	blue/red	2.4 fold ▲	NS
Collagen I	$13x10^{-2}$±$4.5x10^{-2}$	$9.7x10^{-2}$±$1x10^{-2}$	FITC/DAPI	25%▼	NS
Collagen III	$0.4x10^{-2}$±$0.5x10^{-3}$	$0.4x10^{-2}$±$0.3x10^{-3}$	FITC/DAPI	1:1	NS
Collagen IV	0.13 ± 0.03	0.10 ± 0.04	FITC/DAPI	23%▼	NS
TG *in situ* activity	$1.8x10^{-2}$±$0.6x10^{-2}$	$1.8x10^{-2}$±$12x10^{-2}$	Alexa/DAPI	1:1	NS
TG2	$0.2x10^{-2}$±$0.9x10^{-3}$	$1.6x10^{-2}$±$8.5x10^{-3}$	Alexa/DAPI	8 fold ▲	NS
Tubulointerstitial					
MT	0.04 ± 0.01	0.16 ± 0.03	blue/red	4 fold ▲	P<0.001
Collagen I	0.14 ± 0.03	0.1650 ± 0.01684	FITC/DAPI	1.1 fold ▲	NS
Collagen III	0.09 ± 0.14	0.38 ± 0.02	FITC/DAPI	4 fold ▲	P<0.0001
Collagen IV	0.08 ± 0.02	0.19 ± 0.03	FITC/DAPI	2.4 fold ▲	P<0.03
TG *in situ* activity	0.17 ± 0.01	0.25 ± 0.02	Alexa/ DAPI	1.5 fold ▲	P<0.02
TG2	0.07 ± 0.02	0.3 ± 0.08	Alexa/ DAPI	4.3 fold ▲	P<0.03

Table 5.4: Measurements after 140 days of RWI

5.3.4. Correlations

Linear regressions in the tubulointerstitial space showed positive correlations between the TG pathway and renal fibrosis after 28 and 140 days of RWI. Day 28, TG2 and MTS, r^2=0.42, P<0.01. Day 140, collagen III with TG activity and TG2, r^2=0.45, P<0.01 and r^2=0.26, P<0.05, respectively, Figure 5.8. Serum creatinine at day 8, showed a positive linear regression with the level of fibrosis by collagen III (r^2=0.78, P<0.0001) and MTS (r^2=0.48, P<0.01) and the TG pathway by TG *in situ* activity (r^2=0.30, P<0.05) and TG2 (r^2=0.44, P<0.005) at day 140 of RWI. Serum creatinine at day 28 showed high significant correlations with luminal tubular area (r^2=0.74, P<0.001). All linear regressions amongst renal function, tubulointerstitial extracellular matrix expansion/fibrosis and TG pathway techniques are shown in Table 5.5.

5.4. Discussion

5.4.1. Experimental technique

Rat Strain. The ability of the rat to develop renal fibrosis can be an inherited characteristic, the extent of which differs between individual strains. Evidence obtained following subtotal nephrectomy, has previously shown the SD to develop renal fibrosis to a greater extent than Wistar Furth, which was attributed to having both a lower nephron number and lower nitric oxide generating capacity (Erdely *et al.*, 2003). Both SD (Basile *et al.*, 2001a; Basile *et al.*, 2005; Basile *et al.*, 2003; Lloberas *et al.*, 2001; Torras *et al.*, 1999) and Wistar stains (Jain *et al.*, 2000a; Jain *et al.*, 2000b; Jain *et al.*, 2001; Yang *et al.*, 2005) have previously been used to study the chronic effects of RWI, the Wistar only developing tubulointerstitial fibrosis in early renal disease while the SD, a more sensitive strain, also developed glomerulosclerosis. The SD rat was therefore employed in the present study.

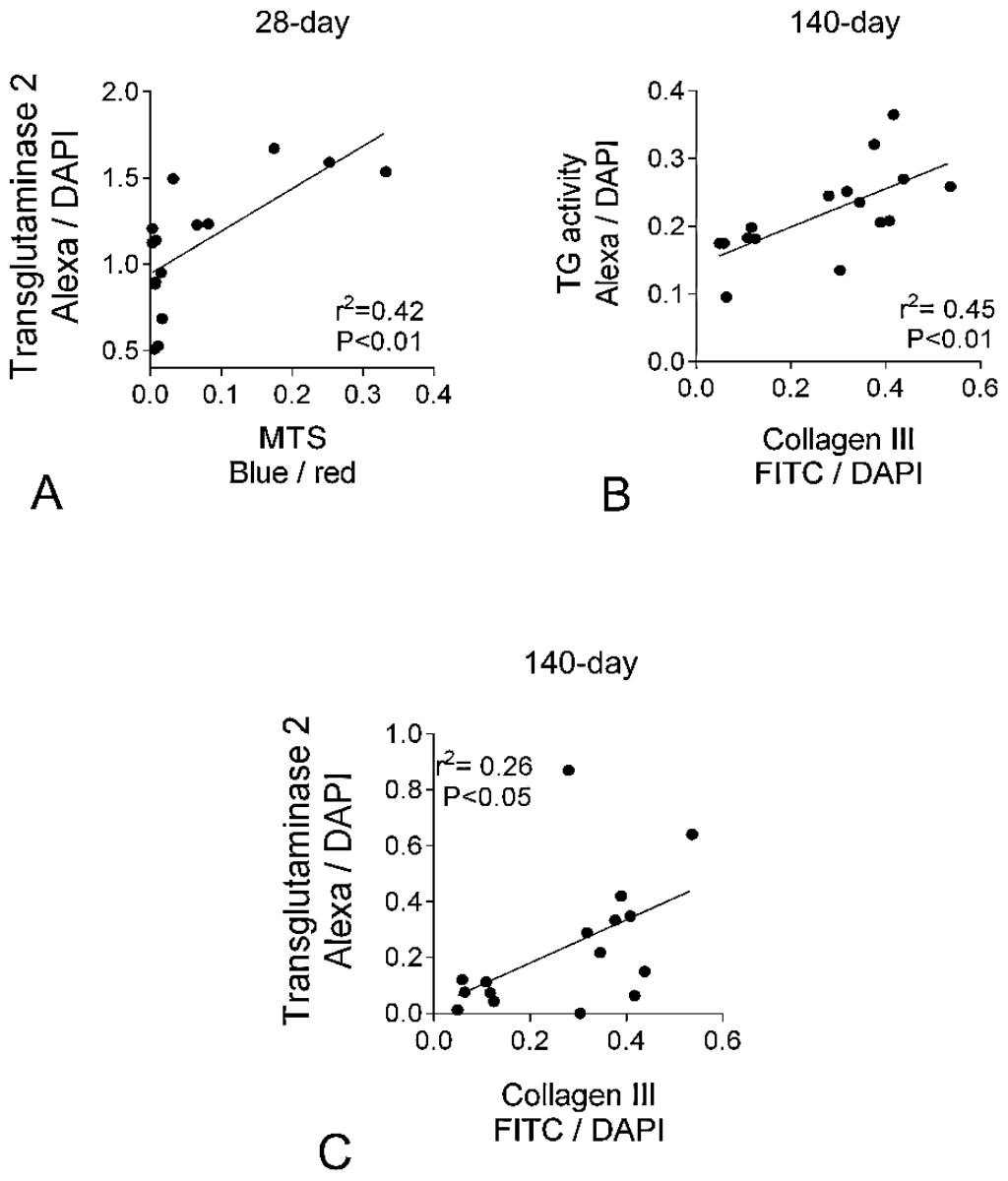

Figure 5.8: Linear regressions between the TG pathway and tubulointerstitial fibrosis

Technique A	Technique B	r^2	P value <
RWI day 8			
TG *in situ* activity	Serum creatinine	0.57	0.02
Serum creatinine	Collagen III	0.84	0.005
RWI day 28			
TG2	Serum creatinine	0.31	0.05
TG2	MTS	0.42	0.01
Luminar tubular area	Serum creatinine	0.74	0.001
Luminar tubular area	MTS	0.27	0.05
Luminar tubular area	TG2	0.28	0.05
RWI day 140			
TG *in situ* activity	Serum creatinine day 8	0.30	0.05
TG *in situ* activity	Serum creatinine day 140	0.45	0.005
TG *in situ* activity	MTS	0.43	0.01
TG *in situ* activity	Collagen III	0.45	0.01
TG2	MTS	0.38	0.05
TG2	Collagen III	0.26	0.05
TG2	Serum creatinine day 8	0.44	0.005
MTS	Collagen III	0.54	0.005
Serum creatinine day 8	MTS	0.48	0.01
Serum creatinine day 8	Collagen III	0.78	0.0001
Serum creatinine day 140	MTS	0.50	0.01
Serum creatinine day 140	Collagen III	0.38	0.02
Serum creatinine day 140	Albumin excretion day 140	0.50	0.01
Serum creatinine day 140	Systemic systolic blood pressure	0.25	0.05

Table 5.5: Tubulointerstitial positive linear regressions at 8, 28 and 140 after RWI

RWI time. Weight et al (1998), using bilateral renal hilum clamping in the SD rat, showed 45 minutes to be the optimal ischaemic time for survival following the induction of renal injury. RWI over 45 minutes may produce a greater degree of renal impairment together with a considerable increase in mortality when rats are nephrectomised on day 0. In the present SD rat study, the right nephrectomy was delayed until day 7, allowing a 60 min RWI stimulus to be employed with a 100% survival. In addition, a 4-fold greater increase than demonstrated by Torras et al (1999) was detected in albuminuria after 5 months.

Body temperature during renal ischaemia. The extend of ischaemia reperfusion injury following a period of RWI is a function of both time and temperature. RWI is always induced under anaesthesia, which suppresses the thermoregulatory system in the hypothalamus, reducing body temperature. The importance maintaining body temperature during a period of "renal warm ischaemia" was recognized by Delbridge et al (2007) who demonstrated a positive correlation between renal damage, assessed by the increase in serum creatinine, and body temperature following 45 min RWI in the SD rat. In the present study, under isoflurane anaesthesia, rat body temperature was maintained (36-37°C) using a thermal blanket, servo-controlled via a rectal temperature probe. In the absence of external body warming, body temperature falls to 32°C under anaesthesia. The thermal blanket also had an advantage over a thermal mat since it could be wrapped around the rat to prevent heat loss by convection. A high wattage lamp was further employed in cases where the body temperature fell down below 36°C, together with procedures to avoid dehydration. An additional consideration could be the diurnal variation in body temperature which may increase by some 2°C during the dark cycle (Brezis *et al.*, 1995) suggesting it may also be important to standardize the time of the day when rats are subjected to RWI.

Nephrectomy: In the present study, a right nephrectomy was performed 7 days after a 60min period of RWI to the left kidney. The nephrectomy was performed for 2 major reasons. Firstly to improve rat survival, maintaining adequate renal function during the period of acute renal injury to the left kidney. A rat survival of only 55% (day 4) was obtained when the right nephrectomy and RWI were performed in the same operation. An alternative approach, using bilateral nephrectomy, produced a lower chronic increase in albumin excretion indicating a lower incidence of glomerular injury (Basile *et al.*, 2001b). Secondly, was the possibility of inducing compensatory hypertrophy in the kidney subjected to ischaemia reperfusion injury, Hypertrophy may

also lead to increased metabolic demand (Brenner *et al.*, 1996), enhancing hypoxaemia and predisposing to medullary injury (Brezis *et al.*, 1995). In addition, an important third but pragmatic reason was to allow the function of the ischaemic kidney to be determined using systemic serum and urine data.

5.4.2. Kidney function

Kidney function: Delaying the right nephrectomy until day 7 improved animal survival, allowing the use of a longer 60 min stimulus of RWI. Day 8, 24h post nephrectomy, was therefore the first study day were the effect of RWI could be demonstrated solely on the function of the left kidney. The effectiveness of RWI (60 min) at inducing ischaemia reperfusion injury was apparent by the 7-fold increase in serum creatinine measured on day 8. Creatinine clearance fell by 94% reflecting a major fall in GFR resulting from the ischaemic insult in the absence of any increase in urine flow or albumin excretion. By 1 month however, the creatinine clearance of the left kidney had recovered to a similar level as the nephrectomised control group without any significant difference in urine flow, albumin excretion or systemic blood pressure. In the 1-4 month period following RWI (60 min), rats developed mild hypertension and albuminuria but little change in creatinine clearance as active creatinine excretion via renal tubes occurs importantly in this species (Darling *et al.*, 1991). By the time the study was terminated, after 5 months, the albuminuria in particular had become much more severe and was associated with an increase in both urine flow and fluid intake.

5.4.3. Kidney histology

Kidney histology: Kidney histology by MT staining also showed evidence of tissue damage and expansion of extracellular matrix at day 8 after RWI. Immunofluorescence analysis showed that collagen III contributed to the expansion of ECM in the tubulointerstitial space. Unexpectedly, tubulointerstitial TG enzyme activity and TG2 protein were elevated in the left kidney at day 8, together within an increase in collagen III. The 28-day study following RWI developed a similar trend in renal damage, tubulointerstitial fibrosis and up-regulation of the transglutaminase 2 than the trend seen in the 8 and 140-day studies. Figure 5.9, upper and lower histograms shows the levels of MTS and TG2, respectively, at 8, 28 and 140-day time point following RWI. Histological evidence supported an increase in matrix protein deposition in the tubulointerstitium, including that for collagen III and collagen IV. The

lack of change in collagen I was an indicator of the presence of the early stages of fibrosis, collagen I increasing at a later stage when the fibrosis becomes more mature (Lavaud *et al.*, 2001; Zager *et al.*, 2009). There was however, little evidence of direct glomerular involvement; glomerular TG2 remained unchanged. Linear regressions at 28 and 140 between renal fibrosis and the TG pathway established a positive association consistent with previous studies in animal models and in the man. Positive correlations were established for renal function and renal fibrosis at day 8, 28 and 140 post RWI. Interestingly, serum creatinine at day 8 showed a positive correlation for both renal fibrosis (MTS and collagen III) and the TG pathway (TG2 and TG activity) at day 140 suggesting that an acute elevation of serum creatinine secondary to RWI may predict the development of fibrosis and therefore TG2. This is evidence that acute renal injury proceeds a series of inflammatory processes of which may trigger CKD.

5.4.4. Downsides of the renal warm ischaemia model

With a relatively simple surgical procedure, renal hilar clamping, the rat model of RWI allows the understanding of tubulointerstitial fibrosis in an accelerated time frame. However, there are important downsides to consider for this model. Body temperature in the rat during anaesthesia is normally unsteady. It has been established that small fluctuations in body temperature in the Sprague Dawley rat cause different degrees of acute renal injury (Delbridge *et al.*, 2007). Sudden fluctuations of temperature may happen in a period of 20 minutes during RWI, therefore a fulltime body temperature assessment have to be performed during all surgical procedure. Rats with fluctuations above or over 36-37 °C should be discard from experimental groups. Small fluctuations (minutes) in the period of RWI change significantly the level of renal injury (Becker *et al.*, 2013) and therefore, high level of attention is necessary to synchronize from the time an accurate clamping (without relocation) is performed to the time the clamp is removed after exact 60 minutes. The clamping of the renal hilar is another vital factor that requires accuracy during placement. Some rats have abundant perirenal fat. Fat tissue may interact with the compression effectiveness of the microvascular clamp over the renal conduits; conversely low fat tissue on renal vessels may predispose to crushing of renal vein after 60 minutes of continues pressure.

5.4.5. 28-days RWI for interventional studies

The disease duration of the 28-day study was determined to develop of a suitable level of renal damage and fibrosis, adequate for interventional studies. A significant level of TG2 was observed when comparing experimental groups. Also it showed a positive linear regression with fibrosis and renal function. Early development of fibrosis, as seen in the 28-day study, was thought to be easier to reduce than well-established mature fibrosis (Jones *et al.*, 1992). Natural matrix remodelling and degradation after renal injury could allow the inhibitor to perform a better effect in an ECM area without continuous build-up of collagen proteins. Therefore, reduction of subtle levels of fibrosis by TG inhibitors would be easier to identify when comparing experimental groups. On the other hand, the level of TG2 was higher in the 28 days study in comparison to the 8 and 140-day study. A TG2 time course from the 3 studies is shown in Figure 5.9, lower histogram. The effect of RWI on TG2 at this time point may be of high relevance, therefore, its inhibition may represent an important effect on the development of fibrosis. Welfare benefits and practicability were also and important factors to take into account; one minipump lasts for 28 days, thus, no multiple surgical procedure would be required to change osmotic pumps reducing surgical procedures together with animal handling, anaesthesia, stress and pain for the studied rats.

5.4.6. Conclusion

The 28-day rat model of RWI allows sufficient degree of acute kidney injury to generate an adequate level of fibrosis in the tubulointerstitial area. The level of fibrosis in this model has shown a correlation with the levels of TG2 in the extracellular space following 60 minutes of RWI. The present study has established a model of tubulointerstitial fibrosis suitable to undertake chemical interventional studies using a chemical TG inhibitor. In the following chapter, inhibition of TG2 will be use on this model to determine whether TG2 is a causal link for the development of renal fibrosis.

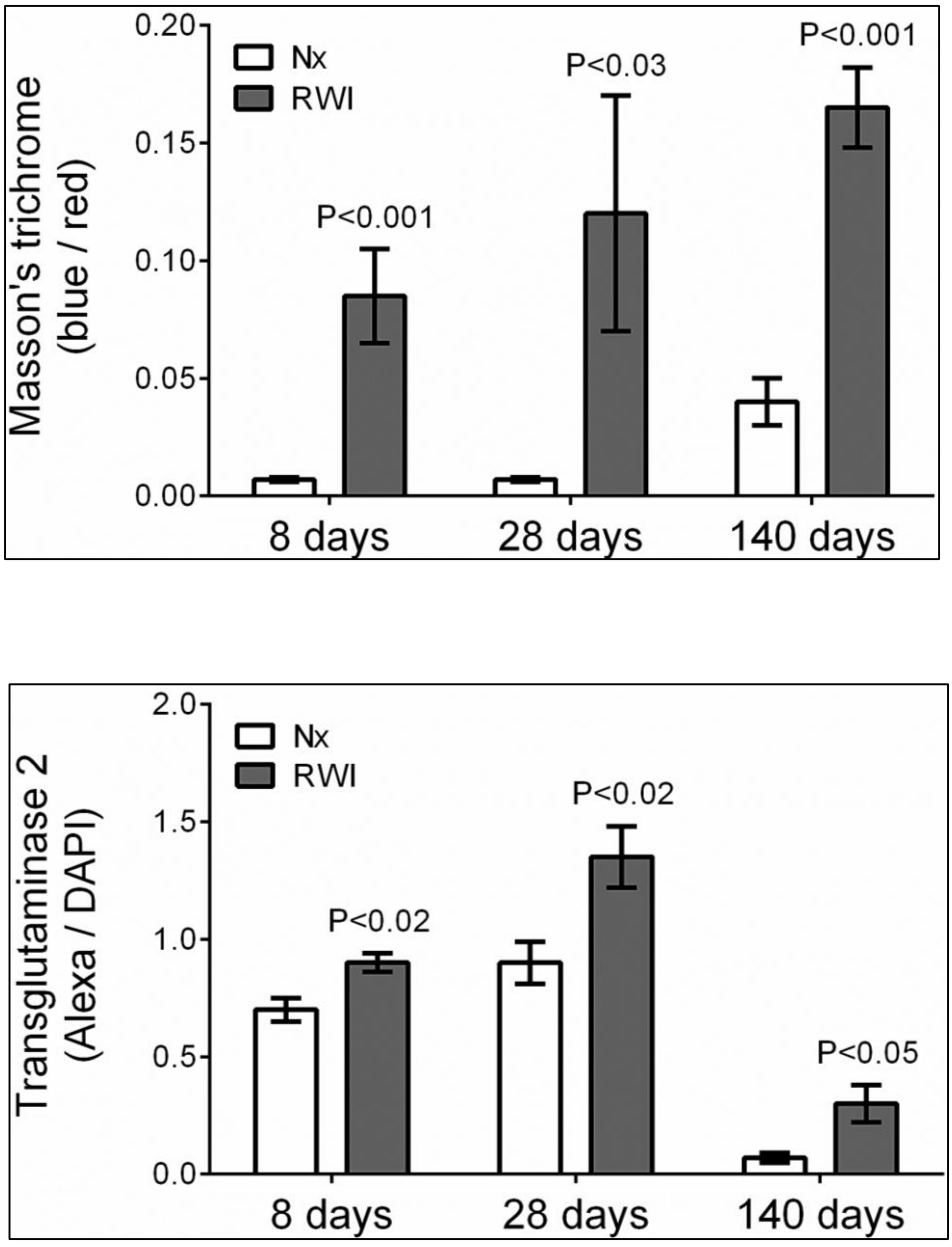

Figure 5.9: Time point effect of RWI on tubulointerstitial fibrosis and TG2

Upper and lower histogram, represent the effect of RWI on renal fibrosis and TG2, respectively, after 8, 28 and 140 days. RWI = renal warm ischaemia (60 min) plus right nephrectomy (day 8, n=4; day 28, n=7; day 140, n=10), Nx = right nephrectomy alone (day 8, n=5; day 28, n=8; day 140, n=6). Vertical bars indicate +/-SEM.

CHAPTER 6

The effect of Transglutaminase 2 inhibition on Tubulointerstitial Fibrosis following Renal Warm Ischaemia

6.1. Introduction

The role transglutaminase 2 in extracellular matrix deposition and inflammatory events (Gundemir *et al.*, 2012) makes this enzyme a potential pharmaceutical target against renal fibrosis. TG2 and its role in renal fibrosis has previously been studied *in vitro* (Huang et al., 2010; Skill et al., 2004), *in vivo* (Fisher *et al.*, 2009; Johnson *et al.*, 2007) and in human renal tissue (Johnson *et al.*, 2003). The inhibition of TG2 and its renal effect in disease has been achieved by using knock out models of TG2 as well as TG2 inhibitors which show a beneficial effect on renal function and structure.

Having established a RWI model, standardizing the time for renal hilar clamping, temperature condition during RWI and time for contralateral nephrectomy (Chapter 5), an interventional approach was necessary to evaluate whether the TG pathway was a causal link for the development of tubulointerstitial fibrosis following RWI. To accomplish this aim, the transglutaminase inhibitor 1,3-dimethyl-2[(2-oxopropyl)thio]imidazolium chloride (TGI), (DOO3, Zedira, Germany), was employed. TGI is an inhibitor for all isoforms of transglutaminase. However, transglutaminase 2, factor XIIIa and prostate transglutaminase are the only three isoforms that can be found extracellularly; while, factor XIIIa and TG2 are the only two isoforms located in the kidney, blood plasma and the intra/extracellular compartments, respectively (Skill *et al.*, 2004; Yee *et al.*, 1994). TGI compound is able to penetrate both intracellular and extracellular compartments, however, its inhibitory effect is just exerted in the extracellular space, as TG2 is activated when exported extracellularly due to the high levels of calcium encountered in this area (Lortat-Jacob *et al.*, 2012). A related compound called N-benzyloxycarbonyl-L-phenylalanyl-6-dimethyl-sulfonium-5-oxo-L-norleucine, used as control in previous chapters, is restricted to the extracellular space due to its high molecular weight (Baumgartner *et al.*, 2004). The chemical structure of TGI is displayed in Figure 6.1.

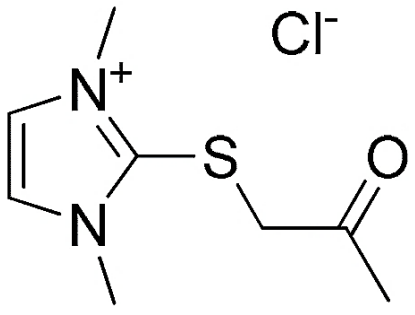

Figure 6.1: TGI chemical structure

The method used to deliver the TGI in this model was first evaluated by Oldroyd et al (1999). The system is based on intrarenal drug delivery through kidney cannulation. The inserted cannula was connected to an osmotic minipump placed subcutaneously in the back of the rat. This method delivered effective concentrations directly into the kidney, reducing the amount of product required to affordable levels and improving its side effect profile, particularly reducing the possibility potential effects on blood clotting and wound healing. The main advantage of the osmotic pump is continuous drug delivery over 28 days (Theeuwes *et al.*, 1976) reducing fluctuations in drug concentration, time and man power for drug administration. Also, the low antigenicity of the pump reduces discomfort to the rat retaining a foreign body subcutaneously.

6.2. Material and Methods

6.2.1. Animals and anaesthesia

Male Sprague-Dawley rats (Harlan, UK), 8-10 weeks, with an initial weight of 250-300 grams were maintained at 20°C, 45% humidity and with a light cycle of 12 hours. Chapter 2, section 2.2. For surgical procedure, rats were induced in an anaesthetic chamber with 5% isoflurane and 8 L/min oxygen. Analgesia was provided by intramuscular injection of buprenorphine 50µg/kg. Maintenance of anaesthesia was achieved with 1.5% of isoflurane and 1 L/min oxygen. During anaesthesia, the rat was placed on an operating board covered with a homeothermic blanket to keep the rat temperature between 36-37°C.

6.2.2. Experimental protocol and surgical procedures

Two interventional studies were performed with a disease progression over either 8 or 28 days. Each study consisted of nephrectomised control rats (Nx) sham operated (day 0) and subjected to right nephrectomy at day 7. The disease groups (RWI and RWI+TGI) were composed of rats subjected to intrarenal cannulation and placement of a subcutaneous osmotic minipump in the dorsal aspect of the back (day -3), see section 2.2.6.4 and 2.2.6.5, and subjected to 60 minutes of left renal hilar clamping (day 0) with right nephrectomy at day 7. The minipumps were loaded with 2ml of either NaCl 0.9% (vehicle) or vehicle + 50 mmol/L of TGI (10 µg/kg/hr). Number of rats used for each terminal experiment is displayed in Table 6.1.

Days after RWI	Number of rats per group		
	Nx	RWI	RWI+TGI
8	5	4	3
28	5	5	6

Table 6.1: Number of rats for each interventional study

6.2.3. Renal function

6.2.3.1. Blood serum and urine

Creatinine was assayed in serum and urine by the Jaffe rate method (Levey *et al.*, 1988) using a SYNCHRON ® System (Beckman Coulter Inc.) machine (section 2.3.1). Assessment of serum and urine creatinine was performed prior to surgical procedure, 24hrs after intrarenal cannulation, day 8 and 28 after RWI, according to each interventional study.

6.2.3.2. Rat albumin

Rat albumin was measured in urine by enzyme-linked immunosorbent assay (ELISA). A 96 well plate was coated with sheep anti-rat albumin antibody and the sample added to the plate. The secondary anti-sheep antibody containing horseradish peroxidase (HRP) was added followed by the enzyme substrate. The change in colour was proportional to the amount of secondary antibody bound to the primary antibody which in turn is bound to albumin. The optical signal was measured by spectrophotometry at 450 nm (section 2.3.2). Assessment of albumin excretion was performed at day 0, 8 and 28 after RWI, according to each interventional study.

6.2.4. Renal fibrosis

6.2.4.1. Masson's trichrome staining

5μm, formalin-fixed, paraffin embedded sections were deparaffinised and rehydrated. Tissue sections were placed in Bouin's and later in working Weigert's iron haematoxylin solutions. Slides were stained with Biebrich scarlet-acid fuchsine, aniline blue, dehydrated and mounted. For IGMA and tubulointerstitial expansion of

extracellular matrix, no less than 10 glomeruli (x 400) and (x 200) of cortex tubules were acquired. The fibrosis index was determined calculating the blue (Masson´s trichrome) / red (cellularity) ratio of total field. Quantification was performed by image analysis (section 2.4.3).

6.2.4.2. Immunofluorescence

8µm thick cryostat sections were blocked and washed. The tissue was probed with a primary antibody (collagen I, III and IV) overnight at 4°C followed by fixation and serial washings. The slides were immunoprobed with a secondary antibody and left at room temperature for 2 hours and mounted with DAPI. No less than 10 glomeruli (x 400) and (x 200) of cortex tubules were acquired. Collagen quantification was determined calculating the intense FITC (collagens) / DAPI (nuclei) ratio of the total field. Quantification was performed by image analysis (section 2.6.1).

6.2.5. Renal transglutaminase

6.2.5.1. Immunofluorescence

8µm thick cryostat sections were blocked and washed. The tissue was probed with a primary antibody (TG2) followed by fixation and serial washings. The slides were immunoprobed with a secondary antibody and left at room temperature for 2 hours and mounted with DAPI. No less than 10 glomeruli (x 400) and (x 200) of cortex tubules were acquired. Collagen quantification was determined calculating the intense Alexa red (TG2) / DAPI (nuclei) ratio of the total field. Quantification was performed by image analysis (section 2.6.1).

6.2.5.2. TG *in situ* activity

8µm thick cryostat sections were incubated with biotin cadaverine and $CaCl_2$. The main negative control consisted in the substitution of $CaCl_2$ by EDTA. The extracellular matrix incorporated biotin cadaverine was revealed by probing the tissue sections with streptavidin Alexa red and mounted with DAPI. No less than 10 glomeruli (x 400) and (x 200) of cortex tubules were acquired. The fluorescent TG activity index was determined calculating the intense Alexa red (TG activity) / DAPI (nuclei) ratio of the total field. Quantification was performed by image analysis (section 2.6.2).

6.2.5.3. Total TG activity

Transglutaminase activity was measured by the incorporation of 3H-putrescine into N,N´dimethylcasein in tissue homogenates using $CaCl_2$ and dithiothreitol (DDT). The TG inhibitor N-benzyloxycarbonyl-L-phenylalanyl-6-dimethyl-sulfonium-5-oxo-L-norleucine (100µM) and the selective TG2 neutralizing monoclonal antibody BB7 (3.3nM) were used as negative controls. The results were expressed units per mg of protein. Unit of activity is equivalent to 1nmol of 3H-putrescine incorporated per hour at 37°C. See section 2.5.2, for kidney homogenates and section 2.5.3 for TG 3H-putrescine assay methodology. Tissue assessment of total TG activity was performed only at 28 days after RWI.

6.2.5.4. Total TG2 protein

Tissue homogenates, were separated on a 10% polyacrylamide gel and electro-blotted. Human recombinant TG2 was used as a positive control. Primary antibodies, either rabbit TG2 (Ab 421, Abcam, UK) or mouse monoclonal antibody (CUB 7402, Abcam, UK) were revealed using a secondary alkaline phosphatase goat anti-rabbit or anti-mouse antibody, respectively. For negative controls, just secondary antibody and mouse monoclonal to B actin (1:2000, Ab 6276, UK) were employed in the blot probed with CUB 702. For blots probed with Ab421, a lane blot was probed with just secondary antibody and another with rabbit serum. Cyclophilin A (Ab 42408, Abcam, UK) was used as loading control. The blots were place in a ChemiDoc machine (Image system, Bio-rad, USA) and quantified using a ChemiDoc software. The results obtained were shown as TG2 optical density mm^2 / cyclophilin A optical density mm^2 (section 2.5.4). Tissue assessment of total TG2 protein was performed only at 28 days after RWI.

6.2.6. Statistics

Longitudinal measurements were assessed using two way analysis of variance (two-way ANOVA); whereas the cross sectional measurements were analysed by one way ANOVA followed by Bonferonni's multiple comparisons test to compare more than two groups. T-test corrected by Mann Whitney U was used to analyse Total TG activity between RWI and RWI+TGI results. To assess correlations between different experiments, analysis r^2 and p values were calculated. For all the statistical analysis, a probability higher than 95% ($p<0.05$) was taken as significant (section 2.7.2).

6.3. Results

6.3.1. Ischaemia and reperfusion

The surface colour of the kidney had changed from reddish to homogeneous dark-brown by 2 minutes after applying the left renal hilar clamping, demonstrating the depletion of oxygen in the renal tissue. Measurement of the kidney length and width was assessed before and after clamping, all clamped kidneys showed an increase after 5 and 60 minutes of renal clamping. 2 minutes after removal of the clamp from the renal hilus, kidney surface colour reverted back to normal in all animals, suggesting homogeneous tissue blood flow and subsequent re-oxygenation had been achieved. All kidneys assessed in this study fulfilled the requirements above described.

6.3.2. Renal Warm Ischaemic - day 28 interventional study

6.3.3.1. Renal function

Serum creatinine. Measurements of serum creatinine for each experimental group at both day 8 and 28 after RWI are shown in Figure 6.2. Serum creatinine prior to any surgical procedure and 24hrs after intra-renal cannulation did not show any significant difference amongst groups. At day 8, the RWI group was associated with a significant 7.5 fold increase in the serum creatinine compared to the Nx. This increase was significantly reduced by the TG inhibitor. At day 28, a similar phenomenon was observed.

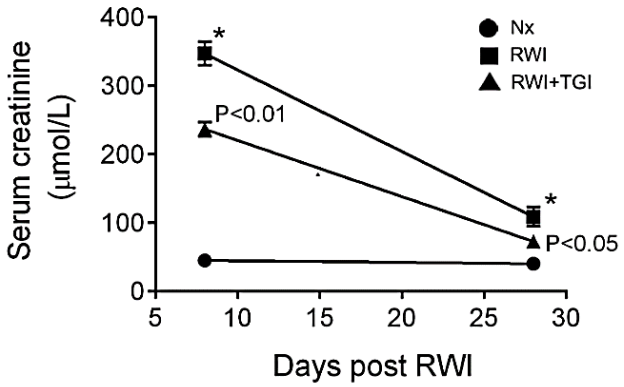

Figure 6.2: Effect of RWI and TG inhibition on s. creatinine after 8 and 28 days

The plot line graph represents the mean serum creatinine µmol/L at day 8 and day 28. Vertical bars indicate ± SEM. P<0.01 and P<0.05, RWI+TGI compared with RWI at day 8 and day 28, respectively. * Denotes P<0.01, RWI compared with Nx group in both time points. Nx, n=5; RWI, n=5; RWI+TGI, n=6.

.**Creatinine clearance.** At day 8 and 28, the RWI and RWI+TGI groups showed a significant decrease compared to the Nx control group. Day 8, Nx, 1.65 ± 0.6; RWI, 0.05 ± 0.01 and RWI+TGI, 0.11 ± 0.01 ml / min. Day 28, Nx, 2.3 ± 0.4; RWI, 0.38 ± 0.1 and RWI+TGI, 0.96 ± 2.4 mmHg. No significant differences between RWI and RWI+TGI groups were observed at day 8 and 28. Creatinine clearance following renal warm ischaemia for 60 minutes at day 8 and 28 showed a modest significant ($P<0.01$) correlation with serum creatinine; $r^2= 0.46$ and 0.64, respectively.

Albumin in urine. Measurements of albumin excretion at 0, 8 and 28 days did not show any significant difference or trend between groups. Day 0, Nx, 0.9 ± 0.7; RWI, 0.47 ± 0.18 and RWI+TGI, 0.13 ± 0.1 mg / 24hrs; Day 8, Nx, 3.1 ± 2.1; RWI, 2 ± 0.45 and RWI+TGI, 2.4 ± 1.4 mg / 24hrs; Day 28, Nx, 3.7 ± 1.8; RWI, 3.2 ± 1.9 and RWI+TGI, 6.8 ± 2.2 mg / 24hrs. However, a significant correlation with serum creatinine at day 28 was identified, $r^2= 0.50$, $P<0.01$.

Kidney weight. Kidney weight did not show any significant difference between groups. Nx, 1.23 ± 0.08 grams; RWI, 1.29 ± 0.1 grams and RWI+TGI, 1.39 ± 0.4 grams.

% of gained body weight. Measurement of % gained body weight over 28 days are shown in Figure 6.3. The RWI group was associated with a significant ($P<0.05$) lower % of gained weight when compared to the Nx group. However, it was partially restored by the administration of the TGI. Nx, 38.4 ± 4.3; RWI, 19.8 ± 3.8 and RWI+TGI, 31 ± 3 % of gained body weight.

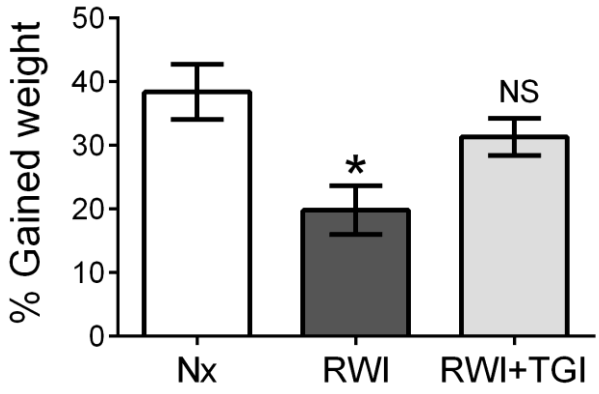

Figure 6.3: Effect of RWI and TG inhibition on % gained weight after 28 days

The histogram represents the gained weight in % after 28 days of renal warm ischaemia. Vertical bars indicate ± SEM. NS denotes no significance between RWI+TGI and RWI groups. * Denotes $P<0.05$, RWI compared with Nx group. Nx, n=5; RWI, n=5; RWI+TGI, n=6.

6.3.3.2. Tubulointerstitial fibrosis

Tubulointerstitial Masson's trichrome staining. Representative examples of tubules and interstitium from MTS sections are shown for each experimental group in Figure 6.4, panel A, B and C. The tubulointerstitial area from the RWI group shows a higher level of blue staining localized in the tubular basement membrane and interstitial area when compared to the example from Nx and RWI+TGI groups. The RWI group was associated with a significant increase (20-fold) in MTS staining compared to the Nx control group. TGI reduced the increase in MTS staining by some 80 % to values which showed no statistical difference from the Nx control group. Nx, 0.001 ± 0.0001; RWI, 0.02 ± 0.005 and RWI+TGI, 0.005 ± 0.001 blue/red ratio. Figure 6.4, panel D.

Tubulointerstitial collagen I. Representative examples of the tubulointerstitial area from immunofluorescence stained sections are shown for each experimental group in Figure 6.5, panel A, B and C. The tubulointerstitial section from the RWI group shows a higher intense green signal (FITC) in the tubulointerstitial area when compared to the example from Nx and RWI+TGI groups. The RWI group was associated with a significant increase (1.8-fold) in collagen I immunofluorescence compared to the Nx control group. TGI abolished the increase in collagen I immunostaining which showed no statistical difference from the Nx control group. Nx, 0.24 ± 0.03; RWI, 0.42 ± 0.06 and RWI+TGI, 0.19 ± 0.03 FITC/DAPI ratio. Figure 6.5, panel D.

Tubulointerstitial collagen III. Representative examples of the tubulointerstitial area from immunofluorescence stained sections are shown for each experimental group in Figure 6.6, panel A, B and C. The tubulointerstitial section from the RWI group shows a higher intense green signal (FITC) in the tubulointerstitial area when compared to the example from Nx and RWI+TGI groups. The RWI group was associated with a significant increase (4.3-fold) in Collagen III immunofluorescence compared to the Nx control group. TGI reduced the increase in Collagen III immunostaining by some 45% to values which also showed statistical difference from the Nx control group, $P<0.001$. Nx, 0.12 ± 0.01; RWI, 0.52 ± 0.04 and RWI+TGI, 0.34 ± 0.03 FITC/DAPI ratio. Figure 6.6, panel D.

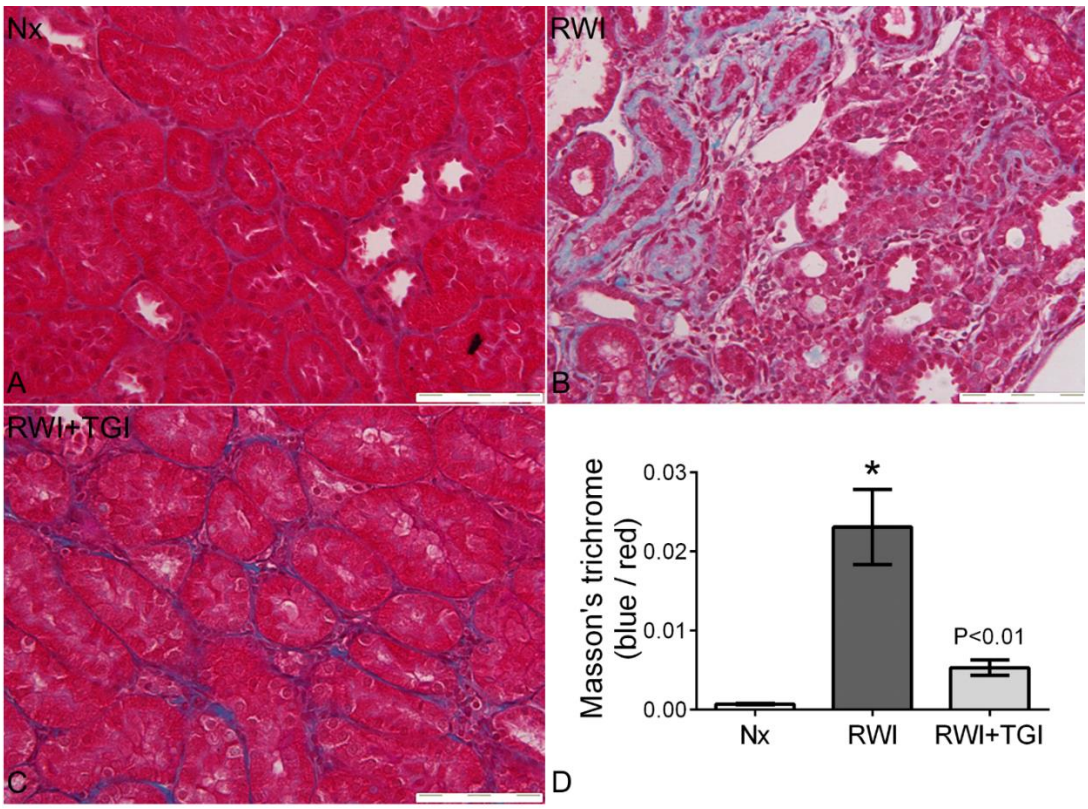

Figure 6.4: Effect of RWI and TG inhibition on tubulointerstitial fibrosis after 28 days

Panel **A**-**C**. Representative images of the tubulointerstitial area under 200x magnification, showing coloration (blue-extracellular matrix expansion; red-cellularity) and structural differences in the Nx (**A**), RWI (**B**) and RWI+TGI (**C**) groups. Panel **D**. The histogram represents the mean blue/red ratio in the tubulointerstitial area. Vertical bars indicate ± SEM. P<0.01, RWI+TGI compared with RWI group. * Denotes P<0.001, RWI compared with Nx group. Nx, n=5; RWI, n=5; RWI+TGI, n=6.

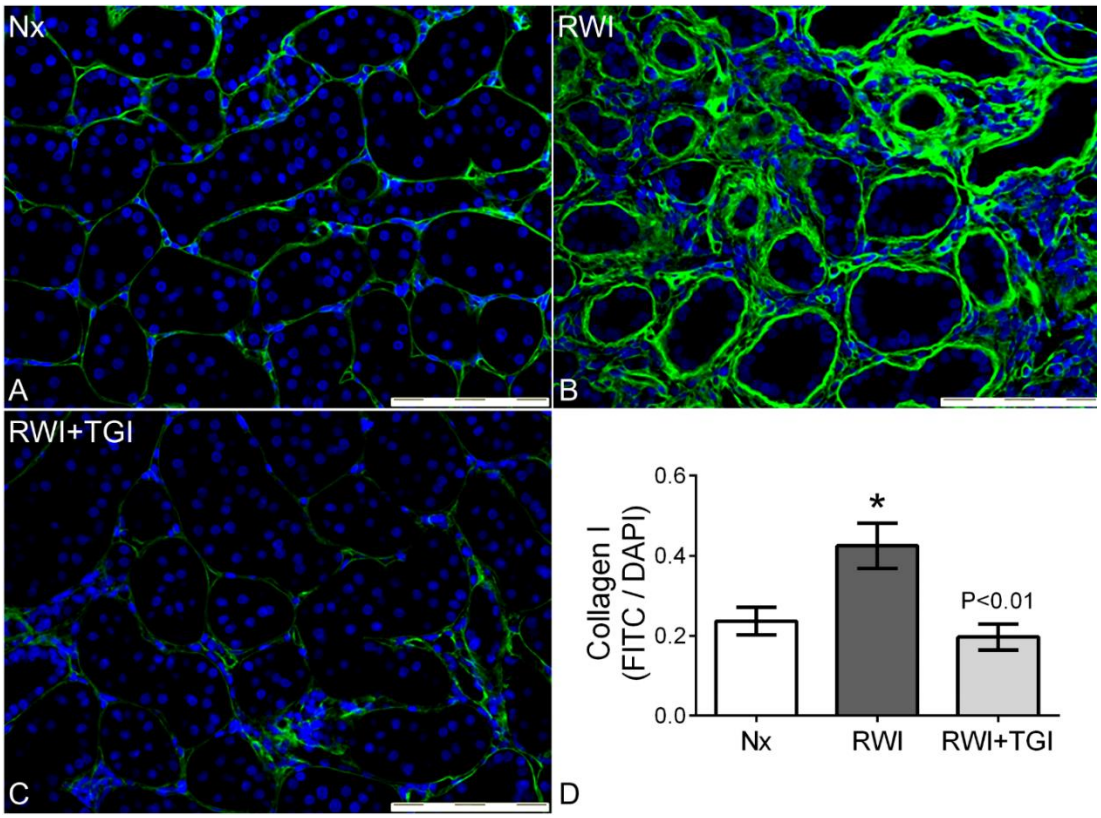

Figure 6.5: Effect of RWI and TG inhibition on tubulointerstitial collagen I after 28 days

Panel **A**-**C**. Representative images of the tubulointerstitial area under 200x magnification, showing coloration differences in collagen I (FITC-green) in the Nx (**A**), RWI (**B**) and RWI+TGI (**C**) groups. Blue dots represent cell nuclei (DAPI). Panel **D**. The histogram represents the mean FITC/DAPI ratio in the IGMA. Vertical bars indicate ± SEM. P<0.01, RWI+TGI compared with RWI group. * Denotes P<0.05, RWI compared with Nx group. Nx, n=5; RWI, n=5; RWI+TGI, n=6.

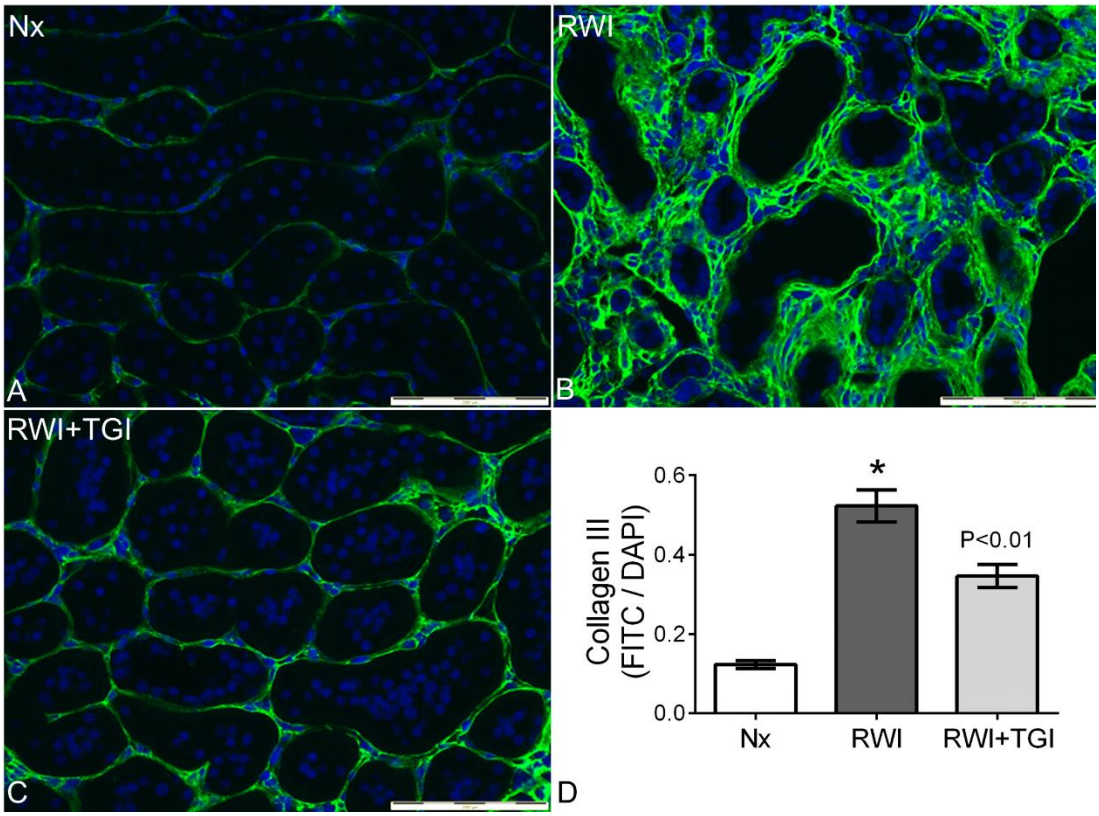

Figure 6.6: Effect of RWI and TG inhibition on tubulointerstitial collagen III after 28 days

Panel **A**-**C**. Representative images of the tubulointerstitial area under 200x magnification, showing coloration differences in collagen III (FITC-green) in the Nx (**A**), RWI (**B**) and RWI+TGI (**C**) groups. Blue dots represent cell nuclei (DAPI). Panel **D**. The histogram represents the mean FITC/DAPI ratio in the IGMA. Vertical bars indicate ± SEM. P<0.01, RWI+TGI compared with RWI group. * Denotes P<0.0001, RWI compared with Nx group. Nx, n=5; RWI, n=5; RWI+TGI, n=6.

Tubulointerstitial collagen IV. Representative examples of the tubulointerstitial area from immunofluorescence stained sections are shown for each experimental group in Figure 6.7, panel A, B and C. The tubulointerstitial section from the RWI group shows a higher intense green signal (FITC) in the peritubular area when compared to the example from Nx and RWI+TGI groups. The RWI group was associated with a significant increase (5.5-fold) in Collagen IV immunofluorescence compared to the Nx control group. TGI reduced the increase in Collagen I immunostaining by some 90% to values which showed no statistical difference from the Nx control group. Nx, 0.04 ± 0.01; RWI, 0.22 ± 0.02 and RWI+TGI, 0.06 ± 0.01 FITC/DAPI ratio. Figure 6.7, panel D.

6.3.3.3. Renal function and tubulointerstitial fibrosis correlations

Significant correlations were obtained for renal fibrosis and serum creatinine in measurements taken at day 8 and 28. A remarkable high correlation was obtained between serum creatinine at day 8 and collagen III, r^2= 0.88, P<0.0001. Masson's trichrome staining showed a considerable positive correlation when compared to collagen I, III and IV; r^2= 0.59, 0.77 and 0.76, respectively. However, when adding the three collagens into one measurement and comparing it with MTS, a higher correlation was obtained, r^2= 0.88, P<0.0001. Linear regressions using renal function and fibrosis parameters are displayed in Table 6.2.

6.3.3.4. Tubulointerstitital pathway

Tubulointerstitial Transglutaminase *in situ* activity. Representative examples of the tubulointerstitial area from immunofluorescence stained sections are shown for each experimental group in Figure 6.8, panel A, B and C. The tubulointerstitial section from the RWI group shows a higher intense red signal (Alexa) in the tubulointerstitial area when compared to the examples from Nx and RWI+TGI groups. The RWI group was associated with a significant increase (1.9-fold) TG activity fluorescence compared to the Nx control group. TGI reduced the increase in TG activity staining by some 80 % to values which showed no statistical difference from the Nx control group. Nx, 0.10 ± 0.017; RWI, 0.19 ± 0.02 and RWI+TGI, 0.12 ± 0.013 Alexa/DAPI ratio. Figure 6.8, panel D.

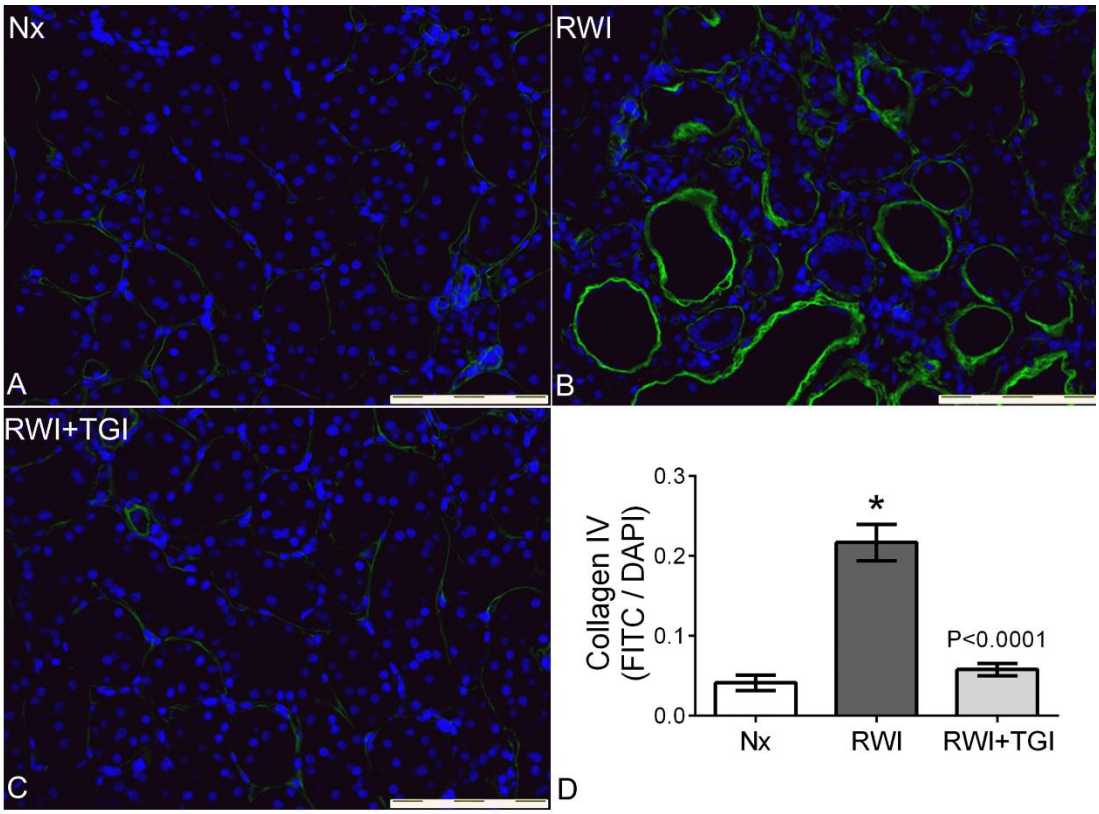

Figure 6.7: Effect of RWI and TG inhibition on tubulointerstitial collagen IV after 28 days

Panel **A**-**C**. Representative images of the tubulointerstitial area under 200x magnification, showing coloration differences in collagen IV (FITC-green) in the Nx (**A**), RWI (**B**) and RWI+TGI (**C**) groups. Blue dots represent cell nuclei (DAPI). Panel **D**. The histogram represents the mean FITC/DAPI ratio in the IGMA. Vertical bars indicate ± SEM. P<0.0001, RWI+TGI compared with RWI group. * Denotes P<0.0001, RWI compared with Nx group. Nx, n=5; RWI, n=5; RWI+TGI, n=6.

Technique A	Technique B	P value <	r^2
Serum creatinine day 8	MTS	0.0001	0.65
Serum creatinine day 8	Collagen I	0.04	0.28
Serum creatinine day 8	Collagen III	0.0001	0.88
Serum creatinine day 8	Collagen IV	0.0005	0.60
Serum creatinine day 28	MTS	0.0001	0.57
Serum creatinine day 28	Collagen I	0.03	0.30
Serum creatinine day 28	Collagen III	0.001	0.65
Serum creatinine day 28	Collagen IV	0.0005	0.61
MTS	Collagen I	0.001	0.59
MTS	Collagen III	0.0001	0.77
MTS	Collagen IV	0.0001	0.76
Collagen I	Collagen III	0.03	0.31
Collagen III	Collagen IV	0.0003	0.65
Collagen IV	Collagen I	0.0003	0.65
Collagens I, III, IV	MTS	0.0001	0.88
Collagens I, III, IV	Serum creatinine day 8	0.0001	0.72
Collagens I, III, IV	Serum creatinine day 28	0.0005	0.64

Table 6.2: Renal function and tubulointerstitial fibrosis correlations

Tubulointerstitial Transglutaminase 2. Representative examples of the tubulointerstitial area from immunofluorescence stained sections are shown for each experimental group in Figure 6.9, panel A, B and C. The tubulointerstitial section from the RWI group shows a higher intense red signal (Alexa) in the tubulointerstitial area when compared to the examples from Nx and RWI+TGI groups. The RWI group was associated with a significant increase (1.9-fold) TG2 immunofluorescence compared to the Nx control group. TGI reduced the increase in TG2 immunostaining by some 80 % to values which showed no statistical difference from the Nx control group. Nx, 0.85 ± 0.12; RWI, 1.6 ± 0.05 and RWI+TGI, 1 ± 0.07 Alexa/DAPI ratio. Figure 6.9, panel D.

6.3.3.1. Tubulointerstitial TG correlations, renal function and fibrosis

Extracellular TG activity showed significant correlations when compared to parameters of renal function. When comparing TG activity with parameters of tubulointerstitial fibrosis, low-moderate correlations were obtained; MTS, collagen I, III, and IV, r^2=0.30, 0.29, 0.34, and 0.41, respectively. Regarding extracellular TG2, slightly higher correlations were obtained when comparing the same measurements of tubulointerstitial fibrosis; MTS, collagen I, III, and IV, r^2=0.53, 0.38, 0.53, and 0.67. Parameters of renal function at day 8 and 28 showed a higher correlation with TG2 in contrast to the correlations obtained with TG activity. A table with linear regressions using tubulointerstitial parameters is displayed in Table 6.3.

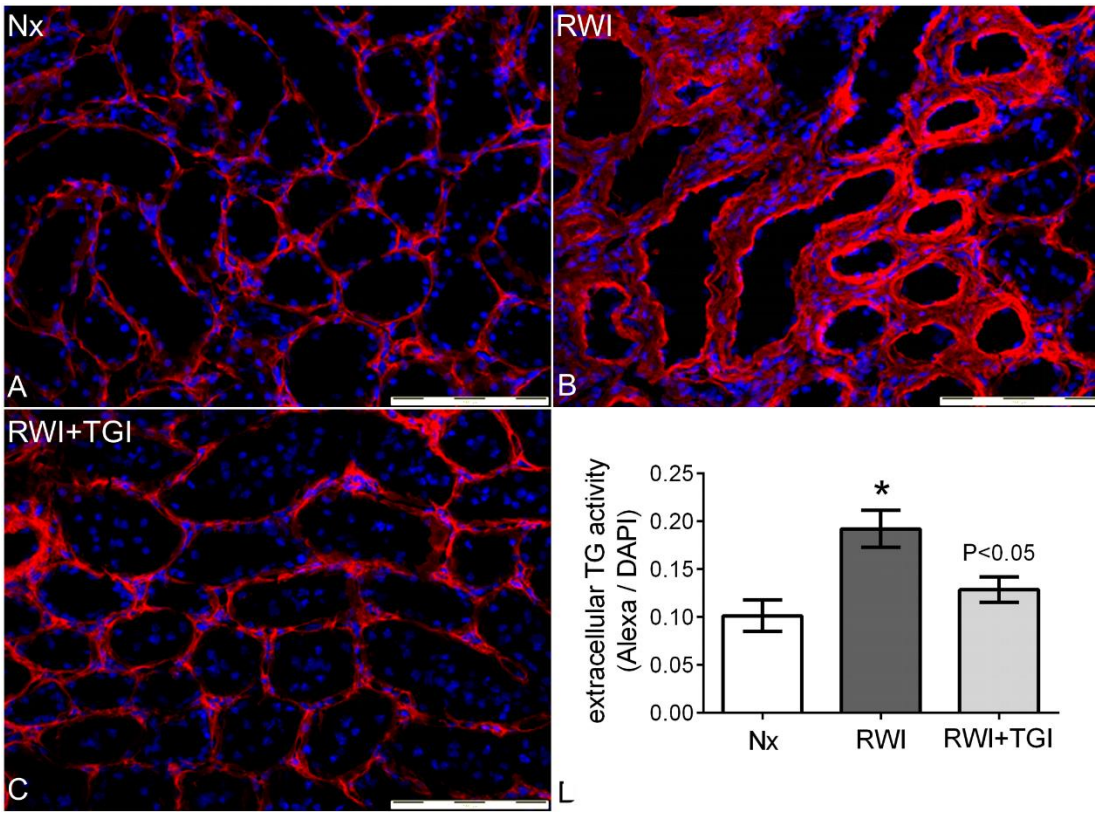

Figure 6.8: Effect of RWI and TG inhibition on tubulointerstitial TG activity after 28 days

Panel **A**-**C**. Representative images of the tubulointerstitial area under 200x magnification, showing coloration differences in TG activity (Alexa-red) in the Nx (**A**), RWI (**B**) and RWI+TGI (**C**) groups. Blue dots represent cell nuclei (DAPI). Panel **D**. The histogram represents the mean Alexa/DAPI ratio in the IGMA. Vertical bars indicate ± SEM. P<0.05, RWI+TGI compared with RWI group. * Denotes P<0.01, RWI compared with Nx group. Nx, n=5; RWI, n=5; RWI+TGI, n=6.

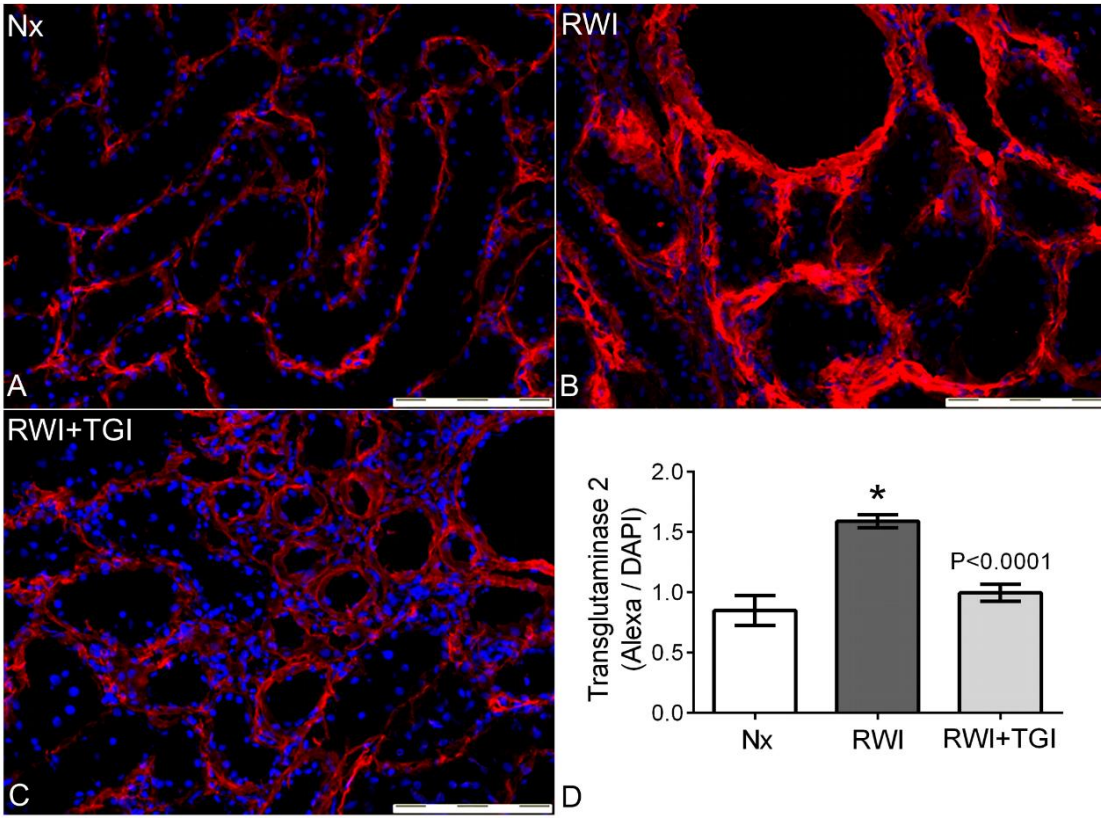

Figure 6.9: Effect of RWI and TG inhibition on tubulointerstitial TG2 after 28 days

Panel **A**-**C**. Representative images of the tubulointerstitial area under 200x magnification, showing coloration differences in TG2 protein (Alexa-red) in the Nx (**A**), RWI (**B**) and RWI+TGI (**C**) groups. Blue dots represent cell nuclei (DAPI). Panel **D**. The histogram represents the mean Alexa/DAPI ratio in the IGMA. Vertical bars indicate ± SEM. P<0.0001, RWI+TGI compared with RWI group. * Denotes P<0.0001, RWI compared with Nx group. Nx, n=5; RWI, n=5; RWI+TGI, n=6.

Technique A	Technique B	P value <	r^2
TG *in situ* activity	Serum creatinine day 8	0.05	0.37
TG *in situ* activity	Creatinine clearance day 28	0.05	0.38
TG *in situ* activity	MTS	0.05	0.30
TG *in situ* activity	Collagen I	0.05	0.29
TG *in situ* activity	Collagen III	0.02	0.34
TG *in situ* activity	Collagen IV	0.01	0.41
TG *in situ* activity	Collagens I, III, IV	0.01	0.42
TG2 protein	Serum creatinine day 8	0.005	0.48
TG2 protein	Serum creatinine day 28	0.01	0.42
TG2 protein	Creatinine clearance day 28	0.01	0.39
TG2 protein	MTS	0.005	0.53
TG2 protein	Collagen I	0.01	0.38
TG2 protein	Collagen III	0.005	0.53
TG2 protein	Collagen IV	0.0001	0.67
TG2 protein	Collagens I, III, IV	0.0005	0.63
TG2 protein	TG *in situ* activity	0.0005	0.60

Table 6.3: Tubulointerstitial Area - General linear regressions

6.3.3.2. Glomerular fibrosis

Glomerular Masson's trichrome staining. Representative examples of glomeruli from MTS sections are shown for each experimental group in Figure 6.10, panel A, B and C. The intraglomerular mesangial area (IGMA) from the RWI group shows a higher level of light blue staining in the capillary basement membranes together with mesangial matrix expansion in contrast to the examples from Nx and RWI+TGI groups. The RWI group was associated with a higher blue/red ratio in contrast to the Nx control group ($P<0.01$). This increase was significantly reduced by the TGI ($P<0.05$) to values not significantly different from the Nx control. Nx, 0.0006 ± 0.0001; RWI, 0.004 ± 0.001 and RWI+TGI, 0.0018 ± 0.0005 Alexa/DAPI ratio. Figure 6.10, panel D.

Glomerular collagen I, III and IV. Representative examples of glomeruli from immunofluorescence stained sections are shown for each experimental group in Figure 6.11, panel A, B and C (collagen I); Figure 6.12, panel A, B and C (collagen III); Figure 6.13, panel A, B and C (collagen IV).

The IGMA for collagen I, from the RWI and RWI+TGI groups shows a lower level of green signal (FITC) when compared to the example from Nx group, Figure 6.11, panel A-C. Collagen I. The RWI group showed a significantly lower FITC/DAPI ratio of some 60% ($P<0.05$) when compared to the Nx control group. This decrease remained unaffected by the administration of the TG inhibitor. Nx, 0.23 ± 0.03; RWI, 0.1 ± 0.06 and RWI+TGI, 0.07 ± 0.03 FITC/DAPI ratio.

The IGMA for collagen III from RWI+TGI group shows a slight increase in green signal when compared to both the examples from Nx and RWI+TGI groups, Figure 6.12, panel A-C. Collagen III. The RWI group did not show any significant difference amongst groups. Nx, 0.004 ± 0.001; RWI, 0.002 ± 0.001 and RWI+TGI, 0.016 ± 0.007 FITC/DAPI ratio.

The IGMA for collagen IV shows a similar fluorescent behaviour to the one seen in IGMA for collagen I, Figure 6.13, panel A-C. Collagen IV. The RWI group showed a significantly lower FITC/DAPI ratio of some 80% ($P<0.01$) when compared to the Nx control group. This decrease remained unaffected by the administration of the TG inhibitor. Nx, 0.25 ± 0.05; RWI, 0.06 ± 0.02 and RWI+TGI, 0.04 ± 0.004 FITC/DAPI ratio

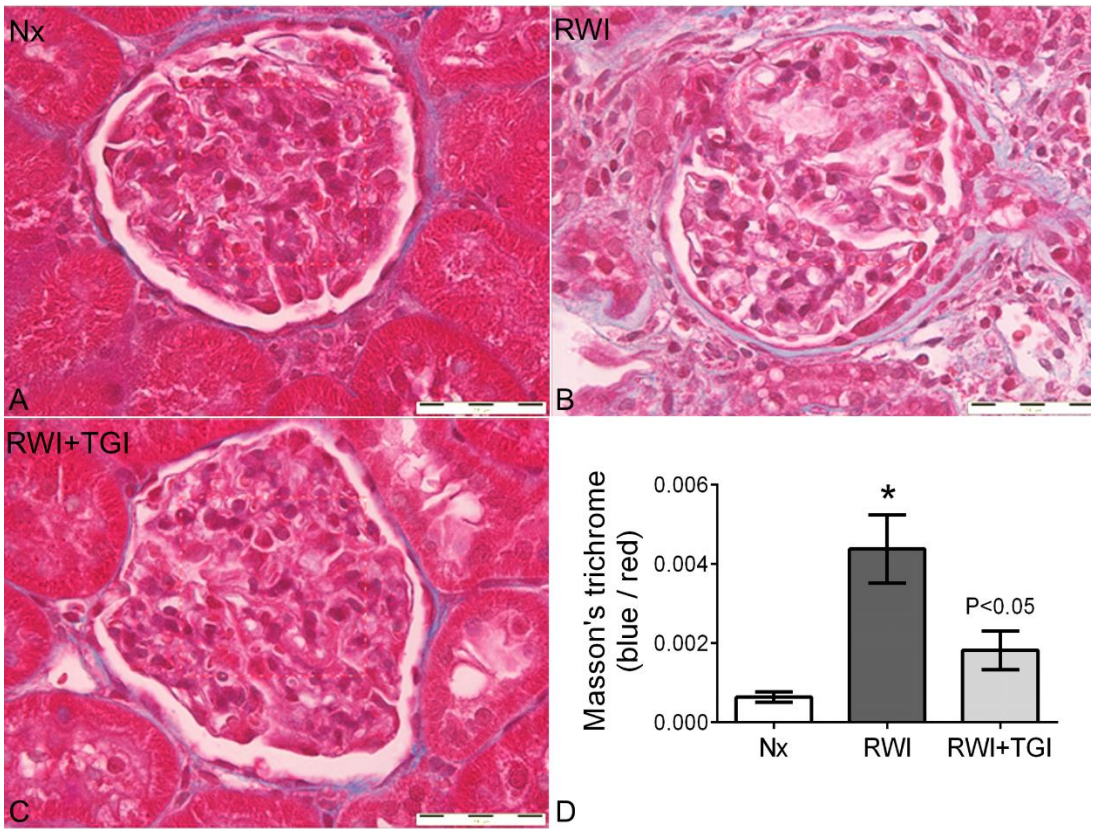

Figure 6.10: Effect of RWI and TG inhibition on glomerular matrix after 28 days

Panel **A**-**C**. Representative images of the intraglomerular mesangial area under 400x magnification, showing coloration (blue-extracellular matrix expansion; red-cellularity) and structural differences in the Nx (**A**), RWI (**B**) and RWI+TGI (**C**) groups. The IGMA is delimited by a squared red frame. Panel **D**. The histogram represents the mean blue/red ratio in the IGMA. Vertical bars indicate ± SEM. P<0.05, RWI+TGI compared with RWI group. * Denotes P<0.01, RWI compared with Nx group. Nx, n=5; RWI, n=5; RWI+TGI, n=6.

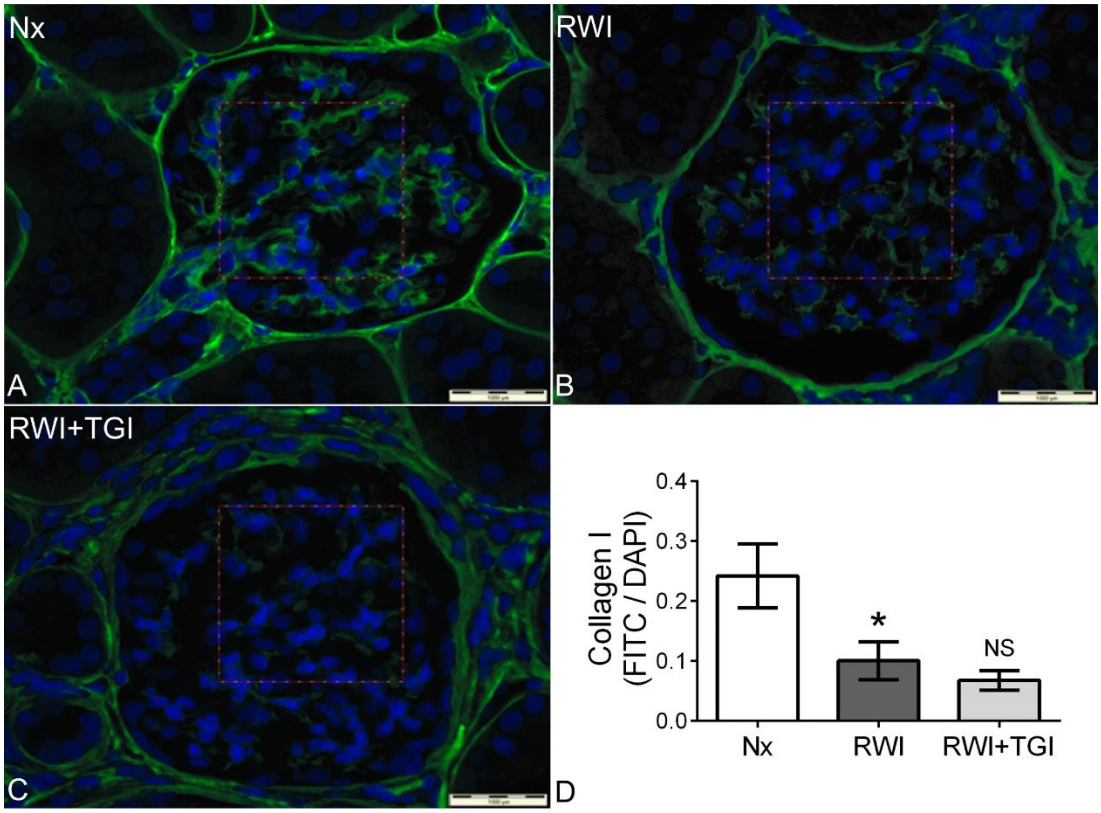

Figure 6.11: Effect of RWI and TG inhibition on glomerular collagen I after 28 days

Panel **A**-**C**. Representative images of the intraglomerular mesangial area under 400x magnification, showing coloration differences in collagen I (FITC-green) in the Nx (**A**), RWI (**B**) and RWI+TGI groups (**C**). Blue dots represent cell nuclei (DAPI). The IGMA is delimited by a squared red frame. Panel **D**. The histogram represents the mean FITC/DAPI ratio in the IGMA. Vertical bars indicate ± SEM. NS denotes no significance between RWI+TGI and RWI groups. * Denotes P<0.05, RWI compared with Nx group. Nx, n=5; RWI, n=5; RWI+TGI, n=6.

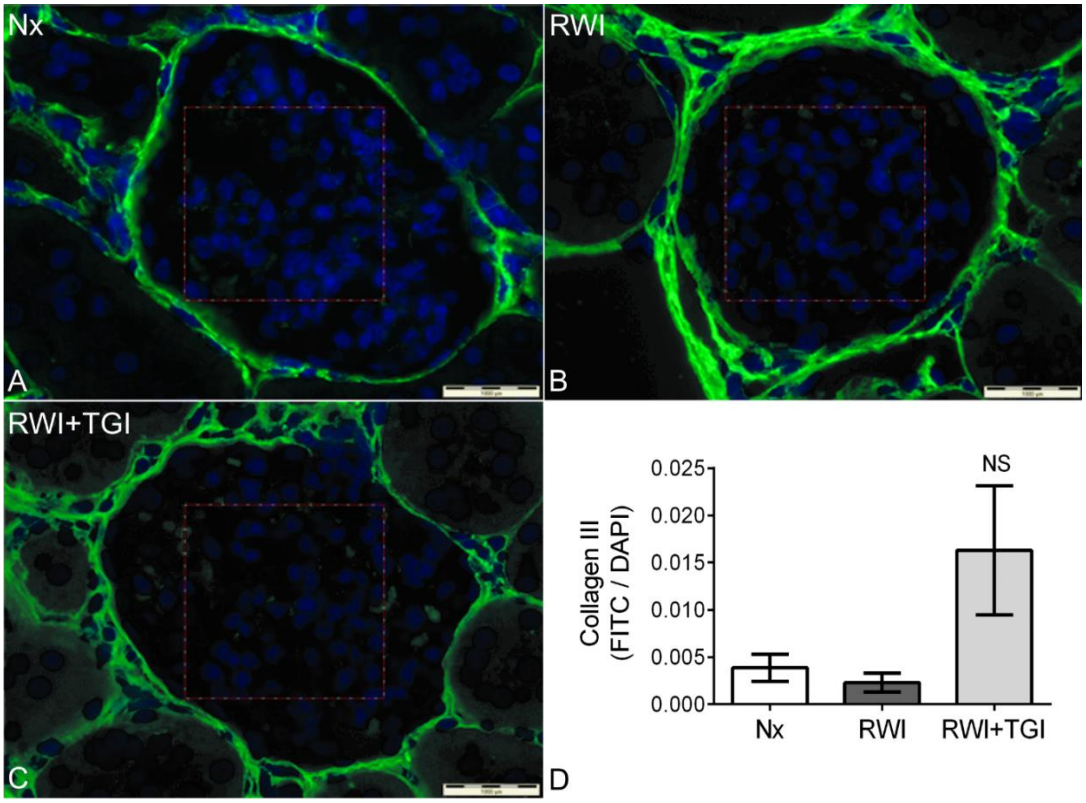

Figure 6.12: Effect of RWI and TG inhibition on glomerular collagen III after 28 days

Panel **A**-**C**. Representative images of the intraglomerular mesangial area under 400x magnification, showing coloration differences in collagen III (FITC-green) in the Nx (**A**), RWI (**B**) and RWI+TGI (**C**) groups. Blue dots represent cell nuclei (DAPI). The IGMA is delimited by a squared red frame. Panel **D**. The histogram represents the mean FITC/DAPI ratio in the IGMA. Vertical bars indicate ± SEM. NS denotes no significance between RWI+TGI and RWI groups. Nx, n=5; RWI, n=5; RWI+TGI, n=6.

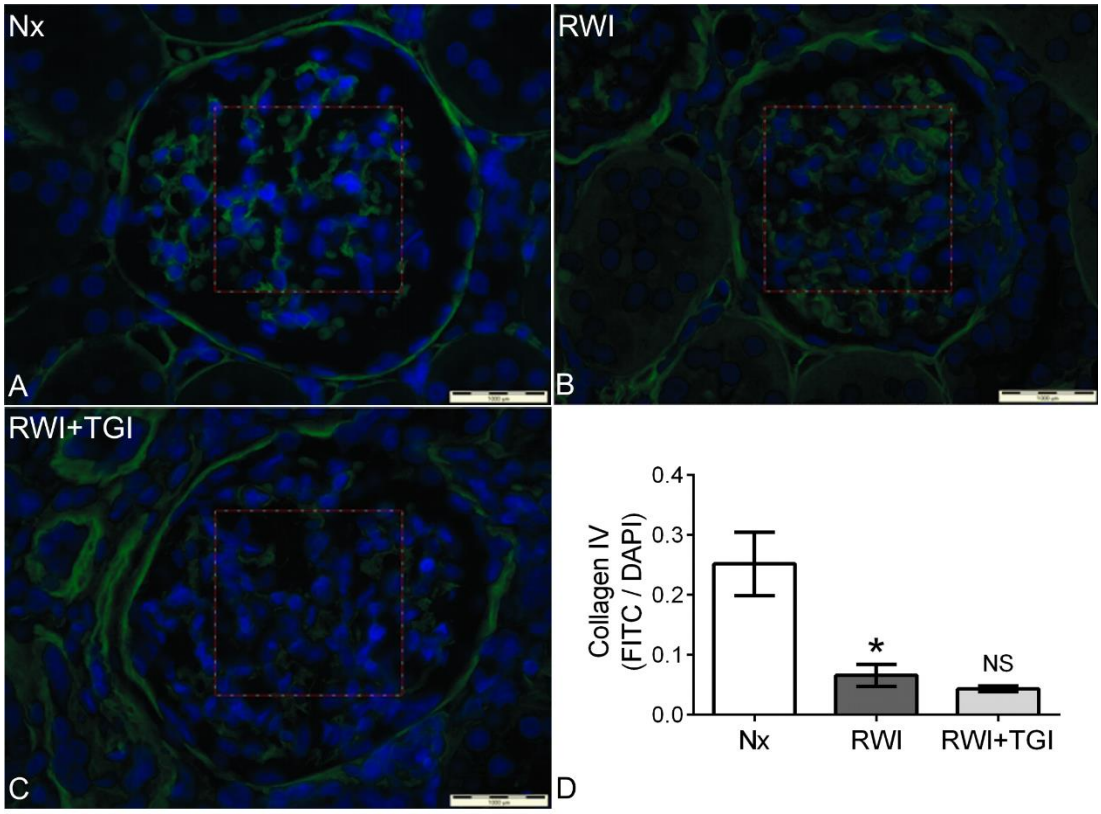

Figure 6.13: Effect of RWI and TG inhibition on glomerular collagen IV after 28 days

Panel **A**-**C**. Representative images of the intraglomerular mesangial area under 400x magnification, showing coloration differences in collagen IV (FITC-green) in the Nx (**A**), RWI (**B**) and RWI+TGI (**C**) groups. Blue dots represent cell nuclei (DAPI). The IGMA is delimited by a squared red frame. Panel **D**. The histogram represents the mean FITC/DAPI ratio in the IGMA. Vertical bars indicate ± SEM. NS denotes no significance between RWI+TGI and RWI groups. * Denotes P<0.01, RWI compared with Nx group. Nx, n=5; RWI, n=5; RWI+TGI, n=6.

6.3.3.3. Glomerular TG pathway

Glomerular Transglutaminase *in situ* activity. Representative examples of glomeruli from immunofluorescence stained sections are shown for each experimental group in Figure 6.14, panel A, B and C. The IGMA from the RWI and RWI+TGI groups show a lower level of red signal (Alexa) compared to the example from Nx group.

The RWI group showed a significantly lower Alexa/DAPI ratio of some 80% ($P<0.0001$) when compared to the Nx control group. This decrease remained unaffected by the administration of the TG inhibitor. Nx, 0.38 ± 0.05; RWI, 0.09 ± 0.027 and RWI+TGI, 0.08 ± 0.03 Alexa/DAPI ratio. Figure 6.14, panel D.

Glomerular Transglutaminase 2. Representative examples of glomeruli from immunofluorescence stained sections are shown for each experimental group in Figure 6.15, panel A, B and C. The IGMA from the RWI and RWI+TGI group show a lower level of red signal (Alexa) when compared to the example from Nx group.

The RWI group showed a significantly lower Alexa/DAPI ratio of some 90% ($P<0.0001$) when compared to the Nx control group. This decrease remained unaffected by the administration of the TG inhibitor. Nx, 0.31 ± 0.04; RWI, 0.03 ± 0.01 and RWI+TGI, 0.05 ± 0.02 Alexa/DAPI ratio. Figure 6.15, panel D.

6.3.3.4. Glomerular correlations with extracellular TG pathway

Extracellular TG activity showed a moderate correlation with parameters of extracellular TG2, $r^2=0.58$, 0.001. Tubulointerstitial renal fibrosis also showed positive correlations with extracellular TG activity. A table with linear regressions using IGMA parameters is displayed in Table 6.4.

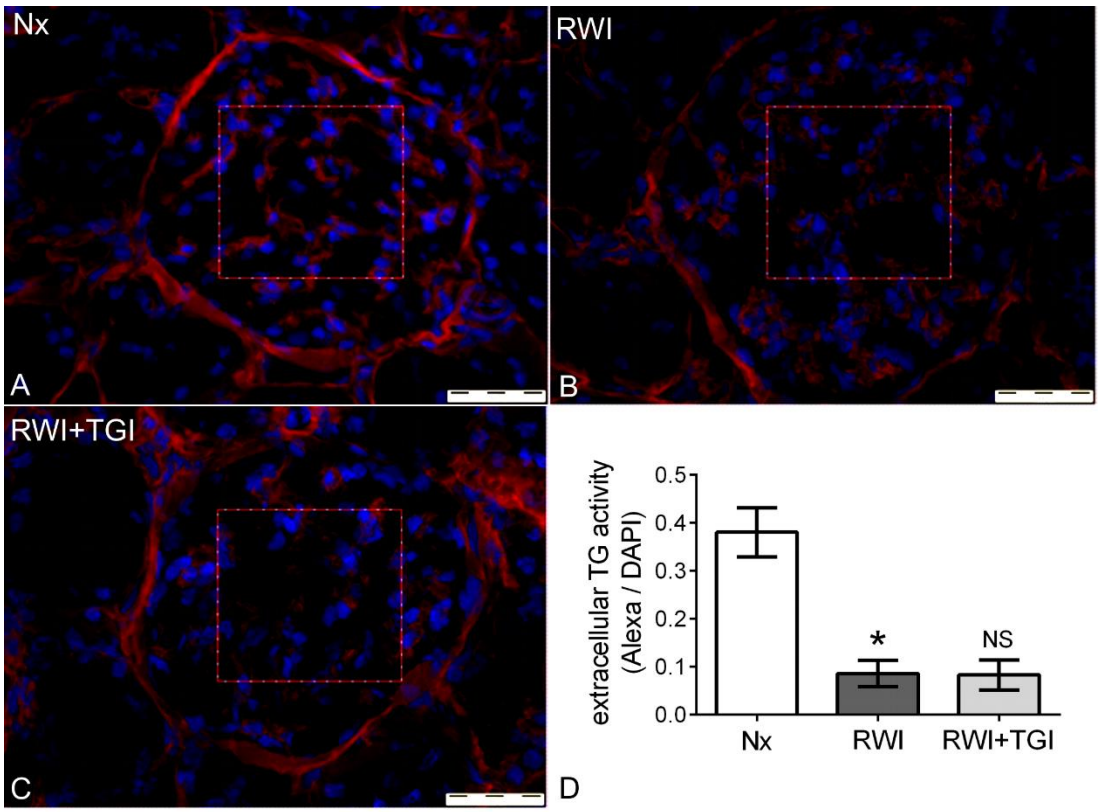

Figure 6.14: Effect of RWI and TG inhibition on glomerular **TG activity** after 28 days

Panel **A**-**C**. Representative images of the intraglomerular mesangial area under 400x magnification, showing coloration differences in TG activity (Alexa-red) in the Nx (**A**), RWI (**B**) and RWI+TGI (**C**) groups. Blue dots represent cell nuclei (DAPI). The IGMA is delimited by a squared red frame. Panel **D**. The histogram represents the mean Alexa/DAPI ratio in the IGMA. Vertical bars indicate ± SEM. NS denotes no significance between RWI+TGI and RWI groups. * Denotes P<0.0001, RWI compared with Nx group. Nx, n=5; RWI, n=5; RWI+TGI, n=6.

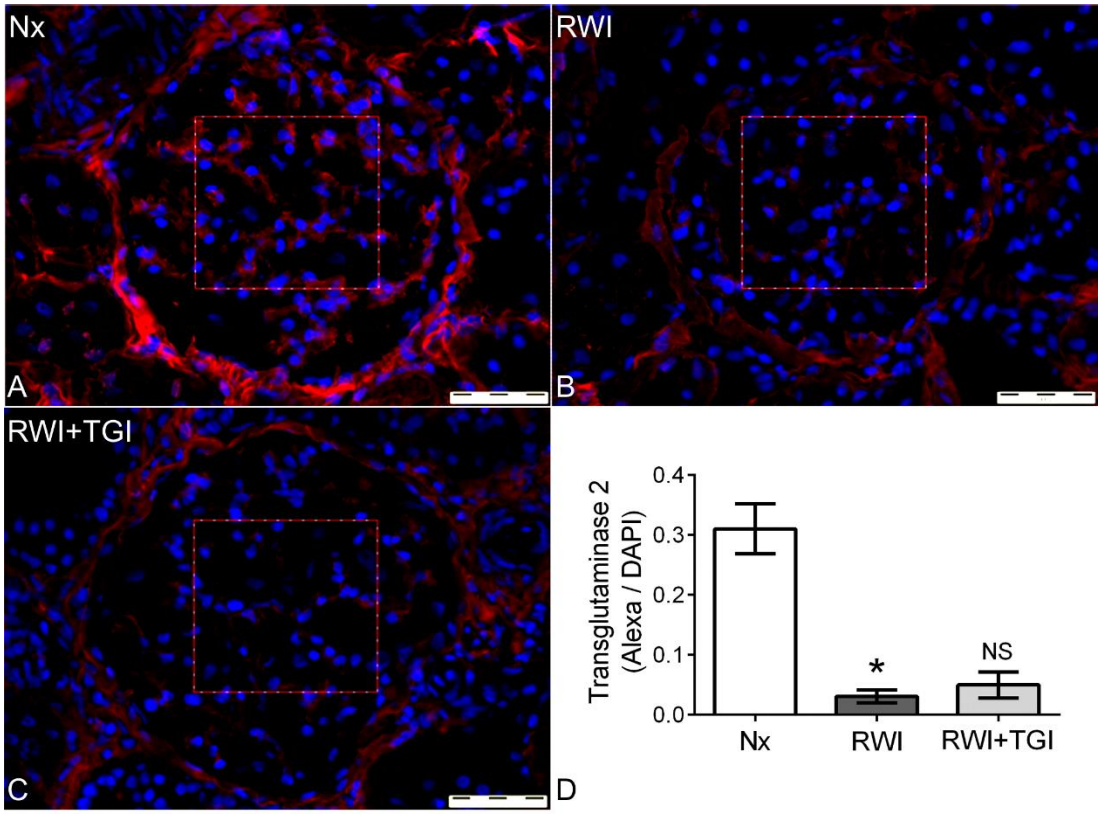

Figure 6.15: Effect of RWI and TG inhibition on glomerular **TG2** after 28 days

Panel **A**-**C**. Representative images of the intraglomerular mesangial area under 400x magnification, showing coloration differences in TG2 protein (Alexa-red) in the Nx (**A**), RWI (**B**) and RWI+TGI (**C**) groups. Blue dots represent cell nuclei (DAPI). The IGMA is delimited by a squared red frame. Panel **D**. The histogram represents the mean Alexa/DAPI ratio in the IGMA. Vertical bars indicate ± SEM. NS denotes no significance between RWI+TGI and RWI groups. * Denotes P<0.0001, RWI compared with Nx group. Nx, n=5; RWI, n=5; RWI+TGI, n=6.

Technique A	Technique B	P value <	r^2
TG *in situ* activity	Collagen I	0.05	0.28
TG *in situ* activity	Collagen IV	0.05	0.38
TG *in situ* activity	Collagen I, III, IV	0.02	0.33
TG2 protein	Collagen IV	0.01	0.43
TG2 protein	Collagen I, III, IV	0.03	0.32
TG2 protein	TG *in situ* activity	0.001	0.58

Table 6.4: Intraglomerular Mesangial Area - General Linear regressions

6.3.3.5. Total TG pathway

Total TG enzyme activity. The RWI and RWI+TGI groups were associated with a significant 3.5 and 5 fold reduction in nmol of 3H-putrescine incorporated per hour at 37˚C when compared to the Nx group, Figure 6.16, panel A. The analysis between the RWI and RWI+TGI showed a significant reduction of the RWI+TGI when contrasted to RWI group. RWI, 0.48 ± 0.07 and RWI+TGI, 0.3 ± 0.05 units / mg of protein, P<0.05. Figure 6.16.

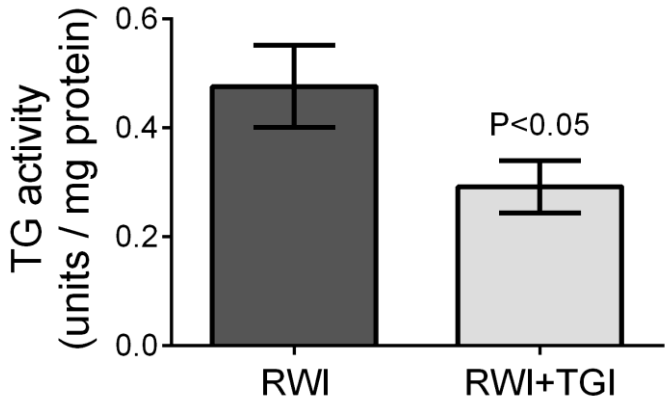

Figure 6.16: Effect of RWI and TG inhibition on total TG activity after 28 days

The histogram represents the total TG activity, determined by 3H-putrescine incorporation, in homogenates of kidneys from RWI and RWI+TGI rats. Vertical bars indicate ± SEM. RWI, n=5; RWI+TGI, n=6.

Total Transglutaminase 2. Representative western blots for each experimental group, immunoprobed with a rabbit polyclonal TG2 antibody (TG2 rpAb) and a mouse monoclonal TG2 antibody (TG100) are shown in Figures 6.17 and 6.18, respectively (sections A). Recombinant rat TG2 (positive control) gave a single band at approximately 73 kDa. When immunoprobing with TG2 rpAb, the rat kidney homogenates gave two intensive bands, 83 and 72kDa (Figure 6.17, section A). When immunoprobing with the TG2 mAb, the rat kidney homogenates gave one intensive band at 72 kDa and multiple faint bands with a lower molecular weight; the more evident ones had molecular weights of 61, 47 and 32 kDa (Figure 6.18, section A). Negative controls using either rabbit serum or mouse IgG to β-actin at an equal concentration to each primary antibody did not show a band with a similar molecular weight to the ones detected when using TG2 antibodies. β-actin antibody (mouse IgG control), gave one band at 40 kDa. The omission of primary antibody for each western blot did not showed any signal band. When immunoprobing a row segment of tissue blot with cyclophilin A (loading control), a band at 17 kDa was detected in all samples with a similar density.

When blot was immunoprobed with the rabbit TG2 antibody (Ab 421), the mean volume density of the 83 (potential factor XIIIa) and 72 kDa (TG2) bands corrected by the mean volume density of cyclophilin A did not show significant difference amongst groups. 83 kDa band. Nx, 0.22 ± 0.03; RWI, 0.19 ± 0.004 and RWI+TGI, 0.18 ± 0.01 $ODmm^2$ / $ODmm^2$. 72 KDa band. Nx, 0.26 ± 0.03; RWI, 0.19 ± 0.012 and RWI+TGI, 0.25 ± 0.06 $ODmm^2$ / $ODmm^2$, Figures 6.17, section B. When blot was immunoprobed with mouse monoclonal TG2 (TG100) the 72 kDa band corrected by the mean volume density of cyclophilin A did not show significant difference amongst groups. Nx, 0.16 ± 0.01; RWI, 0.19 ± 0.01 and RWI+TGI, 0.21 ± 0.03 $ODmm^2$ / $ODmm^2$. Figures 6.18, section B.

No correlations were obtained when compared tubulointerstitial measurements with either total TG activity or TG2 protein.

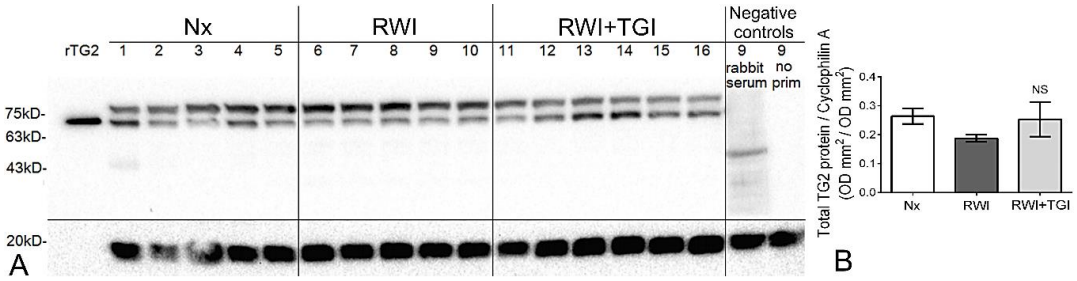

Figure 6.17: Effect of RWI and TG inhibition on total TG2 after 28 days using a rabbit polyclonal antibody

Panel **A**. Representative western blot for transglutaminase 2 (TG2) from Nx (rats 1-5), RWI (rats 6-10) and RWI+TGI (rats 11-16). Homogenates were immunoprobed with a rabbit polyclonal TG2 antibody. Rat recombinant TG2 was the positive control giving a band at 72kDa. Kidney homogenates a band at 71 kDa (TG2). In the negative control set, the first lane kidney homogenate (rat 9) was immunoprobed with rabbit serum giving a faint band at 45kDa band. In the last lane kidney homogenate (rat 9) was probed without primary antibody. Cyclophilin A was employed for loading control giving a band at 17 kDa. Panel **B**. The histogram represents the TG2 mean OD mm^2 / cyclophilin A mean OD mm^2 obtained from kidney homogenates immunoprobed with rabbit polyclonal TG2 antibody. Vertical bars indicate ± SEM. NS denotes no significance between RWI+TGI and RWI groups. Nx, n=5; RWI, n=5; RWI+TGI, n=6.

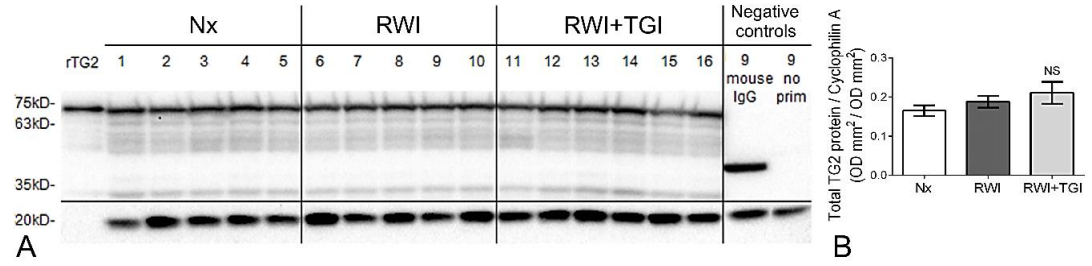

Figure 6.18: Effect of RWI and TG inhibition on total TG2 after 28 days using a mouse monoclonal antibody

Panel **A**. Representative western blot for transglutaminase 2 (TG2) from Nx (rats 1-5), RWI (rats 6-10) and RWI+TGI (rats 11-16). Kidney homogenates were immunoprobed with a mouse monoclonal TG2 antibody. Rat recombinant TG2 was the positive control giving a band at 72kDa. Kidney homogenates a band at 71 kDa (TG2). In the negative control set, the first lane kidney homogenate (rat 9) was immunoprobed with mouse monoclonal to β-actin giving a 40 kDa band. In the last lane kidney homogenate (rat 9) was without primary antibody. Cyclophilin A was employed for loading control giving a band at 17 kDa. Panel **B**. The histogram represents the TG2 mean OD mm^2 / cyclophilin A mean OD mm^2 obtained from kidney homogenates immunoprobed with mouse monoclonal TG2 antibody. Vertical bars indicate ± SEM. NS denotes no significance between RWI+TGI and RWI groups. Nx, n=5; RWI, n=5; RWI+TGI, n=6.

6.3.3. Renal Warm Ischaemia - day 8 interventional study

6.3.2.1. Renal function and kidney weight

Serum creatinine. Measurements of serum creatinine for each experimental group at day 8 after RWI, expressed as mean of μmol/L, are shown in Figure 6.19. The RWI group was associated with a higher serum creatinine compared to the Nx control (P<0.0001), this increase was partially restored by the TGI. Nx, 52 ± 4; RWI, 334 ± 34 and RWI+TGI 251 ± 23 μmol/L. Serum creatinine prior to any surgical procedure and 24hrs after intra-renal cannulation on day -3 did not show any significant difference between experimental groups.

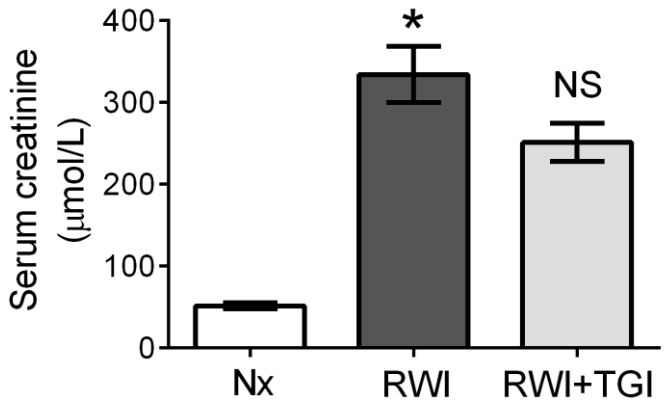

Figure 6.19: Effect of RWI and TG inhibition on serum creatinine at day 8

The histogram represents the level of serum creatinine after 8 days of renal warm ischaemia. Vertical bars indicate ± SEM. NS denotes no significance between RWI+TGI and RWI groups. * Denotes P<0.0001, RWI compared with Nx group. Nx, n=5; RWI, n=4; RWI+TGI, n=3.

Creatinine clearance. The RWI group was associated with a lower creatinine clearance compared to the Nx control (P<0.001), this increase was partially restored by the TGI. Nx, 1.5 ± 0.2; RWI, 0.12 ± 0.4 and RWI+TGI 0.23 ± 0.1 ml/min. Creatinine clearance prior to any surgical procedure and 24hrs after intra-renal cannulation did not show any significant difference between groups.

Albumin in urine. Measurements of albumin excretion at day 8 for each experimental group, did not show any significant difference between groups. Nx, 2.4 ± 0.6; RWI, 0.83 ± 0.16 and RWI+TGI, 1.8 ± 0.7 mg / 24hrs.

Kidney weight. The RWI group was associated with a significantly higher renal weight in grams compared to the Nx control group (P<0.001). TGI significantly reduced the increase in kidney weight by some 90% to values not significantly different from the Nx controls. Nx, 1.24 ± 0.12; RWI, 2.04 ± 0.5 and RWI+TGI 1.32 ± 0.1 grams, Figure 6.20.

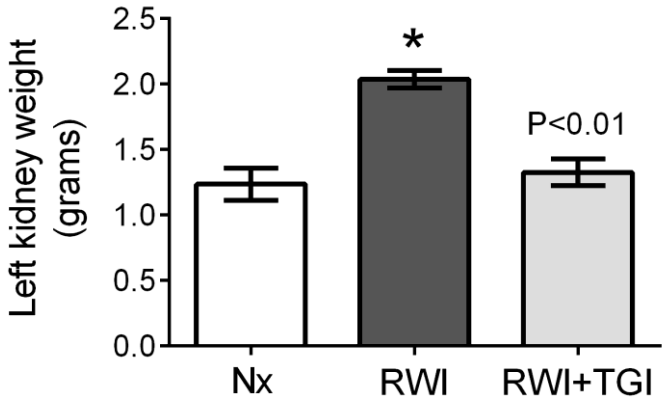

Figure 6.20: Effect of RWI and TG inhibition on the left kidney weight at 8 days

The histogram represents the weight of the left kidney after 8 days of renal warm ischaemia. Vertical bars indicate ± SEM. P<0.01, RWI+TGI compared with RWI group. * Denotes P<0.001, RWI compared with Nx group. Nx, n=5; RWI, n=4; RWI+TGI, n=3.

6.3.2.2. Tubulointerstitial fibrosis

Masson's trichrome staining. The RWI group was associated with a higher blue/red ratio compared to the Nx control (P<0.05). This increase remained unaffected by the administration of the TG inhibitor. Nx, 0.007 ± 0.001; RWI, 0.04 ± 0.01 and RWI+TGI 0.036 ± 0.01 blue/red ratio, Figure 6.21.

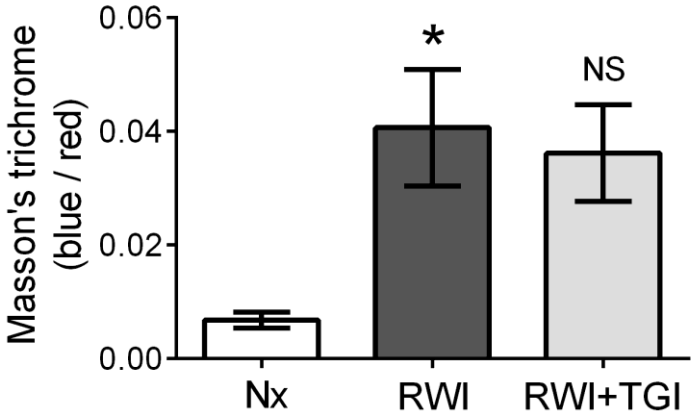

Figure 6.21: Effect of RWI and TG inhibition on extracellular matrix expansion at 8 days

The histogram represents the effect of RWI on extracellular matrix expansion after 8 days. Vertical bars indicate ± SEM. NS denotes no significance between RWI+TGI and RWI groups. Nx, n=5; RWI, n=4; RWI+TGI, n=3.

Collagen III. The RWI group was associated with a higher FITC/DAPI ratio compared to the Nx control (P<0.01). This increase was partially reduced by the TGI Nx, 0.085 ± 0.02; RWI, 0.3 ± 0.03 and RWI+TGI 0.25 ± 0.02 FITC/DAPI ratio. Figure 6.22.

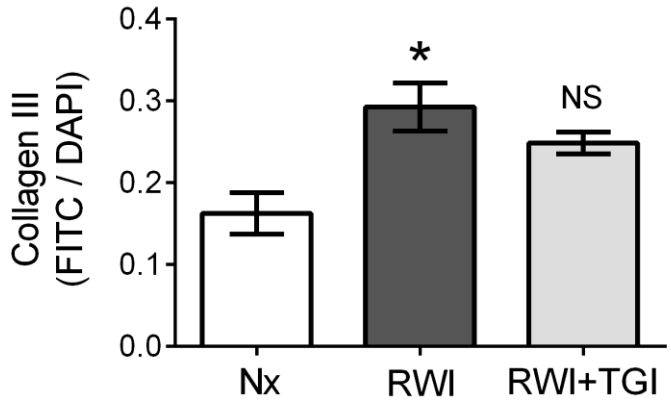

Figure 6.22: Effect of RWI and TG inhibition on tubulointerstitial collagen III at 8 days

The histogram represents the effect of RWI on tubulointerstitial collagen III after 8 days. Vertical bars indicate ± SEM. NS denotes no significance between RWI+TGI and RWI groups. * Denotes P<0.01, RWI compared with Nx group. Nx, n=5; RWI, n=4; RWI+TGI, n=3.

6.3.2.3. Tubulointerstitial TG pathway

Tubulointerstitial transglutaminase *in situ* activity. The RWI group was associated with a significant increase (2.2 fold) in the Alexa/DAPI ratio when compared to the Nx controls. TGI abolished the increase in transglutaminase activity which showed no statistical difference from the Nx control group. Nx, 0.24 ± 0.07; RWI, 0.55 ± 0.07 and RWI+TGI, 0.25 ± 0.05 FITC/DAPI ratio. Figure 6.23.

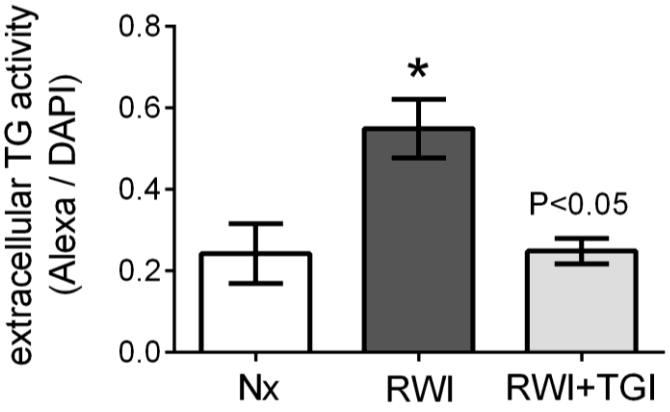

Figure 6.23: Effect of RWI and TG inhibition on tubulointerstitial TG activity at 8 days

The histogram represents the effect of RWI on tubulointerstitial collagen III after 8 days. Vertical bars indicate ± SEM. P<0.05, RWI+TGI compared with RWI group. * Denotes P<0.05, RWI compared with Nx group. Nx, n=5; RWI, n=4; RWI+TGI, n=3

6.4. Discussion

6.4.1. Interstitial transglutaminase and fibrosis

In the present study, the 2-fold increase in TG enzyme activity following RWI, was prevented by the renal infusion of a TG inhibitor, suggesting that adequate drug concentrations had been achieved for enzyme inhibition within the extracellular matrix. Although the distribution of TG inhibitor employed was not confined to the extracellular space, an intracellular effect would seem unlikely as the intracellular calcium concentration is not high enough to activate the enzyme, an essential

requirement for enzyme inhibition. However, in addition to inhibiting extracellular TG enzyme activity, the TG inhibitor, also prevented the increase in extracellular TG2 protein induced by RWI, which is assumed to be a transcriptional event. How could a TG enzyme inhibitor reduce the extracellular renal content of the enzyme protein itself? One possibility maybe through inhibition of its cross-linking effect, reducing the activation of the latent form of TGF-β since, the activated form of TGF-β is known to stimulate the transcription of TG2 in the rat kidney (Huang *et al.*, 2010).

RWI was associated with an increase in extracellular matrix proteins, including collagens I, III & IV. The increase in all three collagens was significantly reduced by the TG inhibitor. Inhibition of TG enzyme activity inhibits transamidation, directly reducing collagen deposition and indirectly unblocking fibrinolytic systems and inhibiting the activation of TGF-β / NF-κβ pathways (Huang *et al.*, 2010; Lee *et al.*, 2004). The lower level of TG activity results in less cross-linked collagen and therefore faster collagen clearance by endogenous proteolytic pathways. Collagen I & IV were reduced down to levels indistinguishable from those found in Nx control animals. Collagen III is the predominant immature form of collagen in incipient forms of fibrosis (Zager *et al.*, 2009), such as 28-day RWI. It is possible that the deposition of all collagens occurred at the same rate, but due to the high bioavailability of collagen III substrate, the reduction in collagen III deposition was less evident. This data provides evidence of a causal link between interstitial TG enzyme activity and interstitial fibrosis. The concept of a causal link between renal TG enzyme activity and renal fibrosis is supported by two previous rat studies where fibrosis, induced following either SNx (Johnson *et al.*, 2007) or the induction of diabetes (Huang *et al.*, 2009), was also reduced following TG inhibition.

6.4.2. Glomerular Transglutaminase and fibrosis

Previous TG inhibitor studies in experimental models of chronic renal disease have shown similar results for both tubulointerstitial and glomerular fibrosis, both being enhanced following either sub-total nephrectomy (Johnson *et al.*, 2007) or the induction of diabetes, and reduced following TG inhibition (Huang *et al.*, 2009). Following RWI however, both glomerular fibrosis and glomerular TG activity were markedly reduced, not increased, with no further reduction seen with the TG inhibitor. RWI (28day) in the rat could therefore be considered as a model of tubulointerstitial fibrosis, and therefore perhaps the most appropriate rat model to parallel changes in the CKD cat. The absence of glomerular involvement in this model is certainly

supported by the lack of proteinuria developing after 28 days. This evidence does not however cast doubt on the causal link between TG and fibrosis, in fact the opposite could be said to be true since in the glomerulus, TG and fibrosis were reduced in parallel.

As far as we are aware this is the first time evidence of a decrease in TG following a renal insult has been demonstrated. This raises a number of important questions, for example:-

1. How can the same RWI stimulus increase TG expression in the interstitium but reduce it within the glomerulus?

2. If it is true however, could a decrease in TG actually provide a mechanism to protect the glomerulus against further injury and actually provide the mechanistic basis for RWI producing a model of interstitial fibrosis?

The down regulation of the glomerular TG pathway in the RWI and RWI+TGI groups at day 28, suggests that hypoxia itself, independent of TG inhibition, could play a major role in such a phenomena. The following hypothesis may explain the results.

The importance of the natural protection of glomeruli under hypoxic environments relies on the rationale that tubules have a high capacity to regenerate following RWI, whereas in glomeruli this mechanism is less active (Park *et al.*, 2000), however still present (Little, 2006). If glomeruli subsist after renal injury, tubular and peritubular vascular networks are more likely to survive and re-establish a functional nephron. Therefore, the glomerulus is a vital structure that has to be protected to ensure a functional renal mass. It has been recognized that hypoxia causes a far milder damage in the glomerular capillaries compared to the tubulointerstitial space (Wang *et al.*, 2015). RWI produces hypoxia and inflammation causing oxidative cellular stress increasing the expression of HIF-1α via podocytes, acting as an immediate mesangial protective mechanism (Wang *et al.*, 2015). HIF system aids the adaptation of cellular homeostasis under hypoxic conditions by regulating a variety of genes to enable angiogenesis through VEGF, energy conservation, metabolic adaptation and cell survival (Gunaratnam *et al.*, 2009). In the kidney, HIF is active

during glomerulogenesis and after that is just active under hypoxic environments (Bernhardt *et al.*, 2006).

Following RWI, HIF-1α in the glomeruli might be more expressed than in the tubulointerstitial space, as a salvage mechanism to protect the glomeruli. In the present study, it is possible that the up-regulation of HIF in the glomeruli caused an indirect down regulation of the TG pathway by promoting mesangial normoxia with the following lower oxidative stress response. The link between TG2 and HIF under hypoxia has been previously study in rat neurons showing that TG2 can promote direct down-regulation of the HIF system (Filiano *et al.*, 2008). However, down regulation of TG2 by from the HIF has never been described. Although unlikely, the possibility of a direct down-regulation of TG2 by the HIF system cannot be totally discarded.

The effect of HIF on glomeruli may be different in the acute and chronic healing stages following RWI. In chronic renal damage, according to long term rat models of RWI (Torras *et al.*, 1999), the HIF protective glomerular mechanism perhaps is overcome when tubulointerstitial fibrosis reaches certain level, allowing the development of glomerulosclerosis. At this stage, if the TG pathway is up-regulated, TG inhibitors may play an important role to slow the progression of glomerulosclerosis by reducing mesangial matrix accumulation/ deposition, as seen in the studies of Johnson et al (2007) and Huang et al (2009).

In acute renal damage, HIF expression may prevent the up-regulation of TG2. The natural down-regulation of the glomerular TG pathway following RWI, reduces the possibility of further activation of NF-κβ attenuating both local inflammation and crosslinking of the accumulated matrix. HIF glomerular system is therefore an endogenous protective glomerular system to reduce acute glomerular damage with the subsequent protective effect to attenuate the development of glomerulosclerosis. Even though the TG pathway seems not to be involved in early RWI, it may provide indirect protection to the glomeruli, since attenuation of glomerulosclerosis can be achieved by reducing inflammation and fibrosis in the tubulointerstitial space, as tubulointerstitial injury precedes glomerular damage (Rodriguez-Iturbe *et al.*, 2010).

There is one piece of information from the shorter 8-day study which may be of some help. In the early days following an ischaemic insult there is an increase in kidney weight, attributed to inflammation and oedema rather than hypertrophy. Yu *et*

al (1998) for example showed a marked increase in kidney tissue malondialdehyde, a peroxidation product and elevated serum eicosanoids (Yu *et al.*, 1998). In the 8-day study presented in this chapter, an increase in kidney wet weight of over 50% was detected, an effect abolished by the TG inhibitor. However, while an increase in tubulointerstitial ECM protein was also apparent, at 8 day, it remained unaffected by TG inhibition presumably since matrix cross-linking had not as yet been established. The early anti-inflammatory effect of TG inhibition could then be a consequence of reduced TGF-β. As a major fibrogenic growth factor, TGF-β is thought to stimulate fibroblast differentiation through inducing a pro-oxidant shift in intracellular redox status mediated via reactive oxygen species, particularly hydrogen peroxide (Sampson *et al.*, 2014), which has shown to play an important role in renal damage in either glomeruli and tubulointerstitium (Shah, 1995). Also, reduction of inflammation via NF-κβ and AKT attenuation due to TG inhibition could also have contributed, as these pathways have been shown to be activated by TG2, in the liver (Mirza *et al.*, 1997) and breast cancer cells (Agnihotri *et al.*, 2013), respectively.

6.4.3. Renal Function

A significant reduction in the GFR assessed by serum creatinine showed renal function impairment after 8 and 28 days following RWI. The RWI+TGI group, on the other hand, showed a marked reduction in serum creatinine when compared to the RWI group at day 8 and day 28, providing evidence that TGI is able to exert a positive effect on renal function after RWI, presumably as a result of the attenuation in inflammation (Lee *et al.*, 2004). The TG inhibitor protected renal function at different time points, however, the mechanism of action may be different according to the time of disease progression. For example, when measuring serum creatinine at day 8, TG inhibition possibly attenuated the inflammatory response to ischaemia reperfusion injury, reducing acute tubular necrosis, thus increasing nephron survival. At day 28, the reduction of serum creatinine was secondary to both the reduction in the acute inflammatory response to RWI and the reduction of matrix deposition in the tubulointerstitial space.

On the other hand, creatinine clearance did not show any significant difference between groups in the present study, a finding secondary to the low sensitivity of the technique, as tubules in rats are able to secrete creatinine in normal conditions (Darling *et al.*, 1991). Regarding albuminuria, no difference between groups was observed, since this model does not able to generate important glomerular damage

before 4 months of disease progression (Torras *et al.*, 1999), also see chapter 5, 140-day RWI study.

Currently, it is well recognised that the decrease of renal inflammation and renal fibrosis have beneficial effects on the conservation of renal function (Eddy, 2000). Interventional studies using transglutaminase inhibitors in rat models of diabetic nephropathy (Huang *et al.*, 2009) and subtotal nephrectomy (Johnson *et al.*, 2007) have shown positive outcomes regarding renal function protection. Therefore, the employment of TG inhibitors in acute and chronic kidney disease is a potential therapeutic approach to prevent renal failure.

6.4.4. Whole Kidney TG Analysis

When kidney homogenates were assessed for total TG activity, the RWI+TGI group showed a lower reduction of activity compared to the RWI group; this provided further evidence for the effectiveness of TGI on transglutaminase inhibition. On the other hand, total TG2 protein did not show any significant difference amongst groups. The lack of correlation between extracellular TG2 protein in cryostat sections and total TG2 in homogenates was due to the difference in concentration of TG2 between the mesangial and tubulointerstitial compartments. When pooling both structures in tissue homogenates, the high expression of tubulointerstitial TG2 was overshadowed by the down-regulation of glomerular TG2, as a result, similar levels were observed between groups. Moreover, it is important to consider that tissue homogenates, apart from cortex, also included medullar tissue. Renal medulla is not importantly affected by inflammation and fibrosis following RWI (Nangaku *et al.*, 2007b), therefore an increase of the TG pathway in medulla was not expected. The inclusion of medula in tissue homogenates may have also contributed to the lack of change in total TG2 between groups. Consistent with our study, Scarpellini et al (2013) showed no differences in total protein concentrations between experimental groups in the mouse models of unilateral ureteral obstruction and aristolochic acid nephropathy, however, a high increase in the extracellular TG2 was observed when compared to the control groups (Scarpellini *et al.*, 2013).

Regarding the upper band (84 kDa) detected when immunoprobing with TG2 rpAb, corresponds to factor XIIIa according to its molecular weight (protein ID ENSRNOP00000021568) (Flicek *et al.*, 2014). A similar result was obtained in the cat study (Chapter 4). It is important to mention that no significant differences were

detected amongst groups for this band, suggesting that Factor XIIIa does not change when renal disease is present following 28 days of RWI. As explained in Chapter 4, the assessment of TG2 in cryostat sections by immunofluorescence using the TG2 rpAb does not alter the measurement of TG2, as the technique for immunofluorescence washes away plasmatic material from tissue sections removing factor XIIIa.

6.4.5. Conclusion

TG inhibition showed a positive effect in renal function and tubulointerstitial fibrosis, therefore TG2 is a causal link for the development of renal tubulointerstitial fibrosis under RWI. TGI effects on tubulointerstitial fibrosis and renal function are secondary to a direct inhibition of TG2 and possibly via indirect reduction of TGF-β1 and NF-κβ. Further studies should be performed to assess the role of TG2 in acute inflammation following RWI. The HIF system is expressed in the glomeruli providing local protection to low tensions of oxygen, as mechanism to glomerular inflammation and subsequently sclerosis. The study of the TG2 down regulatory mechanism in the glomeruli may be an important pathway to understand and generate new glomerular protective therapeutic approaches.

CHAPTER 7A

Rat Kidney Transplantation:

A method using Aortic and Cava conduits

7A.1. Introduction

Chronic allograph nephropathy (CAN) is a renal disease developed in up to 40 % of people following kidney transplantation. It represents the main cause of renal allograft failure. This phenomena often occurs from 1 year to 10 years after operation (Grinyo *et al.*, 2011). CAN has been also described in the cat (De Cock *et al.*, 2004), sharing both functional and histopathological features (tubulointerstitial fibrosis and tubular atrophy) with man (Haas, 2014). CAN has been associated with both alloantigen-dependent and independent factors. Amongst those factors, ischaemia reperfusion injury has been shown to play a major role in the development of post-transplant renal fibrosis (Fellstrom, 2003).

Previous pilot studies undertaken at the Academic Nephrology Unit in the University of Sheffield showed the association between renal fibrosis and transglutaminase 2 in a Fisher to Lewis rodent model of chronic allograft nephropathy (Shrestha et al., 2014); therefore, as a next step, an interventional study on the inhibition of TG2 in this model was proposed. The kidney transplantation technique was first established in a systematic and detailed manner to reduce surgeon and technique-related variables. Eventually, TG2 activity inhibition studies employing a TG2 neutralising antibody (BB7) were intended to occur in this model. However, BB7 antibody was ultimately not available for this project. This chapter describes, at great detail, the kidney transplantation technique (donor and recipient operation) in Sprague Dawley rats.

7A.2. Donor Technique

All the equipment (table, mat, microscope, pen for data recording and anaesthesia machine, including vaporiser and tubes) was disinfected prior to anaesthesia induction. In the theatre, a mask, cap, surgical scrubs and trousers were worn to reduce the risk of infection. All donor data (timings, measures and complications) was recorded during surgery using a donor kidney evaluation form.

7A.2.1. Anaesthesia and Jugular Cannulation

For anaesthesia induction, the rat is placed in an anaesthetic chamber with isoflurane at 5% for 2-5 minutes. After that, a strip of eye ointment (0.25 cm) is applied in both eyes and the rat is placed on the surgical mat in dorsal recumbence position. Anaesthesia was maintained with isoflurane 2-3% delivered through an anaesthetic tube placed over the rat's muzzle, covering nose and mouth. Analgesia is achieved by administering buprenorphine 50µg/kg intramuscularly into the left hind limb. A lubricated rectal probe was introduced gently into the rectum, with prior manual removal of stools to prevent rectum or colon damage and to promote better probe contact with the colon endothelium. A tape was placed around the tail, to fix the probe in position.

A thermostatically controlled heating blanket was employed to maintain body temperature (34.5- 36.5 ^{o}C). The ventral abdominal and the left jugular area, 6 x 12 cm and 2 x 2 cm, respectively, were clipped and aseptically cleaned three times using chlorhexidine 2%. The palmar and plantar surfaces of limbs were meticulously cleaned with chlorhexidine 2% in order to reduce bacterial contamination. The left internal jugular vein was exposed after performing a 2 cm skin incision parallel to the cervical trachea from the left clavicle to the end of the pulsatile area, which runs parallel to the neck. The vein was isolated using blunt dissection. Two loops of ligature were placed around the vein. The cranial end of the vein was tied and the caudal end left untied. After a transversal venotomy using microvascular scissors (1/3 of the jugular vein diameter) caudal to the cranial knot, the cannula (0.58 mm–bore-polyethylene tubing) was introduced no more than 2 cm into the jugular lumen from cranial to caudal. The untied caudal loop was then tied up to hold the intra-jugular portion of the cannula. The cranial loop's free ends were tied around the tube to avoid the tube getting out of the jugular (Figure 7.1; panel A). The cannula tube was attached to the anaesthesia tube with a piece of tape. A continuous infusion of 0.9% NaCl at 6 ml per hour was delivered using a continuous infusion pump.

7A.2.2. Preparation of surgical field and exposure of vascular conduits

An autoclaved surgical kit was employed containing:- 10 cotton buds, 3 swabs (10 x10 cm), 1 square (5 x 5 cm) of autoclave sterilizer paper and 2 sheets of blue paper towel roll (28 x 60 cm) with a 5 x 11 cm medial opening as surgical drapes. The sterile towel paper was placed over the ventral abdominal area covering vertically

from the neck to the half portion of the tail and horizontally covering the entire rat, including the surgical mat. The surgical opening of the double sheets was placed vertically in the centre of the abdominal surgical area. Manipulation of sterile surgical material and instruments was performed using sterile gloves. Prior to the abdominal midline incision, new sterile gloves were worn.

The peritoneal cavity is entered through a midline incision of 10 cm from the xiphoid process to the neck of the bladder. At this stage, anaesthesia was adjusted to 1.5% isoflurane delivered at 1 litre per minute oxygen. The autoclaved paper towel was placed along the right side of the surgical incision. Subsequently, the paper towel was moisten with 0.9% NaCl solution. Autoclave paper was used to prevent desiccation of the abdominal gastrointestinal tract. The caecum was flipped over the right side on the autoclave paper, with the apex *ceci* pointing to the left (Figure 7.1 C/D).

The small bowel, the ascending colon and the first half of the transverse colon (mobile colon) were exteriorized over the caecum and covered by a sterile swab soaked in saline solution. The cranial delimitation of the intra-abdominal surgical area was achieved using a rectangular folded, saline-soaked swab next to the cranial pole of the kidney. The swab allowed the mesenteric fat to be moved toward the spleen and liver, providing protection to these organs. The lateral delimitation was achieved by placing a rectangular saline soaked swab along the left side of the descending colon. The swab protected both the colon epithelium and mesenteric roots. To maximize the visibility of the great vessels and left kidney, a West's retractor is used. One of the jaws of the retractor was placed on the left side of the wound (skin and muscular layers) and the other on the descending colon protective swab (Figure 7.1; panel B).

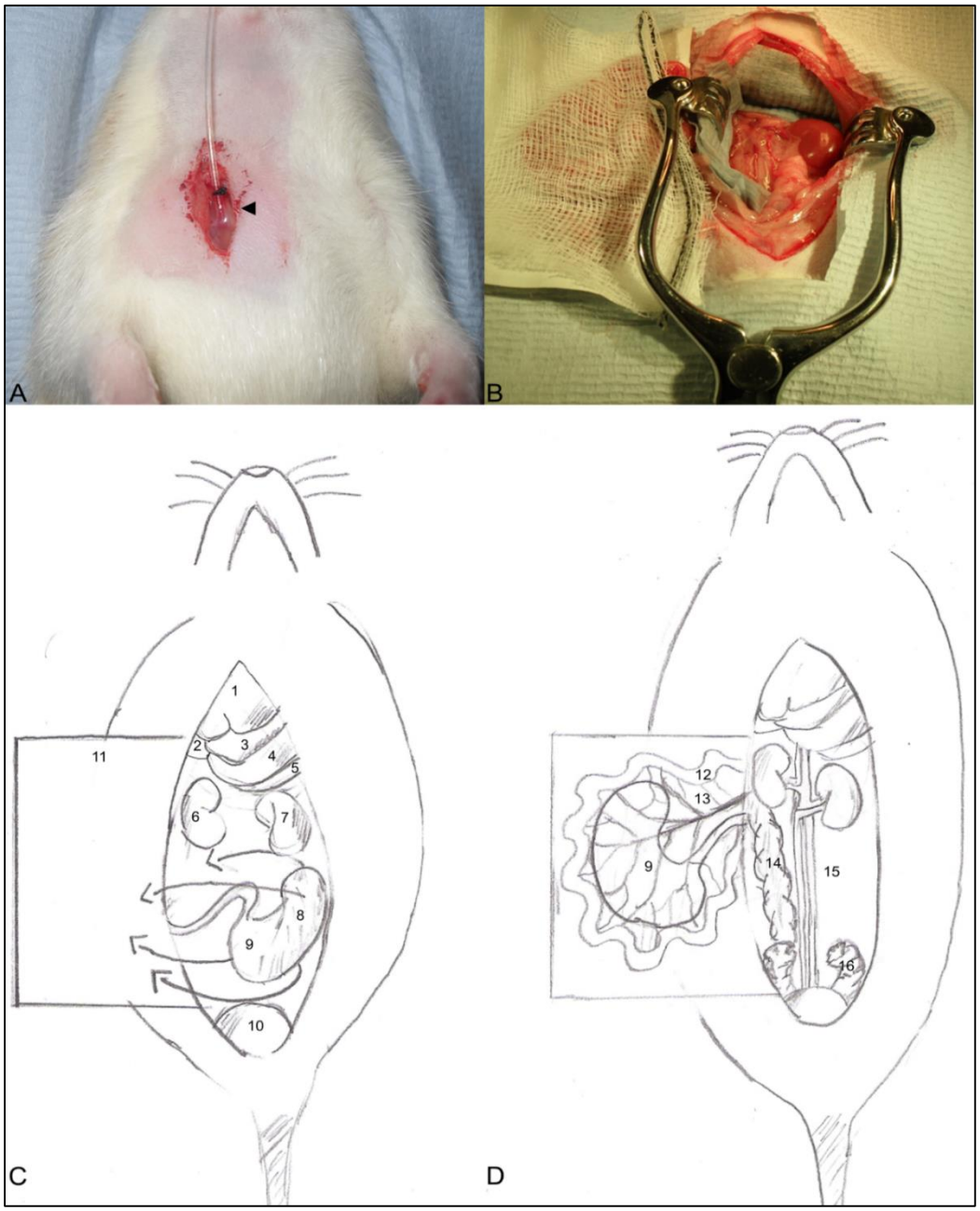

Figure 7.1: Jugular cannulation and surgical delimitation

Panel **A**. Jugular cannulation. **Black arrow** showing cannula in the jugular vein. Panel **B**. Delimitation of the surgical area. Panel **C**. The drawing shows the normal position of the caecum, viscera and the manoeuvre to exteriorize the caecum on the autoclave paper. Panel **D**. The drawing shows the position of the caecum after exteriorization and the display of bowels on it. **1**, liver median lobe; **2**, liver right lateral lobe; **3**, liver left lateral lobe; **4**, stomach; **5**, spleen; **6**, left kidney; **7**, right kidney; **8**, caecum apex ceci; **9**, body of caecum; **10**, bladder; **11**, autoclave paper; **12**, small bowel; **13**, vascular mesenteric root; **14,** descending colon; **15**, great vessels, from right to left, cava and aorta, respectively; **16**, left seminal vesicle.

7A.2.3. Infra-renal Aorta and Cava Dissection

Dissection of the infra-renal aorta and cava was performed by separating the connective tissue around the conduits. This procedure was achieved by performing horizontal tearing dissection with two curved forceps. The mesenteric, adrenal, left and right gonadal artery and vein were ligated and transected close to the main conduits using a triple knot (three simple throws); each throw was formed by wrapping the two strands with each other (Figure 7.2, panel A and Figure 7.3). The left para-lumbar vein and retro-cava venous tributaries branches were ligated, underneath the suprarenal cava. A similar procedure was applied to the retro-arterial branches underneath the suprarenal aorta. The vessels were divided once the rat died due to the limited space of manoeuvre to place the inferior ligatures. The fat tissue over infra-renal cava was removed without damage to the vessel epithelium, using blunt dissection with curved microvascular forceps (dorsal-ventral rubbing) whilst retracting dorsally. Failure to remove peripheral fat tissue interfered with the conduit anastomosis. The supra-renal cava and aorta were marked with a stitch (10-0 suture) in the anterior right side of each conduit in order to aid in the graft orientation and avoid conduits torsion after anastomosis (Figure 7.4, panel A, black arrow).

7A.2.4. Bladder Dissection

The ureter was identified and followed up to the neck of the bladder. The left seminal vesicle was turned to the right side to clear the vesical-ureteral area. The caudal end of the left gonadal vein was ligated and divided approximately 5 mm far away from the ureter. The major vas deferens vein was separated by retraction and dorsal/ventral blunt dissection from the left side of the ureter to the right side of the vas deferens conduit. The vas deferens conduct was ligated and divided to expose the ureter. The caudal ureter was easily dissected using blunt dissection with curved forceps parallel and 5 mm away (right and left side) from the conduit. The small vessels along the ureter (peri-ureteric tributaries vessels and superior vesical artery) were ligated using a double knot with two simple throws. The left gonadal vein, ligated and divided close to the renal vein, was ligated and divided one more time close to the vesical area on the left side of the ureter. The bladder was dissected away from the prostatic lobes and the seminal vesicles. The right ureter was ligated and divided close to the bladder. A loose loop of ligature, constructed by a double-wrap throw, was placed around the neck of the bladder and around infra/supra renal aorta and cava.

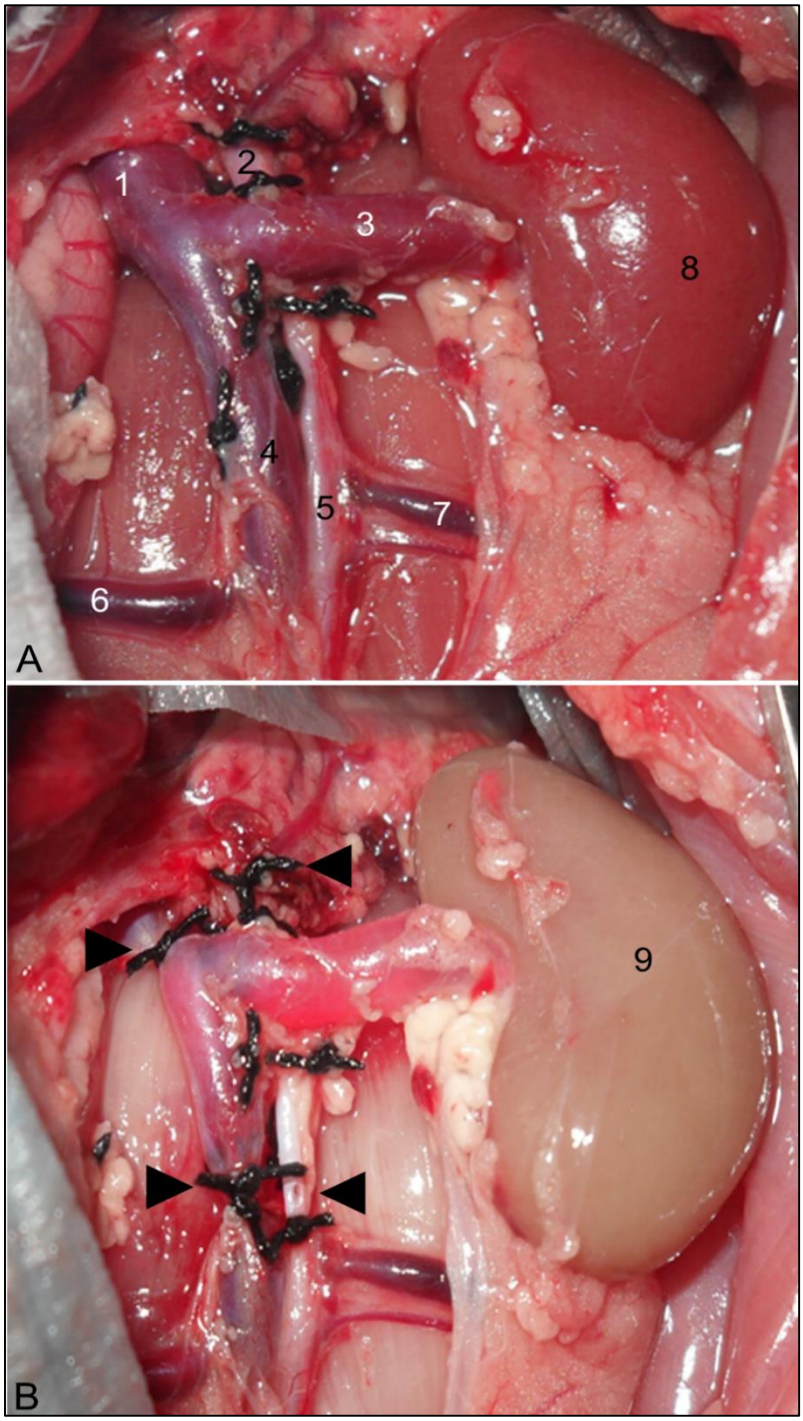

Figure 7.2: Ligation of major and accessory conduits for renal perfusion

Panel **A**. Supra and infra-renal vessels dissections. **1**, suprarenal cava; **2**, suprarenal aorta; **3**, renal vein; **4**, infrarenal cava; **5**, infrarenal aorta; **6**, right iliac vein; **7**, left iliac vein; **8**, normal kidney and **9**, perfused kidney. Panel **B**. Perfused kidney. **Upper left black arrow** pointing suprarenal cava ligature after perfusion. **Lower left black arrow** pointing infrarenal cava ligature. **Upper right black** arrow pointing suprarenal aorta ligature. **Lower right black arrow** pointing the cannula's hole in the infrarenal aorta after perfusion with UW solution. In the same conduit, 1mm caudal to the needle hole, an infrarenal aorta ligature is observed. Black suture ligatures are used to transect main or accessory arteries and veins

7A.2.5. Renal Perfusion

Heparin (300 IU) was administered with a 29G insulin syringe into the supra-renal cava. The loose loop constructed with a double throw in the infra-renal aorta was tied and completed with second double throw forming a double-double surgeon knot. The left para-lumbar vein coming from the infra-renal cava and crossing transversally underneath the aorta is a reference to place the tie. In a similar manner, the infra-renal cava was ligated as caudal as possible. A 26G butterfly cannula was attached to a 20ml syringe of cold UW solution. The catheter tube of the butterfly needle is filled up with UW solution to avoid air emboli. The needle's shaft and bevel (0.5cm) is bent upwards 30° to enhance cannula stability when the cannula is inside the aorta and to avoid puncture of the posterior endothelial layer. The cannula was introduced cranial to the caudal aortic knot using dorsal retraction of the knot's free strands, see Figure 7.2, panel B, right lower arrow and Figure 7.3. The blood pressure of the aorta avoids the collapsing of aortic walls facilitating the introduction of the needle. The cannula was locked with a microclamp. Due to aortic blood pressure, the plastic catheter of the butterfly needle can quickly fill with blood, avoided by pre-clamping the plastic tube with a pair of Rochester forceps. Supra-renal aorta was tied with a double-double knot.

The knots in the suprarenal aorta, infrarenal aorta and cava allow the perfusion solution to drain into the circulatory system through the suprarenal cava, Figure 7.2, panel B, black arrows and Figure 7.3, right drawing. To facilitate the systemic administration of the UW solution, the jugular cannula was removed. Cold perfusion was achieved by administering UW solution with a rate of 4ml/min to avoid tissue damage due to high intra-glomerular pressure. After 10ml of UW solution, cardiac-arrest occurs due to the high levels of potassium and hypothermia.

Once the kidney has been perfused with 20ml UW solution, the supra-renal cava was tied as far as possible to the renal vein with a double-double surgeon knot (Figure 7.2, panel B, upper left black arrow). Eventually, the supra-renal cava was cut transversally, cranial to the infra-renal aortic ligature. The kidney was perfused with the remaining 5ml UW solution to clear any traces of venous blood. By the end of the perfusion, the surface colour of the kidney had changed from reddish to grey/green (Figure 7.2 in panel A-B). The perinephric and ureteral fat was preserved as much as possible. The graft was harvested, cutting the retro-cava and aortic tributaries small

conduits. The double throw of suture placed around the neck of the bladder was tied and completed to get a double-double surgeon knot.

7A.2.6. Kidney, ureter and bladder harvesting

The bladder was removed leaving the knot in the graft. The bladder cuff was transected releasing the urine. The graft was placed in and universal container with iced cold UW solution. The universal container on the other hand was placed onto a metallic container filled up with flaked ice. During the surgical procedure the rat cannot urinate by itself. The accumulation of urine produces bladder over distension affecting the bladder graft. The urine can be collected from the bladder by introducing a needle attached to a 1ml syringe into cranial apex of the bladder (cystocentesis) and aspirating the fluid. Punctured apex is removed at the end of procedure, hence cystocentesis can be performed several times.

7A.3. Recipient Technique

The anaesthesia induction / maintenance, analgesia, surgical aseptic technique and jugular cannulation were performed as described for the donor. Amoxicillin / clavulanic acid was administered subcutaneously at a dose of 21mg/kg.

7A.3.1. Pre-anastomosis preparation of aorta and cava recipient conduits

The suprarenal aorta and cava are dissected in order to prepare the area for anastomosis. The reference of dissection for the anastomosis area is cranially delimited by the convergence of the renal vein and artery with the infra-renal cava and aorta, respectively. Caudally, the left para-lumbar vein coming from the infra-renal cava and crossing transversally underneath the aorta was a reference to delimitate the dissection. The left kidney was removed by tying a double-double surgeon knot 5 mm away from the kidney. See section 2.3.1.2 for right kidney nephrectomy, which also applies to left kidney nephrectomy. A pair of Rochester forceps was placed close to the kidney to avoid spillage of blood when the renal vein and artery were divided between the forceps and the ligature. This technique allows conservation of the adrenal irrigation and the left gonadal vein.

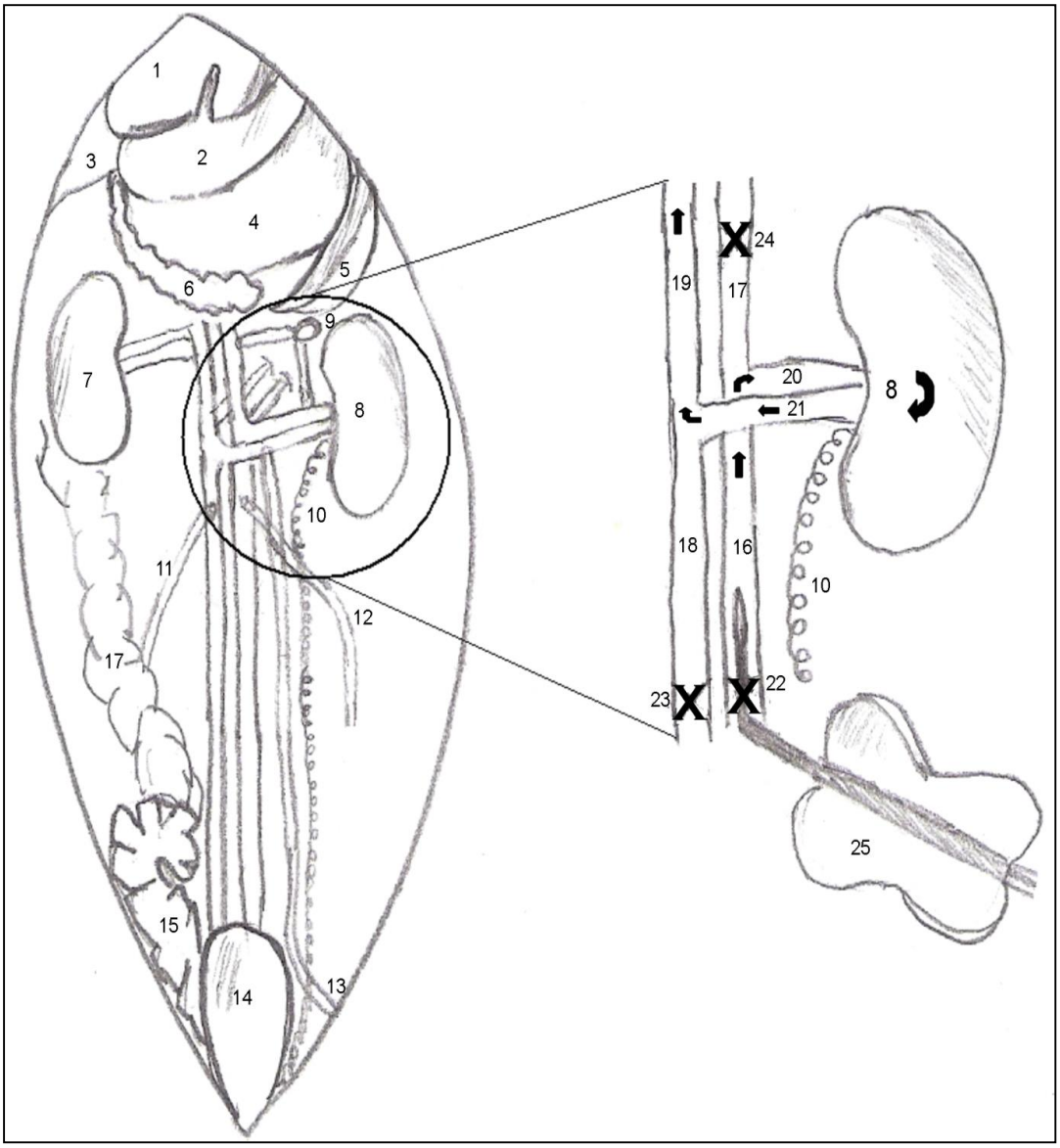

Figure 7.3: Renal perfusion through infrarenal aorta

Cannula insertion into the infrarenal aorta. Doble-doble surgeon knots around the supra and infra renal aorta and cava. **1**, liver median lobe; **2**, liver left lateral lobe; **3**, liver right lateral lobe; **4**, stomach; **5**, spleen; **6**, pancreas; **7**, right kidney; **8**, left kidney; **9**, adrenal gland; **10**, ureter; **11**, right gonadal vein; **12**, left gonadal artery; **13**, left caudal gonadal vein; **14**, bladder; **15**, right seminal vesicle; **16,** infrarenal aorta; **17 left** drawing, descending colon; **17 right** drawing, suprarenal aorta; **18**, infrarenal cava; **19**, suprarenal cava; **20**, renal artery; **21**, renal vein; **22**, infrarenal aortic knot; **23**, infrarenal cava knot; **24,** suprarenal aortic knot; **25**, butterfly needle; **X**, vascular ligatures; **arrows**, UW solution flow.

7A.3.2. Aorta and vena cava end-to-side anastomosis

The first conduit anastomosis was performed on the infra-renal aorta. Occasionally it was necessary to snuggle a lumbar artery or/and the right gonadal artery to avoid bleeding during the arteriotomy. The knots of the snuggled vessels were preferably on the right hand side as the left side would be occupied by the anastomosed vessel. A cranial vascular clamp was placed first (high blood pressure) followed by caudal clamp (low blood pressure) according to the delimitation areas previously described (Figure 7.4, panel A and B) and the arteriotomy performed using a 26G needle. The orifice produced by the needle on the artery was used as a guide to introduce the tip of the microsurgical scissors. The arteriotomy was developed along the conduit (from caudal to cranial) according to the transverse diameter of the donor end-side aorta (2 to 2.5 mm). The arteriotomy had to be performed slightly to the left of the conduit to facilitate blood flow, as the donor vessels adopt a horizontal position once the gastrointestinal tract is placed back into the abdomen (Figure 7.4, panel A). The kidney was taken out from the cold iced UW solution and placed over a gauze (square shaped) pre-soaked in UW solution and pre-cut with a rhomboidal orifice large enough to exteriorize the conduits.

7A.3.3. Vascular Anastomosis

Once the stitch markers on the conduits are identified, the kidney is oriented transversally on the abdominal cavity with the renal hilar pointing cranial and the cranial pole of the kidney pointing the left side of the cavity. The aorta donor end side is faced with the recipient aorta lateral side. The arterial anastomosis is performed using a non-absorbable 10-0 monofilament with a curved non-spatulated needle following the next steps:-

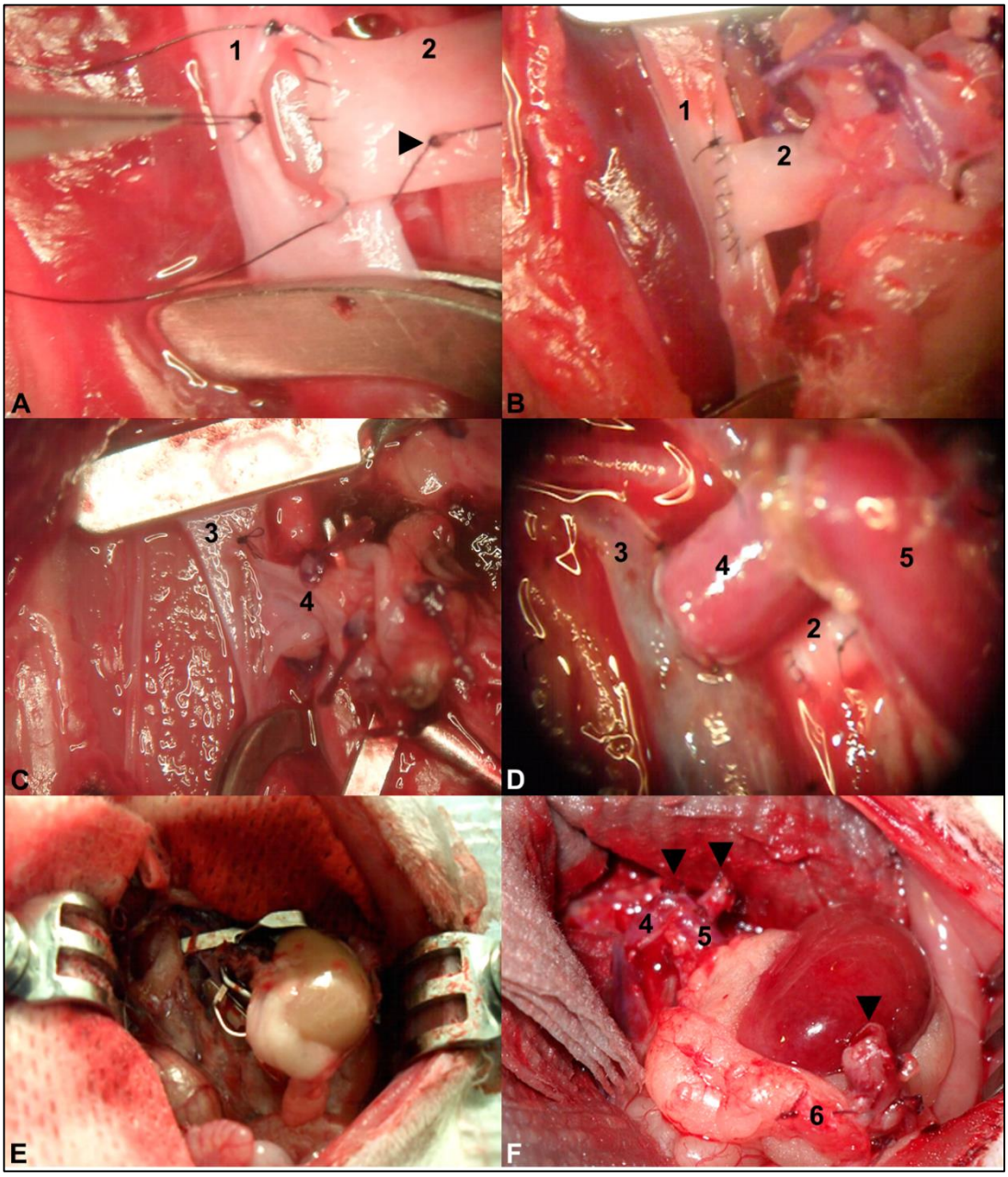

Figure 7.4: Sequence of the recipient technique for kidney transplantation

Panel **A**. Left side aortic anastomosis. **Black arrow** indicates the reference stitch for graft orientation on the recipient. Panel **B**. Completed aortic anastomosis. Panel **C**. Left side cava anastomosis. Panel **D**. Patent cava and aorta after anastomosis, left and right conduit, respectively. Panel **E**. Transplanted non-reperfused kidney. Panel **F**. Reperfusion of transplanted kidney. **Black arrows** pointing down are showing, from left to right, suprarenal cava and aorta conduits stump after ligature and transection and bleeding of donor bladder capillaries suggesting vascular patency. Number **1** and **2** shows recipient and donor aorta, respectively; **3** and **4**, recipient and donor cava, respectively; **5**, renal vein from donor kidney; **6**, ureteral graft cover by peripheral ureteral fat tissue.

A) The needle was passed from the cranial apex of the outer part (the recipient aorta) to the inside part (Figure 7.5; panel A).

B) The needle was passed then on the cranial edge of the donor aorta, inside the apex (lumen), to the outside of the aorta (Figure 7.5; panel B).

C) The first lock stitch was made with a double-double surgeon knot leaving an end strand long enough to knot it with the caudal to cranial strand from the right hand side of the anastomosis (Figure 7.5; panel C).

D) The needle was passed on the inside part of the donor aorta to the outside and on the outside part of the recipient aorta to the inside. The same pattern, in a single movement, was advanced along the perimeter of the recipient aorta until the caudal apex. The stitches were tightened and placed very close to each other (Figure 7.5; panel D).

E) In the caudal extreme of the anastomosis the last stitch that comes out inside the recipient artery (left wall) was passed on the recipient inside part of the right wall to the outside. This was in order to change the suture orientation and develop the other side of the anastomosis (Figure 7.5; panel E).

F) The needle is passed on the outer part of the recipient aorta to the inside. The continue pattern is performed in the same fashion until arriving to the cranial apex of the anastomosis (Figure 7.5; panel F).

G) The free strand was knotted to the free strand of the locking knot (Figure 7.5; panel G).

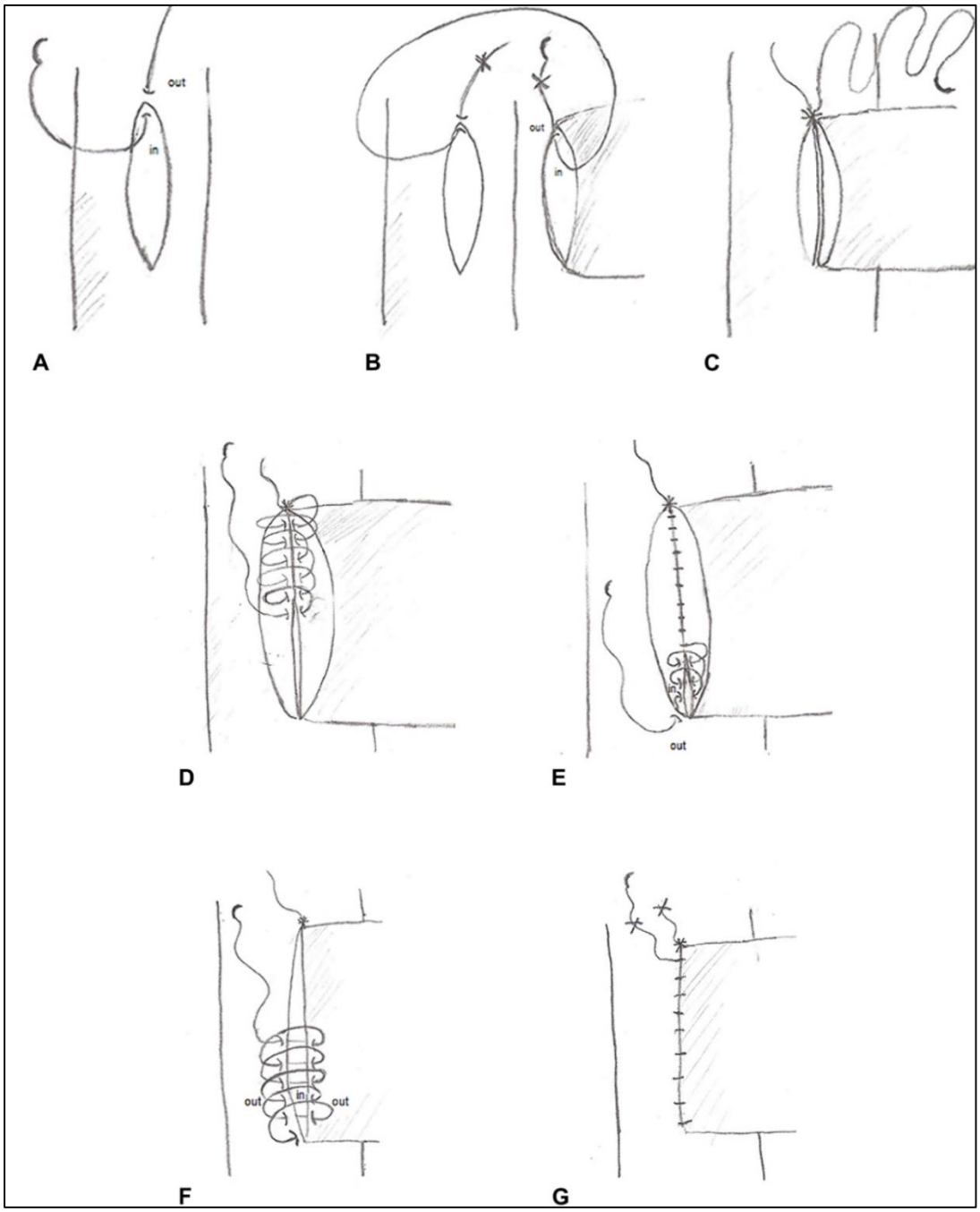

Figure 7.5: Vascular anastomosis technique

Drawing **A**, The needle is passed from the cranial apex of the outer part (the recipient aorta) to the inside part. **B**, the needle passes in the cranial edge of the donor aorta, inside the apex (lumen), to the outside of the aorta. **C**, the free strands are knotted. **D**, the needle is passed on the inside part of the donor aorta to the outside and on the outside part of the recipient aorta to the inside. **E**, The last stitch in the caudal extreme of the anastomosis comes out inside the recipient artery (left wall); the needle is passed on the recipient inside part of the right wall to the outside. **F**, to close the other side of the conduit, the needle passes on the outer part of the recipient aorta to the inside and then from the inside of the recipient conduit to the outside. **G**, the free strand is knotted to the free strand of the locking knot.

Once the anastomosis was completed, a triple square layer of swab was placed below the donor kidney and another one on the right side of the anastomosis. Close to the anastomosis, mini-clamps were placed on the donor aorta to avoid blood flow into the kidney after removing the clamps. To decrease bleeding when releasing the clamps, an oxidized regenerated, cellulose haemostat was placed in both sides of the anastomosis. Firstly, the caudal clamp was released (low blood pressure). If a haemorrhage appeared, it was controlled by exerting gentle pressure with a swab on the anastomosis. If the haemorrhage was profuse, the caudal clamp is re-located and extra-stitches had to be place. If there was no haemorrhage after releasing the caudal clamp, it was necessary to wait some minutes to promote clotting prior to cranial clamp removal. It is possible to have bleeding after the last step; however, this could be controlled as explained previously. The snuggled aortic peripheral vessels were released as soon as possible to avoid vascular maceration.

The steps for the end-to-side cava anastomosis were the same as for end-to-side aorta anastomosis. Vascular anastomosis for aorta and cava conduits is represented in Figure 7.4; panels A-B and C-D, respectively. However, in order to avoid stenosis of the cava anastomosis, the stitches were more separated and the thread not tightened as in the end-to-side aortic anastomosis technique. The cranial venous clamp were first released (low blood pressure) and assessed for haemorrhage. The second clamp to retrieve was the caudal clamp (high pressure) followed by the arterial micro-clamp. The kidney changes immediately from grey/green colour to reddish indicating a proper reperfusion (Figure 7.4; panels E-F). The colour of a reperfused kidney after transplantation must be similar to the colour before perfusion of the donor kidney with UW solution, see Figure 7.2, panel A Ureteral peristalsis, layer bleeding of the vesical capillaries or even urine in the bladder cuff were desirable signs to observe after reperfusion (Figure 7.4, panel F) for bladder bleeding post kidney reperfusion. The exteriorized small intestine, the caecum and the mobile part of the colon were placed back into the abdominal cavity. Two stitches were placed through the abdominal muscular and skin layer so that the abdomen remained open just on the caudal side of the surgical wound.

7A.3.4. Bladder cystoplasty and abdominal closure

Bladder cystoplasty was performed using a one layer full thickness simple continuous suture pattern as explained for the arterial anastomosis with 6-0

polygalactin 910. The donor bladder was developed as the recipient aorta and the recipient bladder as the donor aorta. The initial suture patter runs from left to right, Figure 7.6, panel A. The bladder healing process was quick, allowing an almost imperceptible scarring line after 8 days of cystoplasty, (Figure 7.6, panel B).

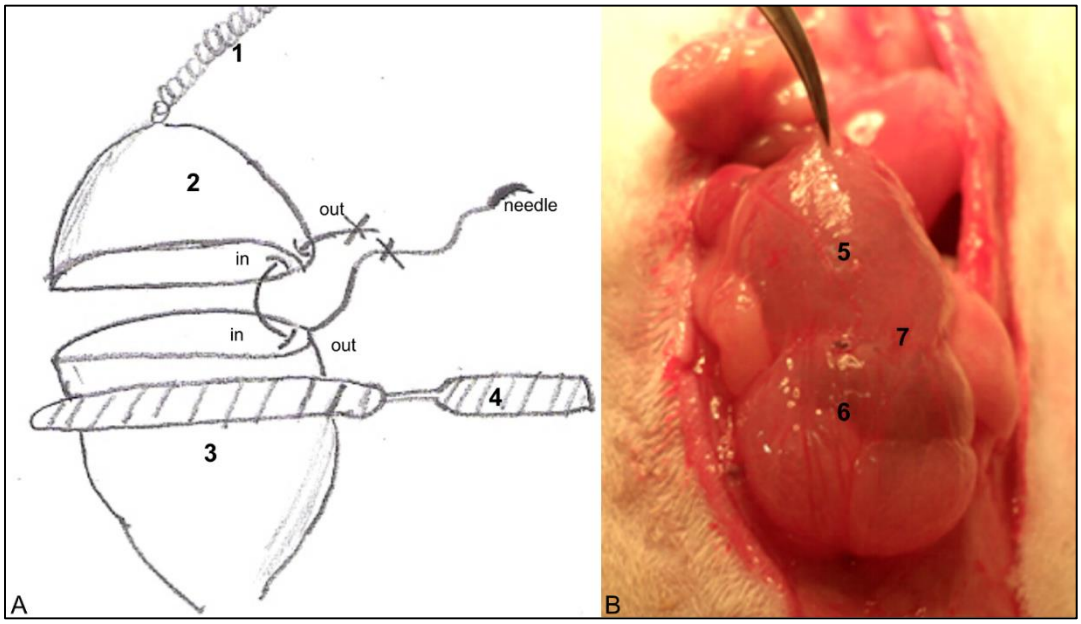

Figure 7.6: Bladder anastomosis

Panel **A**. The needle is first passed from the left apex of the outer part (the donor bladder) to the inside part; then the needle is passed on the left edge of the recipient bladder, inside the apex (lumen), to the outside. **1**, Donor bladder; **2**, recipient bladder; **3**, micro-clamp and **4**, donor ureter. Panel **B**. Filled bladder with urine after 8 days of cystoplasty; **5**, donor b ladder; **6**, recipient bladder and **7**, scarring line post anastomosis

The abdominal muscular layer and eventually the skin were closed using a simple continuous pattern with 4-0 braided polygalactin 910 or not braided absorbable suture (polyglecaprone 25). Both surgical layers were knot-locked in three different areas along the surgical wound. Anaesthesia was stopped and the rat placed in the incubator (30^{o}C). The rat was provided with water once it has recovered from anaesthesia. Eventually, the rat was placed in its respective box with a sheet of fabric covering the floor instead of sawdust. This action maintained the surgical wound clean and avoided the eating of sawdust, a frequent behaviour after kidney transplantation.

CHAPTER 7B

Experiments to establish a model of Kidney Transplantation in the Rat

7B.1. Introduction

The two major surgical methods of kidney transplantation in the rat involve either:-

(A) end-to-end anastomosis of the renal artery and renal vein or
(B) end-to-side anastomosis of aortic/vena caval conduits.

Previous studies have shown that the end-to-end anastomosis of renal vessels requires the use of a high-power surgical microscope. To combat the narrow depth of focus when anastomosing small vessels, foot-powered control of microscope focus is essential. Since this facility was unavailable for this project, the end-to-side anastomosis technique was investigated. This is a technique which had been successfully used in previous studies from this unit concerned with the development of CAN in the rat (Shrestha et al 2014). However a model of such surgical complexity as the end-to-side anastomosis of major conduit vessels requires both practise and evaluation to reduce the variables dependent on surgical skills before undertaking interventional studies.

A methodology was devised to evaluate the success, both qualitatively and quantitatively of the surgical techniques involved for:-

(A) donor kidney harvesting,
(B) renal reperfusion in the recipient following conduit anastomosis,

Two series of experiments were undertaken, firstly to develop a technique of donor kidney removal and secondly, to transplant donor kidneys into recipient rats. Transplants were considered successful if recipient rats produced 24h urine samples following a right nephrectomy, 8-9 days after transplantation. Pilot experiments were then undertaken in non-operated Fisher and Lewis rat strains to establish any differences in the TG pathway prior to undertaking the Lewis-to-Lewis isografts. Once a successful method of kidney transplantation had been achieved, the aim was to test the effectiveness of a selective TG2 inhibitory antibody, possibly a TG2 selective inhibitory antibody, on their ability to slow the progression of fibrosis in the Fisher-to-Lewis rat model of CAN. However, the TG2 inhibitory antibody lacked of specificity to the rat TG2, therefore antibody inhibition of the TG pathway in this model was not available anymore. The intrarenal delivery of TGI in this model was thought to cause excessive parenchymal injury for a transplanted kidney.

7B.2. Material and Methods

Male Sprague-Dawley rats (Harlan, UK) were used during the first study (kidney transplantation). The second phase study (measuring levels of renal TG2) included male Fisher (n=5) and Lewis rats (n=5) (Harlan, UK). All rats were approximated, 8-10 weeks, with an initial weight of 250-300 grams were maintained at 20°C, 45% humidity and with a light cycle of 12 hours. Rats were terminated by placing them in the anaesthetic chamber (isoflurane) followed by cardiac exsanguination. Kidney was placed in liquid nitrogen and storage as described in section 2.2.10. All the animal procedures were carried out under the Animal Scientific Procedures Act 1986, Home Office United Kingdom. The vascular and bladder-patch anastomosis were performed as described in Chapter 7A based on the methods of Karatzas et al (2007) and Salaman et al (1969), respectively (Karatzas *et al.*, 2007; Salaman, 1969).

7B.2.1. Donor Kidney

The technique of donor kidney surgery, without transplantation, was evaluated in an initial group of 23 animals (rat nos 1-23). The quality of the donor kidney was evaluated intra-operatively according to the renal surface visual evaluation of blood clearance after perfusion, total time of procedure, estimated blood loss during procedure and graft structure integrity (Table 7.1).

7B.2.1.1. Blood clearance and superficial tissue damage

The visual evaluation of blood clearance was assessed under surgical microscope straight away after perfusion of 20 ml of UW solution. A proper perfusion was considered as the total renal surface change in colour from bright reddish to green-grey. Visual evaluation of blood clearance was subdivided using uppercase letters. **A**: Total blood clearance; **B**: Total blood clearance with superficial laceration (scratch, puncture or partial decapsulation); **C**: Blood clearance with haematomas covering less than 5% of the renal surface; **D**: Blood clearance with haematomas covering from 5% to 10% of the renal surface; **E**: No blood clearance. The marking A, B, C and D were given 15, 10, 5 and 0 points, respectively.

7B.2.1.2. Time of total procedure

The time of total procedure was counted from the time the rat was placed on the surgical mat to the time the kidney was perfused with the UW solution. The evaluation of the time of surgical procedure was subdivided using numbers. **1**: less than 2 hours 30 minutes; **2**: more than 2 hours 30 minus but less than 3 hours 30 minutes; **3**: more than 3 hours 30 minutes but less than 4 hours 30 minutes; **4**: more than 4 hours 30 minutes. The marking 1, 2, 3 and 4 were given 15, 10, 5 and 0 points, respectively.

7B.2.1.3. Blood loss

The evaluation of haemorrhage during operation was estimated by weighing the gauzes with the absorbed blood. The estimation of haemorrhage during operation was easily achieved by placing the bloody gauzes in a plastic beaker covered by a latex layer made from a sterile surgical latex glove. The latex layer was perforated in the centre to allow the entrance of the gauzes (1 cm diameter) by pushing them through the latex layer with the gloved surgeon's finger to avoid contamination and evaporation of blood. The weight of one of the gauzes (all gauzes same weight) and the beaker was noted before surgery. After finishing the surgery, the beaker with the used gauzes was weighted. The weight subtraction of the used gauzes and beaker with the weight of the clean gauzes and beaker corresponds to the estimated amount of haemorrhage in millilitres (w/v). The evaluation of haemorrhage during operation was subdivided using lower case letters. **a**: No relevant haemorrhage, estimated in less than 1.5ml; **b**: Low haemorrhage, estimated in more than 1.5ml but less than 2.5ml; **c**: Considerable haemorrhage estimated in more than 2.5ml but less than 3.5ml; **d**: High haemorrhage complication, estimated in more than 3.5ml. The marking a, b, c and d were given 15, 10, 5 and 0 points, respectively.

7B.2.1.4. Donor kidney structure integrity

The evaluation of the graft structure integrity was visually performed during and after kidney harvesting aided with a surgical microscope. The evaluation of the structural integrity was subdivided using colours. **Green**: no structural damage; **yellow**: Minimal ureteral torn (less than 1mm), minimal damage of ureteral irrigation (partial removal of peri-ureteral fat), sporadic scattered haematomas in bladder and torn (less than 1mm) or perforation of major vessels; **red**: Considerable structural

damage by ureteral torn, ureteral stricture, cut or avulsion from bladder, major vessels torn in more than 1mm and renal, ureteral or bladder necrosis. The marking green, yellow and red were given 15, 10 and 0 points, respectively.

Collected donor kidneys were marked as excellent, very good, satisfactory and reserved according to the scoring obtained in each subject. A, 1, a / green was identified as excellent graft. A, 2, a or b / green was defined as very good graft. B-C, 2, b / green was identified as satisfactory graft. C-D, 3, c / green or yellow was identified as reserved graft. Donor kidneys were considered unsuitable for transplant if E, 4, d or red marking were involved in any of the sub-scores. The minimal requirement of grafts for kidney transplantation ranged from excellent to satisfactory quality. See Table 7.2.

7B.2.2. Kidney transplant into Recipient Rat

18 kidney transplants were undertaken using donor rats (nos 24-41), transplanted into recipient rats (nos 42-59). The intra-operative viability of the graft was evaluated according to the speediness in renal reperfusion, renal surface alteration, renal hypertrophy, and second warm ischaemia time (Table 7.3).

.

7B.2.2.1. Time of total Reperfusion

Reperfusion time was define as the time between removal of clamps to the time the renal surface is homogeneously reddish (qualitative visual assessment) due to entrance of oxygenated blood to the renal tissue. The speediness in reperfusion was subdivided using uppercase letters. **A**: Rapid reperfusion in less than 10 seconds after releasing vascular clamps; **B**: Hypotensive delayed reperfusion in more than 10 seconds due to hypothermia or hypovolemia; **C**: Delayed reperfusion due to adhesion of vascular walls or vascular stenosis due to anastomosis technique; and **D**: No reperfusion. The marking A, C, D and E were given 15, 10, 5 and 0 points, respectively.

1.- Renal surface blood clearance	
A = 15 points	100% blood clearance
B = 10 points	100% blood clearance + superficial laceration (scratch, puncture or partial decapsulation)
C = 5 points	Blood clearance with minimal haematomas < 5% renal surface
D = 1 points	Blood clearance with haematomas > 5 % < 10% renal surface
E = 0 points	No blood clearance
2.-Time of procedure	
1 = 15 points	< 2 hours 30 minutes
2 = 10 points	> 2 hours 30 minutes, < 3 hours 30 minutes
3 = 5 points	> 3 hours 30 minutes , < 4 hours 30 minutes
4 = 0 points	> 4 hours 30minutes
3.- Surgical haemorrhage	
a = 15 points	No relevant haemorrhage during procedure (blood loss < 1.5ml)
b = 10 points	Low haemorrhage complications (blood loss 1.5 - 2.5ml)
c = 5 points	Considerable haemorrhage complication (blood loss 2.5 - 3.5ml)
d = 0 points	High haemorrhage complication with more than > 3.5ml
4.-Donor kidney structural integrity	
15 points	No ureteral, bladder or major vessels (cava/aorta) damage
10 points	Low ureteral, bladder or vascular damage -Ureteral tare (<1 mm), Minimal damage to ureteral irrigation -Petechiaes or ecchymosis in bladder -Minimal tare (<1 mm) or perforation of major vessels.
0 points	Considerable ureteral, bladder or vascular damage - Ureteral stricture, torn, cut or avulsion - Renal, ureteral or bladder necrosis - Torn (>1mm) or perforation of major vessels

Table 7.1: Scoring System A - Donor Kidney evaluation

Marking	Points	Sub-score 1	Sub-score 2	Sub-score 3	Sub-score 4
Excellent	**60**	A	1	a	
Very good	**50-55**	A	2	a-b	
Satisfactory	**45-50**	B-C	2	b	
Reserved	**45-26**	C-D	3	c	
Not suitable	**If any score**	E	4	d	

Table 7.2: Scoring system A - Overall marking

7B.2.2.2. Renal surface alteration post reperfusion

Renal surface alteration was assessed after 10 minutes of reperfusion by immediate visual assessment and by picturing the kidney surface from both sides with a Samsung PL50, 8 megapixels camera. Evaluation of renal surface alteration was subdivided using numbers. 1: Normal colour surface; 2: Superficial damage such as scratches with less than 5mm length, kidney puncture or partial decapsulation. **3**: Haematomas or ischaemic patches in less than 5% of the renal surface, scratches with more than 5mm length, total renal decapsulation. **4**: Haematomas or ischaemic patches in more than 5% the renal surface but less than 10%. **5**: Renal congestion and ischaemia/necrosis. The marking 1, 2, 3, 4 and 5 were given 15, 10, 5 and 1 and 0 points, respectively.

7B.2.2.3. Renal hypertrophy post reperfusion

Renal hypertrophy was measured by using a digital Vernier calliper after 10 minutes of reperfusion. The length of the kidney was measured placing the calliper's jaws dorsal on the convex side of the kidney just touching cranial and caudal edge of each renal pole. The measurement of the renal width was achieved placing the instrument's jaws in the middle of the kidney transverse to the poles. The measurements were compared with the kidney measurements obtained before perfusion with UW solution in the donor procedure. Evaluation of renal hypertrophy was subdivided using lowercase letter. **A**: Native size; **B**: Renal mass increased in 10%; **C**: Renal mass increased in more than 10% but less than 20%; **D**: Renal mass increased in more than 20%. The marking a, c, d and e were given 15, 10, 5 and 0 points, respectively.

1.- Speediness in reperfusion	
A = 15 points	Rapid reperfusion after releasing vascular clams before 10 seconds
B = 10 points	Hypotensive delayed reperfusion in > than 10 seconds
C = 5 points	Delayed reperfusion due to vascular damage (adhesion of vascular walls or vascular stenosis)
D = 0 points	No reperfusion
2.-Renal surface alteration	
1 = 15 points	Normal colour surface
2 = 10 points	Superficial scratches (<5mm length), puncture or partial decapsulation
3 = 5 points	Minimal haematomas, ischaemic patches (<5%), scratches with more than 5mm length, total decapsulation.
4 = 1 point	Extended hematomas or ischaemic patches (>5%, <10%)
5 = 0 points	Renal congestion or Ischaemia/necrosis.
3.-Renal hypertrophy	
a = 15 points	Native size
b = 10 points	Minimal (increase < 10%)
c = 5 points	Moderate (increase >10%, < 20%
d = 0 points	Severe (increase >20%)
4.- Second warm ischaemia	
15 points	< than 1 hour 30 minutes
10 points	> 1 hour 30 minutes , < 2 hours 30 minutes
0 points	> than 2 hours 30 minutes

Table 7.3: Scoring System B - Graft evaluation after reperfusion

7B.2.2.4. Second warm ischaemic time

Second warm ischaemia time was count from the time the donor kidney is placed in the abdomen to the time the kidney is anastomosed and reperfused; the timing was assessed using a professional chronometer. After clicking the previously disinfected chronometer's button a change of gloves was performed. The evaluation of the second warm ischaemia was subdivided using colours. **Green**: Procedure less than 1 hour 30 minutes; **yellow**: More than 1 hour 30 minutes but less than 2 hours 30 minutes; **red**: More than 2 hours 30 minutes. The marking green, yellow and red were given 15, 10 and 0 points, respectively.

7B.2.3. TG2 by immunofluorescence

8µm thick cryostat sections on adherent slides, previously stored at -80°C. The slides were blocked and washed. The tissue was then probed with a primary antibody (TG2) overnight at 4°C followed by fixation and serial washings. The slides were immunoprobed with a secondary antibody and left at room temperature for 2 hours. Finally, a drop of mounting medium with DAPI was added. No less than 10 glomeruli (x 400) and (x 200) of cortex tubules were acquired. The immunofluorescent fibrosis index was determined calculating the intense Alexa red (TG2) / DAPI (nuclei) of the total field. Quantification was performed by image analysis (section 2.6.1).

7B.3. Results

7B.3.1. Donor Evaluation

The evaluation of donor surgery for 23 individual rats (nos1-23) where no transplant was performed is shown in Table 7.4 and for 18 rats (nos 24-42) transplanted into a recipient in Table 7.5.

7B.3.1.1. Blood Clearance

In **set A**, marking A, B, D and E of blood clearance was shown in 78.26% (18 / 23), 4.3% (1/23), 8.69% (2/23) and 8.86% (2/23) of the rats. Marking C was not reported in this set. In **set B,** marking A of blood clearance was shown in 100%

(18/18) of the rats. The overall score (set A and B) for marking A, B, D and E was 90.2 % (37/41), 2.3% (1/41), 4.9% (2/41) and 4.9% (2/41), respectively.

7B.3.1.2. Time of procedure

In **set A**, marking 1, 2, 3 and 4 of time of total procedure was shown in 8.69% (2/23), 39.1% (9/23), 30.4% (7/23) and 21.7% (5/23) of the rats, respectively. In **set B**, marking 1, 2 and 3 of time of total procedure was shown in 5.5% (1/18), 66.7% (12/18) and 27.8% (5/18) of the rats, respectively. None of the rats were reported with a score of 4.The overall score (set A and B) for marking 1, 2, 3 and 4 was 7.3% (3/41), 48.8% (20/41), 29.3% (12/41) and 12.2% (5/41), respectively.

7B.3.1.3. Surgical haemorrhage

In **set A**, marking a, b, c and d of surgical haemorrhage was shown in 7% (16/23), 17.4 % (4/23), 8.7 (2/23) and 4.3% (1/23) of the rats, respectively. In **set B**, marking a and c of surgical haemorrhage was shown in 94.4% (17/18) and 5.6% (1/18) or the rats, respectively. The overall score (set A and B) for marking a, b, c and d was 7.3% (3/41), 48.8% (20/41), 29.3% (12/41) and 12.2% (5/41), respectively.

7B.3.1.4. Structural integrity of donor kidney

In **set A**, marking green, yellow and red of graft structural integrity was shown in 78.3% (18/23), 17.4% (4/23) and 2.3% (1/23) of the rats, respectively. In **set B**, green marking was shown in 100% (18/18) of the rats were scored green. The overall score (set A and B) for marking green, yellow and red was 87.8% (36/41), 9.8% (4/41) and 2.4% (1/41), respectively

7B.3.2. Score system B- Immediate graft evaluation and urine production

Eighteen donor kidneys with satisfactory to excellent scores were transplanted. 16.7% (3/18) of the rats subjected to the procedure did not survive the surgery; therefore, 83.3% (15/18) of the grafts were evaluated with the scoring system B. See **Table 7.6.**

Rat No	Time	Complications	Score A
1	5:33	Mesenteric artery bleed. Petechiaes/ecchymosis after perfusion	D4d
2	5:12	Hypothermia. Death before perfusion	E4a
3	4:38	Haemorrhage from jugular/cava tear. Cortex scratched (forceps)	E4c
4	4:30	Ureteral bleeding.	A4b
5	5:00	Caudal pole scratch	B3a
6	4:12	The ureter 0.2mm tearing	A3a
7	3:29	Aorta bleeding during cannulation due to fail of ligature	A2c
8	3:25	Bleeding from adrenal vessel	A2b
9	4:00	Haemorrhage from heparin in IVC	A3b
10	4:30	Fat left in IVC. Ruffling of bladder neck knot.	A4a
11	3:52	No relevant complications	A3a
12	4:06	Aorta perforation during cannulation	A3a
13	3:20	No relevant complications	A2a
14	3:01	No relevant complications	A2a
15	3:06	Total transversal ureteral cut	A2a
16	3:30	Renal focal ischaemia (cranial pole)	D2b
17	3:20	Aorta tearing due to butterfly needle.	A2a
18/19	3.55	Delay in vessels isolation and dissection	A3a
20/21	3:20	No relevant complications	A2a
22/23	2:30	No relevant complications	A1a

Table 7.4: Set A - Establishing the donor technique

Rat No	Score system A
29	A1a
22,25,26,28,30,31,32,34,35, 37,38,41	A2a
27	A3c
33,36,39,40	A3a

Table 7.5: Set B - Scoring system A

7B.3.2.1. Speediness in reperfusion

Marking A, C and D for speediness in reperfusion was shown in 86.7% (13/15), 6.7% (1/15), 6.7% (1/15) and 20% (3/15) of the transplanted kidneys, respectively. There were not grafts in classification B.

7B.3.2.2. Renal surface alteration

Marking 1, 2, 3, 4 and 5 for renal surface alteration was shown in 46.7% (7/15), 0% (0/15), 26.7% (4/15), 6.7% (1/15), 20% (3/15) of the transplanted kidneys, respectively.

7B.3.2.3. Renal hypertrophy

Marking a, b, c and d for renal hypertrophy was shown in 33.3% (5/15), 33.3% (5/15), 26.7% (4/15) and 6.7% (1/15) of the transplanted kidneys, respectively.

7B.3.2.4. Second warm ischaemia

Marking green and yellow for second warm ischaemia time was shown in 6.7% (1/15) and 93.3% (14/15) of the transplanted kidneys, respectively.

7B.3.2.5. Urine production at day 8

Kidneys able to produce urine after 8 days of kidney transplantation and 24hrs after contralateral nephrectomy were considered successful kidney transplants.

See Table 7.6 for transplant procedure evaluation by graft scoring B. A summary of successful transplanted kidneys with score A and B is shown in Table 7.7. A representative image of a kidney after 5 minutes and 8 days post transplantation is displayed in Figure 7.7. Some surgical problems encountered after kidneys transplantations are shown in Figure 7.8.

Rat No	AA minutes	CA minutes	BA minutes	SWI h:m	Score B	Recovered	Urine production at day 8
42	52	20	15	1:12	Died	No	NA
43	50	50	20	1:40	C5c	No	NA
44	47	41	13	1:28	D5a	No	NA
45	37	22	22	0:59	A1b	Yes	15 ml
46	38	50	20	1:28	A1b	Yes, for 1h	NA
47	44	40	30	1:24	A1b	Yes	15 ml
48	44	35	15	1:19	A1c	Yes, for 48h	NA
49	40	45	25	1:25	A1b	Yes, for 24h	NA
50	61	55	24	1:56	A1a	Yes	16 ml
51	42	60	19	1:42	Died	No	NA
52	45	60	25	1:45	A5d	No	NA
53	60	44	20	1:45	A3a	Yes, for 48h	NA
54	53	80	25	2:23	A3b	Yes	28 ml
55	40	45	10	1:25	A3c	Yes	18 ml
56	65	45	22	1:45	A3c	No	NA
57	42	32	22	1:04	A1a	Yes	10 ml
58	78	76	20	2:34	Died	No	NA
59	50	93	19	2:38	A4a	Yes	17 ml

Table 7.6: Transplant procedure evaluation by graft scoring system B

AA, aortic anastomosis; **CA**, cava anastomosis; **BA**, bladder anastomosis; **h**, time in hours; **mm**, time in minutes; **SWI**, second warm ischaemia. Rows in blue show the recovered rat until the end of study.

Rat No	Scoring A	Rat No	Scoring B
27	A3c	**45**	A1b
29	A1a	**47**	A1b
32	A2a	**50**	A1b
36	A3a	**54**	A1b
37	A2a	**55**	A3c
39	A3a	**57**	A1a
41	A2a	**59**	A4a

Table 7.7: Summary of scores and points

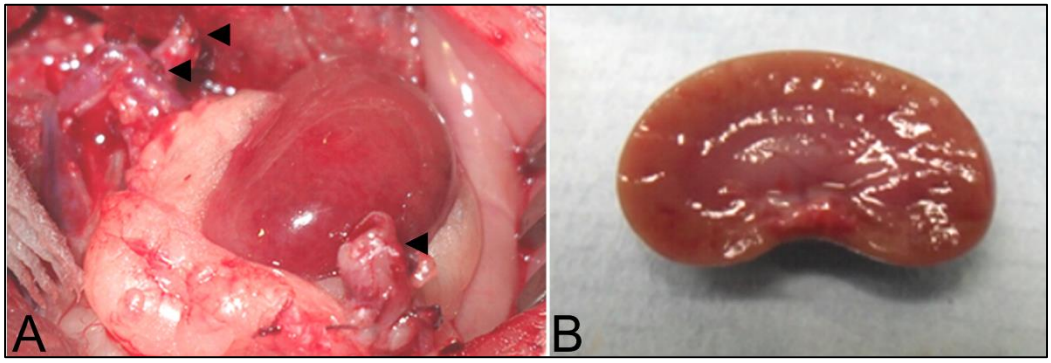

Figure 7.7: Renal isograft after 5 minutes (A) and 8 days of transplantation (B)

Panel **A**. Reperfused kidney after 5 minutes of vascular conduits anastomosis. Black arrow show, from top to bottom, a portion of the ligated donor aorta, renal vein-cava conduit and perfused bladder. Panel **B**. Transversal kidney section of the kidney in picture A after 8 days of transplantation.

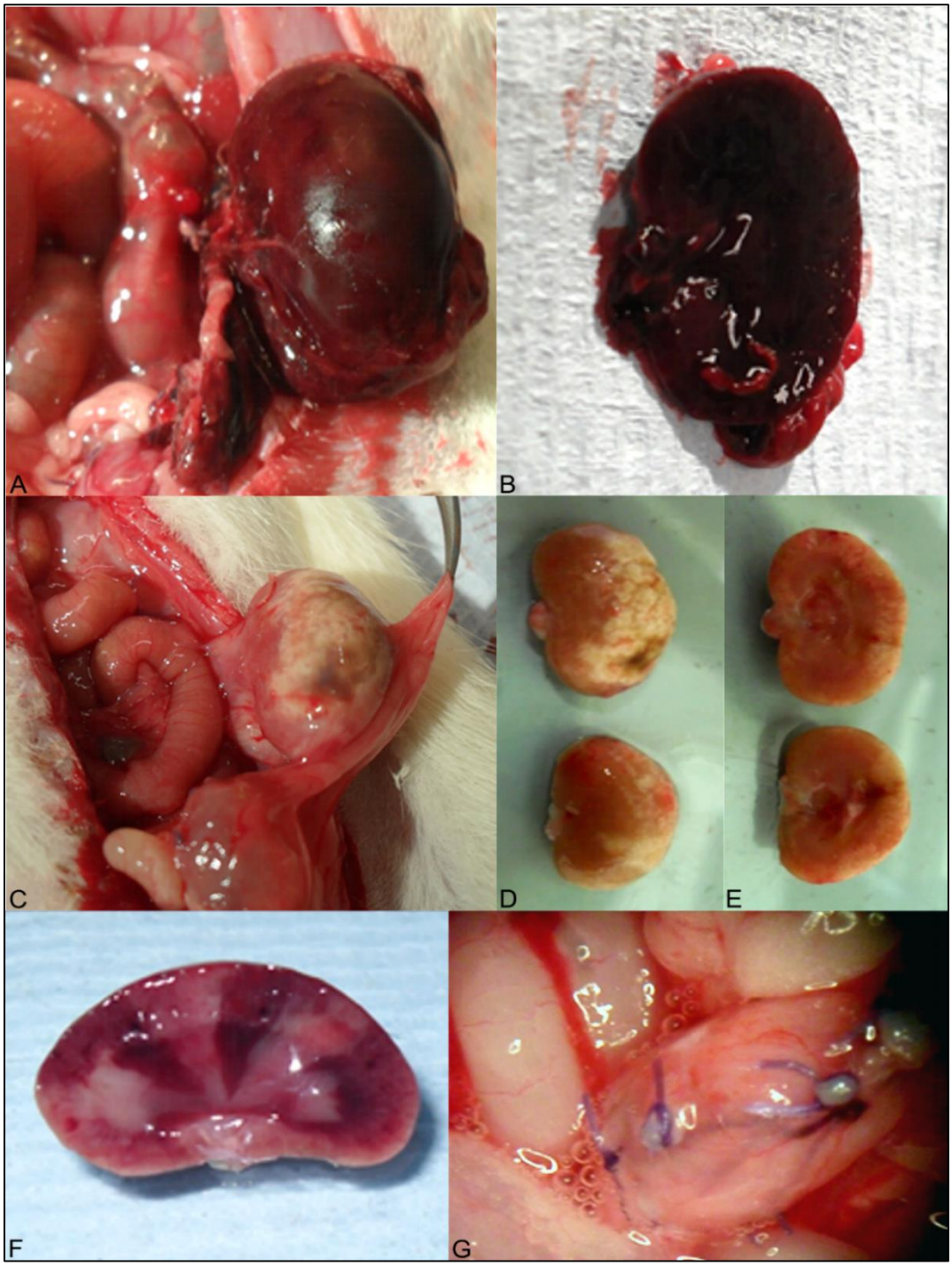

Figure 7.8: Kidney and bladder complications after kidney and bladder transplantation

Panel **A**-**B**. Representative images of renal ischaemia/ necrosis after 2 days of transplantation. Panel **B**, shows the affected kidney transversally cut. Panel **C**-**D**. Representative images of a kidney suspected of pyelonephritis. Panel **F**, kidney with focal ischaemia. Panel **G**. Bladder leakage post bladder cuff anastomosis; notice the air bubbles in the body of the bladder after injecting air into it.

7B.3.3. Evaluation TG2 levels in the Lewis and Fisher rats

Measurements of the IGMA (400x) and tubulointerstitial area (200x) in the Lewis group were associated with a non-significant FITC/DAPI ratio when compared to the Fisher group. IGMA, Lewis, 1.8 ± 0.1; Fisher, 1.9 ± 0.20 FITC/DAPI ratio, NS. Tubulointerstitial, Lewis, 2.5 ± 0.3; Fisher, 2.6 ± 0.2 FITC/DAPI ratio, NS. Figure 7.9, left and right panel for IGMA and tubulointerstitial area, respectively.

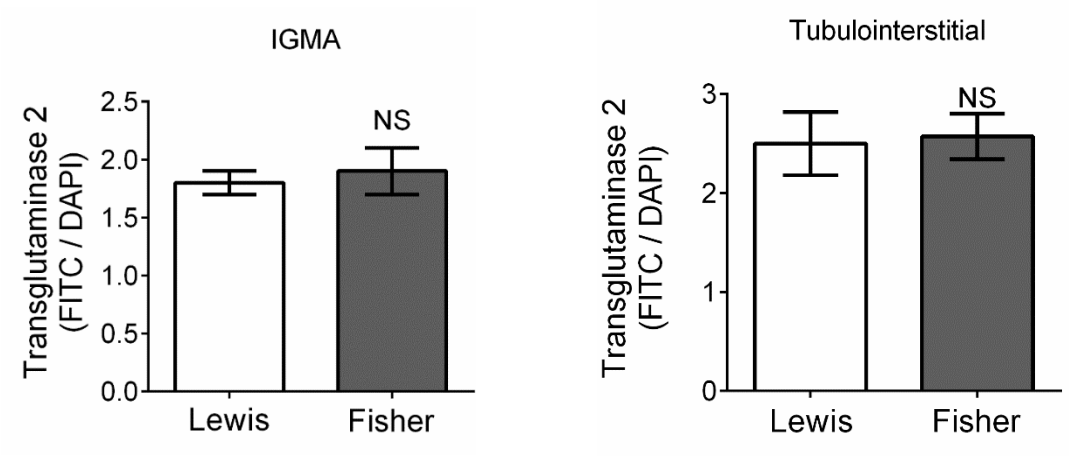

Figure 7.9. TG2 levels in the Lewis and Fisher rats

Left and right histograms represent the levels of TG2 by immunofluorescent expressed as FITC/DAPI ratio in the IGMA and tubulointerstitial space. Lewis (n=5) and Fisher (n=5). Vertical bars indicate +/- SEM.

7B.4. Discussion

7B.4.1. CAN, interventional model of renal fibrosis

In man, currently there is no effective treatment to prevent the irreversible features of CAN. Current research on this subject has focused on four main areas; development of new immunosuppressive drugs, surgical technical improvements, avoidance of ischaemia reperfusion injury by using normothermic organ perfusion machines during/after kidney harvesting (Brasile *et al.*, 1997a; Brasile *et al.*, 1997b;

Stubenitsky *et al.*, 2000) and blocking of inflammatory and fibrogenic pathways to target both deposition and accumulation of ECM (Shrestha *et al.*, 2014b).

The role for TG2 has been proposed since both CAN and CKD share three major factors interconnected with the transglutaminase pathway, inflammation, fibrosis and hypoxia. Hypoxia can be considered an important factor involved in the activation and perpetuation of TG2 activity in the kidney, whereas fibrosis is the end result factor of both diseases which is major substrate source for TG2. Studying KT in the rat allows the assessment of renal fibrosis which represents a major histopathological feature after renal transplantation as well as in CKD. Also, this model facilitates the testing of biological drugs such as TG2 inhibitory monoclonal antibodies.

The practise and evaluation of an appropriate technique for kidney transplantation in the rat was initiated early in the work present for this thesis in parallel with the analysis of CKD in the cat in Chapters 3 & 4. The intention at that time was to undertake interventional studies in a rat model of CAN using a newly developed TG2 selective inhibitory antibody effective in the cat kidney in vitro (Chapter 4). Transplantation project was intended to use Fisher to Lewis rats' allografts to generate a highly renal fibrogenic model. Results in this chapter indicates both Fisher to Lewis rats have similar levels of extracellular TG2 in either the tubulointerstitial or the IGM areas; therefore, excluding the variable of differences in TG2 levels secondary to rat strains. However, initial studies showed the human TG2 neutralising antibody (BB7), while effective in the cat kidney, to be ineffective against the TG2 enzyme in rodents. The epitope binding site of the BB7 antibody did not matched 100% the aminoacid segment in the rat TG2, see Figure. 4.10. This required a change of emphasis to undertake interventional studies in a much simpler experimental model, ischaemia reperfusion injury, where the kidney would be able to withstand the trauma of tissue infusion procedures, required to deliver the pan TG inhibitor (D003), Chapter 6.

The results presented in this chapter would indicate considerably greater experience is required to achieve normal function in the Sprague-Dawley isograft using the technique of end-to-side anastomosis of aortic and caval conduits. The choice of transplant technique was limited by the lack of a suitable high-powered microscope with a foot-controlled focus essential for the anastomosis of small vessels such as the renal vein and artery. The following discussion attempts to identify the

technical issues which, if resolved, might allow a successful end-to-side approach to be employed.

7B.4.2. Kidney Donor

Blood Clearance**.** Currently, a wide variety of solutions are available to preserve solid organs. The University of Wisconsin solution is used worldwide used due to its effectiveness in organs exposed to hypothermic preservation conditions (Bonventre *et al.*, 1992; Ploeg *et al.*, 1992; Southard *et al.*, 1995). An adequate perfusion with at least 20 ml should be enough to flush away the intravascular native cellularity (erythrocytes, lymphocytes and leucocytes). An appropriate balance between perfusion and pressure must be exerted; low pressure must be applied whilst renal perfusion to avoid intraglomerular damage. High hydraulic intraglomerular pressure could disrupt the glomerular filtration barrier allowing temporary proteinuria and subsequently tubular damage from protein overloading in the transplanted kidney (Gorriz *et al.*, 2012). In an *ex vivo* model of rat has been shown that increasing of intraglomerular pressure and mesangial stretching may be a trigger factor for matrix formation (Riser *et al.*, 1992). The extravasation of fluid into the extracellular matrix could seed erythrocytes and leucocytes preloading an inflammatory reaction on top of the reaction caused by reperfusion itself. Fail in flushing away the blood cells may result in thrombosis or acute rejection, probably even with previous treatment with immunosuppressive drugs. Red blood cell aggregates and glomerular disruption could be seen as haematomas after renal perfusion. On the other hand, puncture or superficial cortex scratches and capsular striping might be enough to seed bacteria and inflammation promoting infection after kidney transplantation. Renal decapsulation has been implicated in the impairment of renal interstitial hydrostatic pressure by decreasing the response of pressure natriuresis (Khraibi *et al.*, 1989). The renal surface visual evaluation allows the assessment of renal perfusion. Though this technique is subjective, and just evaluates some micrometres in thickness, it may be relevant to forecast donor kidney quality and survival once implanted in the recipient. Blood clearance was achieved in the majority of kidneys suggesting this is a basic parameter to achieve; therefore, failure in blood clearance is a strong exclusion criteria for the donor kidney.

Surgical Timing. In the present study, an appropriate total surgical time for this technique was less than 2 hours 30 minutes; however, according to some of our kidney transplants, times between 3 hours 30 minutes and 4 hours 30 minutes were

not associated with fail in urine production after contra-lateral nephrectomy. Long intra-operative time and hypotension is a common event during kidney transplantation (Hirata *et al.*, 2009) and it has been associated with delayed graft function in transplant recipients (Sandid *et al.*, 2006). A quick and efficient surgical technique for the donor procedure may prevent infection and hypotension (Sandid *et al.*, 2006). Intra-operative hypotension has been associated to renal infarcts, probably due to low organ perfusion (Goldman *et al.*, 1975). Hypotension during surgery can decrease renal perfusion producing hypoxygenation which may cause cellular endothelial and epithelial damage (Patschan *et al.*, 2012). On the other hand, a long donor technique procedure may sensitize the kidney to infection during the transplantation procedure by tissue environmental contamination. Hypothermia during and post-anaesthetic procedures can cause peripheral vasoconstriction (Ozaki *et al.*, 1995; Sessler *et al.*, 1991) and impaired function of phagocytic leucocytes by reducing reactive oxygen species utilization against bacteria (Wenisch *et al.*, 1996). Kidney injury secondary to hypotension and sepsis during donor kidney harvesting may alert the adaptive immune system by dendritic cells activation before renal implantation (Jantsch *et al.*, 2008; Kerschen *et al.*, 2010).

The last phase of the donor technique is called first warm ischaemia (FWI) which begins when the donor kidney blood flow is totally or partially blocked to the time the kidney is perfused with a cold preservation solution. In the rat, cellular changes compatible with cell survival were identified after 15, 30, 60 and 120 minutes of ischaemia. Nevertheless, partial or total necrosis of proximal tubular cells (P3 segment) was identified after reperfusion followed 3, 6, 12 and 24 hrs of recovery. These findings may suggest that the rat kidney is relatively resistant to first warm ischaemia; however, not resistant to the harm originated after reperfusion. Even though FWI in the rat is not the most relevant issue for tissue integrity and function due to its short time (approximately 5 minutes), long surgical procedures should be avoided as much as possible to decrease the kidney susceptibility to bacterial contamination, innate immune system disabling, and hypotension. Approximately 50 % of the donor procedures in this study were achieved in less than 3 hours and 30 minutes and just 8 % in less than 2 hours 30 minutes. Further training should improve the timing of surgery.

Haemorrhage. Donor or recipient severe haemorrhage can occur during cannulation of infrarenal aorta for perfusion or after anastomosis of great vessels. Low degree haemorrhage can result with a non-adequate ligation technique of small

peripheral vessels. Thrombotic complications (Odland, 1998) and stenosis of the renal artery (Wong *et al.*, 1996) have been described as significant harmful elements for graft survival. Moreover, haemorrhage has also been also associated with acute tubular necrosis, which is an important cellular damage closely related to delayed graft function (Osman *et al.*, 2003). Rats are considered to have around 55-70 ml of blood per kg of bodyweight (Parasuraman *et al.*, 2010). Taking 55ml as reference, a rat weighing 250g would therefore have a total blood volume (TBV) of approximately 14 ml. Haemorrhage of 1.4 ml would be the equivalent of 10% of the total blood volume. The suggested limit for blood sampling is less than 10% (Parasuraman *et al.*, 2010). A surgical procedure with less than 1.5ml in this study was consider as haemorrhage without complications, taking into account the rats were supported with fluid therapy (NaCl 0.9%). In the rat, mean arterial blood pressure of 40mmHg is maintained when the TBV is reduced up to 40%, at this percentage, renal hepatocellular damage (Wang *et al.*, 1990) and circulatory dysfunction even with crystalloids or colloids resuscitation is imminent (Wang *et al.*, 1994). It has been hypothesized that liver dysfunction might bring postoperative multiple organ dysfunction in patients with intraoperative haemorrhage (Ozawa *et al.*, 1983). The importance of a surgical procedure with low haemorrhage during the donor and transplant technique could be translated in better tissue integrity, low incidence of delayed graft function and infection. In the present study 50% and 30% of the subjected rats had less than 2.5 ml and 3.5ml of haemorrhage, respectively, suggesting that haemorrhage of less than 2.5 ml is an achievable and realistic goal to increase in 80% with further training.

Donor kidney integrity. In humans, Wigmore et at (1999) published a large study using data from the National Transplant database (1992-1996) (Wigmore *et al.*, 1999); 1% (98 / 9014) of the cadaveric donor kidneys in that study was not transplanted because of donor kidney damage during surgical harvesting, whereas 19% (1726/9014) of the injured donor kidneys were transplanted and did not show a significant difference 5 years post-transplant when compared to non-damage organs. The damage was mainly associated to capsular tearing and small haematomas, inadvertently short ureters, cut of renal veins, polar renal arteries and the presence of aortic patch. In a recent retrospective study (2000-2010), Ausiana et al (2012) showed that 11.4% (96 / 841) of the recovered kidneys from cadaveric donors were damaged during retrieval procedure. The main damage was associated with ureters and polar artery injury (Ausania *et al.*, 2012). In the present study the kidney damage during kidney retrieval was associated to haematomas, capsular tearing, partial

decapsulation from one of the poles, puncture, ureteral torn, total cut, structure, perforation or torn of major vessels and the main findings were haematomas. However, in overall, almost 90% of the subjected kidneys were scored with a green label. The present study, the results obtained in the first set of donor kidneys suggests that the surgical inexperience is the main factor for graft injury. However, the healing process of transplanted kidneys is able overpass the moderate organ damage (yellow label marking) that may be caused during surgery.

7B.4.3. Kidney Transplant

Reperfusion. Renal reperfusion injury has been described as one of the most important alloantigen independent events for the development of acute inflammation (Patschan *et al.*, 2012) and renal fibrosis (Torras *et al.*, 1999). However, this damage can be exacerbated by extrinsic renal causes such as recipient systemic hypotension, vascular stenosis due to anastomosis and adhesion of vascular walls due to micro-claps pressure. Hypotension during kidney transplantation can be associated with myocardial depression and vasodilatation produced by anaesthesia. This phenomena can be directly reflected in delayed graft function (Sandid *et al.*, 2006) and in the development of thrombosis due to activation of pro-coagulant pathways (Yan *et al.*, 1999), apart from the other mechanisms previously reviewed in hypotension during donor kidney retrieval. An important issue in this section is the lack of perfusion due to vascular disruption such as vascular perforation or vascular clamp injury. Vascular damage has been also associated with the development of thrombus. The activation of the pro-coagulant cascade is triggered by vascular endothelial disruption or conduit narrowing (Bakir *et al.*, 1996; Khouri *et al.*, 1990; Slayback *et al.*, 1976). Vascular clamp injury in the aorta has been also associated with vascular hyporeactivity in the rabbit (Barone *et al.*, 1989). Failure in reperfusion can occur as a result of a variety of aetiologies, special attention has to be focus on surgical timing and vascular integrity during anastomosis, including proper anastomosis and quick timing of vascular anastomosis to avoid damage by compression with vascular clamps. Almost 90% of all the transplanted kidneys in the present study and 100% (7/7) of the recovered group had a total reperfusion time of less than 10 seconds suggesting that hypotension or major vascular damage secondary to microclamps did not impaired the renal graft blood inflow or outflow. However, it is important to bear in mind that the first seconds of reperfusion could have higher pressure than the blood pressure after one minute of renal graft reperfusion, hence, proper perfusion within 10 seconds does not rule out either vascular damage, which eventually can be evident with lower

pressures, or systemic hypotension. This is just an evaluation of major blockage due to important vascular maceration or thrombosis.

Renal surface and hypertrophy post-reperfusion. The implications of superficial lacerations, decapsulation and haematomas during kidney transplantation (recipient technique) are similar to that previously explained for the donor technique. However, renal congestion and ischaemia/necrosis are important phenomena to be addressed. During the end-to-side technique, the graft, suprarenal aorta and suprarenal cava are clamped leading to potential damage in other organs. The low blood flow, crushing of vessels by vascular clamps, excessive conduit manipulation, vascular stenosis during anastomosis technique and low dose of heparin are potential factors for early formation of thrombotic emboli (Pahlavan *et al.*, 2005; Schumacher *et al.*, 2003). Thrombotic emboli represented as focal ischaemic areas may occur just after releasing the clamps with the subsequent renal congestion and low (Salaman, 1969). Renal congestion can be associated with cava anastomosis secondary to surgical anastomosis or vascular clamping as this conduit is susceptible to damage due to its structure. A proper blood flow coming from renal arteries can be slowed down in the blood outlet by cava stenosis. This phenomenon can produce thrombus and renal hypertrophy. High intra-glomerular pressure due to stricture of the venous outflow may intensified nephron loss by ischaemia reperfusion injury affecting the graft acutely and generating chronic damage (Mackenzie *et al.*, 1995; Mackenzie *et al.*, 1996). Sprague Dawley rats were used to generate renal isografts. This is an outbreed strain which means that rats are maintained as closed colonies of genetically variable composition, hence, graft haematomas, renal hypertrophy and necrosis could have been the results of acute rejection or perhaps this could have contributed to further the cava stenosis (previously damage by clamps) due to an inflammatory reaction. In the present study, less than 10% and 20% of renal hypertrophy were seen in 33 and 26% of the grafts, respectively, suggesting there was a certain degree of venous blockage that could have been caused secondary to cava endothelial damage and this might have been potentiated by certain degree of histological antigenicity, maybe not just in the cava conduit, also in the intrarenal vascular system. However, 86% (1/7) in the recovered group showed adequate renal surface colour and no hypertrophy. The graft from the recovered group showed more than 10% but less than 20% hypertrophy and it did not correlate with urine production, which might suggest that the immune response or the vascular damage was mild and could be overcome over time, nevertheless the number of samples was low and no

histological assessment was generated due to lack of time, hence no strong conclusions can be reached from this study.

Second warm ischaemia. SWI is the time the surgeon spends during the graft anastomosis to the time it is properly reperfused. Vasospasm, hypotension, artery stenosis, renal artery embolism, renal or vein misangulation and misalignment are reasons that can lead to a long second warm ischaemia (Qiu *et al.*, 2012). A rat model of ischaemia reperfusion injury by bilateral clamping or renal vein and artery suggests that 30 minutes of SWI allows the kidney to recover from renal damage with minimal complications after kidney transplantation (Weight *et al.*, 1998). In the rat, this timing has been corroborated as a suitable time in kidney transplantation to generate adequate long term graft outcomes (Patschan *et al.*, 2012; Schumacher *et al.*, 2003). Karatzas et al (2007) reported a mean vascular anastomotic time of 15.5 ± 1.5 min with a 15 day survival rate of 87% (Karatzas *et al.*, 2007). In the current study around 90% (14/15) of all transplants were performed in not less than 1 hour 30 minutes. However, a better timing can be achieved with further training. In theory a lack in oxygen increases the production of xanthine oxidase, which in turn generates reactive oxygen species when perfusion occurs affecting renal structures acutely. The generation of ROS is proportional to the ischaemic time. However, probably the University of Wisconsin is able to interrupt effectively the ROS formation as UW has allopurinol as an important compound. Interestingly, even though xanthine oxidase is a key enzyme in the development of ROS, its inhibition through allopurinol in acute renal ischaemia and kidney transplantation has not always been translated to renal integrity improvements in long term (Paller *et al.*, 1984). This shows that ROS is the result of just a part of the injury cascade triggered by a hypoxaemic status; and therefore, other cellular inflammatory mechanisms have to be approached at the same time to promote functional and structural renal integrity following acute renal injury.

In this study, the aortic plus cava anastomotic times represents more a measurement of SWI than the anastomotic times their selves. The start count was performed from the time the clamps were placed in the recipient's vascular conduits to the time the vessels were anastomosed. This action could have added some minutes (10 ± 5 minutes) to the total count as further careful dissection was performed for some of procedures to relocate the vascular clamps or to ligate any missed accessory paralumbar veins and missed venous tributaries branches before the anastomosis started. Even though long SWI did not affected the production of urine

the kidney managed to get classified as acceptable, anastomosis should be achieved in less time with further training.

7B.4.4. Conclusion

Special attention should be addressed to the surgical timings and vascular anastomosis. The surgical technique end-to-side anastomosis using vena cava and aortic conduits provides a good technical option when a high powered microscope is not available, prevents vascular strictures, which may decrease the incidence of thrombosis and long term graft quality. The bladder patch offers a reliable technique to maintain a patent urine outflow during a chronic study. Surgical training should start by performing the donor technique using the scoring system A. Once an adequate donor technique skill and anastomosis surgical pattern has been dominated the next step is developing the transplant technique. The handling of vessels and organs is performed as in the donor technique. In my opinion, the recipient technique is easier to perform than the donor technique, however it requires of more attention and surgical detail. A high quality technique could be achieved if the donor and recipient surgical technique are performed by different surgeons, this can be translated in better timings and less surgical mistakes. Both the vascular and bladder anastomosis are techniques that can be performed under conventional microsurgical microscope. The learning curve for this technique can be achievable by novice surgeons during a PhD programme, along with other major research duties. Setting the surgical technique during PhD studies allows the student to establish stronger postdoctoral projects and pursue a solid career in this subject.

CHAPTER 8

Discussion

8.1. Introduction

The prevalence of CKD in aged cats is over 50% (Marino *et al.*, 2013a) and considered a major cause of death together with cancer, osteoarthritis and cardiac dysfunction secondary to endocrine abnormalities (Gowan *et al.*, 2012). CKD in the human is a major health problem worldwide and is considered the 12th and 17th cause of death and disability, respectively, with many major economic, social and epidemiological implications (Schieppati *et al.*, 2005). Understanding CKD in the human requires the use of experimental animal models under controlled conditions with a shorter period of disease progression to produce reliable findings. Although CKD in the domestic cat is multifactorial, the kidney develops histopathological features similar to that in human CKD, which may be influenced by a wide range of environmental factors which cannot be replicated in the laboratory setting, either *in vivo* or *in vitro*.

In this thesis, a naturally occurring model of CKD in the cat was used to investigate the possibility of an association between the TG2 enzyme and the development of renal fibrosis, as shown in humans with CKD (Johnson *et al.*, 2003). Both an inhibitory antibody against human TG2 and a small molecule pan TG inhibitor were examined in feline tissue *in vitro,* showing that the TG2 enzyme could be inhibited in the cat. This finding suggested that renal fibrosis could be inhibited by a small molecule drug or an inhibitory antibody to human TG2 if administered to cats *in vivo*. Studies on TG2 inhibition in human renal tissue with CKD have yet to be published, showing the potential for a study of naturally occurring animal disease. The results presented in this thesis on CKD studies in the domestic cat may therefore support further investigations into human CKD.

Renal fibrosis however, is not a feature exclusive to CKD (Nangaku, 2006) and is also found in a condition described as chronic allograft nephropathy (CAN) (Rosenberger *et al.*, 2007), a fibrogenic disease generated after renal transplantation. CAN could be considered as a post-transplant form of CKD, as both diseases have histopathological and disease progression similarities. A rat model of renal warm ischaemia (RWI) was employed to mimic the development of renal fibrosis by CKD and CAN, but secondary to ischaemia reperfusion injury. The association between TG2 and the development of fibrosis was successfully demonstrated in this RWI model and a causal link established through chemical inhibition of the enzyme *in vivo* with a positive reduction in tubulointerstitial fibrosis.

Further studies were initiated to examine a possible causal link between TG2 and renal fibrosis following kidney transplantation. Previous work performed in collaboration with Mr Shrestha in the Academic Nephrology Unit had already shown an association between CAN and TG2. A methodology of kidney transplantation was established using aortic and vena caval conduits using the Sprague-Dawley rat. However, this approach was unable to be completed for two major reasons:-

(a) The work-up time taken to establish this complex surgical technique which itself involved the use of some 60 animals,

(b) A lack of sensitivity to rodent TG2 of an antibody inhibitor of the human TG2 enzyme developed in Sheffield by Drs Mamrabouka and Watson since an interventional study was required to establish a causal link between the development of CAN and the TG2 enzyme.

8.2. CKD and the TG pathway in the Rat

A rodent model of RWI was examined with a disease duration of 8, 28 and 140 days providing evidence of a positive association between the development of tubulointerstitial fibrosis and the TG2 enzyme. This model at 28 days did not developed glomerulosclerosis but early tubulointerstitial fibrosis together with renal failure and the up-regulation of the transglutaminase pathway. Hence, the RWI model was considered to be histopathologically similar to feline CKD and suitable for interventional studies. According to the degree of functional decline, tubulointerstitial TG2 and histological damage, a disease progression of 28 days was long enough to provide evidence of a causal link between TG2 and the development of renal fibrosis following RWI. The inhibition of the TG pathway was achieved using a small molecule pan TG inhibitor delivered intrarenally by a perforated cannula positioned within the kidney attached to a subcutaneous osmotic minipump containing the drug.

Drug Delivery System. TGI was delivered to the kidney by tissue infusion using an intrarenal cannula attached to a subcutaneous osmotic minipump. This experimental method of drug delivery, although somewhat crude, has been used successfully within other experimental rat models of CKD published from the Academic Nephrology Unit at the University of Sheffield including both subtotal

nephrectomy (Johnson *et al.*, 2007; Oldroyd *et al.*, 1999) and diabetic nephropathy (Huang *et al.*, 2009). The delivery system using intrarenal cannulation was initially employed by Oldroyd et al (1999), where interferon-Y was shown to reduce fibrosis in the rat following subtotal nephrectomy and subsequently by Johnson et al (2007) to evaluate the effectiveness of TG inhibitors. Further evidence for the effectiveness of this approach was provided by Huang et al (2009) in a rat model of diabetic nephropathy where a TG inhibitor was labelled with dansyl-FITC to evaluate the distribution of the compound within kidney tissue. The results showed both a homogenous distribution of drug and also a very minimal degree of fibrosis from any damage resulting from cannula placement within the kidney.

Osmotic minipumps provide a reliable, versatile and robust method of continuous drug infusion as suggested by their use in some 17,500 articles published over a period of 35-40 years from 1976 onwards. The main advantage of the osmotic pump is the ability to deliver a continuous drug infusion, for experiments within this thesis of a period of up to 28 days (Theeuwes *et al.*, 1976), with the possibility of extending up to 33 days, depending on the batch. Benefits include a reduction in the fluctuation of drug concentrations within the body, a reduction in the time and manpower required for drug administration and indirectly, reducing animal stress. The low antigenicity of the pump also prevents stimulation of the immune system and inflammation following its implantation.

TG2 upregulation in inflammation and fibrosis**.** The inhibition of TG2 is able to attenuate both inflammatory and fibrogenic processes following RWI, since TG2 plays an important role in the upregulation of core cytokines involved in early and late healing processes.

TG2 and NF-κβ interaction. The inhibition of TG2 has been proposed to have an anti-inflammatory effect, as transglutaminase 2 can activate the NF-κβ pathway (Kim, 2006). In a TG2 knock out mouse model of ischaemia reperfusion injury (30 minutes renal hilar clamping), intravenous TNF-α was shown to keep NF-κβ and COX-2 expression to basal levels in contrast to the upregulation of NF-κβ and COX-2 in the wild type. As a result, renal neutrophilic infiltration, function (urea and creatinine) and structure (glomerular and tubulointerstitial) were significantly preserved in the TG2 knockout mouse group at day 3 (Kim *et al.*, 2010).

NF-κβ activation via TG2 has been shown to be associated with I-κβ kinase dependent and independent pathways, upstream paths for NF-κβ signal transduction in the inflammatory cascade. TG2 polymerizes the inhibitory subunit alpha of NF-κβ via cytosolic transamidation, which in turn, produces a dissociation from the NF-κβ inhibitor with its subsequent translocation to the nucleus where it activates transcription (Lee *et al.*, 2004). The activation of NF-κβ via TG2 has been supported by other research groups in the oncology field (Cao *et al.*, 2008; Jang *et al.*, 2010; Kim *et al.*, 2006). Furthermore, NF-κβ has been shown to induce TG2 transcription in liver cells; this event has been proposed to be associated with the NF-κβ binding to the TG2 promoter (Mirza *et al.*, 1997).

Phospholipase A2 activation via TG2. Another implication of TG2 in inflammation is via activation of the secretory form of phospholipase A2 (Miele, 2003), a pathway with special relevance in the reduction and control of inflammation via corticosteroids. This finding was first assessed in a model of conjuctivitis in the guinea pig, where TG2 was proposed to contribute to the activation of phospholipase A2 (Sohn *et al.*, 2003). The role of phospholipase A2 in the kidney has been indirectly tested by determining the induction of inflammation via COX-2 through NF-κβ activation (Kim *et al.,* 2010).

TGF-β1 activation via TG2. TG2 has also been shown to upregulate (Huang et al., 2010; Khalil, 1999) and to be upregulated by TGF-β1. TGF-β1 is secreted inactively as latent form of TGF-β (L-TGF-β1) and later this is catalysed by TG2. TG2 also recruits the non-active form of TGF-β1 into the extracellular matrix where it gets cytokine-activated. In *vivo*, by using a rat model of diabetic nephropathy + TG inhibitor, it was shown that TGF-β1 transcription and protein was significantly reduced in contrast to the diabetic nephropathy group following 8 months of disease progression. Furthermore, in transfected opossum kidney proximal tubular epithelial cells, the higher the TG2 overexpression the higher TGF-β1 transcription was noted (Huang et al., 2010). Conversely, TGF-β1 has been shown to promote TG2 transcription in dermal fibroblasts treated with inflammatory cytokines. Interestingly, TGF-β1 also upregulates fibronectin, a vital component in the ECM during early inflammatory processes (Quan *et al.*, 2005), and important TG2 substrate.

TGF-β1 and NF-κβ interaction. Concerning TGF-β1 and NF-κβ cross-talk, TGF-β1 is able to induce NF-κβ activation to promote osteoclast survival; a similar phenomenon has been seen in squamous cell carcinoma (Freudlsperger *et al.*, 2013;

Gingery *et al.*, 2008). NF-κβ is able to attenuate TGF-β1 transcription via regulation of SMAD7 promoter, a TGF-β1 receptor antagonist. Interestingly TGF-β1 can antagonize transcription of NF-κβ. Also, NF-κβ can block TGF-β1-induced apoptosis in hepatocytes (Nagarajan *et al.*, 2000). The cross talk between these two proteins might be dependent on the cellular context and the causal agent that triggers the gene expression. This protein interaction may be relevant as a regulatory "valve" between renal inflammation and fibrogenesis. A diagram with main TG2 upregulation pathways is displayed in Figure 8.1.

TG2, inflammation and fibrosis following Renal Warm Ischaemia. The rat experiments in this project have shown that renal warm ischaemia is able to cause acute, sub-acute and chronic long term effects in the rat kidney, following 8, 28 and 140 days following RWI, respectively. RWI is able to induce hypoxia and inflammation. Hypoxia and inflammation may interact to each other, however during disease progression both events may run parallel at different rates and may support each other to perpetuate disease. In chronic stages, hypoxia overtakes inflammation in the disease progression placing the inflammatory event as a second actor. Both events promote an increase in NF-κβ and TGF-β1 in the rat and mouse following early RWI (Basile *et al.*, 1996; Supavekin *et al.*, 2003). Basile et al (1996) showed that TGF-β1 gene expression remains up regulated from 12 hours to 14 days following RWI in the outer medulla and tubules, and after that just in regenerating tubules. NF-κβ and TGF-β1 then promote TG2 transcription. The activation of TGF-β1 via TG2 feeds the extracellular matrix with collagen protein, which subsequently gets cross-linked by TG2 in the tubulointerstitial space. A diagram for the up-regulation of the TG pathway in the tubulointerstitial area following RWI is shown in Figure 8.2.

Correlations between tubulointerstitial fibrosis and the TG pathway**.** Taking into account that TG2 is a major causal link for the development of renal matrix deposition a high correlation between fibrosis and TG pathway was expected. However, in all RWI experiments, low but still significant correlations were found between extracellular TG2 protein/activity and tubulointerstitial fibrosis as assessed by MTS or collagen immunofluorescence. One important factor to consider may be the half-life of TG2. Intracellular TG2 half-life has been assessed in monocytes lysates showing that in 2-day and 10 day old cells can reach up to 11h and 7h, respectively of TG2 half-life (Murtaugh *et al.*, 1984). This is evidence that senescence may condition TG2 activity and this might be probably associated with the number of times each enzyme is involved in a transamination reaction. Perhaps, ECM turn over and the location of

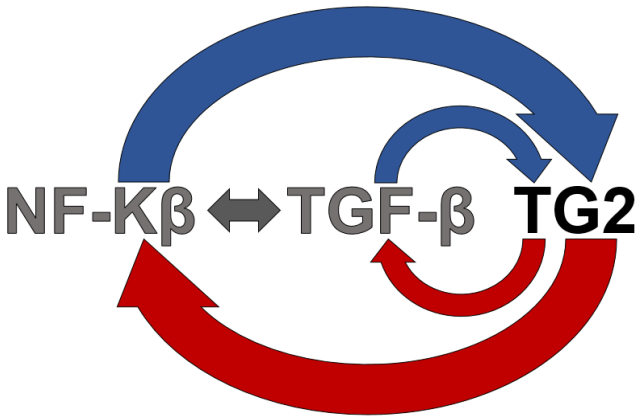

Figure 8.1: Upstream TG2 upregulation

Blue arrows represents the interaction of NF-κβ and TGF-β on TG2 upregulation. Red arrow represents the interaction of TG2 on NF-κβ and TGF-β upregulation. Grey double way arrow represents NF-κβ and TGF-β cross-talk, which involves inhibitory and transcriptional processes.

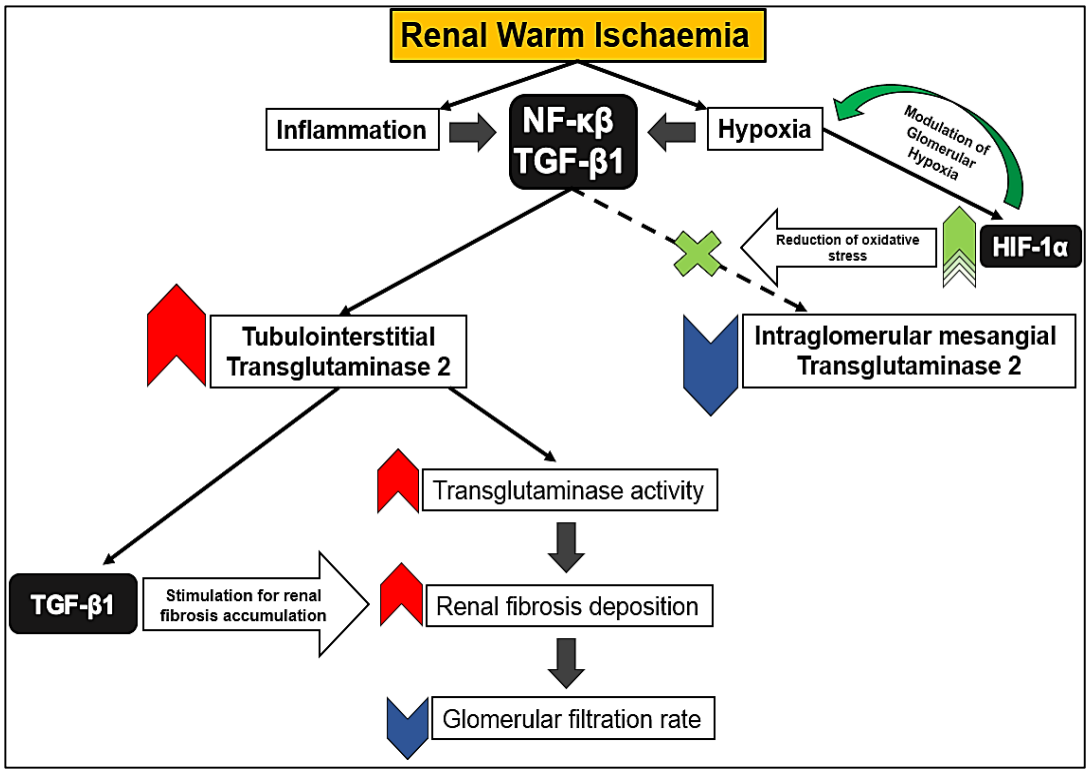

Figure 8.2: Effect of RWI on the tubulointerstitial and IGM areas.

Renal warm ischaemia initiates an inflammatory and hypoxaemic events together with the generation of NF-κβ and TGF-β1 cytokines. Tubulointerstitial space generates an increase in TG2 followed by increase in TG activity, renal fibrosis deposition (fed by TGF- β1 interaction with TG2) and finally reduction in GFR. IGMA is less affected by RWI due to a possible over expression of glomerular HIF-1α (green arrow). A low expression of IGM TG2 together with glomerular conservation is achieved as a result.

the enzymes (intracellular or extracellular space) may contribute to a modification in TG2 activity or TG2 protein degradation. Therefore, measuring of the ε (ɣ-glutamyl)-lysine, the TG2 non-degradable cross-linking product, remains the best method to evaluate the contribution of the TG2 pathway in collagen deposition. Previous publications have shown the value of assessing of ε(ɣ-glutamyl)-lysine in cryostat sections to investigate the previous impact and implication of TG2 in the generation of tubulointerstitial fibrosis (Huang *et al.*, 2009; Johnson *et al.*, 2003; Johnson *et al.*, 2007; Johnson *et al.*, 1997). However, due to the lack of specificity in the used commercial antibodies against the TG2 cross link product, accurate measurement of cross-link *in situ* in the rat was not possible (Johnson *et al.*, 2004a).

Glomerular Resistance to Fibrosis. In marked contrast to the tubulointerstitium, renal fibrosis in the rat following RWI at 28 and 140-day did not generate glomerulosclerosis. This finding was consistent with lack of IGM TG2 protein and activity. Interestingly, in the 28-day study even a significant reduction in glomerular fibrosis (Collagen I and IV) was achieved together with a significant reduction in TG2 protein and activity when the RWI and RWI+TGI groups were compared to nephrectomised control rats. The association (Johnson *et al.*, 2003; Johnson *et al.*, 1997; Liu *et al.*, 2006) and causal link (Fisher *et al.*, 2009; Johnson *et al.*, 2007; Kim *et al.*, 2010) between TG2 and glomerulosclerosis have been shown in a number of studies. Is it possible that hypoxia enables the IGMA with a protective system to down-regulate the TG pathway and therefore preventing the glomeruli from inflammation and sclerosis? Is this the result of a glomerular repairing process or the result of the blocking of renal injury?

Renal regeneration has been widely described during embryogenesis (Quaggin *et al.*, 2008). Post-embryonal nephron-neogenesis is well known to occur in some species such as the adult fish (Watanabe *et al.*, 2009). Some adult amphibians (frog, axolotl) and reptiles (green iguana, turtle and lizard) have shown both glomerular and tubular regeneration (Beuchat *et al.*, 1988; Izaguirre *et al.*, 2008; Solomon, 1985). In mammalians, nephron survival after renal injury is limited to reparation. Nephron reparation is exerted through, proliferation and dedifferentiation of surviving and resident cells which have been shown to play a vital role (Gobe *et al.*, 2007; Lin *et al.*, 2010). However, multipotent progenitor cells and extra-renal cell migration may also contribute to renal repair and may provide some limited regenerative capacity (Benigni *et al.*, 2010). Tubular reparation is highly active process following renal injury when compared to glomeruli, which assumes that the

glomeruli should be enabled with a protective mechanism to perpetuate nephron function. However, recent studies suggest that reparation in glomeruli may not be as passive as previously thought, as renal progenitor cells lining the Bowman capsule in humans and rats have been shown to contribute to important podocyte turnover (Gagliardini *et al.*, 2014).

Glomerular protection may play a role in the prevention of glomerular damage following renal injury. Protective glomerular systems in the domestic feline and the rat model of RWI could be subdivided into:-

Hypoxia sensitive system promoting oxygen homeostasis via:-

a) Up-regulation of oxygen carrier proteins.
b) Up-regulation of pathways involved in vascular regeneration and reparation.
c) Attenuation of cellular oxygen requirements.
d) Maximisation of the available cellular oxygen.

System promoting reduction in inflammation via:-

a) Up-regulation of anti-inflammatory proteins in the mesangial area.
b) Down-regulation of inflammatory proteins in the mesangial area.
c) Reduction of pro-inflammatory cell infiltration in the mesangial area.
d) Increase in the degradation rate of pro-inflammatory mesangial proteins.
e) Up-regulation of pathways involved in glomerular reparation and regeneration.

System promoting reduction in fibrosis via:-

a) Down-regulation of proteins involved in collagen accumulation.
b) Up-regulation of pathways involved in collagen degradation.
c) Attenuation of collagen deposition by down regulation of crosslinking proteins expression and/or activity.
d) Increase in the degradation rate of pro-inflammatory mesangial proteins.
e) Reduction of pro-fibrotic cell infiltration in the mesangial area.

The hypoxia-inducible factor (HIF) could be important part of potential glomerular protective system. Murine glomerular endothelial cells (GECs) under hypoxic conditions have shown to be protected by podocytes rather than mesangial cells (Wang *et al.*, 2015). This protective mechanism is enabled via SUMO-specific protease 1 (SENP-1). Wang et al (2015) showed that by knocking down SENP-1 in GECs the HIF-1α system was abolished together with the GECs protection. The

activation of HIF-1α upregulates genes related to erythropoiesis (e.g. erythropoietin) angiogenesis (e.g. VEGF), vascular tone (e.g. nitric oxide synthase), matrix metabolism (MMP's) and glucose metabolism (e.g. glucose transporters 1 and 3), to mention some (Ke *et al.,* 2006). HIF system regulation may reduce oxidative stress and therefore less initial inflammation. The reduction of inflammation and regulation matrix deposition via HIF may be more regulated in the glomeruli when compared to the tubulointerstitial space. If this is true, the high expression of HIF-1α may have been responsible for reduction of the TG pathway in the IGMA following 28-day of RWI. Perhaps, also other proteins such as mesangial haemoglobin may also contribute tin the modulation of hypoxia after RWI (Nishi *et al.*, 2008). Mesangial haemoglobin could enable the glomerulus to resist ischaemic events by providing more oxygen resources, which in turn may block the generation of nitric oxide and hydroxyl radicals, increased following renal reperfusion (Chatterjee *et al.*, 2002; Murad *et al.*, 1978; Yokozawa *et al.*, 1999). A diagram for the down-regulation of the TG pathway in the IGMA following RWI is shown in Figure 8.2.

Another potential mediator for glomerular protection could be osteogenic protein I (OP-1) also known as bone morphogenetic protein 7 (BMP-7), a protein involved in embryonic nephrogenesis. Luo et al (1995) showed, the OP-1 knockout mouse was not able to survive more than one day due to congenital acute renal failure. Interestingly, the high mRNA expression of OP-1 is not restricted to embryonic states, it is also highly elevated after birth (Ozkaynak *et al.*, 1991). In the ischaemia reperfusion model of rat, OP-1 has been identified highly expressed in the parietal and visceral epithelium of the glomerulus as well as tubuloepithelial cells (Vukicevic *et al.*, 1998). Furthermore, *in vitro* research has shown that OP-1 inhibits TGF-β fibrinogenesis activity in mesangial cells (Wang *et al.*, 2003) suggesting that apart from having a role in acute protection, it is implicated in chronic stages of renal disease and potentially highly active in the mesangium.

Problems associated with TG inhibition. TG2 knockout mice can live without developing major systemic dysfunctions (De Laurenzi *et al.*, 2001). In contrast, TGF-β1 knockout mice were associated with prenatal death due to alterations in haematopoiesis and vasculogenesis (Dickson *et al.*, 1995). Although there are a number of studies showing that the inhibition of TG2 can be beneficial reducing fibrosis in different organs, TG2 knockout mice, have also shown to reduce clearance of apoptotic cells and phagocytosis by macrophages in the liver together with splenomegaly and immunocomplex glomerulonephritis (Szondy *et al.*, 2003). In

another model of induced liver disease in the TG2 knockout mouse, defective apoptotic cell clearance contributed to the release of pro-inflammatory cytokines (IL-12, sTNF-RI) increasing susceptibility to inflammatory disease (Falasca *et al.*, 2005).

Important TG2 functions have been identified in intracellular structures. In the nucleus, TG2 has been implicated in phosphorylation of histones *in vitro*, hence, implicated in chromatin function and structure stability (Kim *et al.*, 2001; Mishra *et al.*, 2006). TG knockout mice also show alterations in mitochondrial physiology with defective ATP production in the heart (Szondy *et al.*, 2006) and in glucose intolerance (Bernassola *et al.*, 2002). The intracellular inhibition of any TG2 function may alter a wide range of cellular signalling important to maintain normal physiology and inflammatory responses in different organ systems.

Extracellular TG2 transamination to promote renal fibrosis represents a small proportion of the full potential of this complex enzyme. The intracellular TG2 implications should never be underestimated when considering TG2 inhibition as potential pharmaceutical approach against fibrosis and inflammation. Temporary inhibition or long-term attenuation of extracellular TG2 and not permanent enzyme disarming should be pursued as an approach to tackle CKD.

8.3. CKD and the TG pathway in the Cat

The data obtained from the Royal Veterinary College for the cat study included plasma and urine analysis. This allowed the generation of two groups, azotaemic and non-azotaemic kidney tissue. However, the clinical history and some parameters of renal function (urinary specific gravity and urea) of the non-azotaemic kidney tissue, did not rule out the possibility of having included early non-azotaemic CKD tissue samples. Although a study limitation, the animals selected were considered to be derived from a realistic sample pool found in a regular clinical setting, where the only tools employed to routinely diagnose CKD are plasma analysis, UPC and urinary specific gravity. The measurements of renal function correlated with tubulointerstitial fibrosis markers in this study. However, more importantly, an association between TG2 and tubulointerstitial fibrosis was found. This is the first time the link TG2-renal fibrosis has been shown in domestic animals, opening a new pathway in the understanding of this condition, supporting the importance of the TG pathway in human CKD and generating a new pharmaceutical approach to tackle the disease.

Interestingly, TG2 and inflammation parameters did not correlate to each other. However, a positive correlation between inflammation and renal fibrosis, by either PASH or MTS was observed, although no difference in interstitial inflammation between cat groups was achieved.

Triad renal hypoxia, inflammation and fibrosis. It has been proposed that tubulointerstitial hypoxia may help to perpetuate the progressive accumulation and deposition of ECM proteins in CKD by affecting peritubular integrity and cellular epithelial death (Basile *et al.*, 2003). Hypoxia may be generated by itself or be also a consequence of inflammation; however, it does not necessarily cause inflammation, in fact hypoxia may even attenuate inflammation via upregulation of HIF and suppression of IL-Iβ-induced NF-Kβ activity, as shown by Scholz et al (2013) in HeLa cells under hydroxylase inhibition (Scholz *et al.*, 2013). In chronic stages of renal disease, hypoxia generates a continuous fibrogenic stimuli (Fine *et al.*, 2008), without the presence of high levels of inflammation, as hypoxia is being perpetuated not via inflammation but by the lack of vascular network and substitution of functional parenchyma by collagen fibrils.

Perhaps, in glomeruli, the attenuation of inflammation via upregulation of the HIF system may be more evident in the glomeruli, explaining the lack of glomerular damage in the cat. Moreover, it has been shown that HIF-1α may contribute to glomerular protection, as seen in murine glomerular endothelial cells via podocytes (Wang *et al.*, 2015). Hence, if the HIF system is more active in the feline glomeruli than the interstitial space, the possibility of the HIF system involvement in feline glomerular protection under hypoxaemic environments could be feasible. This may explain the lack of sclerosis and TG2 expression in the intraglomerular mesangial area when compared to the interstitial space, as hypothesised in the rat.

In the tubulointerstitial area, hypoxia could precede inflammation acutely but in sub-acute and chronic stages of injury, hypoxia and inflammation may develop in parallel to each other albeit at different rates, according to the level of hypoxia. Inflammation by itself may not contribute importantly to the progression of CKD as much as hypoxia does. If this is correct, the longer the chronic kidney disease progression, the greater the tissue hypoxia, and therefore, the lower the level of inflammation. An Australian study in cats with CKD and degenerative joint disease on long-term meloxicam, showed that chronic treatment did not alter the life-span of the studied cats when compared to CKD cats without treatment (Gowan *et al.*, 2011),

perhaps suggesting that hypoxia is a more important actor than inflammation in late stages of renal disease and therefore anti-inflammatory treatment in stable CKD may be unable to provide any substantial benefit.

Inhibition of interstitial inflammation may be beneficial during acute kidney injury or at the very beginning of CKD. If inflammation is a prominent feature of acute renal disease then, reduction of inflammation may be beneficial in cats and humans with early renal injury to avoid the transition from AKI to CKD, or at least to reduce the fibrogenic consequences of AKI in the future development of renal fibrosis. This could be achieved via inhibition of direct NF-κβ pathway or time dependent inhibition of cyclooxygenase 2. It is well established that reduction of inflammation via inhibition of the COX pathway should be avoided in patients with kidney disease, due to the interaction with renal prostaglandins and the reduction of renal perfusion. Although this is a real concern in unstable hypotensive patients with AKI, the use of weak renal cyclooxygenase 2 (COX-2) inhibitors such as meloxicam (Engelhardt, 1996) might be beneficial in stabilised cases of acute renal injury. The modest anti-inflammatory effect of meloxicam on the kidney might be enough to provide an adequate balance between prostaglandin inhibition and the reduction of tubulointerstitial inflammation in stable-late AKI or soon after AKI resolution. However, extensive research in this area should be performed before attempting such approach

Inflammation and hypoxia phases in renal disease may indicate that the staging systems for CKD could include an estimated time for CKD maturation, considering AKI signs or at least the first identified signs of CKD as starting point. This may be highly relevant in the classification and treatment of cats with CKD. In naturally occurring feline CKD a close monitoring to detect asymptomatic AKI and early CKD could only be achieved if urinalysis, haematology and biochemistry analysis were evaluated on a regular basis (every 6 months) in feline patients before 13 years of age. Plasma and urine samples would have to be stored properly (liquid nitrogen or -80°C) for longitudinal retrospective studies at protein and RNA levels. Similar storage systems are required for terminal kidney tissue. Such a research biorepository could be funded by the pharmaceutical industry, government, veterinary insurance companies and small animal teaching hospitals, not necessarily in the UK.

Rabbit PolyclonalTG2 Antibody. The western blot analysis of cat kidney tissue, using a rabbit polyclonal TG2 antibody (rpTG2), detected an additional band at 83 kDa. However, the presence of an 83kDa protein firstly is not consistent with the

molecular weight of feline TG2 and secondly showed no increase in volume density for cats with azotemia. The visualisation of this band is mostly likely explained by cross-reactivity of the rabbit polyclonal antibody with cat factor XIIIa which has a molecular weight of 83-84 kDa (ENSFCAP00000014378) (Flicek *et al.*, 2014).

An alternative explanation could be differences in the glycosylation of the TG2 enzyme itself which cannot be discounted entirely although, no published information is available on either the carbohydrate content or potential glycosylation sites for cat TG2. The possibility that transglutaminase may be a glycoprotein has been raised by the sequence studies of Ikura et al (1988), using TG derived from guinea-pig liver, where the presence of 6 potential Asn-glycosylation sites was deduced from its DNA sequence (Ikura *et al.*, 1988). Earlier studies by Folk and Chung (1973) however, using guinea-pig TG, were unable to detect any carbohydrate content present in this protein (Folk *et al.*, 1973). At present therefore, there is little evidence to support the concept of TG from any species being a glycoprotein. So, the most plausible explanation for the presence of an 83kDa band on the cat kidney western blot would be cross reactivity of the polyclonal rabbit antibody to factor XIIIa present in residual blood stored within kidney tissue obtained at post-mortem.

Although the same rabbit polyclonal antibody was used to assess extracellular TG2 in cryostat sections in situ, there was no possibility of assessing both TG2 and factor XIIIa. Factor XIIIa is localized in blood plasma and the immunostaining technique (washing/fixation) removed blood plasma from tissue leaving just the TG2 attached to collagen proteins and other minor TG2 substrates. The quantification of TG2 in cryostat sections by immunofluorescence was therefore proposed to specifically target transglutaminase 2.

TG2 Degradation. One important issue and potential limitation of the cat kidney data presented in this thesis was the possibility of proteolytic degradation while the kidney remained within the deceased animal during the period between euthanasia and tissue harvesting post-mortem (potentially a period of up to 6 hours). Rapid cold preservation of tissue after euthanasia would be necessary to avoid potential degradation by natural proteases. Matrix metalloproteinases, for example, are enzymes responsible for extracellular matrix degradation (Birkedal-Hansen *et al.*, 1993). Membrane type-1 matrix metalloproteinase (MT1-MMP), a membrane activator of MMP-2 secretion, is involved in the proteolysis of TG2 at 3 different cleavage sites, reducing the activity of the TG2 enzyme (Belkin *et al.*, 2004). Some

degree of tissue degradation might be responsible for the lower correlation between renal function with TG activity than with TG2 protein in cat kidney tissue homogenates as evidenced by the detection of a 66 kDa band, compatible with an inactive fragment of TG2 (Belkin et al 2004), when western blots were performed using a TG2 selective antibody (BB7).

Non-Azotaemic Kidney Tissue. Both the early development of CKD and the presence of concomitant diseases remain a possibility for the non-azotaemic cat group. Their old age (11 to 23.7 years), low urine specific gravity (particularly in cats No 2 and No 5) together with other health issues might have affected renal structure and/or function either directly or indirectly. Cat No 2, more importantly, showed evidence of tissue damage supported by the presence of tubulointerstitial fibrosis and inflammation. The presence of a renal lymphoma was diagnosed in cat No 11, being detected in over 70% of the total kidney section. Interestingly, this sample also showed the lowest level of TG activity and protein for both total and extracellular transglutaminases. However, fibrosis in this sample was high, consistent with the low level of renal function (CKD stage 3). The low expression of TG activity in this kidney could have been due to non-adequate tissue preservation or low innate TG2 activity/expression secondary to renal lymphoma.

The association of cancer and transglutaminase 2 upregulation has previously been established in human glioblastoma, melanoma, pancreatic, ovarian, lung and mammary carcinoma (Mehta *et al.*, 2010). A link between renal cell carcinoma and high expression of TG2 has also been investigated in a xenograft model of rat (Ku *et al.*, 2014). The only evidence concerning the TG2 and cancer in the cat has been in mammary carcinoma where TG2 was also shown to be upregulated (Wakshlag *et al.*, 2006). For other renal cancers and TG2, no information in domestic felines is as yet available. Further assessment of feline renal tissue with CKD and renal lymphoma could be tested to evaluate if lymphoma itself, in contrast to other renal neoplasia, is able to maintain low TG2 expression whilst spreading throughout the kidney. Renal transglutaminase protein and enzyme activity were assumed to remain unaffected by the presence of non-renal metastasis. Cats No. 3, 5, 6, 8 and 11 were diagnosed with non-renal tumours in the stomach, liver, lung, bladder and intestine respectively.

8.4. Renal fibrosis (CKD / CAN) and the TG pathway in the man

In the human, antecedents associated with the increased risk to develop CKD are easy tracked when taking the clinical history of the patient. If a patient has a high level of CKD risk of factors, reduction of them may help in the reversal of the process in very early CKD. If factors are associated with evidence of renal damage (blood and urine analysis), then CKD can be staged followed by the treatment of comorbidity to slow the progression of the disease. Assessment of the reduction of glomerular filtration rate estimates the progression of the disease and it is important to re-evaluate patient and treat complications (Levey *et al.*, 2012). When kidney failure occurs, the patient will die if dialysis or kidney transplantation are not available. Kidney transplantation is the best long term therapeutic alternative. However, chronic allograft nephropathy, a version of CKD post-transplant, may occur. Consequences at any stages of CAN and CKD can cause complications and patients' death. The cardinal histopathological process in either CKD or CAN is renal fibrosis, which reduces GFR. This is represented as tubulointerstitial fibrosis and glomerulosclerosis. See Figure 8.3 for progression of renal fibrosis via CKD or CAN.

Transglutaminase 2 has been identify in the man in both diseases, in either the glomeruli or the tubulointerstitial space (Johnson *et al.*, 2004b; Johnson *et al.*, 2003). Different animal models in the rat have also shown the association and causality of TG2 on CKD (Huang *et al.*, 2009; Johnson *et al.*, 2007; Shweke *et al.*, 2008). However, CAN has been limited to just one animal association study (Shrestha *et al.*, 2014a). Therefore, in order to understand CAN in the man an interventional study using a Fisher to Lewis model of CAN was intended to be part of the current research project. However, due to unavailability of a TG2 inhibitory antibody, specific to the rat, just the establishment of the kidney transplant technique and the TG2 quantification was achieved. The technique description and the data generated regarding TG2 quantification in both rat strains are important foundation for the development of future CAN projects.

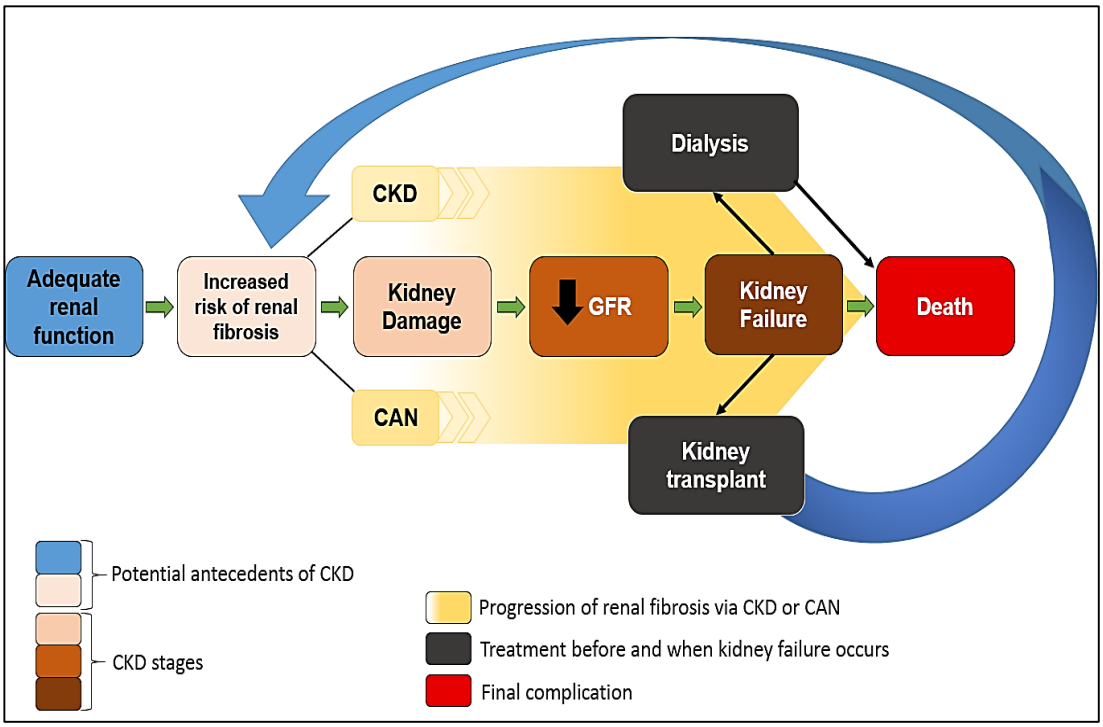

Figure 8.3: Development, progression and therapeutic options for renal fibrosis

Blue represents adequate renal function; pink, the risks to develop renal fibrosis; yellow, represents triggering, establishment and progression of renal fibrosis via CKD or CAN. Dark pink, brown and dark brown, different stages of CKD. Black, last resource treatment for CKD or CAN.

8.5. Comparative medicine between human and feline renal fibrosis

Even though human and non-human animal diseases overlaps tremendously, a communication between physicians and veterinarians is uncommon when approaching illnesses. Understanding a diseases according to each other's expertise allows a wider criteria for the development of research projects. Comparative medicine bridges both disciplines enhancing the understanding of diseases through the study of the similarities and differences in physiopathology amongst animals. Veterinary and medical science, together with molecular biology, is able to generate new treatments and diagnostic methods for the benefit of both animals and humans.

The study of CKD in the domestic cat is emerging. The International Renal Interest Society has boosted research to study feline acute and chronic kidney. As a result, a staging system similar to the one in humans has been developed. This staging system is expected to be further refined when the inclusion of more accurate GFR measurements occurs. The development of CKD staging system was a vital first step for the generation of evidence based veterinary medicine in this field; this is intended to facilitate the setting up of comparative research in renal fibrosis, which is not just limited to CKD, since CAN has been already identify in transplanted cats (De Cock *et al.*, 2004). Likewise, acute kidney disease and dialysis in cats could be very useful research platform for comparative medicine. Furthermore, the genome in the cat has been fully mapped and currently it is in process of refinement, opening the door to comparative genetics (Montague *et al.*, 2014).

8.6. Future Work.

The feline data presented in this thesis could have shown a higher statistical significance if a more rigid system of inclusion criteria had been used; for example, to differentiate non-azotaemic CKD from non-azotaemic tissue samples without CKD, and to rule out tissue samples suspicious of renal tumours.

In a future research project, it would be important to assess the TG pathway and fibrosis in all stages of CKD, separating groups based on differences in either histology or renal function rather than just the presence/absence of azotaemia. If results are obtained as in the present study, then further investigation should be performed to establish if hypoxia is a potential triggering factor in the cat for the TG

pathway up-regulation. To achieve this, analysis of HIF-1α and TG2 protein in renal tissue and urine could be studied. In tissue, glomerular HIF-1α and TG2 could be compared to tubulointerstitial HIF-1α in both cryostat sections and in tissue homogenates. This can be achieved by using micro-dissection, intraglomerular magnetic beads or tissue micro sieves. If HIF-1α is expressed in either tubulointerstitial and glomeruli in the cat kidney with CKD and this expression increase gradually along the progression of the disease, then it could be assumed that hypoxia is an important factor for the development of CKD in the cat. If the HIF-1α system on the other hand, is overexpressed in the glomeruli when compared to the tubulointerstitial area, together with a low expression in the glomerular TG pathway, it could be assumed that indeed HIF-1α is a protective glomerular mechanism under low oxygen tension environment. Furthermore, intra/extracellular HIF-1α / TG2 analysis in the rat model of RWI could be carried out to compare results. If results in the cat are similar to the results obtained in this model then, the RWI in the rat would be a more reliable model to undertake interventional studies for feline CKD.

Moreover, if the triad of hypoxia, inflammation and fibrosis are important to determine the maturation of CKD then the simultaneous evaluation of urinary markers such as TG2 (Da Silva *et al.*, 2013), KIM-1 and HIF-1α could be important to establish CKD maturation and even to develop or modify the current acute and chronic kidney disease staging system in cats.

8.7. Conclusion

CKD in the human and cat share many histological and physiopathological similarities. The study of differences however, such as glomerular resistance to the development of fibrosis in the cat may provide valuable evidence to understand glomerular disease in the human such as in diabetic glomerulosclerosis, considered at present a worldwide epidemic (Rossing, 2006). The study of naturally occurring CKD in the cat could lead to a reduction in the use of experimental laboratory animals, increase safety in the use of drugs during clinical trials, allow a wider variety of analysis due to availability of diseased kidney tissue and allow confirmation of findings from *in vitro* and *vivo* models. Veterinary medicine, on the other hand, would benefit from a stronger evidence based approach, strengthening veterinary basic science, which might accelerate the development of new treatments for domestic animals.

Evidence presented in this thesis showed that inhibition of the transglutaminase pathway may represent an important new target site to reduce both inflammation and accumulation of interstitial fibrosis. Reduction in renal fibrosis could be achieved by TG2 inhibition in the early stages of CKD, however a delay in the progression of CKD may be possible with TG2 inhibition in more mature forms of CKD.

"A finding in Veterinary Research is remarkable if it improves animal health. However, if that finding brings a substantial benefit to public health, it becomes outstanding" ACSL.

CHAPTER 9

References

Abuelo JG (2007). Normotensive ischemic acute renal failure. *N Engl J Med* **357**(8)**:** 797-805.

Acierno MJ (2011). Continuous renal replacement therapy in dogs and cats. *Vet Clin North Am Small Anim Pract* **41**(1)**:** 135-146.

Acland GM, Ray K, Mellersh CS, Gu W, Langston AA, Rine J*, et al.* (1998). Linkage analysis and comparative mapping of canine progressive rod-cone degeneration (prcd) establishes potential locus homology with retinitis pigmentosa (RP17) in humans. *Proc Natl Acad Sci U S A* **95**(6)**:** 3048-3053.

Acland GM, Ray K, Mellersh CS, Langston AA, Rine J, Ostrander EA*, et al.* (1999). A novel retinal degeneration locus identified by linkage and comparative mapping of canine early retinal degeneration. *Genomics* **59**(2)**:** 134-142.

Agnihotri N, Kumar S, Mehta K (2013). Tissue transglutaminase as a central mediator in inflammation-induced progression of breast cancer. *Breast Cancer Res* **15**(1)**:** 202.

Aguirre GD, Baldwin V, Pearce-Kelling S, Narfstrom K, Ray K, Acland GM (1998). Congenital stationary night blindness in the dog: common mutation in the RPE65 gene indicates founder effect. *Mol Vis* **4:** 23.

Ahmed A, Huang L, Raftery AT, Ahmed AK, Fahmy H, El Nahas AM*, et al.* (2004). Cyclosporine A sensitizes the kidney to tubulointerstitial fibrosis induced by renal warm ischemia. *Transplantation* **77**(5)**:** 686-692.

Ameratunga R, Winkelstein JA, Brody L, Binns M, Cork LC, Colombani P*, et al.* (1998). Molecular analysis of the third component of canine complement (C3) and identification of the mutation responsible for hereditary canine C3 deficiency. *J Immunol* **160**(6)**:** 2824-2830.

Anders H, Schlondorff D (2000). Murine models of renal disease: possibilities and problems in studies using mutant mice. *Exp Nephrol* **8**(4-5)**:** 181-193.

Arata S, Ohmi A, Mizukoshi F, Baba K, Ohno K, Setoguchi A*, et al.* (2005). Urinary transforming growth factor-beta1 in feline chronic renal failure. *J Vet Med Sci* **67**(12)**:** 1253-1255.

Arbour J, Blais MC, Carioto L, Sylvestre D (2012). Clinical leptospirosis in three cats (2001-2009). *J Am Anim Hosp Assoc* **48**(4)**:** 256-260.

Ausania F, White SA, Pocock P, Manas DM (2012). Kidney damage during organ recovery in donation after circulatory death donors: data from UK National Transplant Database. *Am J Transplant* **12**(4)**:** 932-936.

Azuma H, Nadeau K, Takada M, Mackenzie HS, Tilney NL (1997). Cellular and molecular predictors of chronic renal dysfunction after initial ischemia/reperfusion injury of a single kidney. *Transplantation* **64**(2)**:** 190-197.

Badr KF, Ichikawa I (1988). Prerenal failure: a deleterious shift from renal compensation to decompensation. *N Engl J Med* **319**(10)**:** 623-629.

Baek RC, Martin DR, Cox NR, Seyfried TN (2009). Comparative analysis of brain lipids in mice, cats, and humans with Sandhoff disease. *Lipids* **44**(3)**:** 197-205.

Bakir N, Sluiter WJ, Ploeg RJ, van Son WJ, Tegzess AM (1996). Primary renal graft thrombosis. *Nephrol Dial Transplant* **11**(1)**:** 140-147.

Barber PJ, Elliott J (1998). Feline chronic renal failure: calcium homeostasis in 80 cases diagnosed between 1992 and 1995. *J Small Anim Pract* **39**(3)**:** 108-116.

Barone GW, Conerly JM, Farley PC, Flanagan TL, Kron IL (1989). Assessing clamp-related vascular injuries by measurement of associated vascular dysfunction. *Surgery* **105**(4)**:** 465-471.

Bartels H, Cikes M (1969). [Chromogens in the creatinine determination of Jaffe]. *Clin Chim Acta* **26**(1)**:** 1-10.

Bartges J (2012). Chronic kidney disease in dogs and cats. *Vet Clin North Am Small Anim Pract* **42**(4)**:** 669-692.

Bartges JaPD (ed) (2011). *Nephrology and Urology of Small Animals*. John Wiley & Sons.

Bartlett PC, Van Buren JW, Bartlett AD, Zhou C (2010). Case-control study of risk factors associated with feline and canine chronic kidney disease. *Vet Med Int* **2010**.

Basile DP (2007). The endothelial cell in ischemic acute kidney injury: implications for acute and chronic function. *Kidney Int* **72**(2)**:** 151-156.

Basile DP (2004). Rarefaction of peritubular capillaries following ischemic acute renal failure: a potential factor predisposing to progressive nephropathy. *Curr Opin Nephrol Hypertens* **13**(1)**:** 1-7.

Basile DP, Donohoe D, Roethe K, Osborn JL (2001a). Renal ischemic injury results in permanent damage to peritubular capillaries and influences long-term function. *Am J Physiol Renal Physiol* **281**(5)**:** F887-899.

Basile DP, Donohoe D, Roethe K, Osborn JL (2001b). Renal ischemic injury results in permanent damage to peritubular capillaries and influences long-term function. *American Journal of Physiology-Renal Physiology* **281**(5)**:** F887-F899.

Basile DP, Donohoe DL, Phillips SA, Frisbee JC (2005). Enhanced skeletal muscle arteriolar reactivity to ANG II after recovery from ischemic acute renal failure. *Am J Physiol Regul Integr Comp Physiol* **289**(6)**:** R1770-1776.

Basile DP, Donohoe DL, Roethe K, Mattson DL (2003). Chronic renal hypoxia after acute ischemic injury: effects of L-arginine on hypoxia and secondary damage. *Am J Physiol Renal Physiol* **284**(2)**:** F338-348.

Basile DP, Rovak JM, Martin DR, Hammerman MR (1996). Increased transforming growth factor-beta 1 expression in regenerating rat renal tubules following ischemic injury. *Am J Physiol* **270**(3 Pt 2)**:** F500-509.

Baumgartner W, Golenhofen N, Weth A, Hiiragi T, Saint R, Griffin M*, et al.* (2004). Role of transglutaminase 1 in stabilisation of intercellular junctions of the vascular endothelium. *Histochem Cell Biol* **122**(1)**:** 17-25.

Becker GJ, Hewitson TD (2013). Animal models of chronic kidney disease: useful but not perfect. *Nephrol Dial Transplant* **28**(10)**:** 2432-2438.

Behrend EN, Grauer GF, Mani I, Groman RP, Salman MD, Greco DS (1996). Hospital-acquired acute renal failure in dogs: 29 cases (1983-1992). *J Am Vet Med Assoc* **208**(4)**:** 537-541.

Belkin AM, Zemskov EA, Hang J, Akimov SS, Sikora S, Strongin AY (2004). Cell-surface-associated tissue transglutaminase is a target of MMP-2 proteolysis. *Biochemistry* **43**(37)**:** 11760-11769.

Bellomo R, Kellum JA, Ronco C (2012). Acute kidney injury. *Lancet* **380**(9843)**:** 756-766.

Benigni A, Morigi M, Remuzzi G (2010). Kidney regeneration. *Lancet* **375**(9722)**:** 1310-1317.

Berent AC (2011). Ureteral obstructions in dogs and cats: a review of traditional and new interventional diagnostic and therapeutic options. *J Vet Emerg Crit Care (San Antonio)* **21**(2)**:** 86-103.

Bernassola F, Federici M, Corazzari M, Terrinoni A, Hribal ML, De Laurenzi V*, et al.* (2002). Role of transglutaminase 2 in glucose tolerance: knockout mice studies and a putative mutation in a MODY patient. *FASEB J* **16**(11)**:** 1371-1378.

Bernhardt WM, Schmitt R, Rosenberger C, Munchenhagen PM, Grone HJ, Frei U*, et al.* (2006). Expression of hypoxia-inducible transcription factors in developing human and rat kidneys. *Kidney Int* **69**(1)**:** 114-122.

Bernsteen L, Gregory CR, Kyles AE, Wooldridge JD, Valverde CR (2000). Renal transplantation in cats. *Clin Tech Small Anim Pract* **15**(1)**:** 40-45.

Bernsteen L, Gregory CR, Pollard RE, Griffey SM, Menwrath V (1999). Comparison of two surgical techniques for renal transplantation in cats. *Vet Surg* **28**(6)**:** 417-420.

Beuchat CA, Braun EJ (1988). Allometry of the kidney: implications for the ontogeny of osmoregulation. *Am J Physiol* **255**(5 Pt 2)**:** R760-767.

Birkedal-Hansen H, Moore WG, Bodden MK, Windsor LJ, Birkedal-Hansen B, DeCarlo A*, et al.* (1993). Matrix metalloproteinases: a review. *Crit Rev Oral Biol Med* **4**(2)**:** 197-250.

Bohle A, von Gise H, Mackensen-Haen S, Stark-Jakob B (1981). The obliteration of the postglomerular capillaries and its influence upon the function of both glomeruli and tubuli. Functional interpretation of morphologic findings. *Klin Wochenschr* **59**(18)**:** 1043-1051.

Bonventre JV (1993). Mechanisms of ischemic acute renal-failure. *Kidney International* **43**(5)**:** 1160-1178.

Bonventre JV, Weinberg JM (1992). Kidney preservation ex vivo for transplantation. *Annu Rev Med* **43:** 523-553.

Boor P, Sebekova K, Ostendorf T, Floege J (2007). Treatment targets in renal fibrosis. *Nephrol Dial Transplant* **22**(12)**:** 3391-3407.

Border WA, Noble NA (1998). Interactions of transforming growth factor-beta and angiotensin II in renal fibrosis. *Hypertension* **31**(1 Pt 2)**:** 181-188.

Bovee KC, Joyce T, Reynolds R, Segal S (1978). The fanconi syndrome in Basenji dogs: a new model for renal transport defects. *Science* **201**(4361)**:** 1129-1131.

Boyd LM, Langston C, Thompson K, Zivin K, Imanishi M (2008). Survival in cats with naturally occurring chronic kidney disease (2000-2002). *J Vet Intern Med* **22**(5)**:** 1111-1117.

Bradley OC (1927). What is Comparative Medicine? *Proc R Soc Med* **21**(1)**:** 129-134.

Brasile L, Green E, Haisch C (1997a). Ex vivo resuscitation of kidneys after postmortem warm ischemia. *ASAIO J* **43**(5)**:** M427-430.

Brasile L, Green E, Haisch C (1997b). Warm ex vivo perfusion prevents reperfusion injury in warm ischemically damaged kidneys. *Transplant Proc* **29**(8)**:** 3422-3423.

Brenner BM, Lawler EV, Mackenzie HS (1996). The hyperfiltration theory: a paradigm shift in nephrology. *Kidney Int* **49**(6)**:** 1774-1777.

Brezis M, Rosen S (1995). Hypoxia of the renal medulla--its implications for disease. *N Engl J Med* **332**(10)**:** 647-655.

Brown DE, Thrall MA, Walkley SU, Wenger DA, Mitchell TW, Smith MO*, et al.* (1994). Feline Niemann-Pick disease type C. *Am J Pathol* **144**(6)**:** 1412-1415.

Cachat F, Lange-Sperandio B, Chang AY, Kiley SC, Thornhill BA, Forbes MS*, et al.* (2003). Ureteral obstruction in neonatal mice elicits segment-specific tubular cell responses leading to nephron loss. *Kidney Int* **63**(2)**:** 564-575.

Cameron ME, Casey RA, Bradshaw JW, Waran NK, Gunn-Moore DA (2004). A study of environmental and behavioural factors that may be associated with feline idiopathic cystitis. *J Small Anim Pract* **45**(3)**:** 144-147.

Cao L, Petrusca DN, Satpathy M, Nakshatri H, Petrache I, Matei D (2008). Tissue transglutaminase protects epithelial ovarian cancer cells from cisplatin-induced apoptosis by promoting cell survival signaling. *Carcinogenesis* **29**(10)**:** 1893-1900.

Carden DL, Granger DN (2000). Pathophysiology of ischaemia-reperfusion injury. *Journal of Pathology* **190**(3)**:** 255-266.

Cecka JM (2000). The UNOS Scientific Renal Transplant Registry--2000. *Clin Transpl***:** 1-18.

Chadha V, Schaefer FS, Warady BA (2010). Dialysis-associated peritonitis in children. *Pediatr Nephrol* **25**(3)**:** 425-440.

Chakrabarti S, Syme HM, Brown CA, Elliott J (2013). Histomorphometry of feline chronic kidney disease and correlation with markers of renal dysfunction. *Vet Pathol* **50**(1)**:** 147-155.

Chakrabarti S, Syme HM, Elliott J (2012). Clinicopathological variables predicting progression of azotemia in cats with chronic kidney disease. *J Vet Intern Med* **26**(2)**:** 275-281.

Chatterjee PK, Patel NS, Kvale EO, Cuzzocrea S, Brown PA, Stewart KN*, et al.* (2002). Inhibition of inducible nitric oxide synthase reduces renal ischemia/reperfusion injury. *Kidney Int* **61**(3)**:** 862-871.

Chevalier RL, Thornhill BA, Forbes MS, Kiley SC (2010). Mechanisms of renal injury and progression of renal disease in congenital obstructive nephropathy. *Pediatr Nephrol* **25**(4).

Chew D, DiBartola SP, Schenck P (2011). Acute Kidney Disease. In: Sciences EH (ed)^(eds). *Canine and Feline Nephrology and Urology*, 2nd edn. p^pp.

Clarke DD, Mycek MJ, Neidle A, Waelsch H (1959). The incorporation of amines into protein. *Archives of Biochemistry and Biophysics* **79:** 338-354.

Collard CD, Gelman S (2001). Pathophysiology, clinical manifestations, and prevention of ischemia-reperfusion injury. *Anesthesiology* **94**(6)**:** 1133-1138.

Collard CD, Lekowski R, Jordan JE, Agah A, Stahl GL (1999). Complement activation following oxidative stress. *Mol Immunol* **36**(13-14)**:** 941-948.

Copeland KR, Yatscoff RW, Thliveris JA, Mehta A, Penner B (1987). Non-enzymatic glycation and altered renal structure and function in the diabetic rat. *Kidney Int* **32**(5)**:** 664-670.

Coresh J, Selvin E, Stevens LA, Manzi J, Kusek JW, Eggers P*, et al.* (2007). Prevalence of chronic kidney disease in the United States. *JAMA* **298**(17)**:** 2038-2047.

Cotter SM, Essex M (1977). Animal model: feline acute lymphoblastic leukemia and aplastic anemia. *Am J Pathol* **87**(1)**:** 265-268.

Cowgill LD (2011). Urea kinetics and intermittent dialysis prescription in small animals. *Vet Clin North Am Small Anim Pract* **41**(1)**:** 193-225.

Cowgill LD, James KM, Levy JK, Browne JK, Miller A, Lobingier RT*, et al.* (1998). Use of recombinant human erythropoietin for management of anemia in dogs and cats with renal failure. *J Am Vet Med Assoc* **212**(4)**:** 521-528.

Creely JJ, DiMari SJ, Howe AM, Haralson MA (1992). Effects of transforming growth factor-beta on collagen synthesis by normal rat kidney epithelial cells. *Am J Pathol* **140**(1)**:** 45-55.

Cummings BJ, Su JH, Cotman CW, White R, Russell MJ (1993). Beta-amyloid accumulation in aged canine brain: a model of early plaque formation in Alzheimer's disease. *Neurobiol Aging* **14**(6)**:** 547-560.

Horton R (ed) (2013). Urinary transglutaminase 2 as a potential biomarker of chronic kidney disease detection and progression. *Spring Meeting for Clinician Scientists in Training*. The Lancet. p S33.

Dager W (2008). Acute Renal Failure. In: DiPiro J (ed)^(eds). *Pharmacotherapy: A Pathophysiologic Approach*, 8 edn: McGraw Hill. p^pp 2700.

Darling IM, Morris ME (1991). Evaluation of "true" creatinine clearance in rats reveals extensive renal secretion. *Pharm Res* **8**(10)**:** 1318-1322.

Daughart.Tm, Ueki IF, Mercer PF, Brenner BM (1974). DYNAMICS OF GLOMERULAR ULTRAFILTRATION IN RAT .5. RESPONSE TO ISCHEMIC-INJURY. *Journal of Clinical Investigation* **53**(1)**:** 105-116.

Daugharty TM, Brenner BM (1975). REVERSIBLE HEMODYNAMIC DEFECT IN GLOMERULAR-FILTRATION RATE AFTER ISCHEMIC-INJURY. *American Journal of Physiology* **228**(5)**:** 1436-1439.

De Cock HE, Kyles AE, Griffey SM, Bernsteen L, Gregory CR (2004). Histopathologic findings and classification of feline renal transplants. *Vet Pathol* **41**(3)**:** 244-256.

de Groot H, Rauen U (2007). Ischemia-reperfusion injury: processes in pathogenetic networks: a review. *Transplant Proc* **39**(2)**:** 481-484.

De Laurenzi V, Melino G (2001). Gene disruption of tissue transglutaminase. *Mol Cell Biol* **21**(1)**:** 148-155.

Debelle FD, Nortier JL, De Prez EG, Garbar CH, Vienne AR, Salmon IJ*, et al.* (2002). Aristolochic acids induce chronic renal failure with interstitial fibrosis in salt-depleted rats. *J Am Soc Nephrol* **13**(2)**:** 431-436.

Delbridge MS, Shrestha BM, Raftery AT, El Nahas AM, Haylor JL (2007). The effect of body temperature in a rat model of renal ischemia-reperfusion injury. *Transplant Proc* **39**(10)**:** 2983-2985.

Dempster WJ, Joekes AM (1953). Functional studies of the kidney autotransplanted to the neck of dogs. *Acta Med Scand* **147**(2)**:** 99-118.

Desmouliere A, Chaponnier C, Gabbiani G (2005). Tissue repair, contraction, and the myofibroblast. *Wound Repair and Regeneration* **13**(1)**:** 7-12.

Devarajan P (2005). Cellular and molecular derangements in acute tubular necrosis. *Curr Opin Pediatr* **17**(2)**:** 193-199.

Devarajan P (2006). Update on mechanisms of ischemic acute kidney injury. *J Am Soc Nephrol* **17**(6)**:** 1503-1520.

Di Donato A, Ghiggeri GM, Di Duca M, Jivotenko E, Acinni R, Campolo J*, et al.* (1997). Lysyl oxidase expression and collagen cross-linking during chronic adriamycin nephropathy. *Nephron* **76**(2)**:** 192-200.

DiBartola SP, Rutgers HC, Zack PM, Tarr MJ (1987). Clinicopathologic findings associated with chronic renal disease in cats: 74 cases (1973-1984). *J Am Vet Med Assoc* **190**(9)**:** 1196-1202.

DiBartola SP, Tarr MJ, Benson MD (1986). Tissue distribution of amyloid deposits in Abyssinian cats with familial amyloidosis. *J Comp Pathol* **96**(4)**:** 387-398.

Dickson MC, Martin JS, Cousins FM, Kulkarni AB, Karlsson S, Akhurst RJ (1995). Defective haematopoiesis and vasculogenesis in transforming growth factor-beta 1 knock out mice. *Development* **121**(6)**:** 1845-1854.

Eardley KS, Kubal C, Zehnder D, Quinkler M, Lepenies J, Savage CO*, et al.* (2008). The role of capillary density, macrophage infiltration and interstitial scarring in the pathogenesis of human chronic kidney disease. *Kidney Int* **74**(4)**:** 495-504.

Eatroff AE, Langston CE, Chalhoub S, Poeppel K, Mitelberg E (2011). Long-term outcome of cats and dogs with acute kidney injury treated with intermittent hemodialysis: 135 cases (1997-2010). *J Am Vet Med Assoc* **241**(11)**:** 1471-1478.

Eddy AA (2000). Molecular basis of renal fibrosis. *Pediatr Nephrol* **15**(3-4)**:** 290-301.

Efstratiadis G, Divani M, Katsioulis E, Vergoulas G (2009). Renal fibrosis. *Hippokratia* **13**(4)**:** 224-229.

Elliott J, Barber PJ (1998). Feline chronic renal failure: clinical findings in 80 cases diagnosed between 1992 and 1995. *J Small Anim Pract* **39**(2)**:** 78-85.

Elliott J, Grauer G (2007). Manual of canine and feline nephrology and urology BSAVA manual of small animal nephrology and urology. In: Association BSAV (ed)^(eds). *BSAVA manual of small animal nephrology and urology*, 2nd edn. London. p^pp 298.

Engelhardt G (1996). Pharmacology of meloxicam, a new non-steroidal anti-inflammatory drug with an improved safety profile through preferential inhibition of COX-2. *Br J Rheumatol* **35 Suppl 1:** 4-12.

Erdely A, Wagner L, Muller V, Szabo A, Baylis C (2003). Protection of wistar furth rats from chronic renal disease is associated with maintained renal nitric oxide synthase. *J Am Soc Nephrol* **14**(10)**:** 2526-2533.

Fabiny DL, Ertingshausen G (1971). Automated reaction-rate method for determination of serum creatinine with the CentrifiChem. *Clin Chem* **17**(8)**:** 696-700.

Falasca L, Iadevaia V, Ciccosanti F, Melino G, Serafino A, Piacentini M (2005). Transglutaminase type II is a key element in the regulation of the anti-inflammatory response elicited by apoptotic cell engulfment. *J Immunol* **174**(11)**:** 7330-7340.

Farrington K, Hodsman A, Casula A, Ansell D, Feehally J (2009). UK Renal Registry 11th Annual Report (December 2008): Chapter 4 ESRD prevalent rates in 2007 in the UK: national and centre-specific analyses. *Nephron Clin Pract* **111 Suppl 1:** c43-68.

Fellstrom (2003). Donor Antigen-Independent Risk Factors for Chronic Allograft Nephropathy. *Transplantation Reviews* **17**(2)**:** 61-63.

Fesus L, Thomazy V (1988). Searching for the function of tissue transglutaminase: its possible involvement in the biochemical pathway of programmed cell death. *Adv Exp Med Biol* **231:** 119-134.

Filiano AJ, Bailey CD, Tucholski J, Gundemir S, Johnson GV (2008). Transglutaminase 2 protects against ischemic insult, interacts with HIF1beta, and attenuates HIF1 signaling. *FASEB J* **22**(8)**:** 2662-2675.

Fine LG, Norman JT (2008). Chronic hypoxia as a mechanism of progression of chronic kidney diseases: from hypothesis to novel therapeutics. *Kidney Int* **74**(7)**:** 867-872.

Finn WF (1993). Recovery from acute renal failure. In: Lazarus J, Brenner BM (ed)^(eds). *Acute Renal Failure*, 3rd ed. edn. New York. p^pp 553-596.

Fisher M, Jones RA, Huang LH, Haylor JL, El Nahas M, Griffin M*, et al.* (2009). Modulation of tissue transglutaminase in tubular epithelial cells alters extracellular matrix levels: A potential mechanism of tissue scarring. *Matrix Biology* **28**(1)**:** 20-31.

Fitch WM (1970). Distinguishing homologous from analogous proteins. *Syst Zool* **19**(2)**:** 99-113.

Flicek P, Amode MR, Barrell D, Beal K, Billis K, Brent S*, et al.* (2014). Ensembl 2014. *Nucleic Acids Res* **42**(Database issue)**:** D749-755.

Flores J, DiBona DR, Beck CH, Leaf A (1972). The role of cell swelling in ischemic renal damage and the protective effect of hypertonic solute. *J Clin Invest* **51**(1)**:** 118-126.

Folk JE, Chung SI (1973). Molecular and catalytic properties of transglutaminases. *Adv Enzymol Relat Areas Mol Biol* **38:** 109-191.

Folk JE, Finlayson JS (1977). The epsilon-(gamma-glutamyl)lysine crosslink and the catalytic role of transglutaminases. *Adv Protein Chem* **31:** 1-133.

Forbes JM, Hewitson TD, Becker GJ, Jones CL (2000). Ischemic acute renal failure: long-term histology of cell and matrix changes in the rat. *Kidney Int* **57**(6)**:** 2375-2385.

Fox JG, Perkins S, Yan L, Shen Z, Attardo L, Pappo J (1996). Local immune response in Helicobacter pylori-infected cats and identification of H. pylori in saliva, gastric fluid and faeces. *Immunology* **88**(3)**:** 400-406.

Fox PR, Liu SK, Maron BJ (1995). Echocardiographic assessment of spontaneously occurring feline hypertrophic cardiomyopathy. An animal model of human disease. *Circulation* **92**(9)**:** 2645-2651.

Fox PR, Maron BJ, Basso C, Liu SK, Thiene G (2000). Spontaneously occurring arrhythmogenic right ventricular cardiomyopathy in the domestic cat: A new animal model similar to the human disease. *Circulation* **102**(15)**:** 1863-1870.

Freudlsperger C, Bian Y, Contag Wise S, Burnett J, Coupar J, Yang X*, et al.* (2013). TGF-beta and NF-kappaB signal pathway cross-talk is mediated through TAK1 and SMAD7 in a subset of head and neck cancers. *Oncogene* **32**(12)**:** 1549-1559.

Freund KF, Doshi KP, Gaul SL, Claremon DA, Remy DC, Baldwin JJ*, et al.* (1994). Transglutaminase inhibition by 2-[(2-oxopropyl)thio]imidazolium derivatives: mechanism of factor XIIIa inactivation. *Biochemistry* **33**(33)**:** 10109-10119.

Frisbie DD, McIlwraith CW (2000). Evaluation of gene therapy as a treatment for equine traumatic arthritis and osteoarthritis. *Clin Orthop Relat Res*(379 Suppl)**:** S273-287.

Fyfe JC, Kurzhals RL, Lassaline ME, Henthorn PS, Alur PR, Wang P*, et al.* (1999). Molecular basis of feline beta-glucuronidase deficiency: an animal model of mucopolysaccharidosis VII. *Genomics* **58**(2)**:** 121-128.

Gagliardini E, Benigni A (2014). Drugs to foster kidney regeneration in experimental animals and humans. *Nephron Exp Nephrol* **126**(2)**:** 91.

Galin FS, Chrisman CL, Cook JR, Jr., Xu L, Jackson PL, Noerager BD*, et al.* (2007). Possible therapeutic vaccines for canine myasthenia gravis: implications for the human disease and associated fatigue. *Brain Behav Immun* **21**(3)**:** 323-331.

Gandhi M, Olson JL, Meyer TW (1998). Contribution of tubular injury to loss of remnant kidney function. *Kidney international* **54**(4)**:** 1157-1165.

Gaudry CA, Verderio E, Jones RA, Smith C, Griffin M (1999). Tissue transglutaminase is an important player at the surface of human endothelial cells: Evidence for its externalization and its colocalization with the beta(1) integrin. *Experimental Cell Research* **252**(1)**:** 104-113.

Geddes RF, Finch NC, Syme HM, Elliott J (2013). The role of phosphorus in the pathophysiology of chronic kidney disease. *J Vet Emerg Crit Care (San Antonio)* **23**(2)**:** 122-133.

Gharahkhani P, O'Leary CA, Kyaw-Tanner M, Sturm RA, Duffy DL (2011). A non-synonymous mutation in the canine Pkd1 gene is associated with autosomal dominant polycystic kidney disease in Bull Terriers. *PLoS One* **6**(7)**:** e22455.

Gilbert J, Nfon CK, Makepeace BL, Njongmeta LM, Hastings IM, Pfarr KM*, et al.* (2005). Antibiotic chemotherapy of onchocerciasis: in a bovine model, killing of adult parasites requires a sustained depletion of endosymbiotic bacteria (Wolbachia species). *J Infect Dis* **192**(8)**:** 1483-1493.

Gingery A, Bradley EW, Pederson L, Ruan M, Horwood NJ, Oursler MJ (2008). TGF-beta coordinately activates TAK1/MEK/AKT/NFkB and SMAD pathways to promote osteoclast survival. *Exp Cell Res* **314**(15)**:** 2725-2738.

Giovannetti S, Biagini M, Balestri P, Navalesi R, Giagnoni P, De Matteis A*, et al.* (1969). Uraemia-like syndrome in dogs chronically intoxicated with methylguanidine and creatinine. *Clinical science* **36**(3)**:** 445.

Go AS, Chertow GM, Fan D, McCulloch CE, Hsu CY (2004). Chronic kidney disease and the risks of death, cardiovascular events, and hospitalization. *N Engl J Med* **351**(13)**:** 1296-1305.

Gobe GC, Johnson DW (2007). Distal tubular epithelial cells of the kidney: Potential support for proximal tubular cell survival after renal injury. *Int J Biochem Cell Biol* **39**(9)**:** 1551-1561.

Goldman MH, Tilney NL, Vineyard GC, Laks H, Kahan MG, Wilson RE (1975). A twenty year survey of arterial complications of renal transplantation. *Surg Gynecol Obstet* **141**(5)**:** 758-760.

Gorriz JL, Martinez-Castelao A (2012). Proteinuria: detection and role in native renal disease progression. *Transplant Rev (Orlando)* **26**(1)**:** 3-13.

Goto Y, Uchio-Yamada K, Anan S, Yamamoto Y, Ogura A, Manabe N (2005). Transforming growth factor-beta1 mediated up-regulation of lysyl oxidase in the kidneys of hereditary nephrotic mouse with chronic renal fibrosis. *Virchows Arch* **447**(5)**:** 859-868.

Gowan RA, Baral RM, Lingard AE, Catt MJ, Stansen W, Johnston L*, et al.* (2012). A retrospective analysis of the effects of meloxicam on the longevity of aged cats with and without overt chronic kidney disease. *J Feline Med Surg* **14**(12)**:** 876-881.

Gowan RA, Lingard AE, Johnston L, Stansen W, Brown SA, Malik R (2011). Retrospective case-control study of the effects of long-term dosing with meloxicam on renal function in aged cats with degenerative joint disease. *J Feline Med Surg* **13**(10)**:** 752-761.

Grassmann A, Gioberge S, Moeller S, Brown G (2005). ESRD patients in 2004: global overview of patient numbers, treatment modalities and associated trends. *Nephrol Dial Transplant* **20**(12)**:** 2587-2593.

Greene JP, Lefebvre SL, Wang M, Yang M, Lund EM, Polzin DJ (2014). Risk factors associated with the development of chronic kidney disease in cats evaluated at primary care veterinary hospitals. *J Am Vet Med Assoc* **244**(3)**:** 320-327.

Griffin M, Casadio R, Bergamini CM (2002). Transglutaminases: Nature's biological glues. *Biochemical Journal* **368:** 377-396.

Grinyo JM, Saval N, Campistol JM, Group IS (2011). Clinical assessment and determinants of chronic allograft nephropathy in maintenance renal transplant patients. *Nephrol Dial Transplant* **26**(11)**:** 3750-3755.

Gunaratnam L, Bonventre JV (2009). HIF in kidney disease and development. *J Am Soc Nephrol* **20**(9)**:** 1877-1887.

Gundemir S, Colak G, Tucholski J, Johnson GV (2012). Transglutaminase 2: a molecular Swiss army knife. *Biochim Biophys Acta* **1823**(2)**:** 406-419.

Gupta M, Greenberg CS, Eckman DM, Sane DC (2007). Arterial vimentin is a transglutaminase substrate: A link between vasomotor activity and remodeling? *Journal of Vascular Research* **44**(5)**:** 339-344.

Haas M (2014). Chronic allograft nephropathy or interstitial fibrosis and tubular atrophy: what is in a name? *Curr Opin Nephrol Hypertens* **23**(3)**:** 245-250.

Haase VH (2006). Hypoxia-inducible factors in the kidney. *Am J Physiol Renal Physiol* **291**(2)**:** F271-281.

Habenicht LM, Webb TL, Clauss LA, Dow SW, Quimby JM (2013). Urinary cytokine levels in apparently healthy cats and cats with chronic kidney disease. *J Feline Med Surg* **15**(2)**:** 99-104.

Halloran P, Aprile M (1988). Factors influencing early renal function in cadaver kidney transplants. A case-control study. *Transplantation* **45**(1)**:** 122-127.

Hang J, Zemskov EA, Lorand L, Belkin AM (2005). Identification of a novel recognition sequence for fibronectin within the NH2-terminal beta-sandwich domain of tissue transglutaminase. *Journal of Biological Chemistry* **280**(25)**:** 23675-23683.

Hardy WD, Jr., Hess PW, MacEwen EG, McClelland AJ, Zuckerman EE, Essex M*, et al.* (1976). Biology of feline leukemia virus in the natural environment. *Cancer Res* **36**(2 pt 2)**:** 582-588.

Haroon ZA, Hettasch JM, Lai TS, Dewhirst MW, Greenberg CS (1999a). Tissue transglutaminase is expressed, active, and directly involved in rat dermal wound healing and angiogenesis. *FASEB J* **13**(13)**:** 1787-1795.

Haroon ZA, Hettasch JM, Lai TS, Dewhirst MW, Greenberg CS (1999b). Tissue transglutaminase is expressed, active, and directly involved in rat dermal wound healing and angiogenesis. *Faseb Journal* **13**(13)**:** 1787-1795.

Harper PA, Healy PJ, Dennis JA (1989). Animal model of human disease. Citrullinemia (argininosuccinate synthetase deficiency). *Am J Pathol* **135**(6)**:** 1213-1215.

Haskins ME, Desnick RJ, DiFerrante N, Jezyk PF, Patterson DF (1984). Beta-glucuronidase deficiency in a dog: a model of human mucopolysaccharidosis VII. *Pediatr Res* **18**(10)**:** 980-984.

Haskins ME, Jezyk PF, Desnick RJ, Patterson DF (1981). Animal model of human disease: Mucopolysaccharidosis VI Maroteaux-Lamy syndrome, Arylsulfatase B-deficient mucopolysaccharidosis in the Siamese cat. *Am J Pathol* **105**(2)**:** 191-193.

He X, Li CM, Simonaro CM, Wan Q, Haskins ME, Desnick RJ*, et al.* (1999). Identification and characterization of the molecular lesion causing mucopolysaccharidosis type I in cats. *Mol Genet Metab* **67**(2)**:** 106-112.

Henson MS, O'Brien TD (2006). Feline models of type 2 diabetes mellitus. *ILAR J* **47**(3)**:** 234-242.

Henthorn PS, Liu J, Gidalevich T, Fang J, Casal ML, Patterson DF*, et al.* (2000). Canine cystinuria: polymorphism in the canine SLC3A1 gene and identification of a nonsense mutation in cystinuric Newfoundland dogs. *Hum Genet* **107**(4)**:** 295-303.

Heyman SN, Khamaisi M, Rosen S, Rosenberger C (2008). Renal parenchymal hypoxia, hypoxia response and the progression of chronic kidney disease. *Am J Nephrol* **28**(6)**:** 998-1006.

Higgins DF, Kimura K, Bernhardt WM, Shrimanker N, Akai Y, Hohenstein B*, et al.* (2007). Hypoxia promotes fibrogenesis in vivo via HIF-1 stimulation of epithelial-to-mesenchymal transition. *J Clin Invest* **117**(12)**:** 3810-3820.

Higgins DF, Kimura K, Iwano M, Haase VH (2008). Hypoxia-inducible factor signaling in the development of tissue fibrosis. *Cell Cycle* **7**(9)**:** 1128-1132.

Hirata ES, Baghin MF, Pereira RI, Alves Filho G, Udelsmann A (2009). Influence of the anesthetic technique on the hemodynamic changes in renal transplantation: a retrospective study. *Rev Bras Anestesiol* **59**(2)**:** 166-176.

Hood JC, Savige J, Seymour AE, Dowling J, Martinello P, Colville D*, et al.* (2000). Ultrastructural appearance of renal and other basement membranes in the Bull terrier model of autosomal dominant hereditary nephritis. *Am J Kidney Dis* **36**(2)**:** 378-391.

Hoppe A, Swenson L, Jonsson L, Hedhammar A (1990). Progressive nephropathy due to renal dysplasia in shih tzu dogs in Sweden: A clinical pathological and genetic study. *Journal of Small Animal Practice* **31**(2)**:** 83-91.

Huang L, Haylor JL, Fisher M, Hau Z, El Nahas AM, Griffin M*, et al.* (2010). Do changes in transglutaminase activity alter latent transforming growth factor beta activation in experimental diabetic nephropathy? *Nephrol Dial Transplant* **25**(12)**:** 3897-3910.

Huang L, Haylor JL, Hau Z, Jones RA, Vickers ME, Wagner B*, et al.* (2009). Transglutaminase inhibition ameliorates experimental diabetic nephropathy. *Kidney Int* **76**(4)**:** 383-394.

Hughson MD, Johnson K, Young RJ, Hoy WE, Bertram JF (2002). Glomerular size and glomerulosclerosis: relationships to disease categories, glomerular solidification, and ischemic obsolescence. *Am J Kidney Dis* **39**(4)**:** 679-688.

Hunter DJ (2005). Gene-environment interactions in human diseases. *Nat Rev Genet* **6**(4)**:** 287-298.

Hynes RO (2009). The extracellular matrix: not just pretty fibrils. *Science* **326**(5957)**:** 1216-1219.

Ientile R, Caccamo D, Griffin M (2007). Tissue transglutaminase and the stress response. *Amino Acids* **33**(2)**:** 385-394.

Ikura K, Nasu T, Yokota H, Tsuchiya Y, Sasaki R, Chiba H (1988). Amino acid sequence of guinea pig liver transglutaminase from its cDNA sequence. *Biochemistry* **27**(8)**:** 2898-2905.

Izaguirre MF, Garcia-Sancho MN, Miranda LA, Tomas J, Casco VH (2008). Expression of cell adhesion molecules in the normal and T3 blocked development of the tadpole's kidney of Bufo arenarum (Amphibian, Anuran, Bufonidae). *Braz J Biol* **68**(3)**:** 561-569.

Jackson CN, Rogers AB, Maurer KJ, Lofgren JL, Fox JG, Marini RP (2008). Cystic renal disease in the domestic ferret. *Comp Med* **58**(2)**:** 161-167.

Jain S, Bicknell GR, Nicholson ML (2000a). Molecular changes in extracellular matrix turnover after renal ischaemia-reperfusion injury. *Br J Surg* **87**(9)**:** 1188-1192.

Jain S, Bicknell GR, Nicholson ML (2000b). Tacrolimus has less fibrogenic potential than cyclosporin A in a model of renal ischaemia-reperfusion injury. *Br J Surg* **87**(11)**:** 1563-1568.

Jain S, Bicknell GR, Whiting PH, Nicholson ML (2001). Rapamycin reduces expression of fibrosis-associated genes in an experimental model of renal ischaemia reperfusion injury. *Transplant Proc* **33**(1-2)**:** 556-558.

Jang GY, Jeon JH, Cho SY, Shin DM, Kim CW, Jeong EM*, et al.* (2010). Transglutaminase 2 suppresses apoptosis by modulating caspase 3 and NF-kappaB activity in hypoxic tumor cells. *Oncogene* **29**(3)**:** 356-367.

Jansen B, Thorner P, Baumal R, Valli V, Maxie MG, Singh A (1986). Samoyed hereditary glomerulopathy (SHG). Evolution of splitting of glomerular capillary basement membranes. *Am J Pathol* **125**(3)**:** 536-545.

Jantsch J, Chakravortty D, Turza N, Prechtel AT, Buchholz B, Gerlach RG*, et al.* (2008). Hypoxia and hypoxia-inducible factor-1 alpha modulate lipopolysaccharide-induced dendritic cell activation and function. *J Immunol* **180**(7)**:** 4697-4705.

Javadi S, Djajadiningrat-Laanen SC, Kooistra HS, van Dongen AM, Voorhout G, van Sluijs FJ*, et al.* (2005). Primary hyperaldosteronism, a mediator of progressive renal disease in cats. *Domest Anim Endocrinol* **28**(1)**:** 85-104.

Jensen J, Henik RA, Brownfield M, Armstrong J (1997). Plasma renin activity and angiotensin I and aldosterone concentrations in cats with hypertension associated with chronic renal disease. *Am J Vet Res* **58**(5)**:** 535-540.

Jiang B, Liu X, Chen H, Liu D, Kuang Y, Xing B*, et al.* (2010). Ischemic postconditioning attenuates renal ischemic/reperfusion injury in mongrel dogs. *Urology* **76**(6)**:** 1519 e1511-1517.

Jin X, Stamnaes J, Klock C, DiRaimondo TR, Sollid LM, Khosla C (2011). Activation of extracellular transglutaminase 2 by thioredoxin. *The Journal of biological chemistry* **286**(43)**:** 37866-37873.

Johnson GV, LeShoure R, Jr. (2004a). Immunoblot analysis reveals that isopeptide antibodies do not specifically recognize the epsilon-(gamma-glutamyl)lysine bonds formed by transglutaminase activity. *J Neurosci Methods* **134**(2)**:** 151-158.

Johnson KH (1970). Globoid leukodystrophy in the cat. *J Am Vet Med Assoc* **157**(12)**:** 2057-2064.

Johnson TS, Abo-Zenah H, Skill JN, Bex S, Wild G, Brown CB*, et al.* (2004b). Tissue transglutaminase: a mediator and predictor of chronic allograft nephropathy? *Transplantation* **77**(11)**:** 1667-1675.

Johnson TS, El-Koraie AF, Skill NJ, Baddour NM, El Nahas AM, Njloma M*, et al.* (2003). Tissue transglutaminase and the progression of human renal scarring. *Journal of the American Society of Nephrology : JASN* **14**(8)**:** 2052-2062.

Johnson TS, Fisher M, Haylor JL, Hau Z, Skill NJ, Jones R*, et al.* (2007). Transglutaminase inhibition reduces fibrosis and preserves function in experimental chronic kidney disease. *J Am Soc Nephrol* **18**(12)**:** 3078-3088.

Johnson TS, Griffin M, Thomas GL, Skill J, Cox A, Yang B*, et al.* (1997). The role of transglutaminase in the rat subtotal nephrectomy model of renal fibrosis. *J Clin Invest* **99**(12)**:** 2950-2960.

Johnson TS, Skill NJ, El Nahas AM, Oldroyd SD, Thomas GL, Douthwaite JA*, et al.* (1999). Transglutaminase transcription and antigen translocation in experimental renal scarring. *J Am Soc Nephrol* **10**(10)**:** 2146-2157.

Jonasdottir TJ, Mellersh CS, Moe L, Heggebo R, Gamlem H, Ostrander EA*, et al.* (2000). Genetic mapping of a naturally occurring hereditary renal cancer syndrome in dogs. *Proc Natl Acad Sci U S A* **97**(8)**:** 4132-4137.

Jones CL, Buch S, Post M, McCulloch L, Liu E, Eddy AA (1992). Renal extracellular matrix accumulation in acute puromycin aminonucleoside nephrosis in rats. *Am J Pathol* **141**(6)**:** 1381-1396.

Jones DB (1982). ULTRASTRUCTURE OF HUMAN ACUTE-RENAL-FAILURE. *Laboratory Investigation* **46**(3)**:** 254-264.

Jones DB (1981). ULTRASTRUCTURE OF HUMAN ACUTE-RENAL-FAILURE (ATN). *Laboratory Investigation* **44**(1)**:** A32-A32.

Kahn LH, Kaplan B, Steele JH (2007). Confronting zoonoses through closer collaboration between medicine and veterinary medicine (as 'one medicine'). *Vet Ital* **43**(1)**:** 5-19.

Kanellis J, Paizis K, Cox AJ, Stacker SA, Gilbert RE, Cooper ME*, et al.* (2002). Renal ischemia-reperfusion increases endothelial VEGFR-2 without increasing VEGF or VEGFR-1 expression. *Kidney Int* **61**(5)**:** 1696-1706.

Karatzas T, Santiago S, Xanthos T, de Faria W, Gandia C, Kostakis A (2007). An easy and safe model of kidney transplantation in rats. *Microsurgery* **27**(8)**:** 668-672.

Kawakami T, Mimura I, Shoji K, Tanaka T, Nangaku M (2014). Hypoxia and fibrosis in chronic kidney disease: crossing at pericytes. *Kidney Int Suppl (2011)* **4**(1)**:** 107-112.

Ke Q, Costa M (2006). Hypoxia-inducible factor-1 (HIF-1). *Molecular pharmacology* **70**(5)**:** 1469-1480.

Keith DS, Nichols GA, Gullion CM, Brown JB, Smith DH (2004). Longitudinal follow-up and outcomes among a population with chronic kidney disease in a large managed care organization. *Arch Intern Med* **164**(6)**:** 659-663.

Keller RC, Switonski M, Jorg H, Ladon D, Arnold S, Schelling C (1998). Chromosomal assignment of two putative canine keratin gene clusters. *Anim Genet* **29**(2)**:** 141-143.

Kerschen E, Hernandez I, Zogg M, Jia S, Hessner MJ, Fernandez JA*, et al.* (2010). Activated protein C targets CD8+ dendritic cells to reduce the mortality of endotoxemia in mice. *J Clin Invest* **120**(9)**:** 3167-3178.

Khalil N (1999). TGF-beta: from latent to active. *Microbes and Infection* **1**(15)**:** 1255-1263.

Khouri RK, Cooley BC, Kenna DM, Edstrom LE (1990). Thrombosis of microvascular anastomoses in traumatized vessels: fibrin versus platelets. *Plast Reconstr Surg* **86**(1)**:** 110-117.

Khraibi AA, Knox FG (1989). Effect of renal decapsulation on renal interstitial hydrostatic pressure and natriuresis. *Am J Physiol* **257**(1 Pt 2)**:** R44-48.

Kidder AC, Chew D (2009). Treatment options for hyperphosphatemia in feline CKD: what's out there? *J Feline Med Surg* **11**(11)**:** 913-924.

Kim DS, Kim B, Tahk H, Kim DH, Ahn ER, Choi C*, et al.* (2010). Transglutaminase 2 gene ablation protects against renal ischemic injury by blocking constant NF-kappaB activation. *Biochem Biophys Res Commun* **403**(3-4)**:** 479-484.

Kim DS, Park SS, Nam BH, Kim IH, Kim SY (2006). Reversal of drug resistance in breast cancer cells by transglutaminase 2 inhibition and nuclear factor-kappaB inactivation. *Cancer Res* **66**(22)**:** 10936-10943.

Kim JH, Choy HE, Nam KH, Park SC (2001). Transglutaminase-mediated crosslinking of specific core histone subunits and cellular senescence. *Ann N Y Acad Sci* **928:** 65-70.

Kim SY (2006). Transglutaminase 2 in inflammation. *Front Biosci* **11:** 3026-3035.

King JN, Gunn-Moore DA, Tasker S, Gleadhill A, Strehlau G, Benazepril in Renal Insufficiency in Cats Study G (2006). Tolerability and efficacy of benazepril in cats with chronic kidney disease. *J Vet Intern Med* **20**(5)**:** 1054-1064.

Kitada H, Sugitani A, Yamamoto H, Otomo N, Okabe Y, Inoue S*, et al.* (2002). Attenuation of renal ischemia-reperfusion injury by FR167653 in dogs. *Surgery* **131**(6)**:** 654-662.

Klauder JV (1958). Interrelations of human and veterinary medicine; discussion of some aspects of comparative dermatology. *N Engl J Med* **258**(4)**:** 170-177.

Kojima S, Nara K, Rifkin DB (1993). Requirement for transglutaminase in the activation of latent transforming growth factor-beta in bovine endothelial cells. *J Cell Biol* **121**(2)**:** 439-448.

Kouwenhoven EA, de Bruin RW, Bajema IM, Marquet RL, Ijzermans JN (2001). Cold ischemia augments allogeneic-mediated injury in rat kidney allografts. *Kidney Int* **59**(3)**:** 1142-1148.

Ku BM, Kim SJ, Kim N, Hong D, Choi YB, Lee SH*, et al.* (2014). Transglutaminase 2 inhibitor abrogates renal cell carcinoma in xenograft models. *J Cancer Res Clin Oncol* **140**(5)**:** 757-767.

Kubinova L, Janacek J, Karen P, Radochova B, Difato F, Krekule I (2004). Confocal stereology and image analysis: methods for estimating geometrical characteristics of cells and tissues from three-dimensional confocal images. *Physiol Res* **53 Suppl 1:** S47-55.

Kuiken T, Rimmelzwaan G, van Riel D, van Amerongen G, Baars M, Fouchier R*, et al.* (2004). Avian H5N1 influenza in cats. *Science* **306**(5694)**:** 241.

Kusaka M, Pratschke J, Wilhelm MJ, Ziai F, Zandi-Nejad K, Mackenzie HS*, et al.* (2000). Activation of inflammatory mediators in rat renal isografts by donor brain death. *Transplantation* **69**(3)**:** 405-410.

Kyllonen LEJ, Salmela KT, Eklund BH, Halme LEH, Hockerstedt KAV, Isoniemi HM*, et al.* (2000). Long-term results of 1047 cadaveric kidney transplantations with special emphasis on initial graft function and rejection. *Transplant International* **13**(2)**:** 122-128.

Laemmli UK (1970). Cleavage of structural proteins during the assembly of the head of bacteriophage T4. *Nature* **227**(5259)**:** 680-685.

Lascelles BD, McFarland JM, Swann H (2005). Guidelines for safe and effective use of NSAIDs in dogs. *Vet Ther* **6**(3)**:** 237-251.

Lavaud S, Poirier B, Mandet C, Belair MF, Irinopoulou T, Heudes D*, et al.* (2001). Inflammation is probably not a prerequisite for renal interstitial fibrosis in normoglycemic obese rats. *Am J Physiol Renal Physiol* **280**(4)**:** F683-694.

Lavelle JP, Meyers SA, Ruiz WG, Buffington CA, Zeidel ML, Apodaca G (2000). Urothelial pathophysiological changes in feline interstitial cystitis: a human model. *Am J Physiol Renal Physiol* **278**(4)**:** F540-553.

Lee J, Kim YS, Choi DH, Bang MS, Han TR, Joh TH*, et al.* (2004). Transglutaminase 2 induces nuclear factor-kappaB activation via a novel pathway in BV-2 microglia. *J Biol Chem* **279**(51)**:** 53725-53735.

Lee ZW, Kwon SM, Kim SW, Yi SJ, Kim YM, Ha KS (2003). Activation of in situ tissue transglutaminase by intracellular reactive oxygen species. *Biochem Biophys Res Commun* **305**(3)**:** 633-640.

Levey AS, Coresh J (2012). Chronic kidney disease. *Lancet* **379**(9811)**:** 165-180.

Levey AS, de Jong PE, Coresh J, El Nahas M, Astor BC, Matsushita K*, et al.* (2010). The definition, classification, and prognosis of chronic kidney disease: a KDIGO Controversies Conference report. *Kidney Int* **80**(1)**:** 17-28.

Levey AS, Perrone RD, Madias NE (1988). Serum creatinine and renal function. *Annu Rev Med* **39:** 465-490.

Levine S, Saltzman A (2001). Are urea and creatinine uremic toxins in the rat? *Ren Fail* **23**(1)**:** 53-59.

Levy AP, Levy NS, Wegner S, Goldberg MA (1995). Transcriptional regulation of the rat vascular endothelial growth factor gene by hypoxia. *J Biol Chem* **270**(22)**:** 13333-13340.

Li YC (2010). Renoprotective effects of vitamin D analogs. *Kidney Int* **78:** 134-139.

Lin L, Faraco J, Li R, Kadotani H, Rogers W, Lin X*, et al.* (1999). The sleep disorder canine narcolepsy is caused by a mutation in the hypocretin (orexin) receptor 2 gene. *Cell* **98**(3)**:** 365-376.

Lin SL, Kisseleva T, Brenner DA, Duffield JS (2008). Pericytes and perivascular fibroblasts are the primary source of collagen-producing cells in obstructive fibrosis of the kidney. *Am J Pathol* **173**(6)**:** 1617-1627.

Lin SL, Li B, Rao S, Yeo EJ, Hudson TE, Nowlin BT*, et al.* (2010). Macrophage Wnt7b is critical for kidney repair and regeneration. *Proc Natl Acad Sci U S A* **107**(9)**:** 4194-4199.

Lingaas F, Aarskaug T, Sletten M, Bjerkas I, Grimholt U, Moe L*, et al.* (1998). Genetic markers linked to neuronal ceroid lipofuscinosis in English setter dogs. *Anim Genet* **29**(5)**:** 371-376.

Lingaas F, Comstock KE, Kirkness EF, Sorensen A, Aarskaug T, Hitte C*, et al.* (2003). A mutation in the canine BHD gene is associated with hereditary multifocal renal cystadenocarcinoma and nodular dermatofibrosis in the German Shepherd dog. *Hum Mol Genet* **12**(23)**:** 3043-3053.

Little MH (2006). Regrow or repair: potential regenerative therapies for the kidney. *J Am Soc Nephrol* **17**(9)**:** 2390-2401.

Liu S, Cerione RA, Clardy J (2002). Structural basis for the guanine nucleotide-binding activity of tissue transglutaminase and its regulation of transamidation activity. *Proc Natl Acad Sci U S A* **99**(5)**:** 2743-2747.

Liu S, Li Y, Zhao H, Chen D, Huang Q, Wang S*, et al.* (2006). Increase in extracellular cross-linking by tissue transglutaminase and reduction in expression of MMP-9 contribute differentially to focal segmental glomerulosclerosis in rats. *Mol Cell Biochem* **284**(1-2)**:** 9-17.

Lloberas N, Cruzado JM, Torras J, Herrero-Fresneda I, Riera M, Merlos M*, et al.* (2001). Protective effect of UR-12670 on chronic nephropathy induced by warm ischaemia in ageing uninephrectomized rats. *Nephrol Dial Transplant* **16**(4)**:** 735-741.

Lorand L, Campbell-Wilkes LK, Cooperstein L (1972). A filter paper assay for transamidating enzymes using radioactive amine substrates. *Anal Biochem* **50**(2)**:** 623-631.

Lorand L, Graham RM (2003). Transglutaminases: crosslinking enzymes with pleiotropic functions. *Nat Rev Mol Cell Biol* **4**(2)**:** 140-156.

Lortat-Jacob H, Burhan I, Scarpellini A, Thomas A, Imberty A, Vives RR*, et al.* (2012). Transglutaminase-2 interaction with heparin: identification of a heparin binding site that regulates cell adhesion to fibronectin-transglutaminase-2 matrix. *J Biol Chem* **287**(22)**:** 18005-18017.

Lowe JK, Kukekova AV, Kirkness EF, Langlois MC, Aguirre GD, Acland GM*, et al.* (2003). Linkage mapping of the primary disease locus for collie eye anomaly. *Genomics* **82**(1)**:** 86-95.

Lowry OH, Rosebrough NJ, Farr AL, Randall RJ (1951). Protein measurement with the Folin phenol reagent. *J Biol Chem* **193**(1)**:** 265-275.

Lucero HA, Kagan HM (2006). Lysyl oxidase: an oxidative enzyme and effector of cell function. *Cell Mol Life Sci* **63**(19-20)**:** 2304-2316.

Lucke VM (1968). Renal disease in the domestic cat. *J Pathol Bacteriol* **95**(1)**:** 67-91.

Lulich JP, Osborne CA, Carlson M, Unger LK, Samelson LL, Koehler LA*, et al.* (1993). Nonsurgical removal of urocystoliths in dogs and cats by voiding urohydropropulsion. *J Am Vet Med Assoc* **203**(5)**:** 660-663.

Lulich JP, Osborne CA, O'Brien TD, Polzin DJ (1992). Feline renal failure: questions, answers, questions. *The Compendium on continuing education for the practicing veterinarian* **14**.

Lund EM, Armstrong PJ, Kirk CA, Kolar LM, Klausner JS (1999). Health status and population characteristics of dogs and cats examined at private veterinary practices in the United States. *J Am Vet Med Assoc* **214**(9)**:** 1336-1341.

Lyons LA, Biller DS, Erdman CA, Lipinski MJ, Young AE, Roe BA*, et al.* (2004). Feline polycystic kidney disease mutation identified in PKD1. *J Am Soc Nephrol* **15**(10)**:** 2548-2555.

Mackenzie HS, Azuma H, Rennke HG, Tilney NL, Brenner BM (1995). Renal mass as a determinant of late allograft outcome: insights from experimental studies in rats. *Kidney Int Suppl* **52:** S38-42.

Mackenzie HS, Azuma H, Troy JL, Rennke HG, Tilney NL, Brenner BM (1996). Augmenting kidney mass at transplantation abrogates chronic renal allograft injury in rats. *Proc Assoc Am Physicians* **108**(2)**:** 127-133.

Maki JM, Sormunen R, Lippo S, Kaarteenaho-Wiik R, Soininen R, Myllyharju J (2005). Lysyl oxidase is essential for normal development and function of the respiratory system and for the integrity of elastic and collagen fibers in various tissues. *Am J Pathol* **167**(4)**:** 927-936.

Mann JF, Schmieder RE, McQueen M, Dyal L, Schumacher H, Pogue J*, et al.* (2008). Renal outcomes with telmisartan, ramipril, or both, in people at high vascular risk (the ONTARGET study): a multicentre, randomised, double-blind, controlled trial. *Lancet* **372**(9638)**:** 547-553.

Manresa MC, Godson C, Taylor CT (2014). Hypoxia-sensitive pathways in inflammation-driven fibrosis. *Am J Physiol Regul Integr Comp Physiol* **307**(12)**:** R1369-R1380.

Marino CL, Lascelles BD, Vaden SL, Gruen ME, Marks SL (2013a). Prevalence and classification of chronic kidney disease in cats randomly selected from four age groups and in cats recruited for degenerative joint disease studies. *Journal of feline medicine and surgery* **16**(6)**:** 465-472.

Marino CL, Lascelles BD, Vaden SL, Gruen ME, Marks SL (2013b). Prevalence and classification of chronic kidney disease in cats randomly selected from four age groups and in cats recruited for degenerative joint disease studies. *J Feline Med Surg*.

Martin KR, Barrett JC (2002). Reactive oxygen species as double-edged swords in cellular processes: low-dose cell signaling versus high-dose toxicity. *Human & Experimental Toxicology* **21**(2)**:** 71-75.

Maxwell SR, Lip GY (1997). Reperfusion injury: a review of the pathophysiology, clinical manifestations and therapeutic options. *Int J Cardiol* **58**(2)**:** 95-117.

Meadows R (1973). Glomerulonephritis with fibrin and crescent formation. *Perspect Nephrol Hypertens* **1 Pt 2**(0)**:** 695-710.

Meguid El Nahas A, Bello AK (2005). Chronic kidney disease: the global challenge. *Lancet* **365**(9456)**:** 331-340.

Mehl ML, Kyles AE, Reimer SB, Flynn AK, Pollard RE, Nyland T*, et al.* (2006). Evaluation of the effects of ischemic injury and ureteral obstruction on delayed graft function in cats after renal autotransplantation. *Vet Surg* **35**(4)**:** 341-346.

Mehta K, Kumar A, Kim HI (2010). Transglutaminase 2: a multi-tasking protein in the complex circuitry of inflammation and cancer. *Biochem Pharmacol* **80**(12)**:** 1921-1929.

Menotti-Raymond M, O'Brien SJ (2008). *The Domestic cat, Felix catus, as a model of hereditary and infectious disease*. edn.

Methven S, MacGregor MS, Traynor JP, O'Reilly DS, Deighan CJ (2010). Assessing proteinuria in chronic kidney disease: protein-creatinine ratio versus albumin-creatinine ratio. *Nephrol Dial Transplant* **25**(9)**:** 2991-2996.

Miele L (2003). New weapons against inflammation: dual inhibitors of phospholipase A2 and transglutaminase. *J Clin Invest* **111**(1)**:** 19-21.

Mimura I, Nangaku M (2010). The suffocating kidney: tubulointerstitial hypoxia in end-stage renal disease. *Nat Rev Nephrol* **6**(11)**:** 667-678.

Minkus G, Breuer W, Wanke R, Reusch C, Leuterer G, Brem G*, et al.* (1994a). Familial nephropathy in Bernese mountain dogs. *Vet Pathol* **31**(4)**:** 421-428.

Minkus G, Reusch C, Horauf A, Breuer W, Darbes J, Kraft W*, et al.* (1994b). Evaluation of Renal Biopsies in Cats and Dogs Histopathology in Comparison with Clinical-Data. *Journal of Small Animal Practice* **35**(9)**:** 465-472.

Mirza A, Liu SL, Frizell E, Zhu J, Maddukuri S, Martinez J*, et al.* (1997). A role for tissue transglutaminase in hepatic injury and fibrogenesis, and its regulation by NF-kappaB. *Am J Physiol* **272**(2 Pt 1)**:** G281-288.

Mishra S, Saleh A, Espino PS, Davie JR, Murphy LJ (2006). Phosphorylation of histones by tissue transglutaminase. *J Biol Chem* **281**(9)**:** 5532-5538.

Mizutani H, Koyama H, Watanabe T, Kitagawa H, Nakano M, Kajiwara K*, et al.* (2006). Evaluation of the clinical efficacy of benazepril in the treatment of chronic renal insufficiency in cats. *J Vet Intern Med* **20**(5)**:** 1074-1079.

Moeller S, Gioberge S, Brown G (2002). ESRD patients in 2001: global overview of patients, treatment modalities and development trends. *Nephrology Dialysis Transplantation* **17**(12)**:** 2071-2076.

Montague MJ, Li G, Gandolfi B, Khan R, Aken BL, Searle SM*, et al.* (2014). Comparative analysis of the domestic cat genome reveals genetic signatures underlying feline biology and domestication. *Proc Natl Acad Sci U S A* **111**(48)**:** 17230-17235.

Morrissey J, Klahr S (1998). Transcription factor NF-kappaB regulation of renal fibrosis during ureteral obstruction. *Semin Nephrol* **18**(6)**:** 603-611.

Mullins JI, Hoover EA, Overbaugh J, Quackenbush SL, Donahue PR, Poss ML (1989). FeLV-FAIDS-induced immunodeficiency syndrome in cats. *Vet Immunol Immunopathol* **21**(1)**:** 25-37.

Murad F, Mittal CK, Arnold WP, Katsuki S, Kimura H (1978). Guanylate cyclase: activation by azide, nitro compounds, nitric oxide, and hydroxyl radical and inhibition by hemoglobin and myoglobin. *Adv Cyclic Nucleotide Res* **9:** 145-158.

Murtaugh MP, Arend WP, Davies PJ (1984). Induction of tissue transglutaminase in human peripheral blood monocytes. *J Exp Med* **159**(1)**:** 114-125.

Nagarajan RP, Chen F, Li W, Vig E, Harrington MA, Nakshatri H*, et al.* (2000). Repression of transforming-growth-factor-beta-mediated transcription by nuclear factor kappaB. *Biochem J* **348 Pt 3:** 591-596.

Nangaku M (2006). Chronic hypoxia and tubulointerstitial injury: a final common pathway to end-stage renal failure. *J Am Soc Nephrol* **17**(1)**:** 17-25.

Nangaku M, Eckardt KU (2007a). Hypoxia and the HIF system in kidney disease. *J Mol Med* **85**(12)**:** 1325-1330.

Nangaku M, Eckardt KU (2007b). Hypoxia and the HIF system in kidney disease. *Journal of molecular medicine* **85**(12)**:** 1325-1330.

Nelson RW, Couto CG (2009). Acute renal failure and chronic kidney disease. In: Nelson RW, Couto CG (ed)^(eds). *Small Animal Internal Medicine*, edn: Mosby-Elsevier. p^pp.

Nielsen S, Kwon TH, Christensen BM, Promeneur D, Frokiaer J, Marples D (1999). Physiology and pathophysiology of renal aquaporins. *J Am Soc Nephrol* **10**(3)**:** 647-663.

Nishi H, Inagi R, Kato H, Tanemoto M, Kojima I, Son D*, et al.* (2008). Hemoglobin is expressed by mesangial cells and reduces oxidant stress. *J Am Soc Nephrol* **19**(8)**:** 1500-1508.

Nolan CR (2005). Phosphate binder therapy for attainment of K/DOQI bone metabolism guidelines. *Kidney Int Suppl*(96)**:** S7-14.

Norman JT, Clark IM, Garcia PL (2000). Hypoxia promotes fibrogenesis in human renal fibroblasts. *Kidney Int* **58**(6)**:** 2351-2366.

Norman JT, Fine LG (2006). Intrarenal oxygenation in chronic renal failure. *Clin Exp Pharmacol Physiol* **33**(10)**:** 989-996.

Nunes I, Gleizes PE, Metz CN, Rifkin DB (1997). Latent transforming growth factor-beta binding protein domains involved in activation and transglutaminase-dependent cross-linking of latent transforming growth factor-beta. *J Cell Biol* **136**(5)**:** 1151-1163.

Nurko S (2006). Anemia in chronic kidney disease: causes, diagnosis, treatment. *Cleve Clin J Med* **73**(3)**:** 289-297.

O'Brien SJ, Troyer JL, Roelke M, Marker, Pecon-Slattery J (2006). Plagues and adaptation: Lessons from the Felidae models for SARS and AIDS. *Biological conservation* **131**(2)**:** 255-267.

Odland MD (1998). Surgical technique/post-transplant surgical complications. *Surg Clin North Am* **78**(1)**:** 55-60.

Oldroyd SD, Thomas GL, Gabbiani G, El Nahas AM (1999). Interferon-gamma inhibits experimental renal fibrosis. *Kidney Int* **56**(6)**:** 2116-2127.

Ollier WE, Kennedy LJ, Thomson W, Barnes AN, Bell SC, Bennett D*, et al.* (2001). Dog MHC alleles containing the human RA shared epitope confer susceptibility to canine rheumatoid arthritis. *Immunogenetics* **53**(8)**:** 669-673.

Osman Y, Shokeir A, Ali-el-Dein B, Tantawy M, Wafa EW, el-Dein AB*, et al.* (2003). Vascular complications after live donor renal transplantation: study of risk factors and effects on graft and patient survival. *J Urol* **169**(3)**:** 859-862.

Ostrander EA, Giniger E (1997). Semper fidelis: what man's best friend can teach us about human biology and disease. *Am J Hum Genet* **61**(3)**:** 475-480.

Overall KL (2000). Natural animal models of human psychiatric conditions: assessment of mechanism and validity. *Prog Neuropsychopharmacol Biol Psychiatry* **24**(5)**:** 727-776.

Ozaki M, Sessler DI, Suzuki H, Ozaki K, Tsunoda C, Atarashi K (1995). Nitrous oxide decreases the threshold for vasoconstriction less than sevoflurane or isoflurane. *Anesth Analg* **80**(6)**:** 1212-1216.

Ozawa K, Aoyama H, Yasuda K, Shimahara Y, Nakatani T, Tanaka J*, et al.* (1983). Metabolic abnormalities associated with postoperative organ failure. A redox theory. *Arch Surg* **118**(11)**:** 1245-1251.

Ozkaynak E, Schnegelsberg PN, Oppermann H (1991). Murine osteogenic protein (OP-1): high levels of mRNA in kidney. *Biochem Biophys Res Commun* **179**(1)**:** 116-123.

Pahlavan PS, Mehrabi A, Kashfi A, Soleimani M, Fani-Yazdi SH, Schemmer P*, et al.* (2005). Guidelines for prevention and management of complications following kidney transplantation in rats. *Transplant Proc* **37**(5)**:** 2333-2337.

Paliege A, Rosenberger C, Bondke A, Sciesielski L, Shina A, Heyman SN*, et al.* (2010). Hypoxia-inducible factor-2alpha-expressing interstitial fibroblasts are the only renal cells that express erythropoietin under hypoxia-inducible factor stabilization. *Kidney Int* **77**(4)**:** 312-318.

Paller MS, Hoidal JR, Ferris TF (1984). Oxygen free radicals in ischemic acute renal failure in the rat. *J Clin Invest* **74**(4)**:** 1156-1164.

Palmarini M (2007). A veterinary twist on pathogen biology. *PLoS Pathog* **3**(2)**:** e12.

Panes J, Perry M, Granger DN (1999). Leukocyte-endothelial cell adhesion: avenues for therapeutic intervention. *Br J Pharmacol* **126**(3)**:** 537-550.

Parasuraman S, Raveendran R, Kesavan R (2010). Blood sample collection in small laboratory animals. *J Pharmacol Pharmacother* **1**(2)**:** 87-93.

Park SK, Kim W, Lee CH, Koh GY (2000). Differential changes of CDK activities in glomeruli and tubules during the active DNA synthetic period after ischemic injury. *Nephron* **86**(3)**:** 306-314.

Patschan D, Patschan S, Muller GA (2012). Inflammation and microvasculopathy in renal ischemia reperfusion injury. *J Transplant* **2012:** 764154.

Paul LC (1999). Chronic allograft nephropathy: An update. *Kidney International* **56**(3)**:** 783-793.

Perico N, Benigni A, Remuzzi G (2008). Present and future drug treatments for chronic kidney diseases: evolving targets in renoprotection. *Nat Rev Drug Discov* **7**(11)**:** 936-953.

Perico N, Codreanu I, Schieppati A, Remuzzi G (2005). Prevention of progression and remission/regression strategies for chronic renal diseases: can we do better now than five years ago? *Kidney Int Suppl*(98)**:** S21-24.

Peterson M (2012). Hyperthyroidism in cats: what's causing this epidemic of thyroid disease and can we prevent it? *J Feline Med Surg* **14**(11)**:** 804-818.

Pillebout E, Burtin M, Yuan HT, Briand P, Woolf AS, Friedlander G*, et al.* (2001). Proliferation and remodeling of the peritubular microcirculation after nephron reduction: association with the progression of renal lesions. *Am J Pathol* **159**(2)**:** 547-560.

Pisano JJ, Finlayson JS, Peyton MP (1968). [Cross-link in fibrin polymerized by factor 13: epsilon-(gamma-glutamyl)lysine.]. *Science* **160**(830)**:** 892-893.

Ploeg RJ, van Bockel JH, Langendijk PT, Groenewegen M, van der Woude FJ, Persijn GG*, et al.* (1992). Effect of preservation solution on results of cadaveric kidney transplantation. The European Multicentre Study Group. *Lancet* **340**(8812)**:** 129-137.

Polzin DJ (2011). *Nephrology and urology of small animals*. edn. Wiley-Backwell.

Pontius JU, Mullikin JC, Smith DR, Lindblad-Toh K, Gnerre S, Clamp M*, et al.* (2007). Initial sequence and comparative analysis of the cat genome. *Genome Res* **17**(11)**:** 1675-1689.

Popov Y, Sverdlov DY, Sharma AK, Bhaskar KR, Li S, Freitag TL*, et al.* (2011). Tissue transglutaminase does not affect fibrotic matrix stability or regression of liver fibrosis in mice. *Gastroenterology* **140**(5)**:** 1642-1652.

Pritchard DH, Napthine DV, Sinclair AJ (1980). Globoid cell leucodystrophy in polled Dorset sheep. *Vet Pathol* **17**(4)**:** 399-405.

Qi WE, Chen XM, Poronnik P, Pollock CA (2006). The renal cortical fibroblast in renal tubulointerstitial fibrosis. *International Journal of Biochemistry & Cell Biology* **38**(1)**:** 1-5.

Qiu T, Zhou J, Liu X, Ge M, Chen Z (2012). The second short-term warm ischemia after vascular anastomosis did not affect early renal function recovery in renal transplantation: a case report. *Front Med* **6**(3)**:** 329-331.

Quaggin SE, Kreidberg JA (2008). Development of the renal glomerulus: good neighbors and good fences. *Development* **135**(4)**:** 609-620.

Quan G, Choi JY, Lee DS, Lee SC (2005). TGF-beta1 up-regulates transglutaminase two and fibronectin in dermal fibroblasts: a possible mechanism for the stabilization of tissue inflammation. *Arch Dermatol Res* **297**(2)**:** 84-90.

Remuzzi G, Bertani T (1998). Pathophysiology of progressive nephropathies. *New England Journal of Medicine* **339**(20)**:** 1448-1456.

Rhodes TH, Vite CH, Giger U, Patterson DF, Fahlke C, George AL, Jr. (1999). A missense mutation in canine C1C-1 causes recessive myotonia congenita in the dog. *FEBS Lett* **456**(1)**:** 54-58.

Risdon RA, Sloper JC, De Wardener HE (1968). Relationship between renal function and histological changes found in renal-biopsy specimens from patients with persistent glomerular nephritis. *Lancet* **2**(7564)**:** 363-366.

Riser BL, Cortes P, Zhao X, Bernstein J, Dumler F, Narins RG (1992). Intraglomerular pressure and mesangial stretching stimulate extracellular matrix formation in the rat. *J Clin Invest* **90**(5)**:** 1932-1943.

Rivas AL, Tintle L, Meyers-Wallen V, Scarlett JM, van Tassell CP, Quimby FW (1993). Inheritance of renal amyloidosis in Chinese Shar-pei dogs. *J Hered* **84**(6)**:** 438-442.

Rodriguez-Iturbe B, Garcia Garcia G (2010). The role of tubulointerstitial inflammation in the progression of chronic renal failure. *Nephron Clin Pract* **116**(2)**:** c81-88.

Rodriguez-Iturbe B, Johnson RJ, Herrera-Acosta J (2005). Tubulointerstitial damage and progression of renal failure. *Kidney Int Suppl*(99)**:** S82-86.

Rosenberger C, Pratschke J, Rudolph B, Heyman SN, Schindler R, Babel N*, et al.* (2007). Immunohistochemical detection of hypoxia-inducible factor-1alpha in human renal allograft biopsies. *J Am Soc Nephrol* **18**(1)**:** 343-351.

Rosenberger C, Rosen S, Heyman SN (2006). Renal parenchymal oxygenation and hypoxia adaptation in acute kidney injury. *Clin Exp Pharmacol Physiol* **33**(10)**:** 980-988.

Ross L (2011). Acute kidney injury in dogs and cats. *Vet Clin North Am Small Anim Pract* **41**(1)**:** 1-14.

Ross LA, Labato MA (2013). Current techniques in peritoneal dialysis. *J Vet Emerg Crit Care (San Antonio)* **23**(2)**:** 230-240.

Rossing P (2006). Diabetic nephropathy: worldwide epidemic and effects of current treatment on natural history. *Curr Diab Rep* **6**(6)**:** 479-483.

Roudebush P, Polzin DJ, Ross SJ, Towell TL, Adams LG, Dru Forrester S (2009). Therapies for feline chronic kidney disease. What is the evidence? *J Feline Med Surg* **11**(3)**:** 195-210.

Rowell JL, McCarthy DO, Alvarez CE (2011). Dog models of naturally occurring cancer. *Trends Mol Med* **17**(7)**:** 380-388.

Salaman JR (1969). Renal transplantation in the rat. *Br J Surg* **56**(11)**:** 818-822.

Sampson N, Berger P, Zenzmaier C (2014). Redox signaling as a therapeutic target to inhibit myofibroblast activation in degenerative fibrotic disease. *Biomed Res Int* **2014:** 131737.

Sandid MS, Assi MA, Hall S (2006). Intraoperative hypotension and prolonged operative time as risk factors for slow graft function in kidney transplant recipients. *Clin Transplant* **20**(6)**:** 762-768.

Scarpellini A, Huang L, Burhan I, Schroeder N, Funck M, Johnson TS*, et al.* (2013). Syndecan-4 Knockout Leads to Reduced Extracellular Transglutaminase-2 and Protects against Tubulointerstitial Fibrosis. *J Am Soc Nephrol*.

Schieppati A, Remuzzi G (2005). Chronic renal diseases as a public health problem: epidemiology, social, and economic implications. *Kidney Int Suppl*(98)**:** S7-S10.

Schmiedt CW, Holzman G, Schwarz T, McAnulty JF (2008). Survival, complications, and analysis of risk factors after renal transplantation in cats. *Vet Surg* **37**(7)**:** 683-695.

Schmiedt CW, Mercurio AD, Glassman MM, McAnulty JF, Brown CA, Brown SA (2009). Effects of renal autograft ischemia and reperfusion associated with renal transplantation on arterial blood pressure variables in clinically normal cats. *Am J Vet Res* **70**(11)**:** 1426-1432.

Schmiedt CW, Nelson SA, Brainard BM, Brown CA, Vandenplas M, Hurley DJ (2011). Bilateral renal ischemia as a model of acute kidney injury in cats. *Res Vet Sci*.

Schmiedt CW, Nelson SA, Brainard BM, Brown CA, Vandenplas M, Hurley DJ (2012). Bilateral renal ischemia as a model of acute kidney injury in cats. *Res Vet Sci* **93**(2)**:** 950-959.

Schnellmann R (1999). Pathophysiology of Nephrotoxic Acute Renal Failure. In: Schrier R (ed)^(eds). *Atlas of Diseases of the Kidney: Disorders of Water, Electrolytes and Acid-base Acute Renal Failure*
First edn, Vol. 1. USA. p^pp.

Scholz CC, Cavadas MA, Tambuwala MM, Hams E, Rodriguez J, von Kriegsheim A*, et al.* (2013). Regulation of IL-1beta-induced NF-kappaB by hydroxylases links key hypoxic and inflammatory signaling pathways. *Proc Natl Acad Sci U S A* **110**(46)**:** 18490-18495.

Schrier RW, Wang W, Poole B, Mitra A (2004). Acute renal failure: definitions, diagnosis, pathogenesis, and therapy. *J Clin Invest* **114**(1)**:** 5-14.

Schumacher M, Van Vliet BN, Ferrari P (2003). Kidney transplantation in rats: an appraisal of surgical techniques and outcome. *Microsurgery* **23**(4)**:** 387-394.

Seal JB, Gewertz BL (2005). Vascular dysfunction in ischemia-reperfusion injury. *Annals of Vascular Surgery* **19**(4)**:** 572-584.

Secin FP (2008). Importance and limits of ischemia in renal partial surgery: experimental and clinical research. *Adv Urol***:** 102461.

Sehgal AR (2002). What is the best treatment for end-stage renal disease? *American Journal of Medicine* **112**(9)**:** 735-736.

Selkoe DJ, Abraham C, Ihara Y (1982). Brain transglutaminase: in vitro crosslinking of human neurofilament proteins into insoluble polymers. *Proc Natl Acad Sci U S A* **79**(19)**:** 6070-6074.

Seltenhammer MH, Heere-Ress E, Brandt S, Druml T, Jansen B, Pehamberger H*, et al.* (2004). Comparative histopathology of grey-horse-melanoma and human malignant melanoma. *Pigment Cell Res* **17**(6)**:** 674-681.

Sent U, Goessl R, Lang I, Stark M (2013). Efficacy of Long Term Treatment with Telmisartan Oral Solution on Quality of Life and Disease Progression in Cats with Chronic Kidney Failure. *ISFM. World Feline Veterinary Congress*.

Sessler DI, Rubinstein EH, Moayeri A (1991). Physiologic responses to mild perianesthetic hypothermia in humans. *Anesthesiology* **75**(4)**:** 594-610.

Shah SV (1995). The role of reactive oxygen metabolites in glomerular disease. *Annu Rev Physiol* **57:** 245-262.

Shah SV, Baliga R, Rajapurkar M, Fonseca VA (2007). Oxidants in chronic kidney disease. *J Am Soc Nephrol* **18**(1)**:** 16-28.

Sharp NJ, Kornegay JN, Van Camp SD, Herbstreith MH, Secore SL, Kettle S*, et al.* (1992). An error in dystrophin mRNA processing in golden retriever muscular dystrophy, an animal homologue of Duchenne muscular dystrophy. *Genomics* **13**(1)**:** 115-121.

Shin DM, Jeon JH, Kim CW, Cho SY, Lee HJ, Jang GY*, et al.* (2008). TGFbeta mediates activation of transglutaminase 2 in response to oxidative stress that leads to protein aggregation. *FASEB J* **22**(7)**:** 2498-2507.

Shoskes DA, Parfrey NA, Halloran PF (1990). Increased major histocompatibility complex antigen expression in unilateral ischemic acute tubular necrosis in the mouse. *Transplantation* **49**(1)**:** 201-207.

Shrestha B, Butt I, Da Silva M, Sanchez-Lara A, Wagner B, Raftery A*, et al.* (2014a). Upregulation of transglutaminase and epsilon (gamma-glutamyl)-lysine in the Fisher-Lewis rat model of chronic allograft nephropathy. *Biomed Res Int* **2014:** 651608.

Shrestha BM, Haylor J (2014b). Biological pathways and potential targets for prevention and therapy of chronic allograft nephropathy. *Biomed Res Int* **2014:** 482438.

Shroff R, Ledermann S (2009). Long-term outcome of chronic dialysis in children. *Pediatr Nephrol* **24**(3)**:** 463-474.

Shweke N, Boulos N, Jouanneau C, Vandermeersch S, Melino G, Dussaule JC*, et al.* (2008). Tissue transglutaminase contributes to interstitial renal fibrosis by favoring accumulation of fibrillar collagen through TGF-beta activation and cell infiltration. *Am J Pathol* **173**(3)**:** 631-642.

Sidjanin DJ, Lowe JK, McElwee JL, Milne BS, Phippen TM, Sargan DR*, et al.* (2002). Canine CNGB3 mutations establish cone degeneration as orthologous to the human achromatopsia locus ACHM3. *Hum Mol Genet* **11**(16)**:** 1823-1833.

Sigurdson CJ, Basaraba RJ, Mazzaferro EM, Gould DH (2002). Globoid cell-like leukodystrophy in a domestic longhaired cat. *Vet Pathol* **39**(4)**:** 494-496.

Skill NJ, Johnson TS, Coutts IG, Saint RE, Fisher M, Huang L*, et al.* (2004). Inhibition of transglutaminase activity reduces extracellular matrix accumulation induced by high glucose levels in proximal tubular epithelial cells. *J Biol Chem* **279**(46)**:** 47754-47762.

Slayback JB, Bowen WW, Hinshaw DB (1976). Intimal injury from arterial clamps. *Am J Surg* **132**(2)**:** 183-188.

Smucker ML, Kaul S, Woodfield JA, Keith JC, Manning SA, Gascho JA (1990). Naturally occurring cardiomyopathy in the Doberman pinscher: a possible large animal model of human cardiomyopathy? *J Am Coll Cardiol* **16**(1)**:** 200-206.

Sohn J, Kim TI, Yoon YH, Kim JY, Kim SY (2003). Novel transglutaminase inhibitors reverse the inflammation of allergic conjunctivitis. *J Clin Invest* **111**(1)**:** 121-128.

Solomon SE (1985). The morphology of the kidney of the green turtle (Chelonia mydas L.). *J Anat* **140 (Pt 3):** 355-369.

Southard JH, Belzer FO (1995). Organ preservation. *Annu Rev Med* **46:** 235-247.

Spugnini EP, Baldi A, Vincenzi B, Bongiorni F, Bellelli C, Citro G*, et al.* (2007). Intraoperative versus postoperative electrochemotherapy in high grade soft tissue sarcomas: a preliminary study in a spontaneous feline model. *Cancer Chemother Pharmacol* **59**(3)**:** 375-381.

Star RA (1998). Treatment of acute renal failure. *Kidney Int* **54**(6)**:** 1817-1831.

Stokes JE, Forrester SD (2004). New and unusual causes of acute renal failure in dogs and cats. *Vet Clin North Am Small Anim Pract* **34**(4)**:** 909-922, vi.

Strutz F, Zeisberg M (2006). Renal fibroblasts and myofibroblasts in chronic kidney disease. *Journal of the American Society of Nephrology* **17**(11)**:** 2992-2998.

Strutz F, Zeisberg M, Ziyadeh FN, Yang CQ, Kalluri R, Muller GA*, et al.* (2002). Role of basic fibroblast growth factor-2 in epithelial-mesenchymal transformation. *Kidney International* **61**(5)**:** 1714-1728.

Stubenitsky BM, Booster MH, Brasile L, Araneda D, Haisch CE, Kootstra G (2000). Exsanguinous metabolic support perfusion--a new strategy to improve graft function after kidney transplantation. *Transplantation* **70**(8)**:** 1254-1258.

Sun J, Kong J, Duan Y, Szeto FL, Liao A, Madara JL*, et al.* (2006). Increased NF-kappaB activity in fibroblasts lacking the vitamin D receptor. *Am J Physiol Endocrinol Metab* **291**(2)**:** E315-322.

Supavekin S, Zhang W, Kucherlapati R, Kaskel FJ, Moore LC, Devarajan P (2003). Differential gene expression following early renal ischemia/reperfusion. *Kidney Int* **63**(5)**:** 1714-1724.

Sutter NB, Ostrander EA (2004). Dog star rising: the canine genetic system. *Nat Rev Genet* **5**(12)**:** 900-910.

Syme H (2011). Hypertension in small animal kidney disease. *Vet Clin North Am Small Anim Pract* **41**(1)**:** 63-89.

Syme HM, Barber PJ, Markwell PJ, Elliott J (2002). Prevalence of systolic hypertension in cats with chronic renal failure at initial evaluation. *J Am Vet Med Assoc* **220**(12)**:** 1799-1804.

Syme HM, Markwell PJ, Pfeiffer D, Elliott J (2006). Survival of cats with naturally occurring chronic renal failure is related to severity of proteinuria. *J Vet Intern Med* **20**(3)**:** 528-535.

Szondy Z, Mastroberardino PG, Varadi J, Farrace MG, Nagy N, Bak I*, et al.* (2006). Tissue transglutaminase (TG2) protects cardiomyocytes against ischemia/reperfusion injury by regulating ATP synthesis. *Cell Death Differ* **13**(10)**:** 1827-1829.

Szondy Z, Sarang Z, Molnar P, Nemeth T, Piacentini M, Mastroberardino PG*, et al.* (2003). Transglutaminase 2-/- mice reveal a phagocytosis-associated crosstalk between macrophages and apoptotic cells. *Proc Natl Acad Sci U S A* **100**(13)**:** 7812-7817.

Szostek M, Kosieradzki M, Chmura A, Pacholczyk M, Lagiewska B, Adadynski L*, et al.* (1999). Does "second warm ischemia time" play a role in kidney allograft function? *Transplant Proc* **31**(1-2)**:** 1037-1038.

Takada M, Nadeau KC, Shaw GD, Marquette KA, Tilney NL (1997). The cytokine-adhesion molecule cascade in ischemia/reperfusion injury of the rat kidney. Inhibition by a soluble P-selectin ligand. *J Clin Invest* **99**(11)**:** 2682-2690.

Telci D, Griffin M (2006). Tissue transglutaminase (TG2) - a wound response enzyme. *Frontiers in Bioscience* **11:** 867-882.

Theeuwes F, Yum SI (1976). Principles of the design and operation of generic osmotic pumps for the delivery of semisolid or liquid drug formulations. *Ann Biomed Eng* **4**(4)**:** 343-353.

Thompson SW (1966). *Selected Histochemical and Histopathological Methods*. edn, vol. 1. Thomas, C.C.

Thornhill BA, Forbes MS, Marcinko ES, Chevalier RL (2007). Glomerulotubular disconnection in neonatal mice after relief of partial ureteral obstruction. *Kidney Int* **72**(9)**:** 1103-1112.

Tonelli M, Wiebe N, Culleton B, House A, Rabbat C, Fok M*, et al.* (2006). Chronic kidney disease and mortality risk: a systematic review. *J Am Soc Nephrol* **17**(7)**:** 2034-2047.

Torras J, Cruzado JM, Riera M, Condom E, Duque N, Herrero I*, et al.* (1999). Long-term protective effect of UR-12670 after warm renal ischemia in uninephrectomized rats. *Kidney Int* **56**(5)**:** 1798-1808.

Tsuchiya K, Wang W, Giebisch G, Welling PA (1992). ATP is a coupling modulator of parallel Na,K-ATPase-K-channel activity in the renal proximal tubule. *Proc Natl Acad Sci U S A* **89**(14)**:** 6418-6422.

Uchide T, Saida K (2006). Primary structure of cat preproendothelin-2 and cat renal mRNA expression of preproendothelin-1 and preproendothelin-2 in naturally occurring renal failure. *Exp Biol Med (Maywood)* **231**(6)**:** 997-1000.

Ueda N, Kaushal GP, Shah SV (2000). Apoptotic mechanisms in acute renal failure. *American Journal of Medicine* **108**(5)**:** 403-415.

Vaden SL (2011). Glomerular disease. *Top Companion Anim Med* **26**(3)**:** 128-134.

Vaden SL, Levine J, Breitschwerdt EB (1997). A retrospective case-control of acute renal failure in 99 dogs. *J Vet Intern Med* **11**(2)**:** 58-64.

Vail DM, MacEwen EG (2000). Spontaneously occurring tumors of companion animals as models for human cancer. *Cancer Invest* **18**(8)**:** 781-792.

van De Sluis B, Rothuizen J, Pearson PL, van Oost BA, Wijmenga C (2002). Identification of a new copper metabolism gene by positional cloning in a purebred dog population. *Hum Mol Genet* **11**(2)**:** 165-173.

van den Berg L, Schilder MB, Knol BW (2003). Behavior genetics of canine aggression: behavioral phenotyping of golden retrievers by means of an aggression test. *Behav Genet* **33**(5)**:** 469-483.

Vanes A, Hermans J, Vanbockel JH, Persijn GG, Vanhooff JP, Degraeff J (1983). EFFECT OF WARM ISCHEMIA TIME AND HLA (A AND B) MATCHING ON RENAL CADAVERIC GRAFT-SURVIVAL AND REJECTION EPISODES. *Transplantation* **36**(3)**:** 255-258.

Vaziri ND (2004). Oxidative stress in uremia: nature, mechanisms, and potential consequences. *Semin Nephrol* **24**(5)**:** 469-473.

Venkatachalam MA, Griffin KA, Lan R, Geng H, Saikumar P, Bidani AK (2010). Acute kidney injury: a springboard for progression in chronic kidney disease. *Am J Physiol Renal Physiol* **298**(5)**:** F1078-1094.

Verderio E, Nicholas B, Gross S, Griffin M (1998). Regulated expression of tissue transglutaminase in Swiss 3T3 fibroblasts: Effects on the processing of fibronectin, cell attachment, and cell death. *Experimental Cell Research* **239**(1)**:** 119-138.

Verderio EA, Johnson T, Griffin M (2004). Tissue transglutaminase in normal and abnormal wound healing: review article. *Amino Acids* **26**(4)**:** 387-404.

Verderio EA, Scarpellini A, Johnson TS (2009). Novel interactions of TG2 with heparan sulfate proteoglycans: reflection on physiological implications. *Amino Acids* **36**(4)**:** 671-677.

Veske A, Nilsson SE, Narfstrom K, Gal A (1999). Retinal dystrophy of Swedish briard/briard-beagle dogs is due to a 4-bp deletion in RPE65. *Genomics* **57**(1)**:** 57-61.

Vite CH, McGowan JC, Braund KG, Drobatz KJ, Glickson JD, Wolfe JH*, et al.* (2001). Histopathology, electrodiagnostic testing, and magnetic resonance imaging show significant peripheral and central nervous system myelin abnormalities in the cat model of alpha-mannosidosis. *J Neuropathol Exp Neurol* **60**(8)**:** 817-828.

Vukicevic S, Basic V, Rogic D, Basic N, Shih MS, Shepard A*, et al.* (1998). Osteogenic protein-1 (bone morphogenetic protein-7) reduces severity of injury after ischemic acute renal failure in rat. *J Clin Invest* **102**(1)**:** 202-214.

Wakshlag JJ, McNeill CJ, Antonyak MA, Boehm JE, Fuji R, Balkman CE*, et al.* (2006). Expression and activity of transglutaminase II in spontaneous tumours of dogs and cats. *J Comp Pathol* **134**(2-3)**:** 202-210.

Wald R, Quinn RR, Luo J, Li P, Scales DC, Mamdani MM*, et al.* (2009). Chronic dialysis and death among survivors of acute kidney injury requiring dialysis. *JAMA* **302**(11)**:** 1179-1185.

Wang L, Zhang T, Fang M, Shen N, Wang D, Teng J*, et al.* (2015). Podocytes protect glomerular endothelial cells from hypoxic injury via deSUMOylation of HIF-1alpha signaling. *Int J Biochem Cell Biol* **58:** 17-27.

Wang P, Ba ZF, Lu MC, Ayala A, Harkema JM, Chaudry IH (1994). Measurement of circulating blood volume in vivo after trauma-hemorrhage and hemodilution. *Am J Physiol* **266**(2 Pt 2)**:** R368-374.

Wang P, Hauptman JG, Chaudry IH (1990). Hepatocellular dysfunction occurs early after hemorrhage and persists despite fluid resuscitation. *J Surg Res* **48**(5)**:** 464-470.

Wang S, Hirschberg R (2003). BMP7 antagonizes TGF-beta -dependent fibrogenesis in mesangial cells. *Am J Physiol Renal Physiol* **284**(5)**:** F1006-1013.

Wang Z, Chamberlain JS, Tapscott SJ, Storb R (2009). Gene therapy in large animal models of muscular dystrophy. *ILAR J* **50**(2)**:** 187-198.

Watanabe N, Kato M, Suzuki N, Inoue C, Fedorova S, Hashimoto H*, et al.* (2009). Kidney regeneration through nephron neogenesis in medaka. *Dev Growth Differ* **51**(2)**:** 135-143.

Watanabe T, Mishina M (2007). Effects of benazepril hydrochloride in cats with experimentally induced or spontaneously occurring chronic renal failure. *J Vet Med Sci* **69**(10)**:** 1015-1023.

Watson AD (1998). Urine specific gravity in practice. *Aust Vet J* **76**(6)**:** 392-398.

Weight SC, Bell PR, Nicholson ML (1996). Renal ischaemia--reperfusion injury. *Br J Surg* **83**(2)**:** 162-170.

Weight SC, Furness PN, Nicholson ML (1998). New model of renal warm ischaemia-reperfusion injury for comparative functional, morphological and pathophysiological studies. *Br J Surg* **85**(12)**:** 1669-1673.

Wen JG, Frokiaer J, Jorgensen TM, Djurhuus JC (1999). Obstructive nephropathy: an update of the experimental research. *Urol Res* **27**(1)**:** 29-39.

Wenisch C, Narzt E, Sessler DI, Parschalk B, Lenhardt R, Kurz A*, et al.* (1996). Mild intraoperative hypothermia reduces production of reactive oxygen intermediates by polymorphonuclear leukocytes. *Anesth Analg* **82**(4)**:** 810-816.

White JD, Norris JM, Baral RM, Malik R (2006). Naturally-occurring chronic renal disease in Australian cats: a prospective study of 184 cases. *Aust Vet J* **84**(6)**:** 188-194.

Wigmore SJ, Seeney FM, Pleass HC, Praseedom RK, Forsythe JL (1999). Kidney damage during organ retrieval: data from UK National Transplant Database. Kidney Advisory Group. *Lancet* **354**(9185)**:** 1143-1146.

Willett BJ, Flynn JN, Hosie MJ (1997). FIV infection of the domestic cat: an animal model for AIDS. *Immunol Today* **18**(4)**:** 182-189.

Williams T, Elliott J, Syme H (2014). Association between urinary vascular endothelial growth factor excretion and chronic kidney disease in hyperthyroid cats. *Research in veterinary science* **96**(3)**:** 436-441.

Williams TL, Elliott J, Syme HM (2013). Renine Angiotensin Aldosterone System Activity in Hyperthyroid Cats with and without Concurrent Hypertension. *Journal of Veterinary Internal Medicine* **27:** 522-529.

Wolfe JH (2009). Gene therapy in large animal models of human genetic diseases. Introduction. *ILAR J* **50**(2)**:** 107-111.

Wong W, Fynn SP, Higgins RM, Walters H, Evans S, Deane C*, et al.* (1996). Transplant renal artery stenosis in 77 patients--does it have an immunological cause? *Transplantation* **61**(2)**:** 215-219.

Worwag S, Langston CE (2008). Acute intrinsic renal failure in cats: 32 cases (1997-2004). *J Am Vet Med Assoc* **232**(5)**:** 728-732.

Yabuki A, Mitani S, Fujiki M, Misumi K, Endo Y, Miyoshi N*, et al.* (2010). Comparative study of chronic kidney disease in dogs and cats: induction of myofibroblasts. *Res Vet Sci* **88**(2)**:** 294-299.

Yamamoto K, Wilson DR, Baumal R (1984). Outer medullary circulatory defect in ischemic acute renal failure. *Am J Pathol* **116**(2)**:** 253-261.

Yan SF, Mackman N, Kisiel W, Stern DM, Pinsky DJ (1999). Hypoxia/Hypoxemia-Induced activation of the procoagulant pathways and the pathogenesis of ischemia-associated thrombosis. *Arterioscler Thromb Vasc Biol* **19**(9)**:** 2029-2035.

Yang B, Jain S, Pawluczyk IZ, Imtiaz S, Bowley L, Ashra SY*, et al.* (2005). Inflammation and caspase activation in long-term renal ischemia/reperfusion injury and immunosuppression in rats. *Kidney Int* **68**(5)**:** 2050-2067.

Yang Z, Xiaohua W, Lei J, Ruoyun T, Mingxia X, Weichun H*, et al.* Uric acid increases fibronectin synthesis through upregulation of lysyl oxidase expression in rat renal tubular epithelial cells. *Am J Physiol Renal Physiol* **299**(2)**:** F336-346.

Yee VC, Pedersen LC, Le Trong I, Bishop PD, Stenkamp RE, Teller DC (1994). Three-dimensional structure of a transglutaminase: human blood coagulation factor XIII. *Proc Natl Acad Sci U S A* **91**(15)**:** 7296-7300.

Ympa YP, Sakr Y, Reinhart K, Vincent JL (2005). Has mortality from acute renal failure decreased? A systematic review of the literature. *Am J Med* **118**(8)**:** 827-832.

Yokozawa T, Chung HY, Kim DW, Goto H (1999). Involvement of superoxide and/or nitric oxide in renal tissue injury. *Exp Toxicol Pathol* **51**(6)**:** 517-521.

Yu DS, Char DL, Chang SY, Ma CP (1998). Pathogenesis of ischemia reperfusion injury of the kidney after transient renal arterial clamping in rats. *J Formos Med Assoc* **97**(9)**:** 606-613.

Yuan HT, Li XZ, Pitera JE, Long DA, Woolf AS (2003). Peritubular capillary loss after mouse acute nephrotoxicity correlates with down-regulation of vascular endothelial growth factor-A and hypoxia-inducible factor-1 alpha. *Am J Pathol* **163**(6)**:** 2289-2301.

Zager RA, Johnson AC (2009). Renal ischemia-reperfusion injury upregulates histone-modifying enzyme systems and alters histone expression at proinflammatory/profibrotic genes. *Am J Physiol Renal Physiol* **296**(5)**:** F1032-1041.

Zeisberg EM, Potenta SE, Sugimoto H, Zeisberg M, Kalluri R (2008). Fibroblasts in Kidney Fibrosis Emerge via Endothelial-to-Mesenchymal Transition. *Journal of the American Society of Nephrology* **19**(12)**:** 2282-2287.

Zemskov EA, Mikhailenko I, Hsia RC, Zaritskaya L, Belkin AM (2011). Unconventional secretion of tissue transglutaminase involves phospholipid-dependent delivery into recycling endosomes. *PloS one* **6**(4)**:** e19414.

Zhang Z, Sun L, Wang Y, Ning G, Minto AW, Kong J*, et al.* (2008). Renoprotective role of the vitamin D receptor in diabetic nephropathy. *Kidney Int* **73**(2)**:** 163-171.

Zheng K, Thorner PS, Marrano P, Baumal R, McInnes RR (1994). Canine X chromosome-linked hereditary nephritis: a genetic model for human X-linked hereditary nephritis resulting from a single base mutation in the gene encoding the alpha 5 chain of collagen type IV. *Proc Natl Acad Sci U S A* **91**(9)**:** 3989-3993.

Zinsstag J, Schelling E, Waltner-Toews D, Tanner M (2011). From "one medicine" to "one health" and systemic approaches to health and well-being. *Prev Vet Med* **101**(3-4)**:** 148-156.

Zoran DL, Buffington CA (2011). Effects of nutrition choices and lifestyle changes on the well-being of cats, a carnivore that has moved indoors. *J Am Vet Med Assoc* **239**(5)**:** 596-606.